

Spring 2010

Kinetic and Thermodynamic Studies of Copper-Catalyzed Atom Transfer Radical Processes in the Presence of Free-Radical Diazo Initiators as Reducing Agents

Marielle Nicole Cajita Balili

Follow this and additional works at: <https://dsc.duq.edu/etd>

Recommended Citation

Balili, M. (2010). Kinetic and Thermodynamic Studies of Copper-Catalyzed Atom Transfer Radical Processes in the Presence of Free-Radical Diazo Initiators as Reducing Agents (Doctoral dissertation, Duquesne University). Retrieved from <https://dsc.duq.edu/etd/261>

This Immediate Access is brought to you for free and open access by Duquesne Scholarship Collection. It has been accepted for inclusion in Electronic Theses and Dissertations by an authorized administrator of Duquesne Scholarship Collection. For more information, please contact phillipsg@duq.edu.

KINETIC AND THERMODYNAMIC STUDIES OF COPPER-CATALYZED ATOM
TRANSFER RADICAL PROCESSES IN THE PRESENCE OF FREE-RADICAL
DIAZO INITIATORS AS REDUCING AGENTS

A Dissertation

Submitted to the Bayer School of Natural and Environmental Sciences

Duquesne University

In partial fulfillment of the requirements for
the degree of Doctor of Philosophy

By

Marielle Nicole Cajita Balili

August 2010

Copyright by
Marielle Nicole Cajita Balili

2010

KINETIC AND THERMODYNAMIC STUDIES OF COPPER-CATALYZED ATOM
TRANSFER RADICAL PROCESSES IN THE PRESENCE OF FREE-RADICAL
DIAZO INITIATORS AS REDUCING AGENTS

By

Marielle Nicole Cajita Balili

Approved April 12, 2010

Dr. Tomislav Pintauer
Assistant Professor of Chemistry and
Biochemistry
Committee Chair

Dr. Jennifer A. Aitken
Associate Professor of Chemistry and
Biochemistry
Committee Member

Dr. Partha Basu
Associate Professor of Chemistry and
Biochemistry
Committee Member

Dr. Krzysztof Matyjaszewski
J. C. Warner Professor of Natural
Sciences
Carnegie Mellon University
External Reviewer

Dr. David W. Seybert
Dean, Bayer School of Natural and
Environmental Sciences
Professor of Chemistry and Biochemistry

Dr. Jeffrey D. Madura
Chair, Department of Chemistry and
Biochemistry
Professor of Chemistry and Biochemistry

ABSTRACT

KINETIC AND THERMODYNAMIC STUDIES OF COPPER-CATALYZED ATOM TRANSFER RADICAL PROCESSES IN THE PRESENCE OF FREE-RADICAL DIAZO INITIATORS AS REDUCING AGENTS

By

Marielle Nicole Cajita Balili

August 2010

Dissertation supervised by Dr. Tomislav Pintauer

The first part of this dissertation focuses on the kinetic aspects of atom transfer radical addition (ATRA) in the presence of reducing agents. The rate of alkene consumption was found to be dependent on the initial concentration of the radical initiator and its decomposition and termination rate constants but not on the concentrations of Cu^{I} and Cu^{II} , which was contrary to the rate law for copper-catalyzed ATRA in the absence of a reducing agent. Kinetic experiments showed that the observed rate of ATRA (k_{obs}) was indeed not dependent on the concentration of the catalyst, which supported the newly derived rate law. However, product selectivity was highly dependent on the nature of the catalyst. The activation ($k_{\text{a,AIBN}}$) and deactivation ($k_{\text{d,AIBN}}$) rate constants of various Cu^{II} /AIBN systems were determined through a combination of

experimental and theoretical methods and were found to control the overall concentrations of Cu^{I} and Cu^{II} at equilibrium.

The effect of the catalyst, alkyl halide, and free radical initiator concentrations on the percent conversion and yield of monoadduct were also investigated. Lower catalyst loadings in ATRA reactions involving reactive monomers led to a decrease in monoadduct yield due to competing polymerization reactions. Low-temperature ATRA reactions were found to significantly increase the formation of the monoadduct as a result of the lowering of the rate constant of propagation (k_p). Reactions of less active halides were more affected by increased alkyl halide concentrations than that of the more active alkyl halides. Higher free radical initiator concentration led to an increase in AIBN-initiated polymer formation.

The second part explores the role of thermodynamic factors on the product selectivity of atom transfer radical cyclization (ATRC). Various derivatives of alkenyl bromoacetate and trichloroacetate were synthesized and characterized by ^1H NMR spectroscopy. Theoretical calculation of the relative energies of the *s-trans* and *s-cis* conformers revealed that the presence of bulky substituents on the carbon atom α to the acetate moiety stabilizes the *s-cis* conformation and, thus, promotes cyclization. This was experimentally confirmed in the ATRC reactions of the synthesized alkenyl haloacetates in which the addition of bulky groups increased the yields of cyclic products.

To my Tatay and my Nanay

ACKNOWLEDGEMENT

First and foremost, I thank my advisor, Dr. Tomislav Pintauer. This work would not have been realized without his guidance and support. I truly appreciate that he had high expectations and pushed me to do my best because “it is for my own good”, but I am also grateful that he was very understanding when it mattered. I feel privileged to have him as my mentor and I am also honored to be his first graduate student.

I am grateful to my committee members, Dr. Jennifer Aitken and Dr. Partha Basu and my external reviewer, Dr. Krzysztof Matyjaszewski, for their valuable feedbacks and insights that helped me improve my dissertation. Dr. Mitch Johnson and his group have been extremely generous with their time and equipment. My UV-irradiated experiments would not have been accomplished without their assistance and for this, I am highly indebted to them.

I also thank the Department of Chemistry and Biochemistry at Duquesne University and the National Science Foundation for their financial support to our research group.

Life as a graduate student can be very challenging, but I am glad to have such amazing labmates who really made working in the lab a lot of fun. To Carolynne Ricardo, William Eckenhoff, Matthew “Machu” Taylor, Ashley Biernesser, Sean Noonan, April Hill, Raj Kaur and Anita Dasu, thanks for all the wonderful memories. I will miss our parties, lunches at Milano’s, and picture-taking sessions. Special thanks to Carol and Will, who have been with me the longest and who have been more than willing to lend an ear to hear me out and a helping hand to pull me up. It has really been fun

working with all of you and I am going to miss you. You can now have my share of the NMR tubes.

Thanks also to Sandy Russell and Amy Stroyne, who were always ready and willing to assist me, from booking rooms for my oral defenses to making sure that I get my per diem when I go to conferences. I also thank Lance Crosby, our go-to guy when it comes to NMR matters, for keeping the NMR machine in tiptop shape so I can run my “usual” 30 samples without any hassle. Dr. Nithya Vaidyanathan and Sue Patil are the unsung heroines of the teaching assistants and I am grateful to them for always having everything ready so that my labs will run smoothly. Thanks also to Heather Costello and Matthew Boyer for their help with administrative and ETD matters.

I also thank the wonderful ladies at the Duquesne University YMCA Child Development Center, Miss Alcira, Miss Caitlin, and Miss Tracy, for taking such great care of my son while my hands were tied up in the lab. They helped me keep my sanity because I knew my son was in good hands.

I will surely miss my friends in the Squirrel Hill community group of City Reformed Presbyterian Church, Gary and Leslie Atcheson, Kate Reilly, Ted and Barb Adair, Dan Reiley, Megan Stehle, Pranav and Trista Shah and Dave and Joanne Faith. Our weekly Bible studies were practically the only life I had outside of school and they not only helped me grow spiritually but were also a nice break from the humdrums of graduate school life. I also thank Dave and Sandy Snoke, Gayathri Withers and our pastor Matthew Koerber and his wife Chrissie for their prayers and for making me and my husband feel welcome and part of the church family.

My parents, Nick and Marlene, deserve special mention. Without their unwavering support and constant encouragement (and not to mention good genes), I would not have made it this far. My Tatay has always been my role model and buddy and my Nanay never fails to remind me that even though I already have a child of my own, I will always be her baby. I also thank my sisters, Maan and Tara, for all their help and prayers. Even if they are my “little” sisters, they helped me a lot financially because they make more money than I do (I guess everyone makes more money than I do). And even though I hate winter in Chicago, I will surely miss spending Christmas with them when I go back home to the Philippines. I guess it is now their turn to visit me. Thanks also to my in-laws, Papa, Mama, Yen, Manoy and Grace, for welcoming me into the Balili family and for helping my husband look after our son while I finish the last lap of the race.

No words can express how thankful I am for Ryan, my husband and best friend. He was always there for me ever since we were undergrads, from tutoring me so I won't fail my phychem undergrad class to picking me up late at night when I had to grade for the Gen Chem exams. I thank God for giving me such a wonderful person to spend the rest of my life with. And though he did not directly contribute to this thesis, I also thank my son, Noah Tristan, who has given me so much joy. I love you both so much and I cannot wait to be with you again.

Above all, I thank our Almighty Father, the source of my strength and the key to my success. I offer this work and everything that I do for His greater glory.

TABLE OF CONTENTS

	Page
Abstract.....	iv
Dedication.....	vi
Acknowledgement	vii
List of Tables	xv
List of Figures.....	xvii
List of Schemes.....	xix
List of Abbreviations	xxi
 Chapter 1. Introduction	
1.1 Origins of Atom Transfer Radical Addition	1
1.2 Fundamentals of Transition Metal Catalyzed Atom Transfer Radical Addition ..	5
1.3 Some Transition Metal Catalysts Used in Atom Transfer Radical Processes	11
1.4 “Greening” of Transition Metal Catalyzed Atom Transfer Radical Processes...	18
1.5 Kinetics of Transition Metal Catalyzed Atom Transfer Radical Processes.....	23
1.6 Project Overview	31
References.....	32
 Chapter 2. Effect of Catalyst, Alkyl Halide, and Reducing Agent Concentrations on Copper-Catalyzed Atom Transfer Radical Addition Reactions	
2.1 Introduction.....	47
2.2 Experimental	50
2.2.1 General Procedures	50
2.2.2 Preparation of Catalyst Solutions.....	50
2.2.3 ATRA Reactions with Varying Cu ^{II} Concentration.....	51

2.2.4 ATRA Reactions with Varying Alkyl Halide Concentration	51
2.2.5 ATRA Reactions with Varying AIBN Concentration	51
2.3 Results and Discussion	52
2.3.1 Effect of Catalyst Concentration on ATRA of CCl ₄ to Alkenes	52
2.3.2 Effect of Alkyl Halide Concentration on ATRA of CCl ₄ , CHCl ₃ , BzCl and BzBr to Alkenes.....	55
2.3.3 Effect of Reducing Agent Concentration on ATRA of CCl ₄ to Alkenes	59
2.4 Conclusions.....	62
References.....	63

Chapter 3. Kinetic Studies of Copper-Catalyzed Atom Transfer Radical Addition in the Presence of Reducing Agents

3.1 Introduction.....	69
3.2 Experimental	72
3.2.1 General Procedures	72
3.2.2 Preparation of Catalyst Solutions.....	73
3.2.3 Kinetic Studies.....	73
3.2.4 Reduction of Copper(II) Complexes in the Presence of AIBN	74
3.3 Effect of Concentration and Nature of Catalyst on Observed Rate Constant (k_{obs})	75
3.4 Effect of AIBN Concentration of Observed Rate Constant (k_{obs}).....	80
3.5 Reduction of Copper(II) to Copper(I) in the Presence of AIBN	81
3.6 Conclusions.....	84
References.....	85

Chapter 4. Determination of Kinetic Parameters for Catalyst Regeneration in Atom Transfer Radical Addition in the Presence of a Reducing Agent: An Experimental and Theoretical Approach

4.1 Introduction.....	88
4.2 Experimental.....	91
4.2.1 General Procedures.....	91
4.2.2 Measurement of the Rate of Decomposition of AIBN.....	91
4.2.3 Measurement of Deactivation Rate Constant.....	92
4.3 Results and Discussion.....	93
4.3.1 Measurement of the Rate of Decomposition of AIBN.....	93
4.3.2 Determination of Deactivation Rate Constant.....	95
4.3.3 Determination of Activation Rate Constant and Equilibrium Constant.....	99
4.3.4 Kinetic Modeling of the Initiation Step in Copper-Catalyzed Atom Transfer Radical Addition in the Presence of Reducing Agents.....	105
4.4 Conclusions.....	112
References.....	113

Chapter 5. Photoinitiated Ambient Temperature Copper-Catalyzed Atom Transfer Radical Addition and Cyclization Reactions in the Presence of AIBN as Reducing Agent

5.1 Introduction.....	121
5.2 Experimental.....	125
5.2.1 General Procedures.....	125
5.2.2 Kharasch Addition of Halogenated Compounds to Alkenes.....	125
5.2.3 Copper-Catalyzed ATRA of Halogenated Compounds to Alkenes.....	126
5.2.4 Kinetic Studies.....	126
5.3 Results and Discussion.....	127
5.3.1 Kharasch Addition of Halogenated Compounds to Highly Active Alkenes.....	127

5.3.2 Photoinitiated Copper Catalyzed ATRA of CCl ₄ and CBr ₄ to Highly Active Alkenes	129
5.3.3 Photoinitiated Copper-Catalyzed ATRA of CHBr ₃ , CHCl ₃ , EtOCOCl ₃ , BzBr and BzCl to Highly Active Alkenes.....	132
5.3.4 Kinetic Studies of Copper-Catalyzed ATRA of CCl ₄ to Highly Active Alkenes at Ambient Temperature	134
5.3.5 Photoinitiated Atom Transfer Radical Cascade Reactions	136
5.4 Conclusions.....	141
References.....	142

Chapter 6. Copper-Catalyzed Free Radical and Atom Transfer Radical Cyclization Processes

6.1 Introduction.....	148
6.2 Experimental	154
6.2.1 General Procedures	154
6.2.2 Synthesis of Copper(I) Hydrotris(pyrazolyl)borate Complexes	155
6.2.3 Synthesis of Alkenyl Bromoacetates	157
6.2.4 Synthesis of Alkenyl Trichloroacetates	157
6.2.5 Free Radical Cyclization of 6-Bromo-1-Hexene	159
6.2.6 ATRC of Alkenyl Haloacetates	159
6.2.7 Modeling of <i>s-cis</i> and <i>s-trans</i> Isomers of Alkenyl Trichloroacetates.....	159
6.3 Results and Discussion	160
6.3.1 Synthesis and Characterization of Cu(I) Homoscorpionate Complexes....	160
6.3.2 Free Radical Cyclization Reactions in the presence of TpCu ^I Complexes	169
6.3.3 Atom Transfer Radical Cyclization of Alkenyl Haloacetates.....	173
6.3.4 Theoretical Elucidation of Thermodynamic Control in Radical Cyclization Regioselectivity.....	179

6.4 Conclusions.....	185
References.....	187
FUTURE DIRECTIONS	197
APPENDIX A. ¹ H NMR Spectra	199
APPENDIX B. X-RAY Crystal Data	211
APPENDIX C. SPARTAN Output Files.....	230

LIST OF TABLES

	Page
Table 1.1. Chain Transfer Constants for CCl ₄ in Free-Radical Polymerization at 60°C ..	3
Table 1.2. Activation Rate Constants (k_a) for Various ATRP Initiators with CuBr/CuCl	26
Table 1.3. Rate Constants of Deactivation (k_d) of 5-Hexenyl and Cyclopropylmethyl Radical by Cu ^{II} Halides and Pseudohalides in CH ₃ CN at 25°C.....	29
Table 2.1. Effect of [CCl ₄] on the ATRA of CCl ₄ to Alkenes at Various Copper(II) Loadings.....	55
Table 2.2. Effect of Alkyl Halide Concentration on ATRA of Less Active Alkyl Halides to Methyl Acrylate and Styrene	58
Table 2.3. Effect of [AIBN] on the ATRA of CCl ₄ to Alkenes at Various Copper(II) Loadings.....	60
Table 3.1. Values of k_{obs} (s ⁻¹) for the ATRA of CCl ₄ to Alkenes with Varying Concentrations of [Cu ^{II} (TPMA)Cl][Cl].....	76
Table 3.2. Values of k_{obs} (s ⁻¹) for the ATRA of CCl ₄ to Styrene and Methyl Acrylate Catalyzed by Different Copper(II) Complexes.....	79
Table 4.1. Decomposition Rate Constant of AIBN at 60°C	94
Table 4.2. Deactivation Rate Constants of Various [Cu ^{II} (L)Cl][Cl] (L=Ligand) with AIBN.....	97
Table 4.3. Values of Parameters Used in Kinetic Modeling.....	103
Table 4.4. Activation Rate Constants and Equilibrium Constants of Various [Cu ^{II} (L)Cl][Cl] Complexes using AIBN as Initiator	104
Table 4.5. Parameters and Reaction Conditions Used in Kinetic Simulation of the Reduction of Cu ^{II} to Cu ^I in Copper-Catalyzed ATRA in the Presence of AIBN.....	105
Table 5.1. Propagation Rate Constants of Highly Active Alkenes	122
Table 5.2. ATRA of CCl ₄ to Highly Active Alkenes at 60°C and Ambient Temperature	123
Table 5.3. Photoinitiated Kharasch Addition of Polyhalogenated Compounds to Highly Active Alkenes at Ambient Temperature	128

Table 5.4. Photoinitiated Copper-Catalyzed ATRA of CCl ₄ and CBr ₄ to Highly Active Alkenes at Ambient Temperature	130
Table 5.5. Photoinitiated Copper Catalyzed ATRA of CHBr ₃ , CHCl ₃ , EtOCOCl ₃ , BzBr and BzCl to Highly Active Alkenes at Ambient Temperature	133
Table 5.6. Values of k_{obs} (s ⁻¹) for the Photoinitiated ATRA of CCl ₄ to Highly Active Alkenes using [Cu ^{II} (TPMA)Cl][Cl] as Catalyst and AIBN as Reducing Agent	135
Table 5.7. Photoinitiated Copper Catalyzed Atom Transfer Radical Cascade Reactions at Ambient Temperature	139
Table 6.1. Selected Bond Distances (Å) and Angles (deg) for [TpCu ^I] ₂	164
Table 6.2. Selected Bond Distances (Å) and Angles (deg) for Tp ^{CF₃} Cu ^I (CH ₃ CN)	166
Table 6.3. Selected Bond Distances (Å) and Angles (deg) for TpCu ^I (6-bromo-1-hexene)	168
Table 6.4. Bu ₃ SnH-Mediated Free Radical Cyclization of 6-bromo-1-hexene in the Presence of TpCu ^I Complexes	171
Table 6.5. Copper-Catalyzed ATRC of Alkenyl Bromoacetates and Trichloroacetates	177
Table 6.6. Calculated Relative Energies of <i>s-cis</i> and <i>s-trans</i> Conformers of Various C3-Substituted Allyl Trichloroacetate Radicals	181
Table 6.7. Electron Density Maps and Dipole Moments (Debye) of <i>s-cis</i> and <i>s-trans</i> Conformers of Various C3-Substituted Allyl Trichloroacetate Radicals	183

LIST OF FIGURES

	Page
Figure 1.1. SOMO-LUMO and SOMO-HOMO Interactions between a Radical and an Alkene (EDG = Electron-Donating Group, EWG = Electron-Withdrawing Group)	7
Figure 1.2. Examples of Halogenated Compounds Used in ATRA Reactions.....	8
Figure 1.3. Examples of Alkenes and 1,6-Dienes Used in ATRA/ATRC Reactions	9
Figure 1.4. Substrates Used in ATRC Reactions (X=Halogen, Y=H or Halogen).....	10
Figure 1.5. Examples of Ruthenium-Based Catalysts Used in ATRA/ATRC Reactions	13
Figure 1.6. Examples of Nitrogen-Based Ligands Commonly Used in Cu-Mediated Atom Transfer Radical Processes	14
Figure 1.7. Examples of Pincer Complexes of Nickel Used as Catalysts in ATRA Reactions (X = Cl, Br)	18
Figure 1.8. Solid-Supported Transition Metal Catalysts Used in Atom Transfer Radical Processes	19
Figure 1.9. Perfluorous Ligands Commonly Used in Biphasic Systems	20
Figure 1.10. Values of k_a ($M^{-1}s^{-1}$) in ATRP for Various Complexing Ligands with EtBriB (ethyl-2-bromoisobutyrate) Measured in CH_3CN at $35^\circ C$	27
Figure 1.11. Values of k_a ($M^{-1}s^{-1}$) in ATRA/ATRP for Various Alkyl Halides with $Cu^I X/PMDETA$ (X = Cl, Br, I) Measured in CH_3CN at $35^\circ C$	28
Figure 2.1. Effect of $[Cu^{II}(TPMA)Cl][Cl]$ on the ATRA of CCl_4 to Alkenes.....	53
Figure 3.1. First-Order Kinetic Plot for the ATRA of CCl_4 to Methyl Acrylate (—), Styrene (----) and 1-Octene (...) Catalyzed by Varying $[Cu^{II}(TPMA)Cl][Cl]$ Concentrations (1 mol% (●), 0.2 mol% (■) and 0.1 mol% (◆)) in the Presence of AIBN.	75
Figure 3.2. Plots of (a) $\ln([M]_0/[M]_t)$ and (b) Percent Yield of Monoadduct Versus Time for the ATRA of CCl_4 to Methyl Acrylate Catalyzed by Copper(II) Complexes with TPMA, PMDETA, bpy, and Me_6TREN Ligands.	78
Figure 3.3. Plot of $\ln(k_{app})$ Versus $\ln[AIBN]$	81
Figure 3.4. Reduction of Copper(II) Complexes with bpy, PMDETA, TPMA and Me_6TREN Ligands in the Presence of AIBN as a Reducing agent in CH_3OH at $60^\circ C$, $[Cu^{II}]_0:[AIBN]_0=1:10$	82

Figure 4.1. ¹ H NMR Spectra of TEMPO-Trapping Experiments showing (a) AIBN Peak at Time = 0, (b) Formation of AIBN-TEMPO Adduct, (c) Formation of AIBN-Cl and AIBN-TEMPO Adducts.....	98
Figure 4.2. ¹ H NMR Spectra showing Increasing AIBN-Cl Formation with Increasing [Cu ^{II} (TPMA)Cl][Cl]-to-[TEMPO] Ratios	98
Figure 4.3. Plot of Mole Ratio of [AIBN-Cl]/[AIBN-TEMPO] versus Initial Concentration Ratio of [Cu ^{II}] ₀ /[TEMPO] ₀ at 40°C in Methanol: [Cu ^{II} (bpy) ₂ Cl][Cl](●), [Cu ^{II} (PMDETA)Cl ₂](■), [Cu ^{II} (TPMA)Cl][Cl](◆), [Cu ^{II} (Me ₆ TREN)Cl][Cl](▲)	99
Figure 4.4. Kinetic Plots for Determination of Activation Rate Constants: Data Points (● for Cu ^{II} and ■ for Cu ^I) show Experimental Copper Concentrations Over Time from UV-Vis Data and Solid Lines (—) are Plotted from Kinetic Modeling	104
Figure 4.5. Simulation of Kinetic Plots for the Regeneration of Cu ^I from Cu ^{II} in the Presence of AIBN: <i>k</i> _{dc} Values Ranging from 3.5-6.5 x 10 ⁻⁶ s ⁻¹ at (A) 10 ⁻¹ M ⁻¹ s ⁻¹ (<i>k</i> _{a,AIBN}) and 10 ⁸ M ⁻¹ s ⁻¹ (<i>k</i> _{d,AIBN}); (B) 10 ² M ⁻¹ s ⁻¹ (<i>k</i> _{a,AIBN}) and 10 ⁸ M ⁻¹ s ⁻¹ (<i>k</i> _{d,AIBN}).	107
Figure 4.6. Simulation of Kinetic Plots for the Regeneration of Cu ^I from Cu ^{II} in the Presence of AIBN: AIBN Concentration Ranging from 1-20 mol% Relative to Alkene at (A) 10 ² M ⁻¹ s ⁻¹ (<i>k</i> _{a,AIBN}) and 10 ⁸ M ⁻¹ s ⁻¹ (<i>k</i> _{d,AIBN}); (B) 10 ⁴ M ⁻¹ s ⁻¹ (<i>k</i> _{a,AIBN}) and 10 ⁷ M ⁻¹ s ⁻¹ (<i>k</i> _{d,AIBN}).....	108
Figure 4.7. Simulation of Kinetic Plots for the Regeneration of Cu ^I from Cu ^{II} in the Presence of AIBN: (A)= <i>k</i> _{a,AIBN} Values Ranging from 0.001 to 5.0 x 10 ⁵ M ⁻¹ s ⁻¹ (<i>k</i> _{d,AIBN} =10 ⁸ M ⁻¹ s ⁻¹) and (B)= <i>k</i> _{d,AIBN} Values Ranging from 10 ⁵ to 10 ⁹ M ⁻¹ s ⁻¹ (<i>k</i> _{a,AIBN} =10 ² M ⁻¹ s ⁻¹).....	110
Figure 5.1. Pseudofirst-Order Kinetic Plot for the Photoinitiated ATRA of CCl ₄ to Methyl Acrylate (MA), Methyl Methacrylate (MMA), Acrylonitrile (AN), Vinyl Acetate (VA), and Styrene (Sty) using [Cu ^{II} (TPMA)Cl][Cl] as Catalyst and AIBN as Reducing Agent.....	135
Figure 6.1. Molecular Structure of [TpCu ^I] ₂ Showing the Atom-Labeling Scheme.. ..	163
Figure 6.2. Molecular Structure of Tp ^{CF3} Cu ^I (CH ₃ CN) Showing the Atom-Labeling Scheme.....	166
Figure 6.3. ¹ H NMR Spectra of 6-bromo-1-hexene and CuTp(6-bromo-1-hexene) Showing Shielding of Olefinic Protons	167
Figure 6.4. Molecular Structure of TpCu ^I (6-bromo-1-hexene) Showing the Atom-Labeling Scheme.....	169
Figure 6.5. Dewar-Chatt-Duncanson Model of Copper-Olefin Binding	170

LIST OF SCHEMES

	Page
Scheme 1.1. Kharasch Addition of Halogenated Compounds to Alkene in the Presence of Peroxide Initiators.....	2
Scheme 1.2. Iron-Catalyzed ATRA of CCl ₄ to Acrylonitrile.....	4
Scheme 1.3. Proposed Mechanism for Transition Metal Catalyzed Atom Transfer Radical Addition (TMC ATRA).....	5
Scheme 1.4. Sequential ATRA/ATRC Resulting in the Formation of Polycyclic Compounds	11
Scheme 1.5. Synthesis of <i>Quercus</i> Lactones via CuCl/bpy-Catalyzed ATRC	15
Scheme 1.6. ATRA of CCl ₄ to Alkenes Using Cu-based Catalyst with Different Tp Ligands.....	16
Scheme 1.7. Proposed Mechanism for ATRA Catalyzed by Tp ^X Cu ^I Complexes	17
Scheme 1.8. Catalyst Regeneration in ATRA in the Presence of Reducing Agents.....	21
Scheme 1.9. Relative K_{ATRP} Values of Various Alkyl Halides	25
Scheme 1.10. Model Reaction for Activation Rate Constant Measurement.....	25
Scheme 1.11. Isomerization and Deactivation of 5-Hexenyl and Cyclopropylmethyl Radicals in the Presence of Cu ^{II} Halides and Pseudohalides	29
Scheme 1.12. Model Reaction for Deactivation Rate Constant Measurements.....	30
Scheme 2.1. Proposed Mechanism for Copper(I) Regeneration in ATRA in the Presence of Free-Radical Diazo Initiator (AIBN) as a Reducing Agent.	48
Scheme 3.1. Initiation, Propagation and Termination Steps in Copper Catalyzed ATRA in the Presence of Free-Radical Initiator AIBN.....	70
Scheme 4.1. Model Reaction for Deactivation Rate Constant ($k_{d,AIBN}$) Measurement ...	96
Scheme 4.2. Model Reaction for Activation Rate Constant ($k_{a,AIBN}$) Measurement	100
Scheme 4.3. Model Reactions for $k_{a,AIBN}$ Estimation through Kinetic Modeling	102
Scheme 5.1. Reaction Pathways in the Atom Transfer Radical Cascade Reaction of Halogenated Compounds to 1,6-Dienes Catalyzed by Copper Complexes (X=Halogen, Pseudohalogen).....	137

Scheme 5.2. Cyclization and Radical Trapping Pathways of the 5-Hexenyl Radical...	139
Scheme 6.1. Tributylstannane (Bu ₃ SnH) and Halogen Atom Transfer Method	149
Scheme 6.2. Synthesis of Spiro-Indoles via Sequential Radical Cyclization.....	150
Scheme 6.3. Proposed Mechanism for Transition Metal-Catalyzed Atom Transfer Radical Cyclization (TMC ATRC) (L = Ligand, X = Halogen)	151
Scheme 6.4. Bu ₃ SnH-Mediated Free Radical Cyclization of 5-Hexenyl Radicals	152
Scheme 6.5. <i>Endo</i> and <i>Exo</i> Mode of Cyclization.....	153
Scheme 6.6. Radical Cyclization of (a) Acyl-Substituted Radicals and (b) Alkenyl Acetate Radicals.....	154
Scheme 6.7. Proposed Mechanism for Copper-Catalyzed ATRC of Haloacetates.....	174
Scheme 6.8. Copper-Catalyzed ATRC of Trichloroacetates and Amides	175
Scheme 6.9. (a) Synthetic Scheme for Alkenyl Bromoacetates and Trichloroacetates, (b) Haloacetate Precursors for ATRC Reactions	176

LIST OF ABBREVIATIONS

AIBN	2,2'-azobis(isobutyronitrile)
ATRA	atom transfer radical addition
ATRC	atom transfer radical cyclization
ATRP	atom transfer radical polymerization
bpy	2,2'-bipyridine
Bu ₃ SnH	tributyltin hydride
BzBr	benzyl bromide
BzCl	benzyl chloride
CBr ₄	carbon tetrabromide
CCl ₄	carbon tetrachloride
CHBr ₃	bromoform
CHCl ₃	chloroform
CH ₃ CN	acetonitrile
Cp*	pentamethylcyclopentadienyl
DCE	1,2-dichloroethane
EDG	electron-donating group
EtBriB	ethyl-2-bromoisobutyrate
EtOCOCl ₃	ethyl trichloroacetate
EWG	electron-withdrawing group
HMTETA	1,1,4,7,10,10-hexamethyltriethylenetetramine
HOMO	highest occupied molecular orbital

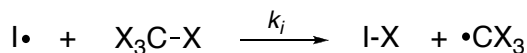
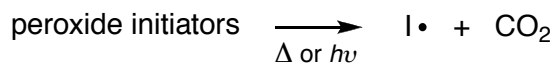
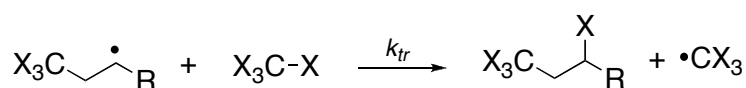
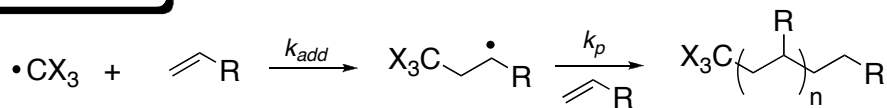
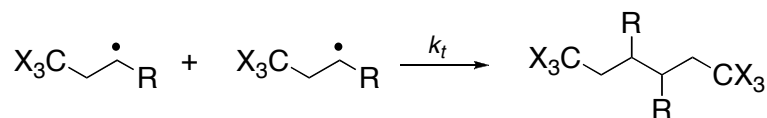
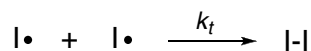
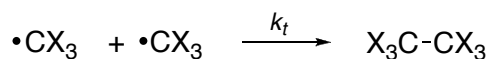
ICAR	initiators for continuous activator regeneration
LUMO	lowest unoccupied molecular orbital
MBriB	methyl-2-bromoisobutyrate
MBrP	methyl-2-bromopropionate
MeOH	methanol
Me ₆ TREN	tris[2-(dimethylaminoethyl)amine]
NMR	nuclear magnetic resonance
NPMI	<i>N</i> -alkyl-2-pyridylmethanimine
PEBr	1-(bromoethyl)benzene
PECl	1-(chloroethyl)benzene
PMDETA	<i>N,N,N',N'',N'''</i> -pentamethyldiethylenetriamine
SOMO	singly occupied molecular orbital
TDHP	tris(1,2-dimethylhydrazino)diphosphane
TEMPO	2,2,6,6-tetramethylpiperidin-1-oxyl
Tp	tris(pyrazolyl)borate
TPEDA	<i>N,N,N',N'</i> -tetrakis(2-pyridylmethyl)ethylenediamine
TPMA	tris[(2-pyridyl)methyl]amine
TMC ATRA	transition metal catalyzed atom transfer radical addition
V70	2,2'-azobis(4-methoxy-2,4-dimethylvaleronitrile)

Chapter 1

Introduction

1.1 Origins of Atom Transfer Radical Addition

The formation of carbon-carbon single bonds is of utmost importance in synthetic organic chemistry. A classic example of this fundamental chemical reaction is Kharasch addition, in which carbon-carbon bond formation results from the anti-Markovnikov addition of halogenated compounds to unsaturated hydrocarbons in the presence of peroxide initiators.¹⁻⁵ As shown in Scheme 1.1, free radicals generated from the decomposition of the peroxide initiators initiate a radical chain reaction through a homolytic cleavage of the carbon-halogen bond of the halogenated compound. The resulting carbon-centered radical species adds across the double bond of an alkene, generating a secondary radical which, in turn, abstracts a halide from a halogenated compound to form a single addition adduct. In the case of simple α -olefins such as 1-hexene, 1-octene and 1-decene, impressive yields of the desired single addition adducts were obtained. However, monoadduct yields significantly decreased when more reactive monomers such as styrene, methyl acrylate and methyl methacrylate were involved. The selectivity towards monoadduct formation from highly reactive monomers was compromised due to the radical-radical termination and the repeated addition of the secondary radical to an alkene. Although, radical-radical termination reactions by

Initiation**Propagation****Termination**

X = Cl, Br, etc.

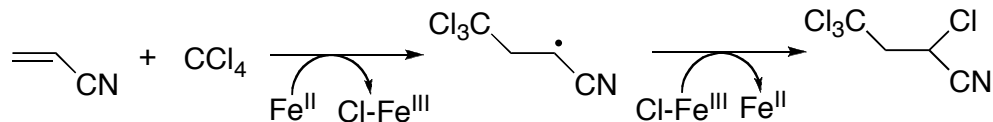
Scheme 1.1. Kharasch Addition of Halogenated Compounds to Alkene in the Presence of Peroxide Initiators

coupling and disproportionation could be suppressed by decreasing the radical concentration ($R_t \propto [\text{radicals}]^2$), the chain transfer constant of these alkenes (Table 1.1) is not high enough to prevent the generation of oligomers/polymers, which results in significantly lower yields of the monoadduct for alkenes that are highly active in free-radical polymerization.

Table 1.1. Chain Transfer Constants for CCl₄ in Free-Radical Polymerization at 60°C⁶

Alkene	k_{tr} (M ⁻¹ s ⁻¹)	k_p (M ⁻¹ s ⁻¹)	k_{tr}/k_p
ethylene	259	16	16.2
1-hexene	320	22	14.5
vinyl acetate	2400	2300	1.04
styrene	1.8	165	0.0109
methyl methacrylate	0.12	515	0.000233
methyl acrylate	0.26	2090	0.000124
acrylonitrile	0.17	1960	0.0000865

In 1956, Minisci and coworkers observed the formation of monoadduct (CCl₃-CH₂-CHClCN with CCl₄ and CHCl₂-CH₂-CHClCN with CHCl₃) in the thermal polymerization of acrylonitrile in CCl₄ and CHCl₃ using a steel autoclave.⁷ This was rather surprising since monoadduct formation was highly unlikely in the addition of CCl₄ to acrylonitrile because the propagation rate constant (k_p) was so much higher than the chain transfer constant (k_{tr}). After observing the same results in a similar experiment in the 1960s, the authors proposed a mechanism in which iron chlorides (arising from corrosion of the autoclave) increase the chain transfer constant and, thus, allowed the formation of single addition adducts from highly active monomers (Scheme 1.2).⁸⁻¹² These findings led to the successful use of transition metal catalysts in Kharasch-type addition processes, which are now more commonly known as transition metal catalyzed atom transfer radical addition (TMC ATRA).

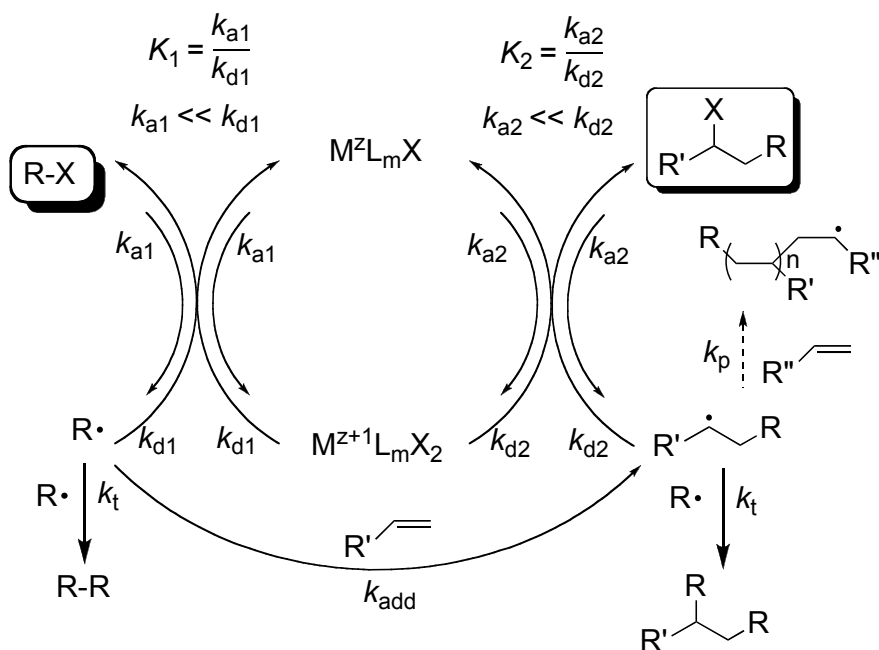


Scheme 1.2. Iron-Catalyzed ATRA of CCl_4 to Acrylonitrile

The use of transition metal catalysts has been a fundamental tool in organic synthesis, enabling a variety of chemical transformations that are difficult to achieve using traditional non-metal catalyzed methods. In many instances, remarkable levels of control in product selectivity in chemical reactions conducted in the presence of a metal catalyst can be accomplished. Since the seminal report by Minisci *et. al.*, a number of transition metal complexes have been successfully utilized in ATRA processes and they included the complexes of Cu, Fe, Ru and Ni,¹³⁻¹⁸ as well as metal oxides^{19,20} and zero valent metals such as Cu(0)^{21,22} and Fe(0).²³⁻²⁵ Furthermore, a variety of functionalized adducts can now be synthesized via ATRA by using different halogenated compounds (alkyl and aryl halides,^{9,26,27} *N*-haloamines,⁹ α -halonitriles,^{28,29} α -haloacetates,^{30,31} α -haloaldehydes,³²⁻³⁴ alkylsulfonyl halides³⁵⁻⁴⁰ and polyhalogenated compounds^{35,38,41,42}), as well as alkenes (styrene, alkyl acrylates and acrylonitrile). As a result, TMC ATRA became a highly useful technique in carbon-carbon bond formation and attracted much interest in synthetic organic chemistry.^{14,15,18,43-45}

1.2 Fundamentals of Transition Metal Catalyzed Atom Transfer Radical Addition

It is generally accepted that the mechanism of TMC ATRA involves free radical intermediates (Scheme 1.3). A metal catalyst in a lower oxidation state, M^zL_mX (M represents a metal ion in oxidation state z , L is a complexing ligand, and X is a halide or a pseudohalide), undergoes inner sphere oxidation via abstraction of a halogen atom from an alkyl halide, RX ($X = Cl, Br$), generating a carboradical species and the corresponding higher oxidation state metal catalyst ($M^{z+1}L_mX_2$). The generated radical can either terminate by coupling with another radical (k_t), abstract the halogen atom from the oxidized metal catalyst to reform the original dormant alkyl halide species (k_{d1}), or add across the double bond of an alkene and form a secondary radical (k_{add}).



Scheme 1.3. Proposed Mechanism for Transition Metal Catalyzed Atom Transfer Radical Addition (TMC ATRA)

If abstraction of the halogen atom from the oxidized metal catalyst occurs after the formation of the secondary radical, the desired monoadduct is produced. The reduction of the metal catalyst through abstraction of the halogen atom completes the catalytic cycle. In order to achieve high selectivity of the target monoadduct, the following conditions should be met: firstly, radical concentration should be low in order to prevent radical coupling reactions and accumulation of the deactivator species (rate constant of activation [k_{a1} and k_{a2}] \ll rate constant of deactivation [k_{d1} and k_{d2}]). Secondly, further activation of the monoadduct should be avoided ($k_{a1} \gg k_{a2}$, where k_{a2} is ideally zero). And lastly, oligomerization and polymerization side reactions should be suppressed, indicating that the rate of deactivation of the radical generated from the addition of the primary alkyl halide radical to the alkene ($k_{d2}[M^{z+1}L_mX]$) should be much larger than the rate of propagation ($k_p[\text{alkene}]$). Ideally, the alkyl halide of choice should result in the formation of a secondary radical that is much less stable than the initial radical and will be irreversibly deactivated by a higher oxidation state metal complex to form an inactive monoadduct.

Addition of the radical to the alkene can also occur intramolecularly when the alkyl halide and the unsaturated moiety are part of the same molecule. Intramolecular TMC ATRA or atom transfer radical cyclization (ATRC) is a powerful tool in organic synthesis and is widely used in the construction of functionalized ring systems that can be used as precursors for the preparation of complex organic molecules.^{15,46} Furthermore, if the functionalized substrate contains more than one unsaturated moiety, sequential intramolecular addition can lead to the formation of polycyclic compounds, which are

highly useful because they mimic the basic skeletons of biologically active natural products.⁴⁷⁻⁵²

Alkenes and alkyl halides are the two main reactants in atom transfer radical process. Radicals are formed from the homolytic cleavage of the alkyl halide bond in the presence of a metal catalyst which then adds to an alkene to form a functionalized adduct. Though polar, steric, and electronic effects are known to influence the orientation of the free radical addition, radical attack typically occurs on the less substituted part of the alkene.⁵³⁻⁵⁵ It is also known that both the SOMO-LUMO and SOMO-HOMO interactions are important in predicting the relative reactivity of a radical to various alkenes (Figure 1.1).^{56,57}

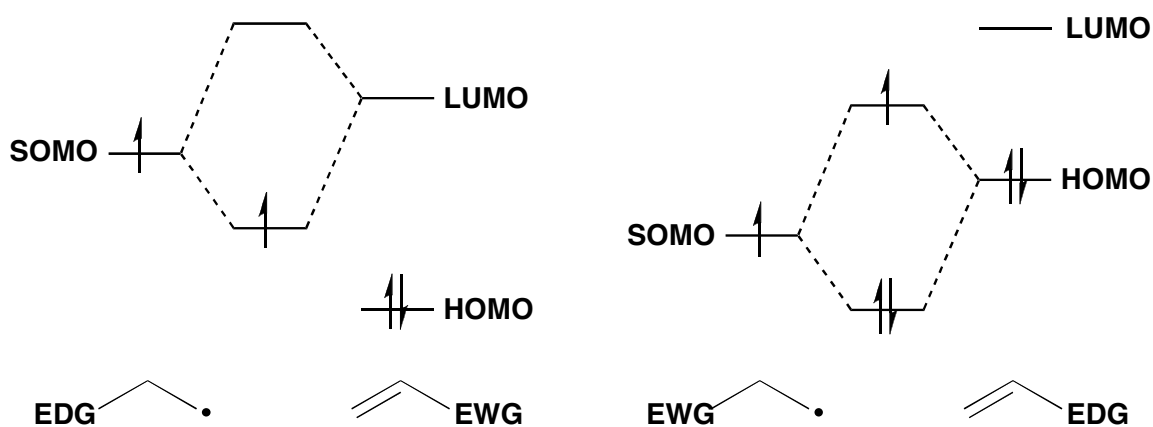


Figure 1.1. SOMO-LUMO and SOMO-HOMO Interactions between a Radical and an Alkene (EDG = Electron-Donating Group, EWG = Electron-Withdrawing Group)

An electron-rich free radical behaves as a nucleophile and its singly occupied molecular orbital (SOMO) interacts with the lowest unoccupied molecular orbital (LUMO) of an alkene. In contrast, a carboradical with electron-withdrawing groups acts

as an electrophile and SOMO-HOMO (highest occupied molecular orbital) interactions are expected between the radical and an alkene. Radical reactions will proceed smoothly when the energy difference is small and, thus, radicals with electron-donating groups preferentially attack an alkene with electron-withdrawing groups and vice versa.

As previously mentioned, a number of halogenated compounds such as alkyl and aryl halides,^{9,26,27} *N*-haloamines,⁹ α -halonitriles,^{28,29} α -haloacetates,^{30,31} α -haloaldehydes,³²⁻³⁴ alkylsulfonyl halides³⁵⁻⁴⁰ and polyhalogenated compounds^{35,38,41,42} have been used in ATRA reactions (Figure 1.2). Generally, multiple functional groups increase the reactivity of an alkyl halide and its corresponding radical, e.g. $\text{CCl}_4 > \text{CHCl}_3 > \text{CH}_2\text{Cl}_2$, towards addition to an alkene. Also, the activity of the alkyl halide typically follows the order of $3^\circ > 2^\circ > 1^\circ$. The activity of the leaving group also decreases in the order $\text{I} \geq \text{Br} > \text{Cl}$.

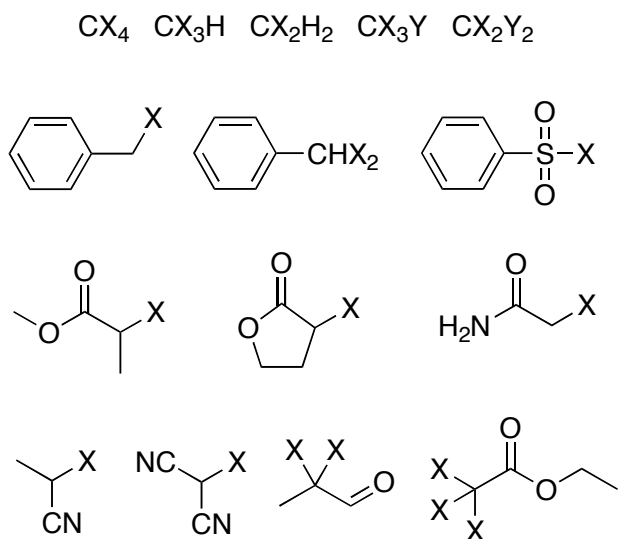


Figure 1.2. Examples of Halogenated Compounds Used in ATRA Reactions
 [X = Halogen (Cl, Br), Pseudohalogen (CN); Y = Alkyl or Aryl Group, Halogen, Pseudohalogen]

Alkenes typically used to probe reactions in ATRA include, but are not limited to, simple α -olefins (1-hexene, 1-octene, 1-decene), methyl acrylate, methyl methacrylate, styrene, vinyl acetate, and acrylonitrile (Figure 1.3). 1,6-Dienes have also been used in transition metal catalyzed atom transfer radical processes, leading to the formation of 1,2-disubstituted cyclopentanes via sequential addition and cyclization.⁵⁸⁻⁶¹ Various transition metal complexes, such as dimanganese decacarbonyl^{58,59} and dinuclear metal-THDP complexes (metal = Ru, Rh, Ir; THDP = tris(1,2-dimethylhydrazino)diphosphane)⁶¹ have

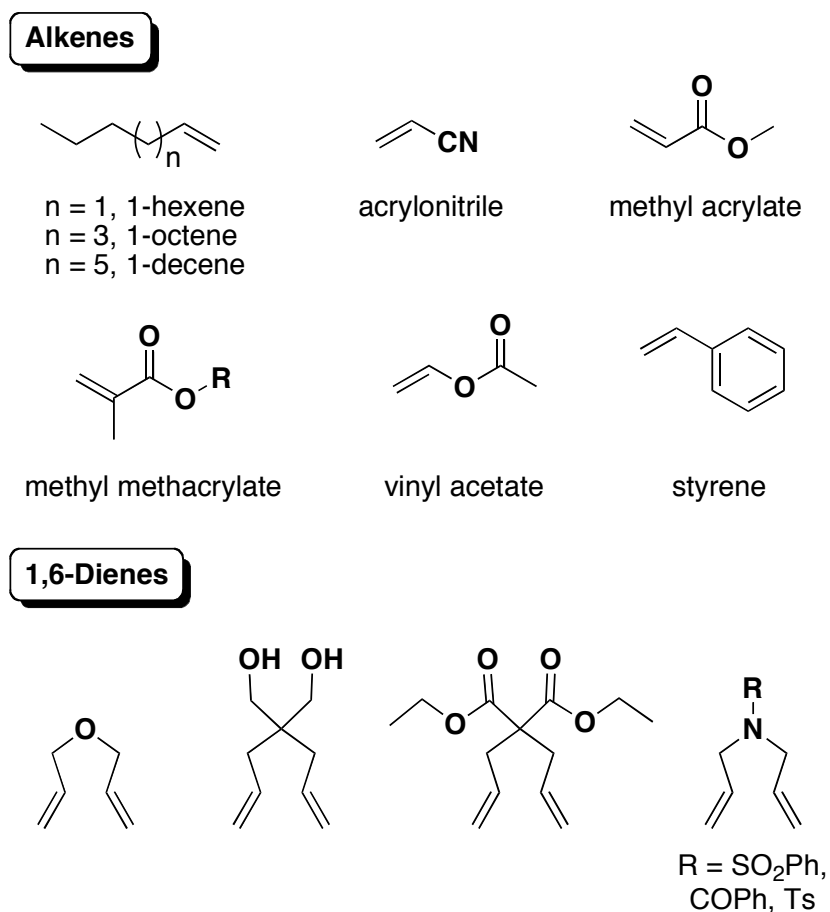


Figure 1.3. Examples of Alkenes and 1,6-Dienes Used in ATRA/ATRC Reactions

been utilized in these sequential/cascade reactions. The diastereoselectivity in the cyclization of these dienes was found to be independent of the catalyst, having a strong preference for the formation of the *cis* isomer.

When a halogen (or pseudohalogen) is present on the alkene framework, intramolecular addition of the generated radical can occur, resulting in the formation of cyclic products. Cyclization reactions play a very important role in organic synthesis because many naturally-occurring organic molecules possess carbo- and heterocyclic rings. A range of substrates (shown in Figure 1.4) has been used in ATRC reactions furnishing a vast array of cyclic products with varying ring sizes.^{15,44,46,62-73}

Tri-halogenated substrates often lead to higher yields than their di- or monohalogenated counterparts. Various factors, such as steric and electronic nature of the catalysts used, substituents on the alkene, solvents, etc., were found to affect the regioselectivity of these cyclization reactions, and will be further discussed in Chapter 6. Furthermore, the presence of two or more unsaturated moieties on the substrate presents an opportunity for sequential addition and cyclization reactions, which will lead to the formation of multi-ring systems (an example is shown in Scheme 1.4).⁷⁴

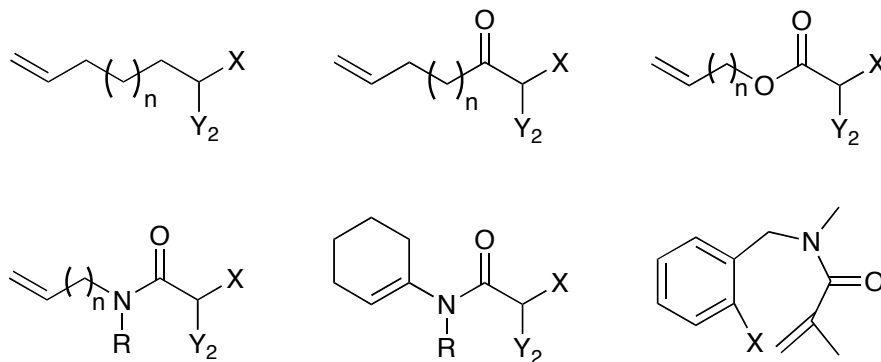
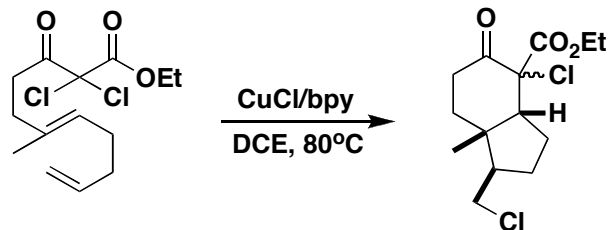


Figure 1.4. Substrates Used in ATRC Reactions (X=Halogen, Y=H or Halogen)



Scheme 1.4. Sequential ATRA/ATRC Resulting in the Formation of Polycyclic Compounds⁷⁴

1.3 Some Transition Metal Catalysts Used in Atom Transfer Radical Processes

As aforementioned, the use of transition metal complexes, which serve as effective halogen transfer agents, has brought about dramatic improvements to the conventional non-metal catalyzed Kharasch addition. In the presence of such complexes, increased yields and high selectivity towards the formation of the monoadduct were observed at high catalyst loadings for alkenes that typically undergo fast radical polymerization processes.^{45,75-79} The transition metal complex plays a significant role in regulating the dynamic equilibrium between the dormant and active species that mediate control in ATRA, which is established between a low oxidation-state transition metal complex and its higher oxidation-state complex. Thus, the characteristics that a transition metal center must possess in order to be an efficient catalyst include having at least two accessible oxidation states separated by one electron, reasonable affinity towards a halogen, and an expandable coordination sphere to selectively accommodate a (pseudo)halogen.⁸⁰ The catalyst should also not participate in any side reactions, which would result in the lowering of the catalytic activity.

In 1973, Matsumoto and coworkers first reported the use of a ruthenium complex, $[\text{RuCl}_2(\text{PPh}_3)_3]$ **1** (Figure 1.5), as a catalyst in the addition of CCl_4 and CHCl_3 to α -olefins.⁸¹ Since then, a number of ruthenium-based catalysts with superior performance in the radical addition of polyhalogenated alkanes to alkenes have been reported in the literature.^{78,79,82-90} One of them is the half-sandwich ruthenium complex $[\text{Ru}^{\text{II}}\text{ClCp}^*(\text{PAr})_2]$ **2** (Cp^* = pentamethylcyclopentadienyl) (Figure 1.5), which is an air stable and readily available complex which promoted the Kharasch addition of CCl_4 and CHCl_3 to alkenes under mild conditions (as low as 40°C).⁷⁸ A similar air stable ruthenium complex, $[\text{Ru}^{\text{II}}\text{Cl}_2(p\text{-cymene})(\text{PAr})_2]$ **3**, also displayed moderately good yields of monoadduct in the ATRA of CCl_4 to various alkenes.⁸⁴ For both complexes, incorporation of electron-withdrawing substituents at the *para* position of the aryl groups (PAr) was found to produce less efficient ATRA catalysts as compared to the unsubstituted rings or rings with electron-donating aryl groups. Another Ru-based catalyst used in atom transfer radical processes is the 1st generation Grubbs' complex **4** (Figure 1.5), a ruthenium carbene complex which is easily synthesized from complex **1**, phenyldiazomethane and tricyclohexylphosphine in a one-pot synthesis.^{91,92} The Grubbs' catalyst has been effectively applied in sequential Kharasch addition of trichloroalkanes across alkenes and hydrolysis of the chlorinated adducts resulting in the carbonylation of the alkenes.^{82,93} Other complexes of Ru that have also been used in ATRA with comparable results include ruthenium amidates (**5**), Ru-Schiff base complexes (**6**) and ruthenacarboranes (**7**), which are illustrated in Figure 1.5.^{84-87,94-98}

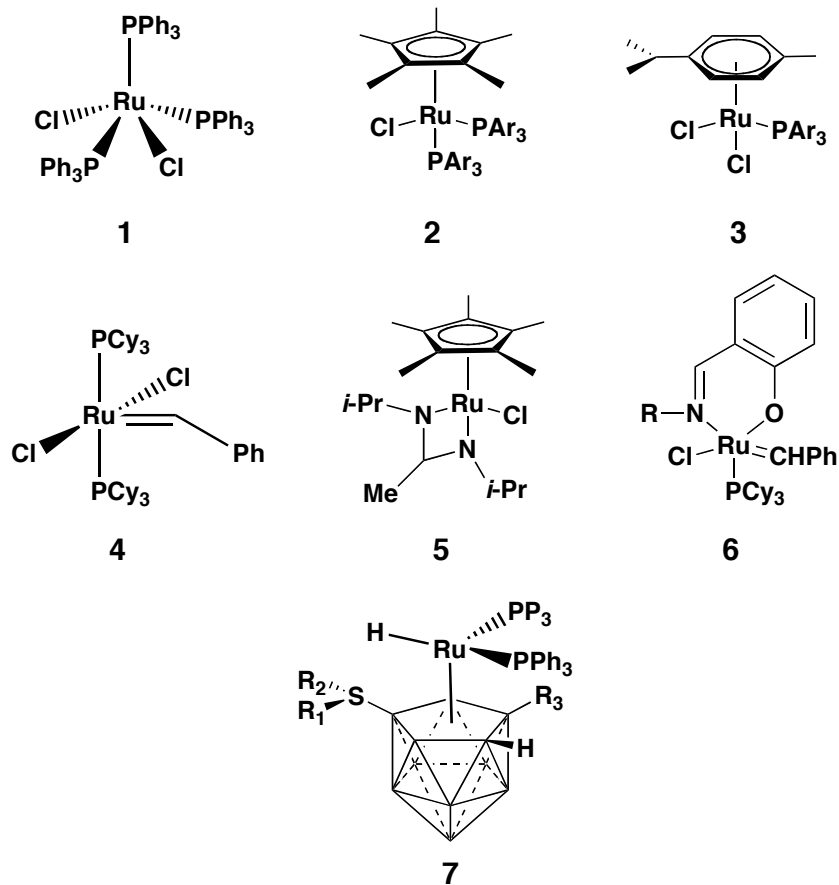


Figure 1.5. Examples of Ruthenium-Based Catalysts Used in ATRA/ATRC Reactions

Copper complexes have also been widely used in ATRA/ATRC reactions and are a cheaper alternative to the Ru catalyst. Earlier Kharasch addition reactions employed copper chloride as a chlorine-atom transfer agent in the addition of CCl_4 , CHCl_3 , and sulfonyl chlorides to alkenes, resulting in moderate yields at 70-145°C.⁹⁹⁻¹⁰¹ Nowadays, various bi-, tri-, and tetradentate nitrogen-based ligands have been widely used in copper catalyzed atom transfer radical processes (Figure 1.6).^{15,45,46,62-67,74,102,103}

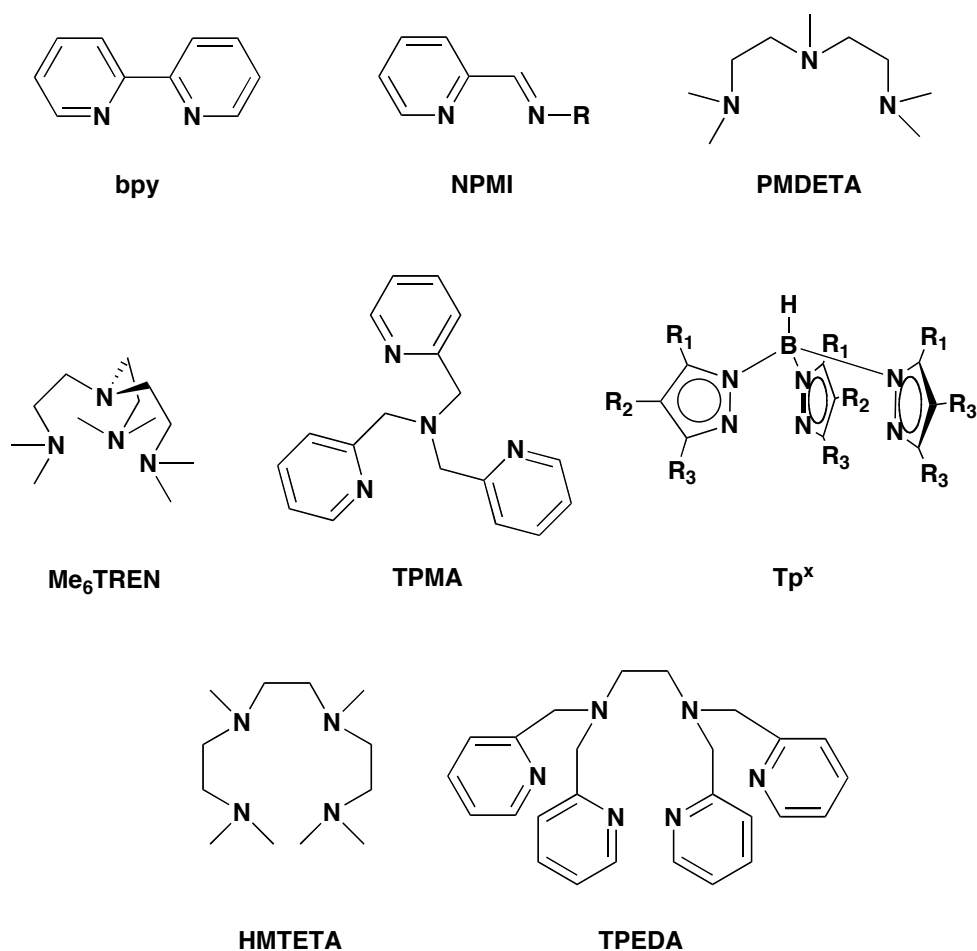
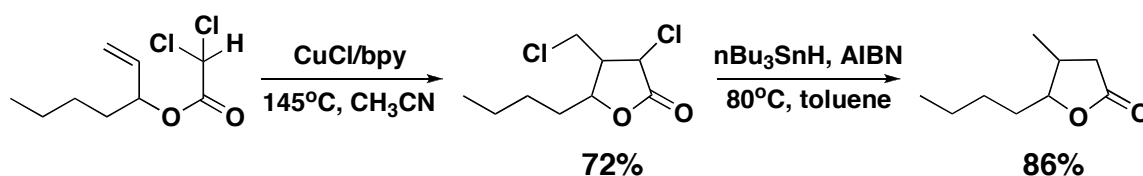


Figure 1.6. Examples of Nitrogen-Based Ligands Commonly Used in Cu-Mediated Atom Transfer Radical Processes

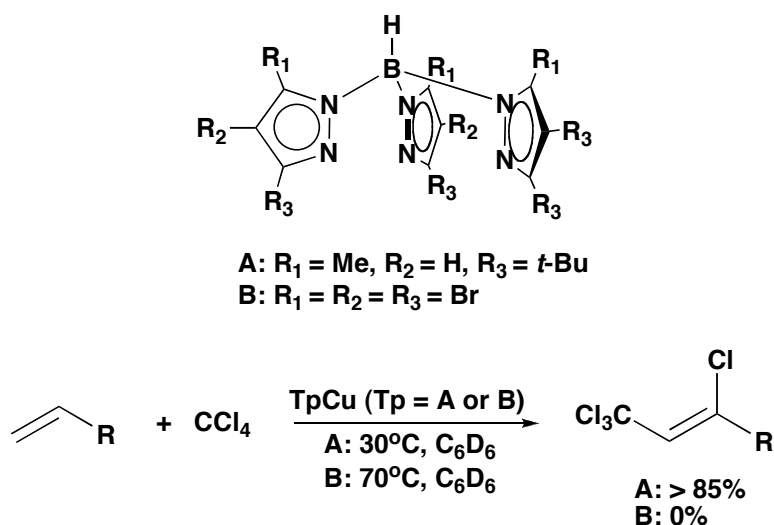
Some of the most commonly used N-based ligands (shown in Figure 1.6) are 2,2'-bipyridine (bpy), *N*-alkyl-2-pyridylmethanimines (NPMI), *N,N,N',N'',N'''*-pentamethyldiethylenetriamine (PMDETA), tris[2-(dimethylamino)ethyl]amine (Me₆TREN), tris[(2-pyridyl)methyl]amine (TPMA), tris(pyrazolyl)borates (Tp^x, where x can be any alkyl group or a halogen), 1,1,4,7,10,10-hexamethyltriethylenetetramine (HMTETA), and *N,N,N',N'*-tetrakis(2-pyridylmethyl)ethylenediamine (TPEDA). Copper complexes with the 2,2'-bipyridine ligand are not particularly active catalysts for ATRA

reactions but are found to be ideal for ATRC processes carried out under harsh reaction conditions ($> 140^{\circ}\text{C}$).⁷¹ The CuCl/bipyridine catalyst system was used in the synthesis of *Quercus* lactones via ATRC of dichlorinated esters of secondary allylic alcohols, with high yields of the targeted cyclic products obtained after reductive dehalogenation of the chlorinated lactones (Scheme 1.5).⁷¹



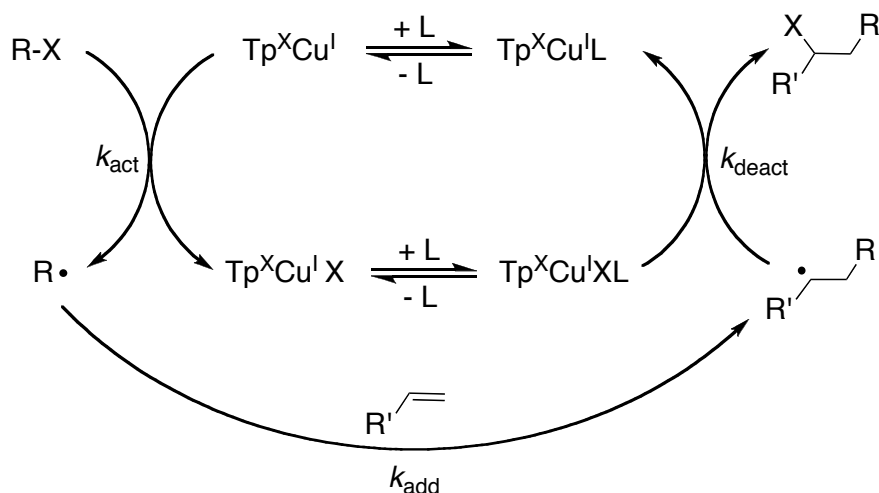
Scheme 1.5. Synthesis of *Quercus* Lactones via CuCl/bpy-Catalyzed ATRC

Copper(I) tris(pyrazolyl)borate (TpCu^{I}) complexes have also been successfully used as catalysts in ATRA reactions. An attractive feature of this type of compound is the ability to tune the catalytic activity of the resulting metal complexes by incorporating substituents with varying steric and electronic properties on the ligand framework. The most efficient TpCu^{I} catalysts reported so far are those with hindered as well as electron-donating Tp ligands such as $\text{Tp}^{\text{tBu,Me}}\text{Cu}(\text{NCCH}_3)$ and $\text{Tp}^{\text{tBu}}\text{Cu}(\text{NCCH}_3)$ **5** (Scheme 1.6), which resulted in nearly quantitative yields and conversions in the addition of CCl_4 , CHCl_3 , sulfonyl chlorides and ethyl trichloroacetate to styrene and methyl methacrylate under mild conditions (30°C).⁴⁵



Scheme 1.6. ATRA of CCl₄ to Alkenes Using Cu-based Catalyst with Different Tp Ligands

On the other hand, TpCu^I catalysts with electron-withdrawing substituents (e.g. Br) on the C3, C4, C5 positions of the pyrazole ring were found to be inactive in the ATRA of CCl₄ to alkene (methyl methacrylate, styrene, 1-hexene) even at elevated temperatures.⁴⁵ Additionally, these catalysts were not very efficient in ATRA reactions involving α -olefins such as 1-hexene, 1-octene, and 1-decene. Perez and coworkers proposed a mechanism wherein the activator Tp^xCu^I equilibrates with an 18 e⁻ Tp^xCu^IL in the presence of a relatively labile ligand such as acetonitrile (Scheme 1.7), which regulates the amounts of Tp^xCu^I available in the solution.^{45,103}



Scheme 1.7. Proposed Mechanism for ATRA Catalyzed by $\text{Tp}^{\text{X}}\text{Cu}^{\text{I}}$ Complexes^{45,103}

Similarly, varying the steric and electronic nature of the *N*-alkyl-2-pyridylmethanimines (NPMI) ligand (Figure 1.6) through substitution on the imine group and on the pyridine ring has shown to affect the observed rate in the copper-catalyzed ATRC of *N*-tosylallylacetamides.^{62,64,66} Substitution on the imine moiety with sterically demanding alkyl groups caused a significant decrease in the rate of ATRC.⁶⁴ Furthermore, introduction of electron-withdrawing groups, such as NO_2 , on the carbon β to the nitrogen atom on the pyridine ring also resulted in slower ATRC reactions.⁶²

Some iron and nickel complexes have also been shown to catalyze atom transfer radical processes.^{14,104-108} Pincer complexes of nickel(II) (depicted in Figure 1.7) are active homogenous catalysts for ATRA reactions using various polyhalogenated alkanes (e.g. CCl_4 , CBr_4 , CF_3CCl_3 , etc.) and a variety of alkenes (e.g. 1-octene, methyl methacrylate, styrene, etc.) under mild reactions conditions.¹⁴ Furthermore, solid-supported arylnickel catalysts, which are soluble in both polar and nonpolar solvents depending on the solid support, were shown to possess good catalytic activity.^{104,105}

Iron(II) chloride has also been successfully used in intramolecular chloroamination of unsaturated alkoxy carbonyl azides for the synthesis of substituted oxazolidinones.²⁴ The $\text{Fe}^0\text{-FeCl}_3$ catalyst system also promoted the addition of CCl_4 and methyl-2,2-dihalocarboxylates to alkenes.²⁵ Other non-transition metal catalysts, such as triethylborane, are also shown to be effective in aqueous ATRA reactions.^{109,110}

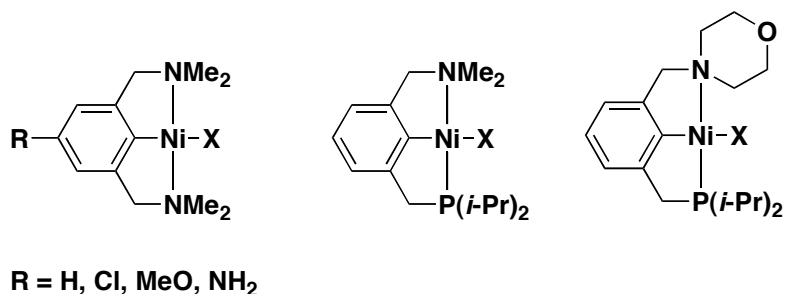


Figure 1.7. Examples of Pincer Complexes of Nickel Used as Catalysts in ATRA Reactions (X = Cl, Br)

1.4 “Greening” of Transition Metal Catalyzed Atom Transfer Radical Processes

Despite the successful use of transition metal catalysts in ATRA, the irreversible accumulation of the deactivator species (transition metal complex in the higher oxidation state) due to the unavoidable radical termination reactions necessitates the use of large amounts of the catalyst (as high as 30 mol% relative to alkene) in order to achieve high selectivity towards the desired target compound.¹¹¹ High metal concentration in the reactions requires additional purification of the final products, making it unsuitable for large scale syntheses and industrial applications. Over the years, various techniques have been developed in order to overcome these limitations. One such methodology is the use of solid-supported transition metal

catalysts which can be easily recovered from the reaction mixture and can also be recycled in subsequent reactions. Examples of solid-supported metal catalysts that have been successfully used in ATRA and ATRC processes include a silica-tethered Cu catalyst **1**, a carbosilane-supported arylnickel catalyst **2** and an amphilic resin-supported Ru complex **3** (Figure 1.8).^{65,67,104,105,112}

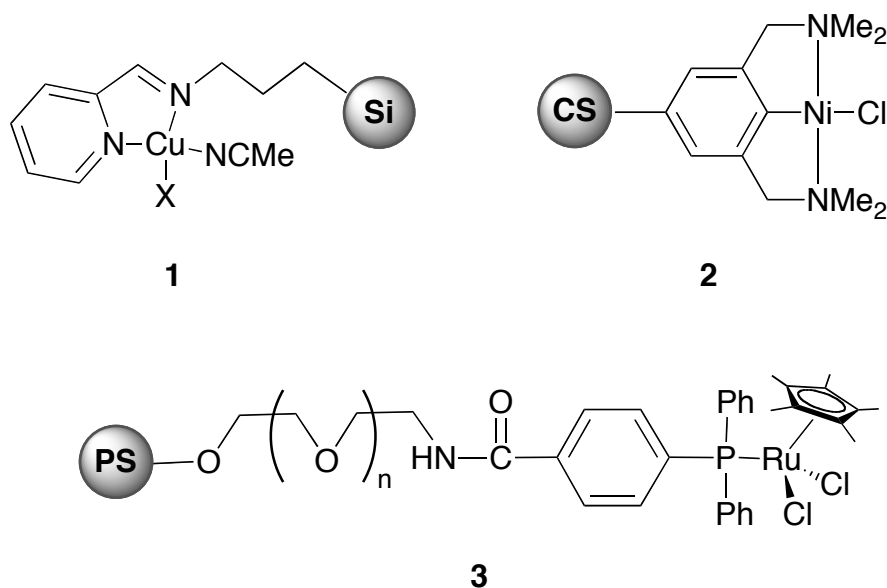


Figure 1.8. Solid-Supported Transition Metal Catalysts Used in Atom Transfer Radical Processes

Another technique that had been explored is the use of biphasic systems (usually a mixture of water or fluorosolvents and an organic solvent).^{106,113} In this method, highly fluorinated ligands (Figure 1.9) were complexed with metal centers, which allowed the catalyst to be soluble in water/fluorous solvent with the resulting products miscible only in the organic layer. Biphasic solvent systems become homogenous at elevated temperatures, which enables the reaction to be conducted

under single phase conditions. Product separation is then performed at lower temperatures under biphasic conditions.

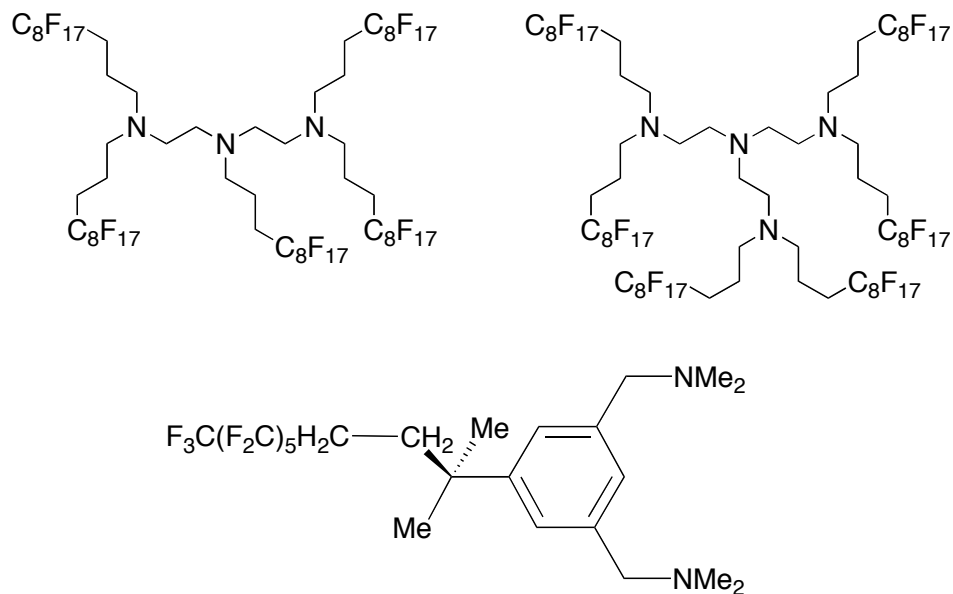
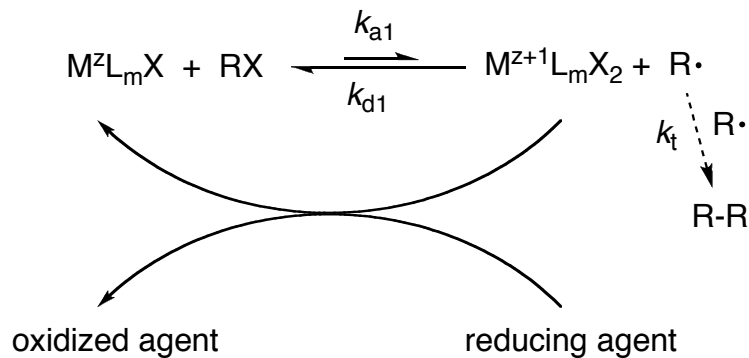
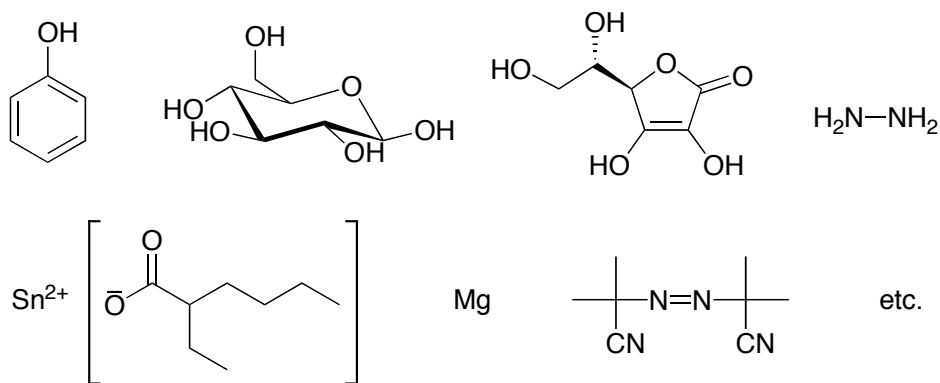


Figure 1.9. Perfluorous Ligands Commonly Used in Biphasic Systems

By far the most attractive technique in the “greening” of TMC atom transfer radical processes is catalyst regeneration using environmentally benign reducing agents, which has been originally found for copper catalyzed atom transfer radical polymerization (ATRP),^{111,114-117} and was subsequently applied first to ruthenium⁷⁷ and then copper^{76,118,119} catalyzed ATRA reactions.



Reducing Agents



Scheme 1.8. Catalyst Regeneration in ATRA in the Presence of Reducing Agents

In all of these processes, reducing agents such as phenols, glucose, ascorbic acid, hydrazine, tin(II) 2-ethylhexanoate, magnesium, and free radical initiators are utilized to reduce the higher oxidation state metal complex ($\text{M}^{\text{Z}+1}\text{L}_m\text{X}_2$) that is present as a persistent radical to the corresponding lower oxidation state activator species (Scheme 1.8). Such constant regeneration of the catalyst compensates for the unavoidable radical-radical termination reactions and, thus, dramatically reduced the amount of metal catalyst required for these processes.

Severin and other groups have successfully used $[\text{Ru}^{\text{III}}\text{Cl}_2\text{Cp}^*\text{PPh}_3]$ and its derivatives in atom transfer radical processes using AIBN or Mg as reducing agents with impressive yields and high turnover numbers (TON) using different substrate combinations.^{31,75,77,96,120} In the presence of AIBN, yields as high as 85% were obtained for CCl_4 and styrene using 0.005 mol% of the catalyst relative to alkene, which was a significant improvement from the 0.3 mol% required to achieve the same yields using $[\text{Ru}^{\text{II}}\text{ClCp}^*(\text{PPh}_3)_2]$ without AIBN.^{77,96} In the same manner, Ru-catalyzed ATRA of CCl_4 to styrene in the presence of Mg as reducing agent resulted in nearly quantitative yields of the monoadduct at an alkene-to-catalyst ratio of 5000:1.⁷⁵ The use of Mg led to higher monoadduct yields due to the suppression of the competing free radical polymerization, which is a common side reaction when free radical initiators are used as reducing agents. However, utilizing Mg is still less preferred because it required agitation under N_2 atmosphere for 10 days prior to use and it also increased the total metal concentration in the reaction system.

Reducing agents have also been successfully used for catalyst regeneration in Cu-catalyzed atom transfer radical processes. One of the best Cu catalysts described so far that was used in conjunction with AIBN was $[\text{Cu}^{\text{I}}(\text{TPMA})\text{X}]$ ($\text{X} = \text{Cl}, \text{Br}$).^{76,118} Turnover numbers (TONs) ranging between 4900-7200 (1-hexene) and 4350-6700 (1-octene) were obtained in the ATRA of CCl_4 catalyzed by $[\text{Cu}^{\text{I}}(\text{TPMA})\text{Cl}]$.¹¹⁸ In the case of styrene and methyl acrylate, lower yields (42-85% for styrene, 60% for methyl acrylate) were observed due to the competing free radical polymerization of these highly active alkenes.¹¹⁸ However, in the ATRA of CBr_4 to styrene and methyl acrylate using $[\text{Cu}^{\text{I}}(\text{TPMA})\text{Br}]/\text{AIBN}$ catalytic system, nearly quantitative monoadduct yields were

observed using as low as 5 ppm Cu catalyst, which was by far the lowest amount of catalyst used in transition metal-mediated ATRA.⁷⁶ Additionally, Cu-catalyzed ATRA reactions conducted at ambient temperature using a low temperature free radical initiator (2,2'-azobis(4-methoxy-2,4-dimethylvaleronitrile) or V70) also allowed the selective formation of monoadduct for highly active alkenes as a result of a decrease in the propagation rate.¹¹⁹

1.5 Kinetics of Transition Metal Catalyzed Atom Transfer Radical Processes

According to Scheme 1.3, the rate of monomer consumption in transition metal catalyzed ATRA in the absence of a reducing agent is given by the following expression:

$$-\frac{d[alkene]}{dt} = k_{add}[R\bullet][alkene] \quad (1.1)$$

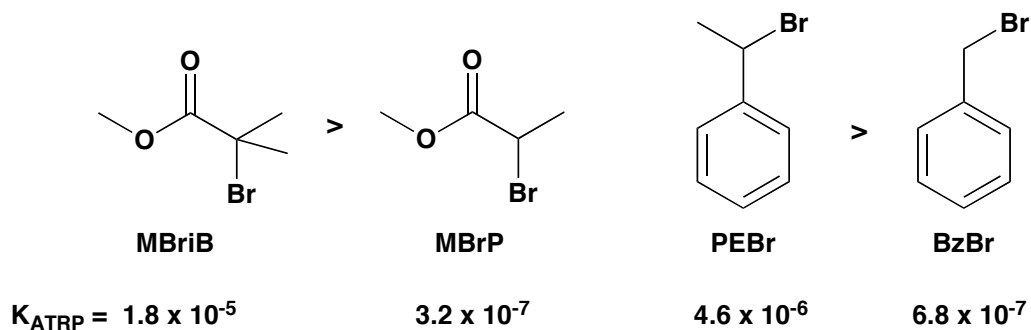
By ignoring radical termination reactions due to persistent radical effect, monoadduct activation (assuming $k_{a2} = 0$) and using a fast equilibrium approximation, the rate law can then be derived by substitution of the expression for the radical concentration ($[R\bullet]$) (Eq. 1.2) into Eq. 1.1:

$$[R\bullet] = \frac{k_{a1}[M^zL_mX][RX]}{k_{d1}[M^{z+1}L_mX_2]} \quad (1.2)$$

$$-\frac{d[alkene]}{dt} = \frac{k_{a1}k_{add}[M^zL_mX][RX][alkene]}{k_{d1}[M^{z+1}L_mX_2]} = \frac{K_{ATRA}k_{add}[M^zL_mX][RX][alkene]}{[M^{z+1}L_mX_2]}$$

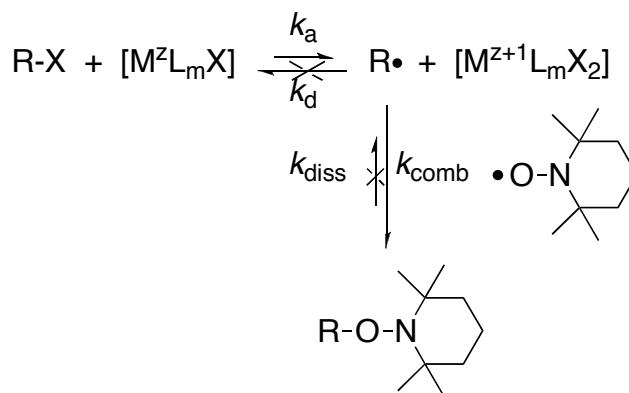
where $K_{\text{ATRA}} = k_{\text{a1}}/k_{\text{d1}}$. Hence, the rate of alkene consumption in TMC ATRA relies on the rate constant for the addition of the radical to the alkene (k_{add}), the equilibrium constant (K_{ATRA}), molar concentrations of alkyl halide (RX) and alkene, and the ratio of the concentrations of the activator (M^zL_mX) and the deactivator ($M^{z+1}L_mX_2$). A constant radical concentration in the system would allow for the determination of the apparent rate constant from the pseudo-first order kinetic plot of the alkene consumption as a function of time.

The success of atom transfer radical addition lies on the reversible activation-deactivation process, wherein a dynamic equilibrium exists between the dormant species (R-X) and the active carboradical species (R•). The position of the equilibrium between the dormant and active species (established by the equilibrium constant K_{ATRA}) is strongly affected by the complexing ligand on the metal center, halogen and the nature and structure of the alkyl groups. For instance, in the mechanistically similar ATRP, the relative activity of the catalyst bearing N-based ligands (based on the K_{ATRP} values) increased in the order bpy (1) < PMDETA (20) < TPMA (2500) < Me₆TREN (40 000) for EtBriB (ethyl-2-bromoisobutyrate).^{121,122} Additionally, the order of the reactivity of the alkyl halides is as follows: tertiary > secondary > primary, which is demonstrated in the relative K_{ATRP} values between MBriB (methyl-2-bromoisobutyrate) and MBrP (methyl-2-bromopropionate) and also between PEBr (1-(bromoethyl)benzene) and (BzBr) benzyl bromide (Scheme 1.9).^{121,122} Lastly, K_{ATRP} values of alkyl bromides are 6 to 10 times larger than their Cl-based counterparts.^{121,122}



Scheme 1.9. Relative K_{ATRP} Values of Various Alkyl Halides

Prior to the development of analytical solution of the persistent radical effect for TMC ATRA and ATRP, K_{ATRP} values were typically estimated by independently measuring the activation (k_a) and deactivation (k_d) rate constants. Activation rate constants are typically determined from model studies (Scheme 1.10) in which the activation process is kinetically isolated from the deactivation step by trapping the generated radical with a radical scavenger, such as TEMPO.¹²³⁻¹²⁶ Addition of a large



Scheme 1.10. Model Reaction for Activation Rate Constant Measurement

excess of the $[M^Z L_m X]$ complex with respect to R-X provides first-order kinetic conditions and the disappearance of R-X can be monitored over time to determine the activation rate constant, as given in the expression below.

$$-\frac{d[R-X]}{dt} = k_{act}[M^Z L_m X][R-X] = k_{obs}[R-X]$$

Activation rate constants were found to depend on the structures of the complexing ligand, alkyl halide, solvent and temperature.¹²⁷⁻¹³⁰ For instance, in a study on the activation rate constants of 1-phenylethylbromide (PEBr) and 1-phenylethylchloride (PECl) with CuBr/CuCl, k_a values for PEBr were larger than that for PECl, indicating that the C-Br bond was easily cleaved compared to the C-Cl bond (Table 1.2).¹²⁴ Also, the presence of an α -methyl substituent increased the k_a value, as evident in the k_a values for PEBr compared to that for benzyl bromide (BzBr).

In a separate study, Matyjaszewski *et al.* reported that mixed halogen systems (RBr/Cu^ICl) provides better control in polymerization than homo-halogen systems (RBr/Cu^IBr) due to an increase in the rate of initiation relative to the rate of propagation.¹³¹ As evident in Table 1.2, the k_a for the PEBr/CuCl system is slightly

Table 1.2. Activation Rate Constants (k_a) for Various ATRP Initiators with CuBr/CuCl¹²⁴

Initiator	Cu Catalyst	k_a (M ⁻¹ s ⁻¹)
PEBr	CuBr	0.42
PEBr	CuCl	0.52
PECl	CuCl	0.018
PECl	CuBr	0.010
BzBr	CuBr	0.18

larger than that for PEBr/CuBr, since PECl, which has a stronger carbon-halogen bond than PEBr, is preferentially formed.¹²⁴ For the same reason, the PECl/CuBr system exhibited a smaller activation rate constant than PECl/CuCl.¹²⁴

The activities of the Cu^I complexes based on their complexing ligand generally follows the order: tetradentate (cyclic-bridged) > tetradentate (branched) > tetradentate (cyclic) > tridentate > tetradentate (linear) > bidentate ligands (Figure 1.10).¹²⁷ The nature of N atoms also affected the k_a values and follows the order pyridine \geq aliphatic amine > imine.¹²⁷ The activation rate constants are also influenced by the degree of substitution of the alkyl halide, which typically follow the order of 3° > 2° > 1° and by the radical stabilizing group in the order of phenyl ester > cyanide > ester > benzyl > amide (Figure 1.11). The activity of the leaving atom/group for the alkyl halide decreases in the order of I \geq Br > Cl >> SCN \approx NCS (Figure 1.11).¹²⁸

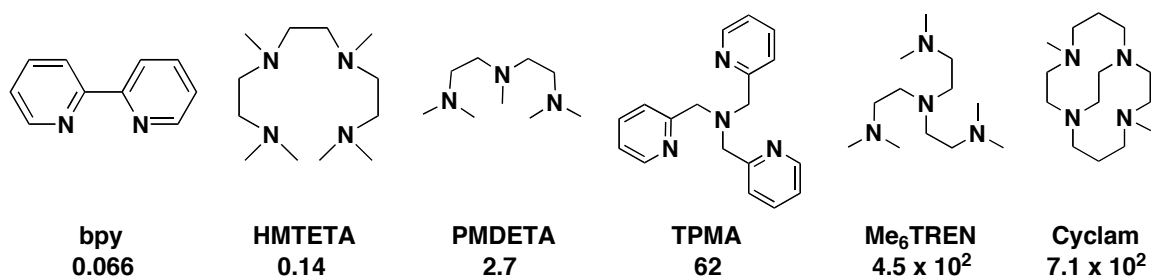
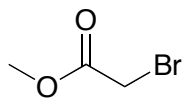


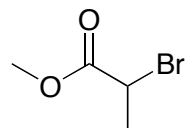
Figure 1.10. Values of k_a ($M^{-1}s^{-1}$) in ATRP for Various Complexing Ligands with EtBriB (ethyl-2-bromoisobutyrate) Measured in CH_3CN at 35°C¹²⁷

Studies on the deactivation rate constants (k_d) are much less common due to the lack of experimental techniques for measuring fast deactivation process, which is typically in the order of 10^8 - 10^9 $M^{-1}s^{-1}$.¹²² In one of the earlier studies, deactivation rate

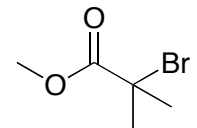
Degree of Substitution



0.030

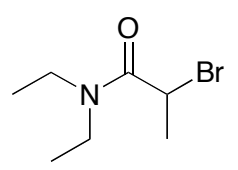


0.33

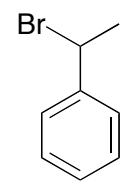


2.6

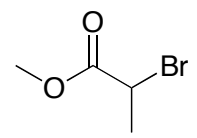
Radical Stabilizing Group



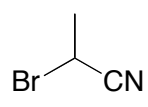
0.040



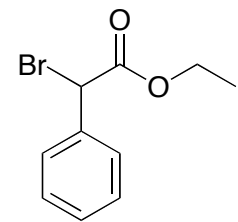
0.17



0.33

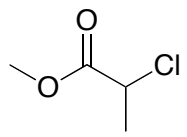


23

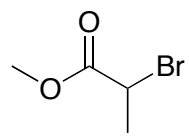


5.3 x 10³

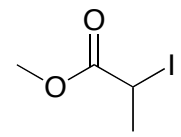
Leaving Atom



0.015



0.33

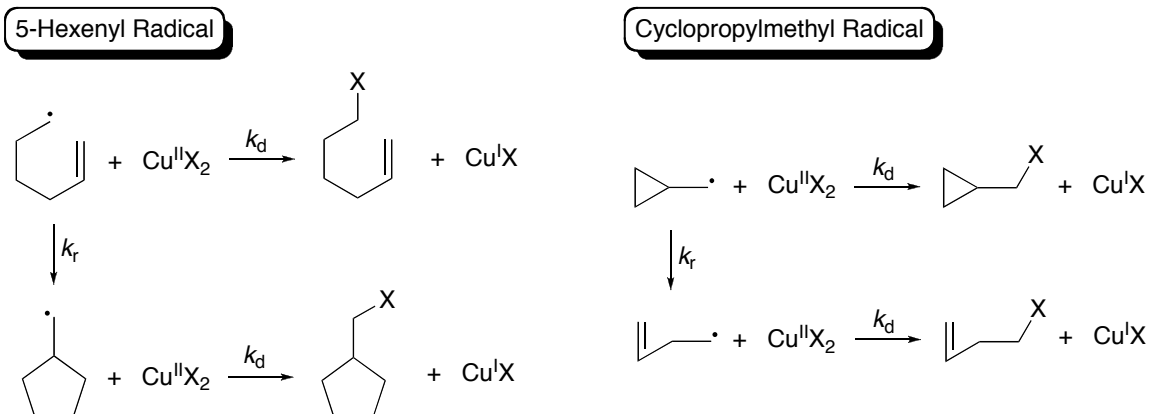


53

Figure 1.11. Values of k_a ($M^{-1}s^{-1}$) in ATRA/ATRP for Various Alkyl Halides with $Cu^I X/PMDETA$ ($X = Cl, Br, I$) Measured in CH_3CN at $35^\circ C$ ¹²⁸

constants for 5-hexenyl and cyclopropylmethyl radicals in the presence of copper halides and pseudohalides were determined by taking into account the known rates of radical rearrangement that are available in literature⁵⁷ (Scheme 1.11).¹³²⁻¹³⁴ By assuming that the k_d values for both isomers of the radical to be approximately the same and that the isomerization is irreversible, the deactivation rate constant can be determined from Eq.

1.3.



Scheme 1.11. Isomerization and Deactivation of 5-Hexenyl and Cyclopropylmethyl Radicals in the Presence of Cu^{II} Halides and Pseudohalides¹³²⁻¹³⁴

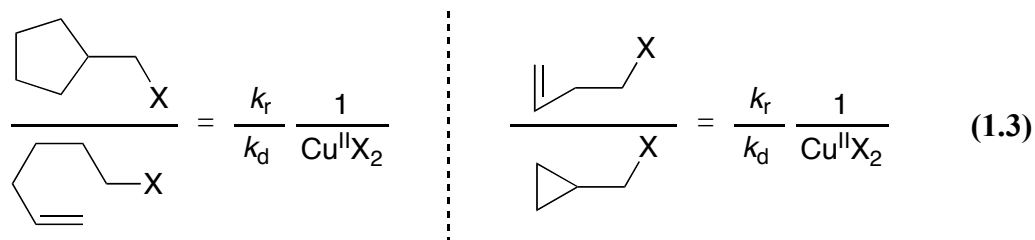


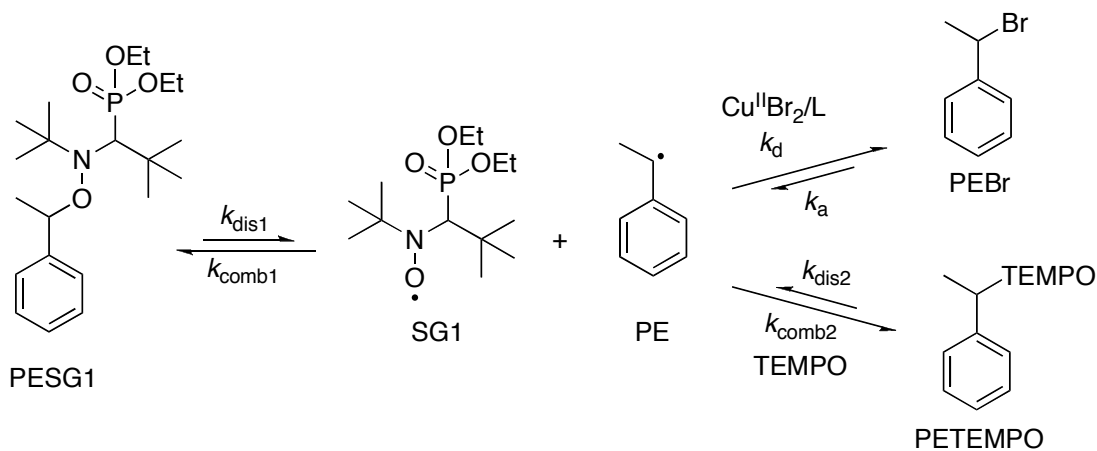
Table 1.3. Rate Constants of Deactivation (k_d) of 5-Hexenyl and Cyclopropylmethyl Radical by Cu^{II} Halides and Pseudohalides in CH₃CN at 25°C¹³²⁻¹³⁴

Radical	Cu ^{II} Catalyst ^a	k_r/k_d ^b	k_d (M ⁻¹ s ⁻¹)
5-hexenyl	CuBr ₂	4.0×10^{-4}	2.0×10^8
5-hexenyl	CuCl ₂	4.0×10^{-4}	2.0×10^8
5-hexenyl	Cu(NCS) ₂	3.9×10^{-4}	2.6×10^8
cyclopropylmethyl	CuBr ₂	2.3×10^{-2}	4.3×10^9
cyclopropylmethyl	CuCl ₂	9.2×10^{-2}	1.1×10^9
cyclopropylmethyl	Cu(NCS) ₂	2.7×10^{-1}	3.6×10^8

^a[Cu^{II}X₂]₀ = 1.0M. ^b k_r (5-hexenyl radicals) = $1.0 \times 10^5 \text{ s}^{-1}$ and k_r (cyclopropylmethyl radicals) = $1.0 \times 10^5 \text{ s}^{-1}$ ⁵⁷

As shown in Table 1.3, the relatively large k_d values indicates that the deactivation of the 5-hexenyl and cyclopropylmethyl radicals occurred through an atom rather than an electron transfer process, which is consistent with the proposed mechanism for TMC ATRA shown in Scheme 1.3.

Determination of the deactivation rate constants were also performed in mechanistically similar ATRP using a competitive kinetic experiment with formation of a TEMPO adduct in a clock reaction, as shown in Scheme 1.12.¹²³ However, this can only be applied to model reaction systems and can be difficult for reactions with relatively low deactivation rate constants, i.e. radical coupling with TEMPO is much faster than the trapping of radical by Cu^{II} . Activation and deactivation rate constant measurements in copper-catalyzed ATRA reactions are further discussed in Chapter 4.



Scheme 1.12. Model Reaction for Deactivation Rate Constant Measurements¹²³

1.6 Project Overview

This dissertation is organized as follows. In Chapter 2, the effects of the concentrations of the catalyst, alkyl halide, and reducing agent on the ATRA of CCl_4 to 1-octene, styrene, and methyl acrylate are reported. Additional experiments involving less active alkyl halides, such as chloroform, benzyl chloride and benzyl bromide are presented in order to further investigate the effect of alkyl halide concentration. Kinetic studies on the effect of the concentration and nature of the catalyst and the concentration of the reducing agent on the observed reaction rate are discussed in Chapter 3. The reduction of Cu^{II} in the presence of AIBN was also probed in UV-Vis experiments on model systems containing only the Cu^{II} catalyst and AIBN and the results are also discussed in Chapter 3.

In Chapter 4, the activation ($k_{\text{a,AIBN}}$) and deactivation ($k_{\text{d,AIBN}}$) rate constants are determined using both experimental and theoretical techniques. Kinetic modeling was also performed in order to demonstrate the effect of $k_{\text{a,AIBN}}$ and $k_{\text{d,AIBN}}$ as well as the concentration of AIBN and its rate of decomposition on the concentrations of Cu^{I} and Cu^{II} at ATRA equilibrium. Various low temperature ATRA and ATRC experiments using a V70 as reducing agent and employing UV-irradiation to photochemically decompose AIBN are discussed in Chapter 5.

Chapter 6 details free radical cyclization and atom transfer radical cyclization experiments in the presence of a copper catalyst. In particular, the effect of the catalyst on the regioselectivity of the cyclization is investigated. Theoretical analysis on the role of thermodynamic factors on product selectivity is also presented.

References

- (1) Kharasch, M. S.; Engelmann, H.; Mayo, F. R. The peroxide effect in the addition of reagents to unsaturated compounds. XV. The addition of hydrogen bromide to 1- and 2-bromo- and chloropropenes. *J. Org. Chem.* **1937**, *2*, 288-302.
- (2) Kharasch, M. S.; Jensen, E. V.; Urry, W. H. Addition of carbon tetrachloride and chloroform to olefins. *Science.* **1945**, *102*, 128.
- (3) Kharasch, M. S.; Jensen, E. V.; Urry, W. H. Addition of derivatives of chlorinated acetic acids to olefins. *J. Am. Chem. Soc.* **1945**, *67*, 1626.
- (4) Kharasch, M. S.; Potts, W. M. The peroxide effect in the addition of hydrogen bromide to ethylene compounds. XIV. The addition of hydrogen bromide to higher alkenes. *J. Org. Chem.* **1937**, *2*, 195-197.
- (5) Kharasch, M. S.; Rossin, E. H.; Fields, E. K. The Peroxide Effect in the Addition of Halogen Acids to Olefins. XXVI. The Addition of Halogen Acids to Trichloromethylethylene. *J. Am. Chem. Soc.* **1941**, *63*, 2558-2560.
- (6) Odian, G., *Principles of Polymerization*, 4th ed., Wiley, New York, **2004**.
- (7) De Malde, M.; Minisci, F.; Pallini, U.; Volterra, E.; Quilico, A. Reactions between Acrylonitriles and Aliphatic Halogen Derivatives. *Chim. Ind. (Milan)*. **1956**, *38*, 371-382.
- (8) Minisci, F. Radical reactions in solution. Dipolar character of free radicals from decomposition of organic peroxides. *Gazz. Chim. Ital.* **1961**, *91*, 386-389.
- (9) Minisci, F. Free-radical addition to olefins in the presence of redox systems. *Acc. Chem. Res.* **1975**, *8*, 165-171.
- (10) Minisci, F.; Galli, R. Influence of the electrophilic character on the reactivity of free radicals in solution. Reactivity of alkoxy, hydroxy, alkyl, and azido radicals in the presence of olefins. *Tetrahedron Lett.* **1962**, 533-538.
- (11) Minisci, F.; Galli, R. Addition of N-chloroamines to styrene and butadiene, catalyzed by iron and copper salts. *Chim. Ind. (Milan)*. **1963**, *45(11)*, 1400-1401.

- (12) Minisci, F.; Pallini, U. Radical reactions in solution. Haloalkylation of acrylic acid derivatives. *Gazz. Chim. Ital.* **1961**, *91*, 1030-1036.
- (13) Iqbal, J.; Bhatia, B.; Nayyar, K. Transition Metal-Promoted Free-Radical Reactions in Organic Synthesis: The Formation of Carbon-Carbon Bonds. *Chem. Rev.* **1994**, *94*, 519-564.
- (14) Gossage, R. A.; van de Kuil, L. A.; van Koten, G. Diaminoarylnickel(II) "Pincer" Complexes: Mechanistic Considerations in the Kharasch Addition Reaction, Controlled Polymerization, and Dendrimeric Transition Metal Catalysts. *Acc. Chem. Res.* **1998**, *31*, 423-431.
- (15) Clark, A. J. Atom transfer radical cyclisation reactions mediated by copper complexes. *Chem. Soc. Rev.* **2002**, *31*, 1-11.
- (16) Nagashima, H., *Ruthenium in Organic Synthesis*, ed. S.-I. Murahashi. Wiley-VCH, Weinheim, Germany, **2004**.
- (17) Delaude, L.; Demonceau, A.; Noels, A. F., In *Topics in Organometallic Chemistry*, C. Bruneau and P.H. Dixneuf, Editors. **2004**, Springer: Berlin, Germany. p. 155-171.
- (18) Severin, K. Ruthenium catalysts for the Kharasch reaction. *Curr. Org. Chem.* **2006**, *10*(2), 217-224.
- (19) Hajek, M.; Silhavy, P.; Malek, J. Free Radical Addition Reactions Initiated by Metal Oxides. XI. Metal-Oxide Induced Redox Chain Addition of Tetrachloromethane to a Carbon-Carbon Double Bond. *Collection Czechoslov. Chem. Commun.* **1980**, *45*, 3488-3501.
- (20) Hajek, M.; Silhavy, P.; Malek, J. Free Radical Addition Reactions Initiated by Metal Oxides. XII. Catalytic Activity of Copper Oxides and Chlorides in the Redox Chain Addition of Tetrachloromethane to Styrene. *Collection Czechoslov. Chem. Commun.* **1980**, *45*, 3502-3509.
- (21) Steiner, E.; Martin, P.; Bellius, D. Metal-Catalyzed Radical Addition of Polyhalogenated Compounds to Olefins. Part 2. A New Simple Synthesis of 2,3,5-Trichloropyridine. *Helv. Chim. Acta.* **1982**, *65*, 983-985.

- (22) Metzger, J. O.; Mahler, R. Radical Additions of Activated Haloalkanes to Alkenes Initiated by Electron Transfer from Copper in Solvent-Free Systems. *Angew. Chem. Int. Ed.* **1995**, *34*, 902-904.
- (23) Bellesia, F.; Forti, L.; Ghelfi, F.; Pagnoni, U. M. The Fe⁰ Promoted Addition of CCl₄ and CCl₃Br to Olefins. *Synth. Commun.* **1997**, *27*, 961-971.
- (24) Forti, L.; Ghelfi, F.; Libertini, E.; Pagnoni, U. M.; Soragni, E. Halogen Atom Transfer Radical Addition of α -Polychloroesters to Olefins Promoted by Fe⁰ Filings. *Tetrahedron.* **1997**, *53*(52), 17761-17768.
- (25) Forti, L.; Ghelfi, F.; Pagnoni, U. M. Fe⁰ Initiated Halogen Atom Transfer Radical Addition of Methyl 2-Br-2-Cl-Carboxylates to Olefins. *Tetrahedron Letters.* **1996**, *37*(12), 2077-2078.
- (26) Caronna, T.; Citterio, A.; Ghirardini, M.; Minisci, F. Nucleophilic character of alkyl radicals—XIII: Absolute rate constants for the addition of alkyl radicals to acrylonitrile and methyl acrylate. *Tetrahedron.* **1977**, *33*, 793-796.
- (27) Baban, J. A.; Roberts, B. P. An electron spin resonance study of alkyl radical addition to diethyl vinylphosphonate. *J. Chem. Soc., Perkin Trans. 2.* **1981**, *1*, 161-166.
- (28) Miniotte, H. G.; Hubert, A. J.; Teyssie, P. The Role of Copper(I) Complexes in the Selective Formation of Oxazoles from Unsaturated Nitriles and Diazoesters. *J. Organomet. Chem.* **1975**, *88*, 115-120.
- (29) Julia, M.; Thuillier, G. I.; Saussine, L. Additions D'Chloronitriles sur les Olefines par Catalyse Redox. *J. Organomet. Chem.* **1979**, *177*, 211-220.
- (30) Murai, S.; Sonoda, N.; Tsutsumi, S. Copper Salts Induced Addition of Ethyl Trichloroacetate to Olefins. *J. Org. Chem.* **1964**, *31*, 3000-3003.
- (31) Fernandez-Zumel, M. A.; Thommes, K.; Kiefer, G.; Sienkiewicz, A.; Pierzchala, K.; Severin, K. Atom-Transfer Radical Addition Reactions Catalyzed by RuCp* Complexes: A Mechanistic Study. *Chem. Eur. J.* **2009**, *15*(43), 11601-11607.
- (32) Steiner, E.; Martin, P.; Bellius, D. Metal-Catalyzed Radical Addition of Polyhalogenated Compounds to Olefins. Part 2. A New Simple Synthesis of 2,3,5-Trichloropyridine. *Helv. Chim. Acta.* **1982**, *65*, 983-985.

- (33) Pierre, M.; Eginhard, S.; Streith, J.; Winkler, T.; Bellius, D. Metal-Catalyzed Addition of Organic Polyhalides to Olefins. 4. Convenient Approaches to Heterocycles via Copper-Catalyzed Additions of Organic Polyhalides to Activated Olefins. *Tetrahedron*. **1985**, *41*, 4057-4078.
- (34) Bellius, D. Copper-Catalyzed Addition of Polyhalides to Olefins: a Versatile Synthetic Tool. *Pure Appl. Chem.* **1985**, *57*, 1827-1838.
- (35) Asscher, M.; Vofsi, D. Chlorine activation by redox-transfer. Part I. The reaction between aliphatic amines and carbon tetrachloride. *J. Chem. Soc.* **1961**, 2261-2264.
- (36) Sinnreich, J.; Asscher, M. Redox-transfer. Part VII. Addition of ethylene and butadiene to functionally substituted aromatic sulphonyl chlorides. *J. Chem. Soc., Perkin Trans. 1*. **1972**, *1*, 1543-1545.
- (37) Kamigata, N.; Sawada, H.; Kobayashi, M. Reactions of arenesulfonyl chlorides with olefins catalyzed by ruthenium(II) complex. *J. Org. Chem.* **1983**, *48*, 3793-3796.
- (38) Truce, W. E.; Wolf, G. C. Adducts of sulfonyl iodides with acetylenes. *J. Org. Chem.* **1971**, *36*, 1727-1732.
- (39) Block, E.; Aslam, M.; Eswarakrishnan, V.; Gebreyes, K.; Hutchinson, J.; Iyer, R. S.; Laffitte, J. A. α -Haloalkanesulfonyl Bromides in Organic Synthesis. 5. Versatile Reagents for the Synthesis of Conjugated Polyenes, Enones, and 1,3-Oxathiole 1,1-Dioxides. *J. Am. Chem. Soc.* **1986**, *108*, 4568-4580.
- (40) Amiel, Y. The thermal and the copper-catalyzed addition of sulfonyl bromides to phenylacetylene. *J. Org. Chem.* **1974**, *39*, 3867-3870.
- (41) Freidlina, R. K.; Velichko, F. K. Synthetic applications of homolytic addition and telomerization reactions of bromine-containing addends with unsaturated compounds containing electron-withdrawing substituents. *Synthesis*. **1977**, *3*, 145-154.
- (42) Julia, M.; Sasussine, L.; Thuillier, G. I. Addition du chloracetate de methyle sur les olefines. *J. Organomet. Chem.* **1979**, *174*, 359-366.
- (43) Curran, D. P., *Comprehensive Organic Synthesis*. Pergamon, New York, **1992**.

- (44) De Campo, F.; Lastecoueres, D.; Verlhac, J.-B. New copper(I) and iron(II) complexes for atom transfer radical macrocyclisation reactions. *J. Chem. Soc., Perkin Trans.* **2000**, *1*, 575-580.
- (45) Munoz-Molina, J. M.; Caballero, A.; Diaz-Requejo, M. M.; Trofimenko, S.; Belderrain, T. R.; Perez, P. J. Copper-Homoscorpionate Complexes as Active Catalysts for Atom Transfer Radical Addition to Olefins. *Inorg. Chem.* **2007**, *46*(19), 7725-7730.
- (46) Clark, A. J.; Battle, G. M.; Bridge, A. Efficient β -lactam synthesis via 4-exo atom transfer radical cyclisation using CuBr(tripyrindylamine) complex. *Tetrahedron Letters.* **2001**, *42*, 4409-4412.
- (47) Ghelfi, F.; Roncaglia, F.; Pattarozzi, M.; Giangiordano, V.; Petrillo, G.; Sancassan, F.; Parsons, A. F. Atom transfer radical cyclization of *O*-allyl-2,2-dichlorohemiacetal acetates: an expedient method to dichloro- γ -lactones. *Tetrahedron.* **2009**, *65*, 10323-10333.
- (48) Wetter, C.; Studer, A. Microwave-assisted free radical chemistry using the persistent radical effect. *Chem. Commun.* **2004**, 174-174.
- (49) Iwamatsu, S. I.; Matsubara, K.; Nagashima, H. Synthetic Studies of *cis*-3a-Aryloctahydroindole Derivatives by Copper-Catalyzed Cyclization of *N*-Allyltrichloroacetamides: Facile Construction of Benzylic Quaternary Carbons by Carbon-Carbon Bond-Forming Reactions. *J. Org. Chem.* **1999**, *64*, 9625-9631.
- (50) Yoshimitsu, T.; Nakajima, H.; Nagaoka, H. Synthesis of the CD ring system of paclitaxel by atom-transfer radical annulation reaction. *Tetrahedron Lett.* **2002**, *43*, 8587-8590.
- (51) Yanada, R.; Koh, Y.; Nishimori, N.; Matsumara, A.; Obika, S.; Mitsuya, H.; Fujii, N.; Takemoto, Y. Indium-Mediated Atom-Transfer and Reductive Radical Cyclizations of Iodoalkynes: Synthesis and Biological Evaluation of HIV-Protease Inhibitors. *J. Org. Chem.* **2004**, *69*, 2417-2422.
- (52) Stevens, C. V.; Meenen, E. V.; Eeckhout, Y.; Vanderhoydonck, B.; Hooghe, W. Synthesis of highly functionalized spiro-indoles by a halogen atom transfer radical cyclization. *Chem. Commun.* **2005**, 4827-4829.

- (53) Fischer, H.; Radom, L. Factors Controlling the Addition of Carbon-Centered Radicals to Alkenes – An Experimental and Theoretical Perspective. *Angew. Chem. Int. Ed.* **2001**, *40*, 1340-1371.
- (54) Fischer, H.; Radom, L. Factors Controlling the Addition of Carbon-Centered Radicals to Alkenes. *Macromol. Symp.* **2002**, *182*, 1-14.
- (55) Lalevée, J.; Allonas, X.; Fouassier, J.-P. Addition of Carbon-Centered Radicals to Double Bonds: Influence of the Alkene Structure. *J. Org. Chem.* **2005**, *70*, 814-819.
- (56) Parsons, A. F., *An Introduction to Free Radical Chemistry*. Blackwell Science Ltd., Oxford, UK, **2000**.
- (57) Togo, H., *Advanced Free Radical Reactions for Organic Synthesis*. Elsevier, Oxford, UK, **2004**.
- (58) Gilbert, B. C.; Kalz, W.; Lindsay, C. I.; McGrail, P. T.; Parsons, A. F.; Whittaker, D. T. E. Initiation of radical cyclisation reactions using dimanganese decacarbonyl. A flexible approach to preparing 5-membered rings. *J. Chem. Soc., Perkin Trans. 1.* **2000**, 1187-1194.
- (59) Huther, N.; McGrail, P. T.; Parsons, A. F. Radical Reactions Using Decacarbonyldimanganese under Biphasic Conditions. *Eur. J. Org. Chem.* **2004**, 1740-1749.
- (60) Nakamura, T.; Yorimitsu, H.; Shinokubo, H.; Oshima, K. Triethylborane-Induced Radical Addition of Halogenated Compounds to Alkenes and Alkynes in Water. *Synlett.* **1998**, 1351-1352.
- (61) Diaz-Alvarez, A. E.; Crochet, P.; Zablocka, M.; Duhayon, C.; Cadierno, V.; Majoral, J. P. Developing the Kharasch Reaction in Aqueous Media: Dinuclear Group 8 and 9 Catalysts Containing the Bridging Cage Ligand Tris(1,2-dimethylhydrazino)diphosphane. *Eur. J. Inorg. Chem.* **2008**, 786-794.
- (62) Clark, A. J.; Battle, G. M.; Heming, A. M.; Haddleton, D. M.; Bridge, A. Ligand electronic effects on rate of copper mediated atom transfer radical cyclisation and polymerisation. *Tetrahedron Lett.* **2001**, *42*, 2003-2005.

- (63) Clark, A. J.; Dell, C. P.; Ellard, J. M.; Hunt, N. A.; McDonagh, J. P. Efficient room temperature copper(I) mediated 5-endo radical cyclisations. *Tetrahedron Letters*. **1999**, *40*(49), 8619-8623.
- (64) Clark, A. J.; Duncalf, D. J.; Filik, R. P.; Haddleton, D. M.; Thomas, G. H.; Wongtap, H. N-Alkyl-2-pyridylmethanimines as Tuneable Alternatives to Bipyridine Ligands as Copper Mediated Atom Transfer Radical Cyclisation. *Tetrahedron Lett.* **1999**, *40*, 3807-3810.
- (65) Clark, A. J.; Filik, R. P.; Haddleton, D. M.; Radigue, A.; Sanders, C. J.; Thomas, G. H.; Smith, M. E. Solid-Supported Catalysts for Atom-Transfer Radical Cyclization of 2-Haloacetamides. *J. Org. Chem.* **1999**, *64*, 8954-8957.
- (66) Clark, A. J.; Filik, R. P.; Thomas, G. H. Ligand Geometry Effects in Copper Mediated Atom Transfer Radical Cyclisations. *Tetrahedron Letters*. **1999**, *40*, 4885-4888.
- (67) Clark, A. J.; Geden, J. V.; Thom, S. Solid-Supported Copper Catalysts for Atom-Transfer Radical Cyclizations: Assessment of Support Type and Ligand Structure on Catalyst Performance in the Synthesis of Nitrogen Heterocycles. *J. Org. Chem.* **2006**, *71*(4), 1471-1479.
- (68) Clark, A. J.; Wilson, P. Copper mediated atom transfer radical cyclisations with AIBN. *Tetrahedron Letters*. **2008**, *49*, 4848-4850.
- (69) Bull, J. A.; Hutchings, M. G.; Lujan, C.; Quayle, P. New reactivity patterns of copper(I) and other transition metal NHC complexes: application to ATRC and related reactions. *Tetrahedron Letters*. **2008**, *49*, 1352-1356.
- (70) Edlin, C.; Faulkner, J.; Helliwell, M.; Knight, C. K.; Parker, J.; Quayle, P.; Raftery, J. Atom transfer radical cyclization reactions (ATRC): synthetic applications. *Tetrahedron*. **2006**, *62*, 3004-3015.
- (71) Felluga, F.; Forzato, C.; Ghelfi, F.; Nitti, P.; Pitacco, G.; Pagnoni, U. M.; Roncaglia, F. Atom transfer radical cyclization (ATRC) applied to a chemoenzymatic synthesis of Quercus lactones. *Tetrahedron: Assymetry*. **2007**, *18*, 527-536.
- (72) Seigal, B. A.; Fajardo, C.; Snapper, M. L. Tandem Catalysis: Generating Multiple Contiguous Carbon-Carbon Bonds through a Ruthenium-Catalyzed Ring-Closing Metathesis/Kharasch Addition. *J. Am. Chem. Soc.* **2005**, *127*, 16329-16332.

- (73) Nagashima, H.; Seki, K.; Ozaki, N.; Wakamatsu, H.; Itoh, K.; Tomo, Y.; Tsuji, J. Transition-Metal-Catalyzed Radical Cyclization: Copper-Catalyzed Cyclization of Allyl Trichloroacetates to Trichlorinated γ -Lactones. *J. Org. Chem.* **1990**, *55*, 985-990.
- (74) Yang, D.; Yan, Y.; Zheng, B.; Gao, Q.; Zhu, N. Copper(I)-Catalyzed Chlorine Atom Transfer Radical Cyclization Reactions of Unsaturated α -Chloro β -Keto Esters. *Organic Letters*. **2006**, *8*, 5757-5760.
- (75) Thommes, K.; Icli, B.; Scopelliti, R.; Severin, K. Atom-Transfer Radical Addition (ATRA) and Cyclization (ATRC) Reactions Catalyzed by a Mixture of [RuCl₂Cp*(PPh₃)] and Magnesium. *Chem. Eur. J.* **2007**, *13*, 6899-6907.
- (76) Eckenhoff, W. T.; Garrity, S. T.; Pintauer, T. Highly Efficient Copper-Mediated Atom-Transfer Radical Addition (ATRA) in the Presence of Reducing Agent. *Eur. J. Inorg. Chem.* **2008**(4), 563-571.
- (77) Quebatte, L.; Thommes, K.; Severin, K. Highly Efficient Atom Transfer Radical Addition Reactions with a Ru^{III} Complex as a Catalyst Precursor. *J. Am. Chem. Soc.* **2006**, *128*, 7440-7441.
- (78) Simal, F.; Wlodarczak, L.; Demonceau, A.; Noels, A. F. Highly efficient Kharasch addition catalysed by RuCl(Cp*)(PPh₃)₂. *Tetrahedron Letters*. **2000**, *41*(32), 6071-6074.
- (79) Simal, F.; Wlodarczak, L.; Demonceau, A.; Noels, A. F. New, Highly Efficient Catalyst Precursors for Kharasch Additions – [RuCl(Cp*)(PPh₃)₂] and [RuCl(Ind)(PPh₃)₂]. *Eur. J. Org. Chem.* **2001**, 2689-2695.
- (80) Matyjaszewski, K.; Davis, T. P., eds. *Handbook of Radical Polymerization*. 2002, John Wiley and Sons, Inc.: Hoboken.
- (81) Matsumoto, H.; Nakano, T.; Nagai, Y. Radical reactions in the coordination sphere I. Addition of carbon tetrachloride and chloroform to 1-olefins catalyzed by ruthenium(II) complexes. *Tetrahedron Lett.* **1973**, *14*(51), 5147-5150.
- (82) Lee, B. T.; Schrader, T. O.; Martin-Matute, B.; Kauffman, C. R.; Zhang, P.; Snapper, M. L. (PCy₃)₂Cl₂Ru=CHPh Catalyzed Kharasch additions. Application in a formal olefin carbonylation. *Tetrahedron*. **2004**, *60*, 7391-7396.

- (83) Richel, A.; Delfosse, S.; Cremasco, C.; Delaude, L.; Demonceau, A.; Noels, A. F. Ruthenium catalysts bearing N-heterocyclic carbene ligands in atom transfer radical reactions. *2003*, *44*, 6011-6015.
- (84) Richel, A.; Demonceau, A.; Noels, A. F. Electrochemistry as a correlation tool with the catalytic activities in [Ru(Cl₂(p-cymene)(PAr₃)]-catalyzed Kharasch additions. *Tetrahedron Lett.* **2006**, *47*, 2077-2081.
- (85) De Clercq, B.; Verpoort, F. Kharasch addition and vinylation reactions mediated by ruthenium(II) complexes bearing Schiff base ligands. *Catalysis Letters.* **2002**, *83*(1-2), 9-13.
- (86) Motoyama, Y.; Hanada, S.; Niibayashi, S.; Shimamoto, K.; Takaoka, N.; Nagashima, H. Atom-transfer radical reactions catalyzed by a coordinatively unsaturated diruthenium amidate, $[(\eta^5\text{-C}_5\text{Me}_5)\text{Ru}(\mu_2\text{-}i\text{-PrN}=\text{C}(\text{Me})\text{Ni-Pr})\text{Ru}(\eta^5\text{-C}_5\text{Me}_5)]^+$. *Tetrahedron.* **2005**, *61*, 10216-10226.
- (87) Motoyama, Y.; Hanada, S.; Shimamoto, K.; Nagashima, H. A coordinatively unsaturated ruthenium methoxide as a highly effective catalyst for the halogen atom-transfer radical cyclization of *N*-allyl dichloroacetamides and related reactions. *Tetrahedron.* **2006**, *62*, 2779-2788.
- (88) Simal, F.; Sebillé, S.; Demonceau, A.; Noels, A. F.; Nunez, R.; Abad, M.; Teixidor, F.; Vinas, C. Radical reactions catalysed by ruthenium(II) complexes with anionic carborane phosphine ligands: Kharasch addition to olefins and controlled polymerisation. *Tetrahedron Letters.* **2000**, *41*(28), 5347-5351.
- (89) Tutusaus, O.; Delfosse, S.; Demonceau, A.; Noels, A. F.; Viñas, C.; Teixidor, F. Kharasch addition catalysed by half-sandwich ruthenium complexes. Enhanced activity of ruthenacarboranes. *Tetrahedron Lett.* **2003**, *44*, 8421-8425.
- (90) Tutusaus, O.; Viñas, C.; Nuñez, R.; Teixidor, F.; Demonceau, A.; Delfosse, S.; Noels, A. F.; Mata, I.; Molins, E. The Modulating Possibility of Dicarborane Clusters: Optimizing the Kharasch Catalysts. *J. Am. Chem. Soc.* **2003**, *125*, 11830-11831.
- (91) Grubbs, R. H., In *Handbook of Metathesis*, S.-I. Murahashi, Editor. **2003**, Wiley-VCH: Weinheim, Germany.
- (92) Grubbs, R. H.; Trnka, T. M., In *Ruthenium in Organic Synthesis*, S.-I. Murahashi, Editor. **2004**, Wiley-VCH: Weinheim, Germany.

- (93) Schmidt, B.; Pohler, M. Ruthenium-catalyzed tandem ring closing metathesis (RCM) – atom transfer radical cyclization (ATRC) sequences. *J. Organomet. Chem.* **2005**, *690*, 5552-5555.
- (94) De Clercq, B.; Verpoort, F. Radical reactions catalysed by homobimetallic ruthenium(II) complexes bearing Schiff base ligands: atom transfer radical addition and controlled polymerization. *Tetrahedron Lett.* **2002**, *43*, 4687-4690.
- (95) Lundgren, R. J.; Rankin, M. A.; McDonald, R.; Stradiotto, M. Neutral, Cationic, and Zwitterionic Ruthenium(II) Atom Transfer Radical Addition Catalysts Supported by P,N-Substituted Indene or Indenide Ligands. *Organometallics.* **2008**, *27*(2), 254-258.
- (96) Nair, R. P.; Kim, T. H.; Frost, B. J. Atom Transfer Radical Addition Reactions of CCl₄, CHCl₃, and *p*-Tosyl Chloride Catalyzed by Cp'Ru(PPh₃)(PR₃)Cl Complexes. *Organometallics.* **2009**, *28*(16), 4681-4688.
- (97) Quebatte, L.; Haas, M.; Solari, E.; Scopelliti, R.; Nguyen, Q. T.; Severin, K. Atom-Transfer Radical Reactions under Mild Conditions with [$\{\text{RuCl}_2(1,3,5\text{-C}_6\text{H}_3\text{iPr}_3)\}_2$] and PCy₃ as the Catalyst Precursors. *Angew. Chem. Int. Ed.* **2005**, *44*, 1084-1088.
- (98) Quebatte, L.; Solari, E.; Scopelliti, R.; Severin, K. A Bimetallic Ruthenium Ethylene Complex as a Catalyst Precursor for the Kharasch Reaction. *Organometallics.* **2005**, *24*, 1404-1406.
- (99) Asscher, M.; Vofsi, D. Chlorine-activation by redox transfer. II. The addition of carbon tetrachloride to olefins. *J. Chem. Soc.* **1963**, 1887-1896.
- (100) Asscher, M.; Vofsi, D. Chlorine-activation by redox transfer. III. The abnormal addition of chloroform to olefins. *J. Chem. Soc.* **1963**, 3921-3927.
- (101) Asscher, M.; Vofsi, D. Chlorine-activation by redox transfer. IV. The addition of sulfonyl chlorides to vinyl monomers and other olefins. *J. Chem. Soc.* **1964**, 4962-4971.
- (102) Muñoz-Molina, J. M.; Belderrain, T. R.; Perez, P. J. Copper-Catalyzed Synthesis of 1,2-Disubstituted cyclopentanes from 1,6-Dienes by Ring-Closing Kharasch Addition of Carbon Tetrachloride. *Adv. Synth. Catal.* **2008**, *350*, 2365-2372.

- (103) Munoz-Molina, J. M.; Belderrain, T. R.; Perez, P. J. An Efficient, Selective and Reducing Agent-Free Copper Catalyst for the Atom-Transfer Radical Addition of Halo Compounds to Activated Olefins. *Inorg. Chem.* **2010**.
- (104) Kleij, A. W.; Gossage, R. A.; Gebbink, R. J. M.; Brinkmann, N.; Reijerse, E. J.; Kragl, U.; Lutz, M.; Spek, A. L.; van Koten, G. A "Dendritic Effect" in Homogeneous Catalysis with Carbosilane-Supported Arylnickel(II) Catalysts: Observation of Active-Site Proximity Effects in Atom-Transfer Radical Addition. *J. Am. Chem. Soc.* **2000**, *122*(49), 12112-12124.
- (105) Kleij, A. W.; Gossage, R. A.; Jastrzebski, J. T. B. H.; Boersma, J.; van Koten, G. The "Dendritic Effect" in Homogenous Catalysts with Carbosilane-Supported Arylnickel(II) Catalysts: Observation of Active-Site Proximity Effects in Atom-Transfer Radical Addition. *Angew. Chem. Int. Ed.* **2000**, *39*(1), 176-178.
- (106) Kleijn, H.; Jastrzebski, J. T. B. H.; Gossage, R. A.; Kooijman, H.; Spek, A. L.; van Koten, G. *Ortho*-bis(amino)arylnickel(II) Halide Complexes Containing Perfluoroalkyl Chains as Model Catalyst Precursors for Use in Fluorous Biphasic Systems. *Tetrahedron.* **1998**, *54*, 1145-1152.
- (107) Spasyuk, D. M.; Zargarian, D.; van der Est, A. New POCN-Type Pincer Complexes of Nickel(II) and Nickel(III). *Organometallics.* **2009**, *28*, 6531-6540.
- (108) van de Kuil, L. A.; Grove, D. M.; Gossage, R. A.; Zwikker, J. W.; Jenneskens, L. W.; Drenth, W.; van Koten, G. Mechanistic Aspects of the Kharasch Addition Reaction Catalyzed by Organonickel(II) Complexes Containing the Monoanionic Terdentate Aryldiamine Ligand System $[C_6H_2(CH_2NMe_2)_2-2,6-R-4]$. *Organometallics.* **1997**, *16*(23), 4985-4994.
- (109) Yorimitsu, H.; Nakamura, T.; Shinokubo, H.; Oshima, K.; Omoto, K.; Fujimoto, H. Powerful Solvent Effect of Water in Radical Reaction: Triethylborane-Induced Atom-Transfer Radical Cyclization in Water. *J. Am. Chem. Soc.* **2000**, *122*(45), 11041-11047.
- (110) Yorimitsu, H.; Shinokubo, H.; Matsubara, S.; Oshima, K.; Omoto, K.; Fujimoto, H. Triethylborane-Induced Bromine Atom-Transfer Radical Addition in Aqueous Media: Study of the Solvent Effect on Radical Addition Reactions. *J. Org. Chem.* **2001**, *66*(23), 7776-7785.
- (111) Pintauer, T.; Matyjaszewski, K. Atom Transfer Radical Addition and Polymerization Reactions Catalyzed by ppm Amounts of Copper Complexes. *Chem. Soc. Rev.* **2008**, *37*, 1087-1097.

- (112) Oe, Y.; Uozumi, Y. Highly Efficient Heterogeneous Aqueous Kharasch Reaction with an Amphiphilic Resin-Supported Ruthenium Catalyst. *Adv. Synth. Catal.* **2008**, *350*, 1771-1775.
- (113) De Campo, F.; Lastécouères, D.; Vincent, J.-M.; Verlhac, J.-B. Copper(I) Complexes Mediated Cyclization Reaction of Unsaturated Ester under Fluoro Biphasic Procedure. *J. Org. Chem.* **1999**, *64*, 4969-4971.
- (114) Matyjaszewski, K.; Jakubowski, W.; Min, K.; Tang, W.; Huang, J.; Braunecker, W. A.; Tsarevsky, N. V. Diminishing catalyst concentration in atom transfer radical polymerization with reducing agents. *Proc. Natl. Acad. Sci. USA.* **2006**, *103*, 15309-15314.
- (115) Wang, J.-S.; Matyjaszewski, K. Controlled/"living" radical polymerization. Atom transfer radical polymerization in the presence of transition-metal complexes. *J. Am. Chem. Soc.* **1995**, *117*, 5614-5615.
- (116) Jakubowski, W.; Matyjaszewski, K. Activators Regenerated by Electron Transfer for Atom-Transfer Radical Polymerization of (Meth)acrylates and Related Block Copolymers. *Angew. Chem. Int. Ed.* **2006**, *45*, 4482-4486.
- (117) Jakubowski, W.; Min, K.; Matyjaszewski, K. Activators Regenerated by Electron Transfer for Atom Transfer Radical Polymerization of Styrene. *Macromolecules.* **2006**, *39*, 39-45.
- (118) Eckenhoff, W. T.; Pintauer, T. Atom Transfer Radical Addition in the Presence of Catalytic Amounts of Copper(I/II) Complexes with Tris(2-pyridylmethyl)amine. *Inorg. Chem.* **2007**, *46*, 5844-5846.
- (119) Pintauer, T.; Eckenhoff, W. T.; Ricardo, C.; Balili, M. N. C.; Biernesser, A.; Noonan, S.; Taylor, M. Highly efficient ambient-temperature copper-catalyzed atom transfer radical addition (ATRA) in the presence of free-radical initiator (V70) as a reducing agent. *Chem. Eur. J.* **2009**, *15*, 38-41.
- (120) Thommes, K.; Kiefer, G.; Scopelliti, R.; Severin, K. Olefin Cyclopropanation by a Sequential Atom-Transfer Radical Addition and Dechlorination in the Presence of a Ruthenium Catalyst. *Angew. Chem. Int. Ed.* **2009**, *48(43)*, 8115-8119.

- (121) Tang, W.; Tsarevsky, N. V.; Matyjaszewski, K. Determination of Equilibrium Constants for Atom Transfer Radical Polymerization. *J. Am. Chem. Soc.* **2006**, *128*(5), 1598-1604.
- (122) Tang, W.; Kwak, Y.; Braunecker, W.; Tsarevsky, N. V.; Coote, M. L.; Matyjaszewski, K. Understanding Atom Transfer Radical Polymerization: Effect of Ligand and Initiator Structures on the Equilibrium Constants. *J. Am. Chem. Soc.* **2008**, *130*(32), 10702-10713.
- (123) Matyjaszewski, K.; Paik, H.-j.; Zhou, P.; Diamanti, S. J. Determination of Activation and Deactivation Rate Constants of Model Compounds in Atom Transfer Radical Polymerization. *Macromolecules*. **2001**, *34*(15), 5125-5131.
- (124) Goto, A.; Fukuda, T. Determination of the activation rate constants of alkyl halides initiators for atom transfer radical polymerization. *Macromol. Rapid Commun.* **1999**, *20*, 633-636.
- (125) Pintauer, T.; Braunecker, W.; Collange, E.; Poli, R.; Matyjaszewski, K. Determination of Rate Constants for the Activation Step in Atom Transfer Radical Polymerization Using the Stopped-Flow Technique. *Macromolecules*. **2004**, *37*(8), 2679-2682.
- (126) Nanda, A. K.; Matyjaszewski, K. Effect of Penultimate Unit on the Activation Process in ATRP. *Macromolecules*. **2003**, *36*, 8222-8224.
- (127) Tang, W.; Matyjaszewski, K. Effect of Ligand Structure on Activation Rate Constants in ATRP. *Macromolecules*. **2006**, *39*(15), 4953-4959.
- (128) Tang, W.; Matyjaszewski, K. Effects of Initiator Structure on Activation Rate Constants in ATRP. *Macromolecules*. **2007**, *40*(6), 1858-1863.
- (129) Chambard, G.; Klumperman, B.; German, A. L. Effect of Solvent on the Activation Rate Parameters for Polystyrene and Poly(butyl acrylate) Macroinitiators in Atom Transfer Radical Polymerization. *Macromolecules*. **2000**, *33*(12), 4417-4421.
- (130) Seeliger, F.; Matyjaszewski, K. Temperature Effect on Activation Rate Constants in ATRP: New Mechanistic Insights into the Activation Process. *Macromolecules*. **2009**, *42*, 6050-6055.

(131) Matyjaszewski, K.; Shipp, D. A.; Wang, J.-L.; Grimaud, T.; Patten, E. Utilizing Halide Exchange to Improve Control of Atom Transfer Radical Polymerization. *Macromolecules*. **1998**, *31*, 6836-6840.

(132) Jenkins, C. L.; Kochi, J. K. Solvolytic Routes via Alkylcopper Intermediates in the Electron-Transfer Oxidation of Alkyl Radicals. *J. Am. Chem. Soc.* **1972**, *94*, 843-855.

(133) Jenkins, C. L.; Kochi, J. K. Homolytic and Ionic Mechanisms in the Ligands-Transfer Oxidation of Alkyl Radicals by Copper(II) Halides and Pseudohalides. *J. Am. Chem. Soc.* **1972**, *94*, 856-865.

(134) Kochi, J. K., *Free Radicals*. Vol. 1. John Wiley & Sons, New York, **1973**.

Chapter 2

Effect of Catalyst, Alkyl Halide, and Reducing Agent Concentrations on Copper-Catalyzed Atom Transfer Radical Addition Reactions

Reproduced in part with permission from Balili, M. N. C.; Pintauer, T., *Inorg. Chem.* **2009**, 48, 2891-2902. Copyright 2009 American Chemical Society

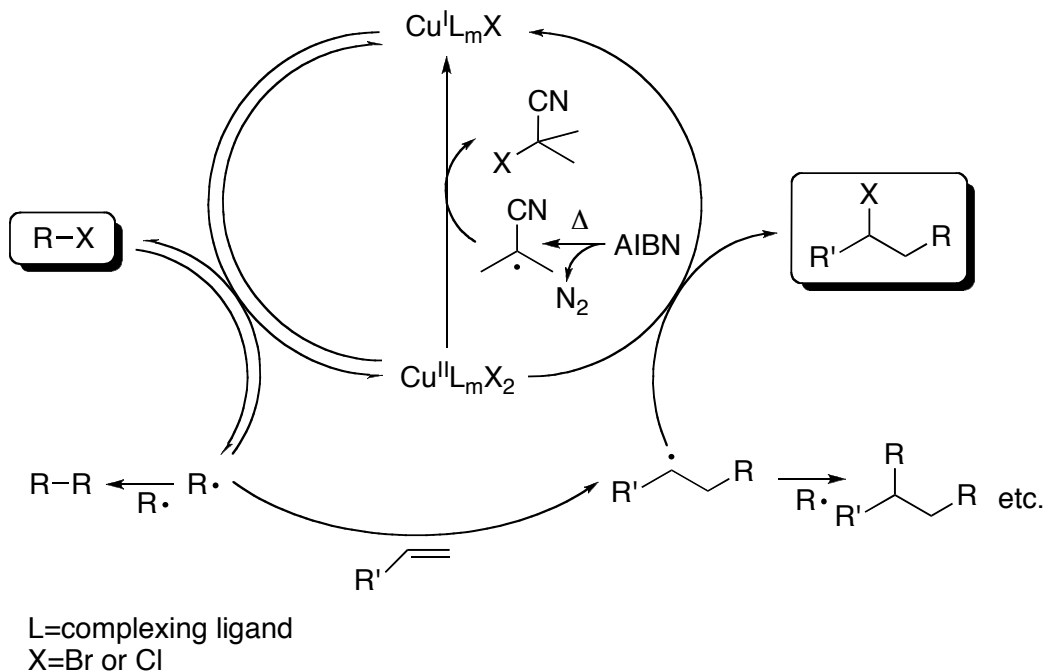
The effect of the copper(II) catalyst, alkyl halide, and reducing agent concentrations on atom transfer radical addition (ATRA) of various alkenes catalyzed by $[\text{Cu}^{\text{II}}(\text{TPMA})\text{X}][\text{X}]$ (TPMA=tris(2-pyridylmethyl)amine, X = Cl, Br) in the presence of free-radical diazo initiator (AIBN) as a reducing agent were investigated. For 1-octene, the catalyst concentration was found to affect the alkene conversion and the yield of monoadduct for $[\text{1-octene}]_0:[\text{Cu}^{\text{II}}]_0$ ratios above 10000:1. More pronounced effect of the catalyst loading was observed in the case of methyl acrylate and styrene, due to the formation of AIBN-initiated oligomeric/polymeric side products. It was also found that excess CCl_4 was not necessary in ATRA reactions that utilize AIBN as a reducing agent. However, reactions of less active halides were more affected by increased alkyl halide concentrations. For all three alkenes, the optimum reaction conditions were achieved using 5 mol% of AIBN relative to alkene. Higher free radical initiator concentration only led to an increase in the formation of AIBN-initiated polymers.

2.1 Introduction

Transition metal catalyzed atom transfer radical addition (TMC ATRA) provides an efficient technique for carbon-carbon bond formation in a catalytic manner.¹⁻⁵ In a typical ATRA, a transition metal complex (Cu,⁴⁻⁸ Ru,⁹⁻¹⁴ Fe¹⁵⁻¹⁸ or Ni¹⁹⁻²⁴) in a lower oxidation state homolytically cleaves a carbon-halogen bond to generate a higher oxidation state metal complex and a carbon-centered radical. The generated radical can either add across the double bond of an alkene, terminate by radical coupling or disproportionate or be reversibly deactivated by the metal complex in a higher oxidation state. If the deactivation happens after the first addition step, the desired monoadduct will be formed. The alkyl halide of choice should result in the formation of a radical after the first addition step that is much less stabilized than the initial radical and will immediately react with a higher-oxidation state metal complex to produce the monoadduct.

Traditionally, ATRA reactions required relatively large amounts of metal catalysts (10-30 mol%).²⁵⁻²⁸ Catalyst regeneration is often a problem in these reaction systems since radical termination side reactions cause the accumulation of the deactivator species and, consequently, a decrease in catalytic activity. Recently, a new methodology for catalyst regeneration in ATRA has been developed,^{8,29} known as initiators for continuous activator regeneration (ICAR), following its success in mechanistically similar atom transfer radical polymerization (ATRP).³⁰ In ICAR ATRA,^{31,32} reducing agents such as 2,2'-azobisisobutyronitrile (AIBN) continuously regenerates the catalytically active lower oxidation state transition metal complex (activator) by the abstraction of a halogen atom from the higher oxidation state complex (deactivator) (Scheme 2.1). This catalyst regeneration technique has been recently employed with great

success in ATRA reactions using $[\text{Ru}^{\text{III}}\text{Cl}_2\text{Cp}^*(\text{PPh}_3)]^{29,33}$ and $[\text{Cu}^{\text{II}}(\text{TPMA})\text{X}][\text{X}]$ ($\text{X} = \text{Cl}$ or Br)^{8,34} as catalysts. The $[\text{Cu}^{\text{II}}(\text{TPMA})\text{Br}][\text{Br}]$ catalyst was found to be approximately 10 times more active than $[\text{Cu}^{\text{II}}(\text{TPMA})\text{Cl}][\text{Cl}]$ based on the catalyst loading, conversion of the alkene and monoadduct yield in the ATRA of polybrominated compounds to alkenes in the presence of AIBN. The catalytic activity of $[\text{Cu}^{\text{II}}(\text{TPMA})\text{Br}][\text{Br}]$ even exceeded that of the $[\text{RuCl}_2\text{Cp}^*(\text{PPh}_3)]$ for comparable monomers and alkyl halides. Development of the ICAR ATRA techniques for catalyst regeneration have allowed these reactions to be conducted using ppm amounts of metal catalysts,^{1,8,29,31,32,34,35} making this process environmentally friendly with an enormous potential for various industrial applications.



Scheme 2.1. Proposed Mechanism for Copper(I) Regeneration in ATRA in the Presence of Free-Radical Diazo Initiator (AIBN) as a Reducing Agent.

TMC ATRA is a multicomponent system, which comprises of an alkene, an alkyl halide and a transition metal catalyst. In an ICAR ATRA reaction, a free radical initiator is added into the system as a reducing agent. Alkenes typically used in ATRA reactions include, but are not limited to, simple α -olefins (1-hexene, 1-octene, 1-decene), methyl acrylate, methyl methacrylate, styrene, vinyl acetate, and acrylonitrile. Simple α -olefins do not readily undergo free radical polymerization in the presence of radical initiators ($k_p \approx 10 \text{ M}^{-1}\text{s}^{-1}$) and, thus, low amounts of the metal catalyst does not lead to an increase in the formation of free-radical initiated polymers. On the other hand, methyl acrylate, methyl methacrylate, styrene and acrylonitrile have high propagation rate constants ($k_p \approx 10^2\text{-}10^3 \text{ M}^{-1}\text{s}^{-1}$) and ICAR ATRA reactions with low catalyst loadings often result to a decrease in monoadduct yields.

Formation of oligomers/polymers can also be a result of the insufficient trapping of the radical generated from the addition of the primary alkyl halide to the alkene or from the reactivation of the monoadduct and the repeated addition to the monomer. Typically, reactivation of the monoadduct can be suppressed by using excess alkyl halide relative to the alkene (as high as 4 equiv), making the activation of the alkyl halide in the presence of a lower oxidation metal catalyst far more favored over the activation of the monoadduct.

Clearly, the selective formation of the monoadduct can be influenced by the relative concentrations of the reactant components in an ATRA reaction. The effects of the concentrations of the Cu^{II} catalyst, alkyl halide, and reducing agent on the yields of the monoadduct for 1-octene, styrene, and methyl acrylate will be addressed in this chapter.

2.2 Experimental

2.2.1 General Procedures

All reagents were obtained from commercial sources. Styrene, 1-octene, and methyl acrylate were dried over calcium hydride and degassed prior to use. 2,2'-Azobis(isobutyronitrile) (AIBN) was recrystallized from cold methanol and dried at room temperature under vacuum. Solvent (acetonitrile) was degassed and deoxygenated using Innovative Technology solvent purifier. Carbon tetrachloride, chloroform, benzyl chloride, benzyl bromide and anisole were deoxygenated by bubbling argon for 30 min before use. Tris(2-pyridylmethyl)amine (TPMA)³⁶ and copper(II) complexes $[\text{Cu}^{\text{II}}(\text{TPMA})\text{Cl}][\text{Cl}]^8$ and $[\text{Cu}^{\text{II}}(\text{TPMA})\text{Br}][\text{Br}]^8$ were synthesized according to published procedures. All other reagents were used as received. Manipulations were performed under argon in a dry box (<1.0 ppm of O₂ and <0.5 ppm of H₂O) or using standard Schlenk line techniques. ¹H NMR spectra were obtained at room temperature on a Bruker Avance 400 MHz spectrometer with chemical shifts given in ppm relative to the residual solvent peak (CDCl₃, 7.26 ppm).

2.2.2 Preparation of Catalyst Solutions

Two solutions of $[\text{Cu}^{\text{II}}(\text{TPMA})\text{Cl}][\text{Cl}]$ were prepared using volumetric flasks to accommodate various catalyst loadings. Catalyst solution **A** was made by dissolving the previously synthesized $[\text{Cu}^{\text{II}}(\text{TPMA})\text{Cl}][\text{Cl}]$ (106 mg, 0.25 mmol) in 10.0 ml of acetonitrile to give a 0.025M solution. Catalyst solution **B** was prepared by diluting 2.1 ml of the 0.025M solution to 10.0 ml using acetonitrile as solvent to yield a 5.25×10^{-3} M solution. A 0.025 M solution of $[\text{Cu}^{\text{II}}(\text{TPMA})\text{Br}][\text{Br}]$ was also prepared by dissolving $[\text{Cu}^{\text{II}}(\text{TPMA})\text{Br}][\text{Br}]$ (128 mg, 0.25 mmol) in 10 ml of acetonitrile.

2.2.3 ATRA Reactions with Varying Cu^{II} Concentration

A stock solution containing CCl₄, an alkene, AIBN, and an internal standard (anisole for 1-octene and styrene, *p*-dimethoxybenzene for MA) was prepared ([CCl₄]₀:[alkene]₀:[AIBN]₀ = 4:1:0.05). The desired amount of [Cu^{II}(TPMA)Cl][Cl] was added to 1.0 ml of the stock solution in a vial. The total volume was adjusted by adding acetonitrile to obtain consistent alkene concentration in each reaction system ([alkene]₀ = 0.95M). The resulting solution was then stirred at 60°C for 24 h under argon.

2.2.4 ATRA Reactions with Varying Alkyl Halide Concentration

The Cu^{II} catalyst ([Cu^{II}(TPMA)Cl][Cl] for chlorinated alkanes and [Cu^{II}(TPMA)Br][Br] for benzyl bromide (BzBr)), alkene, AIBN, and an internal standard were dissolved in acetonitrile to make up stock solution **A** ([alkene]₀:[AIBN]₀ = 100:5). Varying amounts of the alkyl halide (CCl₄, CHCl₃, BzCl, BzBr) was then added to 1.0 ml of stock solution **A** in separate vials. The alkene concentration in each reaction system was maintained at 0.95M by adding acetonitrile to adjust the total volume of each reaction mixture. The reaction flask was immersed in a 60°C oil bath and stirred for 24 h under argon.

2.2.5 ATRA Reactions with Varying AIBN Concentration

The corresponding alkene, CCl₄, [Cu^{II}(TPMA)Cl][Cl] ([alkene]₀:[CCl₄]₀ = 100:400) and an internal standard were placed in a vial and stirred (stock solution **A**). AIBN (82.1 mg, 0.5 mmol) was dissolved in 1.0 ml acetonitrile to obtain a 0.5M AIBN solution. To a vial was added 1.0 ml of stock solution **A** and the required amount of

AIBN solution. Acetonitrile was added to increase the total volume of each reaction mixture ($[\text{alkene}]_0 = 0.95\text{M}$). The reaction was run under argon for 24 h at 60°C.

2.3 Results and Discussion

2.3.1 Effect of Catalyst Concentration on ATRA of CCl_4 to Alkenes

The effect of catalyst concentration on the alkene conversion and the yield of monoadduct in the ATRA of CCl_4 to alkenes was systematically investigated by varying the molar ratio of the catalyst with respect to alkene from 100:1 to 10000:1, while keeping other reactant concentrations constant. The corresponding plots for the alkene conversion and the percent yield of monoadduct versus time are shown in Figure 2.1. $[\text{Cu}^{\text{II}}(\text{TPMA})\text{Cl}][\text{Cl}]$ complex was quite effective in the ATRA of CCl_4 to 1-octene using as low as 0.02 mol % of the catalyst. A slight decrease in the yield of monoadduct was observed at even lower catalyst loadings (7500:1 (0.013 mol%) and 10000:1 (0.010 mol%)), which was attributed to incomplete alkene conversions. These results clearly indicate that free-radical diazo initiator (AIBN) provides a constant source of radicals, which continuously reduce $[\text{Cu}^{\text{II}}(\text{TPMA})\text{Cl}][\text{Cl}]$ to $\text{Cu}^{\text{I}}(\text{TPMA})\text{Cl}$. The activator or copper(I) complex is needed to homolytically cleave the $\text{CCl}_3\text{-Cl}$ bond. More pronounced effect of the catalyst loading on the alkene conversion and the yield of monoadduct was observed in the case of styrene and methyl acrylate. For styrene, relatively high yield of the monoadduct was observed at much higher catalyst loadings (alkene-to-catalyst ratio=100:1). A further increase in the styrene-to- $[\text{Cu}^{\text{II}}(\text{TPMA})\text{Cl}][\text{Cl}]$ ratio still resulted in high conversions; however, a more pronounced decrease in the yield of monoadduct was observed. The decrease in

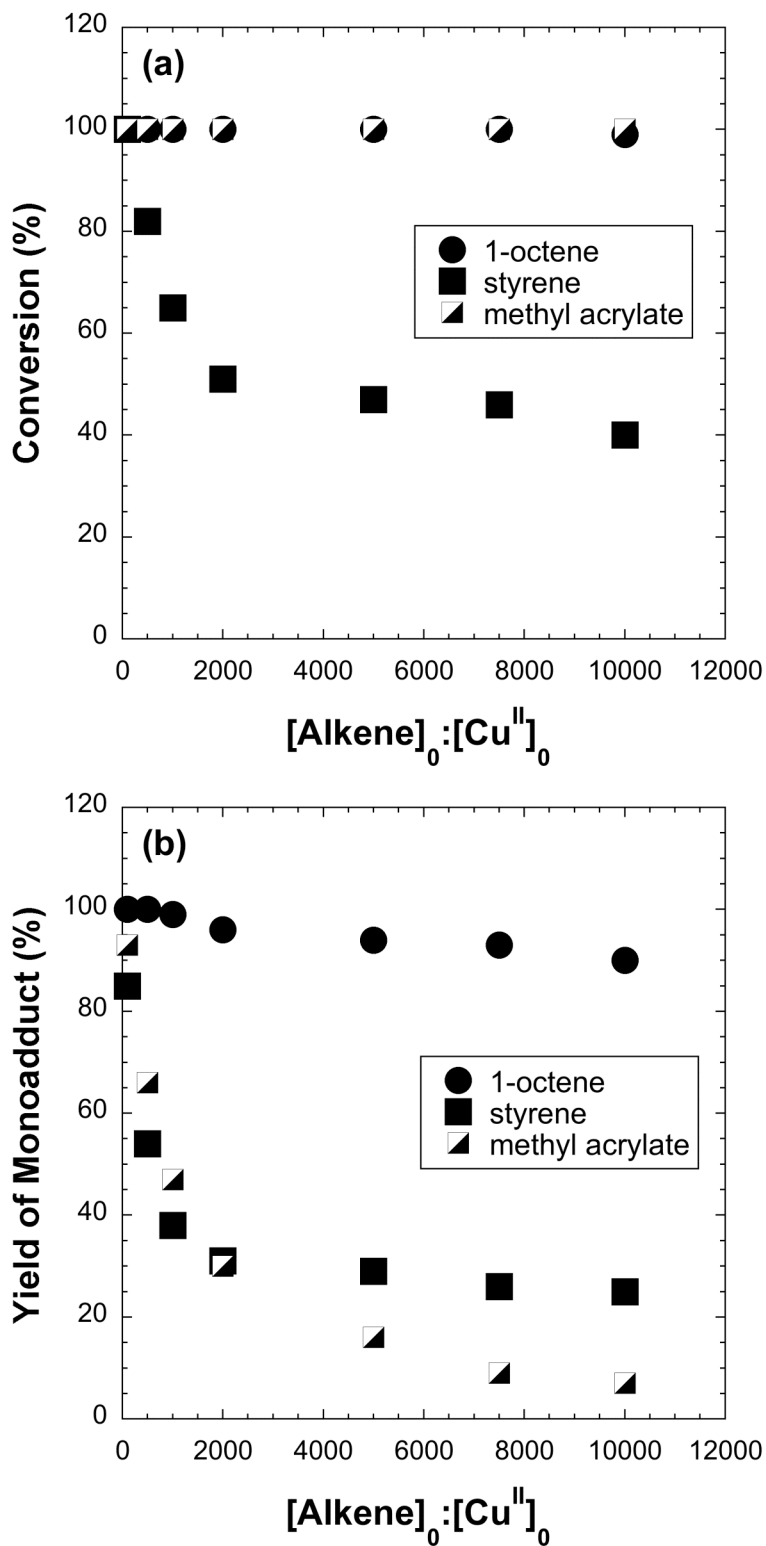


Figure 2.1. Effect of $[\text{Cu}^{\text{II}}(\text{TPMA})\text{Cl}][\text{Cl}]$ on the ATRA of CCl_4 to Alkenes. Experimental Conditions: time=24 h, solvent= CH_3CN , $[\text{alkene}]_0:[\text{CCl}_4]_0:[\text{AIBN}]_0=1:4:0.05$, $[\text{alkene}]_0=0.95$ M.

the yield of monoadduct was mostly due to the formation of oligomers/polymers, as a result of insufficient trapping of radicals generated from either AIBN (free radical polymerization) or addition of $\text{CCl}_3\cdot$ to alkene (ATRA) by the copper(II) complex.

Even more noticeable effect on the yield of monoadduct was observed in the addition of CCl_4 to methyl acrylate. For this alkene, quantitative conversions were observed regardless of the copper(II) concentrations in the system. However, the percent yield of the monoadduct was found to strongly depend on the alkene-to-catalyst molar ratio. At 100:1 ratio of methyl acrylate to $[\text{Cu}^{\text{II}}(\text{TPMA})\text{Cl}][\text{Cl}]$ the monoadduct was obtained in 93% yield. Furthermore, the yield continuously decreased at lower catalyst loadings, and reached the value of only 7% when the ratio of methyl acrylate to copper(II) was 10000:1.

The results on the effect of $[\text{Cu}^{\text{II}}(\text{TPMA})\text{Cl}][\text{Cl}]$ clearly indicate that AIBN is not very effective reducing agent for alkenes that have high propagation rate constants in free radical polymerization, such as styrene and methyl acrylate. For such alkenes, low temperature free-radical diazo initiators such as V-70 (2,2'-azobis(4-methoxy-2,4-dimethylvaleronitrile) can be used. In our previous report, this initiator has been shown to be a very effective reducing agent, enabling selective formation of the ATRA product with α -olefins and highly active monomers such as methyl acrylate, methyl methacrylate and vinyl acetate at ambient temperatures using as low as 0.002 mol% of copper.³⁷ Alternatively, redox-reducing agents that do not generate free radicals, such as magnesium, can also be utilized.³⁸

2.3.2 Effect of Alkyl Halide Concentration on ATRA of CCl₄, CHCl₃, BzCl and BzBr to Alkenes

Formation of oligomers/polymers is a common side reaction in ATRA especially when highly active monomers, such as styrene and methyl acrylate, are used. In the absence of free-radical initiators, oligomers/polymers are formed during ATRA as a result of further monoadduct activation and/or insufficient trapping of radicals generated in the first addition step by the copper(II) complex (Scheme 2.1). In order to suppress re-activation of the monoadduct, typically an excess of alkyl halide relative to alkene is used (as high as 4 equivalents). The results for the effect of CCl₄ concentration on the ATRA with 1-octene, styrene and methyl acrylate are summarized in Table 2.1.

Table 2.1. Effect of [CCl₄] on the ATRA of CCl₄ to Alkenes at Various Copper(II) Loadings^a

		conversion (%) / yield (%) ^b							
[alkene] ₀ :	1-octene	styrene			methyl acrylate				
[CCl ₄] ₀	1 mol% Cu ^{II}	1 mol% Cu ^{II}	0.2 mol% Cu ^{II}	0.02 mol% Cu ^{II}	1 mol% Cu ^{II}	1 mol% Cu ^{IIc}	0.2 mol% Cu ^{IIc}	0.1 mol% Cu ^{IIc}	0.02 mol% Cu ^{IIc}
1:1.0	83/83	100/86	67/40	41/25	100/74	80/71	90/45	95/35	92/22
1:1.5	100/100	100/89	70/48	41/27	100/79	nd	nd	nd	nd
1:2.0	100/100	100/90	71/46	42/27	100/92	84/72	91/48	94/36	92/21
1:2.5	100/100	100/88	76/48	41/25	100/81	nd	nd	nd	nd
1:3.0	100/100	100/84	82/53	43/26	100/81	82/69	88/47	94/32	90/20
1:4.0	100/100	100/89	84/55	43/27	100/80	80/68	88/50	95/36	93/21
1:5.0	100/100	100/86	76/50	45/26	100/81	82/71	88/50	92/34	91/20
1:6.0	100/100	100/85	67/46	44/26	100/82	79/67	88/51	92/30	91/19

^aAll reactions were performed in CH₃CN at 60°C for 24 h with [alkene]₀/[AIBN]₀ = 1:0.05 and [alkene]₀ = 0.95M. ^bThe yield is based on the formation of monoadduct and was determined using ¹H NMR spectroscopy (relative errors are ±10%). ^cReaction time=2 h.

Using 1 mol% of $[\text{Cu}^{\text{II}}(\text{TPMA})\text{Cl}][\text{Cl}]$, a complete conversion of 1-octene was not observed when $[\text{1-octene}]_0:[\text{CCl}_4]_0$ ratio was 1:1. Further increase in the ratio of CCl_4 to 1-octene allowed for the total consumption of the alkene and quantitative yield of the monoadduct, which remained constant using as high as 6 equivalents of CCl_4 . Re-activation of the monoadduct is not expected for 1-octene because the resulting C-Cl bond is quite strong.³⁹ Also, free radical polymerization should not compete with the deactivation processes because α -olefins are known to have very low propagation rate constants.⁴⁰

Complete conversion of styrene and methyl acrylate was also observed in the ATRA using stoichiometric amounts of CCl_4 with 1 mol% of copper catalyst. However, in comparison with 1-octene, the yields of the monoadduct were slightly lower for both alkenes. In addition, they remained relatively independent on the ratio of alkene to CCl_4 . At lower copper(II) catalyst loadings (0.2 and 0.02 mol%, Table 2.1), a further decrease in the conversion and the yield of monoadduct was observed, but the amount of CCl_4 added did not have a significant effect. These results clearly show that further activation of the monoadduct for methyl acrylate and styrene is much slower than the formation of CCl_3^\bullet radicals generated from the homolytic cleavage of $\text{CCl}_3\text{-Cl}$ bond. Additionally, the formation of the monoadduct via the cleavage of the $\text{CCl}_3\text{-Cl}$ bond by radicals generated from the decomposition of AIBN only (non-metal catalyzed Kharasch addition) is negligible since higher concentrations of CCl_4 in the system have no significant effect on the monoadduct yield. Consistent with our previous studies,^{27,41} a decrease in the yield of monoadduct in the ATRA of CCl_4 to methyl acrylate and styrene at lower catalyst loadings (0.2

and 0.02 mol%, Table 2.1) is induced by free-radical polymerization initiated by AIBN.

Since the conversion of alkene and yield of monoadduct was not dependent on the concentration of a highly active alkyl halide (CCl_4), the effect of the concentration of less active alkyl halides, such as chloroform (CHCl_3), benzyl chloride (BzCl) and benzyl bromide (BzBr) on ATRA to methyl acrylate and styrene was further investigated. Less active alkyl halides are known to be less prone to add across alkenes and, oftentimes, harsh reaction conditions and high catalyst loadings are required to achieve quantitative monoadduct formation.^{4,8} Thus, ATRA reactions involving less active alkyl halides were done with 1 mol% Cu^{II} catalyst relative to the alkene and the results are summarized in Table 2.2.

Addition of 1 equivalent of CHCl_3 relative to methyl acrylate resulted in nearly quantitative conversion of the alkene and 77% yield of the monoadduct (entry 1, Table 2.2). When 2 equiv of CHCl_3 relative to methyl acrylate was used, the monoadduct was obtained in 93% yield (entry 2, Table 2.2). A further increase in the amount of CHCl_3 added resulted in quantitative conversions and monoadduct yields (entries 3 and 4, Table 2.2). The increase in monoadduct yield with increasing CHCl_3 concentrations clearly shows that reactivation of the monoadduct is suppressed at higher CHCl_3 concentrations. Furthermore, a more pronounced effect was observed in the ATRA of benzyl chloride and benzyl bromide to methyl acrylate. Stoichiometric amounts of the alkyl halide and alkene resulted in 37% and 55% yield of the BzCl -methyl acrylate and BzBr -methyl acrylate adducts, respectively (entries 5 and 9, Table 2.2). At higher alkyl halide concentrations, the monoadduct yields significantly increased, with approximately twice

Table 2.2. Effect of Alkyl Halide Concentration on ATRA of Less Active Alkyl Halides to Methyl Acrylate and Styrene^a

Entry	Alkene	Alkyl Halide	[Alkene] ₀ : [R-X] ₀	%Conv	%Prod	%Yield ^c
1			1:1	>99	77	77
2	Methyl	CHCl ₃	1:2	100	93	93
3	Acrylate		1:4	100	100	100
4			1:6	100	100	100
5			1:1	85	43	37
6	Methyl	BzCl	1:2	87	55	48
7	Acrylate		1:4	90	72	65
8			1:6	91	84	76
9			1:1	91	60	55
10	Methyl	BzBr ^b	1:2	93	70	65
11	Acrylate		1:4	95	81	77
12			1:6	95	90	86
13			1:1	94	78	73
14	Styrene	CHCl ₃	1:2	100	96	96
15			1:4	100	99	99
16			1:6	100	100	100
17			1:1	58	50	29
18	Styrene	BzCl	1:2	63	63	40
19			1:4	69	77	53
20			1:6	75	89	67
21			1:1	64	63	40
22	Styrene	BzBr ^b	1:2	69	72	50
23			1:4	74	84	62
24			1:6	80	93	74

^a[alkene]₀: [Cu^{II}]₀: [AIBN]₀ = 100:1:5, catalyst = [Cu^{II}(TPMA)Cl][Cl], solvent = CH₃CN, time = 24 h, T = 60°C; ^b[Cu^{II}(TPMA)Br][Br] was used as catalyst. ^cThe yield is based on the formation of monoadduct and was determined using ¹H NMR spectroscopy (relative errors are ±10%).

as much formed at alkene-to-alkyl halide ratio of 1:6 (entries 8 and 12, Table 2.2). Evidently, higher concentrations of the less active alkyl halides minimized the formation of oligomers due to monoadduct reactivation, resulting to higher yields without a significant change in alkene conversion.

Similar results were observed in the ATRA of CHCl_3 , BzCl and BzBr to styrene (entries 13 to 24, Table 2.2). Stoichiometric amounts of the alkene and alkyl halide resulted in low yields of the single addition adducts due to the formation of oligomers from the repeated addition of the activated monoadduct to an alkene. Higher concentrations of the alkyl halide led to an increase in the monoadduct yield, and, therefore, effectively suppressing the reactivation of the monoadduct.

2.3.3 Effect of Reducing Agent Concentration on ATRA of CCl_4 to Alkenes

So far, we have considered the effects of alkyl halide (CCl_4 , CHCl_3 , BzCl and BzBr) and $[\text{Cu}^{\text{II}}(\text{TPMA})\text{Cl}][\text{Cl}]$ concentrations on the alkene conversion and the yield of monoadduct in ATRA reactions utilizing free-radical diazo initiator (AIBN) as reducing agent. AIBN is very important component of the reaction mixture because its slow decomposition provides a constant source of radicals that are essential for the regeneration of the activator or $\text{Cu}^{\text{I}}(\text{TPMA})\text{Cl}$ complex. Table 2.3 shows the results of the effect of varying AIBN concentrations on the ATRA of CCl_4 to 1-octene, styrene, and methyl acrylate.

For all three alkenes, the conversion and the yield of monoadduct increased as the ratio of AIBN to alkene increased from 0.01:1 to 0.05:1, however, the maximum is achieved at approximately 5 mol% of AIBN (relative to alkene), consistent with our previous observations. At high catalyst loadings ($[\text{alkene}]_0:[\text{Cu}^{\text{II}}]_0=100:1$), further increase in the AIBN concentration had a small effect on the monomer conversion and the percent yield of monoadduct.

Table 2.3. Effect of [AIBN] on the ATRA of CCl₄ to Alkenes at Various Copper(II) Loadings^a

		conversion (%) / yield (%) ^b					
[alk] ₀ :	1-octene	styrene			methyl acrylate		
[AIBN] ₀	1 mol% Cu ^{II}	1 mol% Cu ^{II}	0.2 mol% Cu ^{II}	0.1 mol% Cu ^{II}	1 mol% Cu ^{II}	0.2 mol% Cu ^{IIc}	0.1 mol% Cu ^{IIc}
1:0.01	98/94	82/70	70/37	28/24	100/79	67/40	71/28
1:0.05	100/100	100/89	84/55	45/33	100/80	88/50	95/36
1:0.10	100/99	100/85	90/49	47/35	100/84	93/51	96/35
1:0.15	100/99	100/85	93/47	55/38	100/77	96/52	99/39
1:0.20	100/100	100/85	100/49	65/38	100/79	98/50	100/40

^aAll reactions were performed in CH₃CN at 60°C for 24 h with [alkene]₀: [CCl₄]₀ = 1:4 and [alkene]₀ = 0.95M. ^bThe yield is based on the formation of monoadduct and was determined using ¹H NMR spectroscopy (relative errors are ±10%). ^cReaction time=2 h.

As aforementioned, the major side reaction in copper catalyzed ATRA in the presence of free-radical diazo initiators as reducing agents is competing radical polymerization. This side reaction is minimized with alkenes that have slow propagation rate constants, but is significantly pronounced for alkenes that rapidly polymerize in the presence of radical initiators. Therefore, the effect of varying free-radical initiator concentration at low catalyst loadings (0.2 and 0.1 mol%) was also investigated for the ATRA of CCl₄ to the highly active alkenes (styrene and methyl acrylate). ATRA reactions involving methyl acrylate was stopped before complete conversion of methyl acrylate was achieved in order to quantitatively observe the effect of free-radical concentration on the percent conversion.

As evident in Table 2.3, a significant increase in the percent conversion of the alkene was observed with increasing AIBN concentration. However, the yield of monoadduct remained nearly constant. Since AIBN is a reducing agent in the system, one could speculate that higher AIBN concentrations would result in lowering of the overall copper(II) concentration. This in turn could decrease the rate of trapping of $\text{CCl}_3\text{-CH}_2\text{-CHR}'\cdot$ radicals generated from the addition of $\text{CCl}_3\cdot$ to an alkene ($\text{rate} \propto [\text{Cu}^{\text{II}}]$), resulting in polymerization/oligomerization. However, this explanation appears to be rather unlikely, because a decrease in copper(II) concentration should result in a decrease of the monoadduct yield (see Table 2.3). However, the monoadduct yield remained constant at varying AIBN concentrations. Therefore, the increase in the conversion for methyl acrylate and styrene is most likely induced by free radical polymerization initiated by AIBN.

2.4 Conclusions

In summary, the effect of the concentrations of the Cu^{II} catalyst, alkyl halide and reducing agent on ATRA reactions catalyzed by $[\text{Cu}^{\text{II}}(\text{TPMA})\text{Cl}][\text{Cl}]$ in the presence of free-radical diazo initiator (AIBN) as a reducing agent were investigated. AIBN was a very effective reducing agent for alkenes that have slow propagation rate constants in free radical polymerization such as α -olefins (1-octene), enabling selective formation of the monoadduct using as low as 0.01 mol% of $[\text{Cu}^{\text{II}}(\text{TPMA})\text{Cl}][\text{Cl}]$ complex. For highly active alkenes such as methyl acrylate and styrene, significantly higher catalyst loadings were required in order to minimize free-radical polymerization initiated by AIBN. The conversion of the alkene and monoadduct yields were found to be independent on the concentration of a highly active alkyl halide (CCl_4). However, a more pronounced effect on the monoadduct yield was observed with varying concentrations of less active alkyl halides. This was attributed to the effective suppression of the reactivation of the monoadduct when a higher equivalent of the alkyl halide relative to the alkene was used. For all three alkenes, the optimum reaction conditions were achieved using 5 mol% of free-radical diazo initiator and as low as 1 equivalent of CCl_4 relative to alkene. Monoadduct yield remained unchanged at higher AIBN concentrations, however, higher conversions due to an increase in the yield of the AIBN-initiated polymers were observed.

References

- (1) Pintauer, T.; Matyjaszewski, K. Atom transfer radical addition and polymerization reactions catalyzed by ppm amounts of copper complexes. *Chem. Soc. Rev.* **2008**, *37*, 1087-1097.
- (2) Severin, K. Ruthenium catalysts for the Kharasch reaction. *Curr. Org. Chem.* **2006**, *10*(2), 217-224.
- (3) Iqbal, J.; Bhatia, B.; Nayyar, K. Transition Metal-Promoted Free-Radical Reactions in Organic Synthesis: The Formation of Carbon-Carbon Bonds. *Chem. Rev.* **1994**, *94*, 519-564.
- (4) Eckenhoff, W. T.; Pintauer, T. Atom Transfer Radical Addition in the Presence of Catalytic Amounts of Copper(I/II) Complexes with Tris(2-pyridylmethyl)amine. *Inorg. Chem.* **2007**, *46*, 5844-5846.
- (5) Munoz-Molina, J. M.; Caballero, A.; Diaz-Requejo, M. M.; Trofimenko, S.; Belderrain, T. R.; Perez, P. J. Copper-Homoscorpionate Complexes as Active Catalysts for Atom Transfer Radical Addition to Olefins. *Inorg. Chem.* **2007**, *46*(19), 7725-7730.
- (6) Pintauer, T.; Eckenhoff, W. T.; Ricardo, C.; Balili, M. N. C.; Biernesser, A.; Noonan, S.; Taylor, M. Highly efficient ambient-temperature copper-catalyzed atom transfer radical addition (ATRA) in the presence of free-radical initiator (V70) as a reducing agent. *Chem. Eur. J.* **2009**, *15*, 38-41.
- (7) Munoz-Molina, J. M.; Belderrain, T. R.; Perez, P. J. An Efficient, Selective and Reducing Agent-Free Copper Catalyst for the Atom-Transfer Radical Addition of Halo Compounds to Activated Olefins. *Inorg. Chem.* **2010**.
- (8) Eckenhoff, W. T.; Garrity, S. T.; Pintauer, T. Highly Efficient Copper-Mediated Atom-Transfer Radical Addition (ATRA) in the Presence of Reducing Agent. *Eur. J. Inorg. Chem.* **2008**(4), 563-571.
- (9) Borguet, Y.; Richel, A.; Delfosse, S.; Leclerc, A.; Delaude, L.; Demonceau, A. Microwave-enhanced ruthenium-catalysed atom transfer radical additions. *Tetrahedron Letters.* **2007**, *48*(36), 6334-6338.

- (10) De Clercq, B.; Verpoort, F. Synthesis and evaluation of a new class of ruthenium-based catalytic systems for atom transfer radical addition and enol ester synthesis. *J. Organomet. Chem.* **2003**, *672*, 11-16.
- (11) Lundgren, R. J.; Rankin, M. A.; McDonald, R.; Stradiotto, M. Neutral, Cationic, and Zwitterionic Ruthenium(II) Atom Transfer Radical Addition Catalysts Supported by P,N-Substituted Indene or Indenide Ligands. *Organometallics*. **2008**, *27*(2), 254-258.
- (12) Opstal, T.; Verpoort, F. From atom transfer radical addition to atom transfer radical polymerization of vinyl monomers mediated by ruthenium indenylidene complexes. *New J. Chem.* **2003**, *27*(2), 257-262.
- (13) Richel, A.; Delfosse, S.; Cremasco, C.; Delaude, L.; Demonceau, A.; Noels, A. F. Ruthenium catalysts bearing N-heterocyclic carbene ligands in atom transfer radical reactions. **2003**, *44*, 6011-6015.
- (14) Richel, A.; Demonceau, A.; Noels, A. F. Electrochemistry as a correlation tool with the catalytic activities in [Ru(Cl₂(p-cymene)(PAR₃)]-catalyzed Kharasch additions. *Tetrahedron Lett.* **2006**, *47*, 2077-2081.
- (15) Bach, T.; Schlummer, B.; Harms, K. Intramolecular Iron(II)-catalyzed Nitrogen Transfer Reactions of Unsaturated Alkoxy carbonyl Oxides: A Facile and Stereoselective Route to 4,5-Disubstituted Oxazolidinones. *Chem. Eur. J.* **2001**, *7*(12), 2581-2594.
- (16) Bellesia, F.; Forti, L.; Gallini, E.; Ghelfi, F.; Libertini, E.; Pagnoni, U. M. Telechelic oligomers by halogen atom transfer radical addition. *Tetrahedron*. **1998**, *54*(27), 7849-7856.
- (17) Forti, L.; Ghelfi, F.; Libertini, E.; Pagnoni, U. M.; Soragni, E. Halogen Atom Transfer Radical Addition of α -Polychloroesters to Olefins Promoted by Fe⁰ Filings. *Tetrahedron*. **1997**, *53*(52), 17761-17768.
- (18) Forti, L.; Ghelfi, F.; Pagnoni, U. M. Fe⁰ Initiated Halogen Atom Transfer Radical Addition of Methyl 2-Br-2-Cl-Carboxylates to Olefins. *Tetrahedron Letters*. **1996**, *37*(12), 2077-2078.
- (19) Granel, C.; Dubois, P.; Jerome, R.; Teyssie, P. Controlled Radical Polymerization of Methacrylic Monomers in the Presence of a Bis(ortho-chelated) Arylnickel(II) Complex and Different Activated Alkyl Halides. *Macromolecules*. **1996**, *29*(27), 8576-8582.

- (20) Kleij, A. W.; Gossage, R. A.; Gebbink, R. J. M.; Brinkmann, N.; Reijerse, E. J.; Kragl, U.; Lutz, M.; Spek, A. L.; van Koten, G. A "Dendritic Effect" in Homogeneous Catalysis with Carbosilane-Supported Arylnickel(II) Catalysts: Observation of Active-Site Proximity Effects in Atom-Transfer Radical Addition. *J. Am. Chem. Soc.* **2000**, *122*(49), 12112-12124.
- (21) Kleij, A. W.; Gossage, R. A.; Jastrzebski, J. T. B. H.; Boersma, J.; van Koten, G. The "Dendritic Effect" in Homogenous Catalysts with Carbosilane-Supported Arylnickel(II) Catalysts: Observation of Active-Site Proximity Effects in Atom-Transfer Radical Addition. *Angew. Chem. Int. Ed.* **2000**, *39*(1), 176-178.
- (22) Kleijn, H.; Jastrzebski, J. T. B. H.; Gossage, R. A.; Kooijman, H.; Spek, A. L.; van Koten, G. *Ortho*-bis(amino)arylnickel(II) Halide Complexes Containing Perfluoroalkyl Chains as Model Catalyst Precursors for Use in Fluorous Biphasic Systems. *Tetrahedron.* **1998**, *54*, 1145-1152.
- (23) Spasyuk, D. M.; Zargarian, D.; van der Est, A. New POCN-Type Pincer Complexes of Nickel(II) and Nickel(III). *Organometallics.* **2009**, *28*, 6531-6540.
- (24) van de Kuil, L. A.; Grove, D. M.; Gossage, R. A.; Zwikker, J. W.; Jenneskens, L. W.; Drenth, W.; van Koten, G. Mechanistic Aspects of the Kharasch Addition Reaction Catalyzed by Organonickel(II) Complexes Containing the Monoanionic Terdentate Aryldiamine Ligand System [C₆H₂(CH₂NMe₂)₂-2,6-R-4]. *Organometallics.* **1997**, *16*(23), 4985-4994.
- (25) Clark, A. J.; Battle, G. M.; Bridge, A. Efficient β-lactam synthesis via 4-exo atom transfer radical cyclisation using CuBr(tripyridylamine) complex. *Tetrahedron Letters.* **2001**, *42*, 4409-4412.
- (26) Clark, A. J. Atom transfer radical cyclisation reactions mediated by copper complexes. *Chem. Soc. Rev.* **2002**, *31*, 1-11.
- (27) Tallarico, J. A.; Malnick, L. M.; Snapper, M. L. New Reactivity from (PCy₃)₂Cl₂Ru=CHPh: A Mild Catalyst for Kharasch Additions. *J. Org. Chem.* **1999**, *64*, 344-345.
- (28) Clark, A. J.; Filik, R. P.; Thomas, G. H. Ligand Geometry Effects in Copper Mediated Atom Transfer Radical Cyclisations. *Tetrahedron Letters.* **1999**, *40*, 4885-4888.

- (29) Quebatte, L.; Thommes, K.; Severin, K. Highly Efficient Atom Transfer Radical Addition Reactions with a Ru^{III} Complex as a Catalyst Precursor. *J. Am. Chem. Soc.* **2006**, *128*, 7440-7441.
- (30) Matyjaszewski, K.; Jakubowski, W.; Min, K.; Tang, W.; Huang, J.; Braunecker, W. A.; Tsarevsky, N. V. Diminishing catalyst concentration in atom transfer radical polymerization with reducing agents. *Proc. Natl. Acad. Sci. USA.* **2006**, *103*, 15309-15314.
- (31) Eckenhoff, W. T.; Pintauer, T. Copper catalyzed atom transfer radical addition (ATRA) and cyclization (ATRC) reactions in the presence of reducing agents. *Catalysis Reviews.* **2010**, *52(1)*, 1-59.
- (32) Pintauer, T. "Greening" of copper catalyzed atom transfer radical addition (ATRA) and cyclization (ATRC) reactions. *ACS Symp. Ser.* **2009**, *1023*, 63-84.
- (33) Thommes, K.; Icli, B.; Scopelliti, R.; Severin, K. Atom-Transfer Radical Addition (ATRA) and Cyclization (ATRC) Reactions Catalyzed by a Mixture of [RuCl₂Cp*(PPh₃)] and Magnesium. *Chem. Eur. J.* **2007**, *13*, 6899-6907.
- (34) Balili, M. N. C.; Pintauer, T. Persistent Radical Effect in Action: Kinetic Studies of Copper-Catalyzed Atom Transfer Radical Addition in the Presence of Free-Radical Diazo Initiators as Reducing Agents. *Inorg. Chem.* **2009**, *48*, 9018-9026.
- (35) Ricardo, C.; Pintauer, T. Copper catalyzed atom transfer radical cascade reactions in the presence of free-radical diazo initiators as reducing agents. *Chem. Commun.* **2009**, *21*, 3029-3031.
- (36) Tyeklar, Z.; Jacobson, R. R.; Wei, N.; Murthy, N. N.; Zubieta, J.; Karlin, K. D. Reversible Reaction of Dioxygen (and Carbon Monoxide) with a Copper(I) Complex. X-Ray Structures of Relevant Mononuclear Cu(I) Precursor Adducts and the Trans-(μ^{-1,2}-peroxy)dicopper(II) Product. *J. Am. Chem. Soc.* **1993**, *115(7)*, 2677-2689.
- (37) Pintauer, T.; Eckenhoff, W. T.; Ricardo, C.; Balili, M. N. C.; Biernesser, A. B.; Noonan, S. J.; Taylor, M. J. W. Highly Efficient, Ambient-Temperature Copper-Catalyzed Atom-Transfer Radical Addition (ATRA) in the Presence of Free-Radical Initiator (V-70) as a Reducing Agent. *Chem. Eur. J.* **2009**, *15*, 38-41.

(38) Thommes, K.; Icli, B.; Scopelliti, R.; Severin, K. Atom-Transfer Radical Addition (ATRA) and Cyclization (ATRC) Reactions Catalyzed by a Mixture of $[\text{RuCl}_2\text{Cp}^*(\text{PPh}_3)]$ and Magnesium. *Chem. Eur. J.* **2007**, *13*(24), 6899-6907.

(39) Gillies, M. B.; Matyjaszewski, K.; Norrby, P.-O.; Pintauer, T.; Poli, R.; Richard, P. A. A DFT Study of R-X Bond Dissociation Enthalpies of Relevance to the Initiation Process in Atom Transfer Radical Polymerization. *Macromolecules.* **2003**, *36*, 8551-8559.

(40) Odian, G., *Principles of Polymerization*, 4th ed., John Wiley & Sons, Hoboken, **2004**.

(41) Simal, F.; Wlodarczak, L.; Demonceau, A.; Noels, A. F. New, Highly Efficient Catalyst Precursors for Kharasch Additions – $[\text{RuCl}(\text{Cp}^*)(\text{PPh}_3)_2]$ and $[\text{RuCl}(\text{Ind})(\text{PPh}_3)_2]$. *Eur. J. Org. Chem.* **2001**, 2689-2695.

Chapter 3

Kinetic Studies of Copper-Catalyzed Atom Transfer Radical Addition in the Presence of Reducing Agents

Reproduced in part with permission from Balili, M. N. C.; Pintauer, T., *Inorg. Chem.* **2009**, 48, 2891-2902. Copyright 2009 American Chemical Society

Kinetic features of atom transfer radical addition (ATRA) of CCl_4 to 1-octene, styrene and methyl acrylate catalyzed by $[\text{Cu}^{\text{II}}(\text{TPMA})\text{Cl}][\text{Cl}]$ (TPMA=tris(2-pyridylmethyl)amine) in the presence of free-radical diazo initiator (AIBN) as a reducing agent were investigated. The amounts of copper(II) and copper(I) complexes in ATRA in the presence of AIBN were found to be governed by both $k_{\text{d,AIBN}}$ and $k_{\text{a,AIBN}}$. Kinetic studies of the ATRA process revealed that the rate of alkene consumption was dependent on the concentration and rate of decomposition of radical initiator, but independent on the concentration of copper catalyst. However, selectivity of the desired monoadduct ultimately depended on the nature of the catalyst.

3.1 Introduction

The reaction kinetics for the ATRA process in the presence of free-radical diazo initiators such as AIBN appear to be rather complex. The principal reason is the incorporation of additional reactions steps that involve AIBN. These steps are: (a) decomposition of AIBN to generate free radicals, (b) reduction of copper(II) to copper(I) in the presence of AIBN and (c) free radical polymerization of alkene initiated by AIBN. The elementary reactions for these processes are shown in Scheme 3.1.

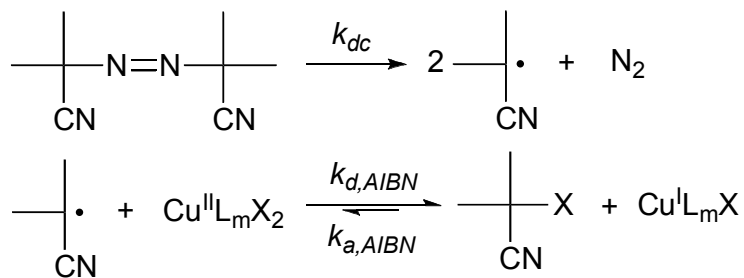
The rate of disappearance of alkene (assuming fast trapping of radicals generated in the first addition step ($k_{d2}[\text{Cu}^{\text{II}}\text{L}_m\text{X}_2] \gg k_p[\text{alkene}]$) and neglecting monoadduct re-activation ($k_{a2} \approx 0$)) is given by the following expression:

$$-\frac{d[\text{alkene}]}{dt} = k_{add}[\text{R}^*][\text{alkene}] + k_{add,\text{AIBN}}[\text{I}^*][\text{alkene}] + k_p[\text{I-Alk}^*][\text{alkene}]$$

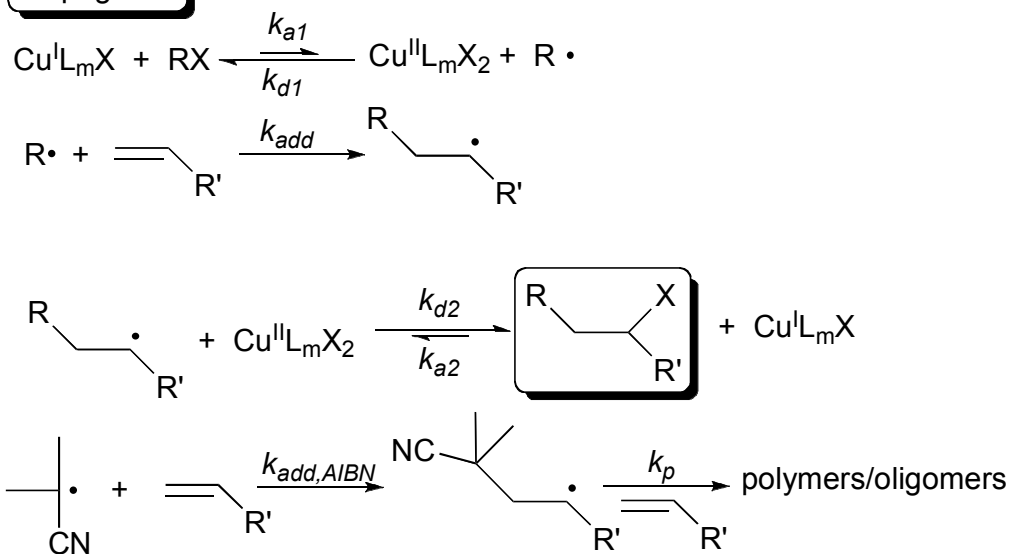
where the first term corresponds to ATRA process and the second and third ones to free-radical polymerization initiated by AIBN (I^* denotes radicals formed from the decomposition of AIBN and I-Alk^* radicals formed in subsequent additions of I^* to alkene). In free radical polymerization, the number of molecules reacting in the initiation step is far less than the number in the propagation step for a process producing high molecular weight polymer. To a very close approximation the former can be neglected and the polymerization rate is given simply by the rate of propagation.¹ Therefore, the above equation can be simplified to:

$$-\frac{d[\text{alkene}]}{dt} = k_{add}[\text{R}^*][\text{alkene}] + k_p[\text{I}^*][\text{alkene}]$$

Initiation

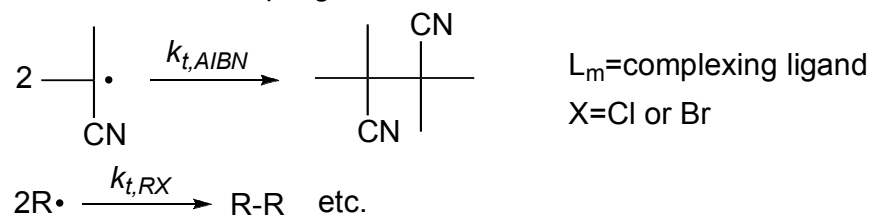


Propagation



Termination

radical-radical coupling:



Scheme 3.1. Initiation, Propagation and Termination Steps in Copper Catalyzed ATRA in the Presence of Free-Radical Initiator AIBN.

If we combine the equilibrium expressions for copper(I) regeneration and activation/deactivation of alkyl halide (RX), the radical concentration (R^\bullet) in the system is equal to:

$$\frac{[Cu^I L_m X][I - X]}{[Cu^{II} L_m X_2][I^\bullet]} = \frac{k_{d,AIBN}}{k_{a,AIBN}} = \frac{1}{K_{ATRA,AIBN}}$$

$$\frac{[Cu^{II} L_m X_2][R^\bullet]}{[Cu^I L_m X][R - X]} = \frac{k_{a,1}}{k_{d,1}} = K_{ATRA,RX}$$

$$[R^\bullet] = \frac{K_{ATRA,RX}}{K_{ATRA,AIBN}} \frac{[R - X]}{[I - X]} [I^\bullet]$$

Substituting this $[R^\bullet]$ expression into the original equation for the rate of disappearance of alkene in ATRA yields:

$$-\frac{d[alkene]}{dt} = k_{add} \frac{K_{ATRA,RX}}{K_{ATRA,AIBN}} \frac{[R - X]}{[I - X]} [I^\bullet][alkene] + k_p [I^\bullet][alkene]$$

This equation is not directly usable because it contains a term for the concentration of radicals $[I^\bullet]$ generated from the decomposition of AIBN. However, using steady-state approximation, this concentration can be easily estimated by assuming that the rate of initiation is equal to the rate of termination. In other words:

$$\frac{d[I^\bullet]}{dt} = 2k_{dc}[AIBN] = 2k_t[I^\bullet]^2 \approx 0$$

$$[I^\bullet] = \sqrt{\frac{k_{dc}}{k_t}[AIBN]}$$

Final substitution of the expression for $[I^*]$ gives the rate of disappearance of alkene in copper catalyzed ATRA containing free-radical initiator as a reducing agent (Eq. 3.1):

$$-\frac{d[alkene]}{dt} = \sqrt{\frac{k_{dc}}{k_t}} [AIBN] \left(k_{add} \frac{K_{ATRA,RX}}{K_{ATRA,AIBN}} \frac{[R-X]}{[I-X]} + k_p \right) [alkene] \quad (3.1)$$

From this equation, it is apparent that the rate depends not only on the concentrations of alkene, R-X and I-X, but also on the equilibrium constants $K_{ATRA,RX}$ and $K_{ATRA,AIBN}$, addition (k_{add}) and propagation (k_p) rate constants for alkene, as well as decomposition (k_{dc}) and termination (k_t) rate constants for AIBN. Surprisingly, the rate of alkene consumption is not dependent on the concentrations of copper(I) and copper(II) complexes. This is contrary to the derived rate law for copper catalyzed ATRA in the absence of a reducing agent (Eq. 3.2):²

$$-\frac{d[alkene]}{dt} = \frac{k_{a,1} k_{add} [Cu^I L_m X][RX][alkene]}{k_{d,1} [Cu^{II} L_m X_2]} = \frac{K_{ATRA} k_{add} [Cu^I L_m X][RX][alkene]}{[Cu^{II} L_m X_2]} \quad (3.2)$$

Several experimental results are consistent with the rate expression for alkene consumption derived in Eq. 3.1 and are further discussed in this chapter.

3.2 Experimental

3.2.1 General Procedures

All reagents were obtained from commercial sources. Styrene, 1-octene, and methyl acrylate were dried over calcium hydride and degassed prior to use. 2,2'-Azobis(isobutyronitrile) (AIBN) was recrystallized from cold methanol and dried at room

temperature under vacuum. Acetonitrile was degassed and deoxygenated using Innovative Technology solvent purifier. Carbon tetrachloride and anisole were deoxygenated by bubbling argon for 30 min before use. Tris(2-pyridylmethyl)amine (TPMA),³ tris[2-(*N,N*-dimethylamino)ethyl]amine (Me₆TREN)⁴ and copper(II) complexes [Cu^{II}(TPMA)Cl][Cl],⁵ [Cu^{II}(Me₆TREN)Cl][Cl],⁶ Cu^{II}(PMDETA)Cl⁷ (PMDETA=*N,N,N',N'',N''*-pentamethyldiethylenetriamine) and [Cu^{II}(bpy)₂Cl][Cl]⁸ (bpy=2,2'-bipyridine) were synthesized according to published procedures. All other reagents were used as received. Manipulations were performed under argon in a dry box (<1.0 ppm of O₂ and <0.5 ppm of H₂O) or using standard Schlenk line techniques. ¹H NMR spectra were obtained at room temperature on a Bruker Avance 400 MHz spectrometer with chemical shifts given in ppm relative to the residual solvent peak (CDCl₃, 7.26 ppm). UV-Vis spectra were recorded using Beckman DU-530 spectrometer.

3.2.2 Preparation of Catalyst Solutions

Cu^{II} catalysts solutions (0.025M) were prepared by dissolving the appropriate amount of Cu^{II} complex ([Cu^{II}(TPMA)Cl][Cl] = 106 mg, [Cu^{II}(Me₆TREN)Cl][Cl] = 91 mg, [Cu^{II}(PMDETA)Cl₂] = 77 mg, [Cu^{II}(bpy)₂Cl][Cl] = 112 mg) in 10 ml of acetonitrile.

3.2.3 Kinetic Studies

The desired amount of [Cu^{II}(TPMA)Cl][Cl], [Cu^{II}(Me₆TREN)Cl][Cl], Cu^{II}(PMDETA)Cl₂ or [Cu^{II}(bpy)Cl][Cl] (225 μL, 0.025 M solution in acetonitrile) was added to 2.0 mL of the acetonitrile solution containing CCl₄, alkene, AIBN, and the internal standard ([CCl₄]₀:[alkene]₀:[AIBN]₀ = 4:1:0.05, [alkene]₀=1.4 M) in a 10 ml

Schlenk flask equipped with a stirring bar. The alkene concentration in each reaction mixture was maintained at 0.95M by adding 900 μL of acetonitrile. The reaction flask was then immersed in a 60°C oil bath. Samples (approximately 100 μL) were taken periodically using purged syringes and analyzed using ^1H NMR spectroscopy.

3.2.4 Reduction of Copper(II) Complexes in the Presence of AIBN

Copper(II) solutions were prepared with the following initial concentrations using methanol as solvent: $[\text{Cu}^{\text{II}}(\text{Me}_6\text{TREN})\text{Cl}][\text{Cl}]_0=0.0028$ M, $[\text{Cu}^{\text{II}}(\text{TPMA})\text{Cl}][\text{Cl}]_0=0.0045$ M, $[\text{Cu}^{\text{II}}(\text{PMDETA})\text{Cl}_2]_0=0.0045$ M and $[\text{Cu}^{\text{II}}(\text{bpy})_2\text{Cl}][\text{Cl}]_0=0.01$ M. Catalyst solution (3 mL) and AIBN (10 eq. relative to copper(II) complex) were placed in airtight 10 mm quartz cell. The reaction mixture was heated at 60 °C for 3 h and the absorbance at λ_{max} ($[\text{Cu}^{\text{II}}(\text{Me}_6\text{TREN})\text{Cl}][\text{Cl}]=938$ nm, $[\text{Cu}^{\text{II}}(\text{TPMA})\text{Cl}][\text{Cl}]=967$ nm, $\text{Cu}^{\text{II}}(\text{PMDETA})\text{Cl}_2=698$ nm and $[\text{Cu}^{\text{II}}(\text{bpy})_2\text{Cl}][\text{Cl}]=736$ nm) monitored at timed intervals. The concentration of Cu^{II} was determined using extinction coefficient values calculated from Beer-Lambert's law: $\epsilon([\text{Cu}^{\text{II}}(\text{Me}_6\text{TREN})\text{Cl}][\text{Cl}])=413.9$ $\text{Lmol}^{-1}\text{cm}^{-1}$, $\epsilon([\text{Cu}^{\text{II}}(\text{TPMA})\text{Cl}][\text{Cl}])=192.1$ $\text{Lmol}^{-1}\text{cm}^{-1}$, $\epsilon(\text{Cu}^{\text{II}}(\text{PMDETA})\text{Cl}_2)=214.3$ $\text{Lmol}^{-1}\text{cm}^{-1}$ and $\epsilon([\text{Cu}^{\text{II}}(\text{bpy})_2\text{Cl}][\text{Cl}])=179.0$ $\text{Lmol}^{-1}\text{cm}^{-1}$.

3.3 Effect of Concentration and Nature of Catalyst on Observed Rate Constant (k_{obs})

First order kinetic plots for the ATRA of CCl_4 to methyl acrylate, styrene and 1-octene catalyzed by varying $[\text{Cu}^{\text{II}}(\text{TPMA})\text{Cl}][\text{Cl}]$ concentrations in the presence of AIBN as a reducing agent are shown in Figure 3.1. Linear plots were observed for all three alkenes, indicating constant concentration of radicals.

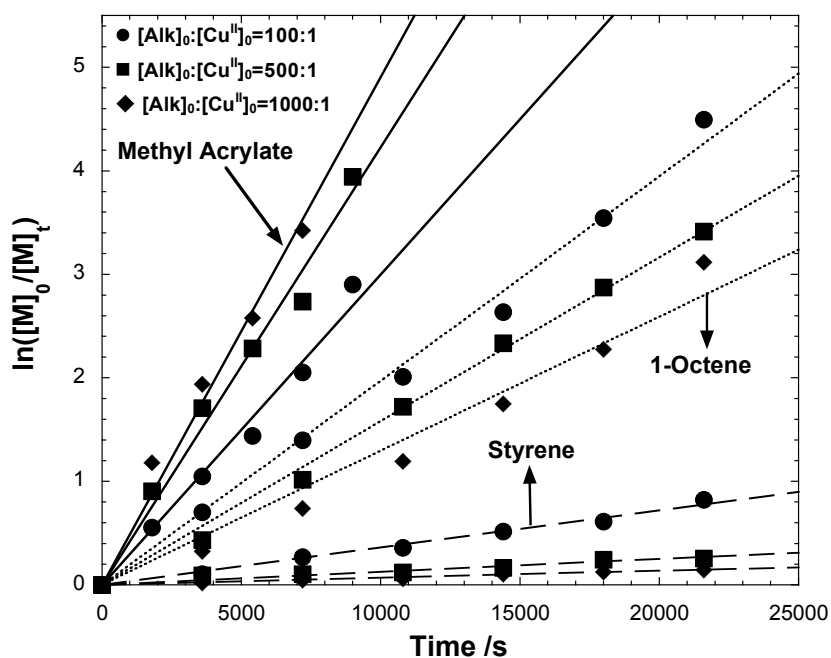


Figure 3.1. First-Order Kinetic Plot for the ATRA of CCl_4 to Methyl Acrylate (—), Styrene (----) and 1-Octene (...) Catalyzed by Varying $[\text{Cu}^{\text{II}}(\text{TPMA})\text{Cl}][\text{Cl}]$ Concentrations (1 mol% (\bullet), 0.2 mol% (\blacksquare) and 0.1 mol% (\blacklozenge)) in the Presence of AIBN. Experimental Conditions: $[\text{alkene}]_0:[\text{CCl}_4]_0:[\text{AIBN}]_0 = 1:4:0.05$, $[\text{alkene}]_0 = 0.95\text{M}$, solvent = CH_3CN , $T = 60^\circ\text{C}$.

The observed rate constants (k_{obs}) were calculated from the slopes and the results are summarized in Table 3.1. The order of the k_{obs} values were as follows: methyl acrylate > 1-octene > styrene.

Table 3.1. Values of k_{obs} (s^{-1}) for the ATRA of CCl_4 to Alkenes with Varying Concentrations of $[Cu^{II}(TPMA)Cl][Cl]^a$

$[alkene]_0:[Cu^{II}]_0$	1-octene	styrene	methyl acrylate
100:1	$(2.1 \pm 0.09) \times 10^{-4}$	$(3.8 \pm 0.20) \times 10^{-5}$	$(3.2 \pm 0.28) \times 10^{-4}$
500:1	$(1.7 \pm 0.04) \times 10^{-4}$	$(1.0 \pm 0.14) \times 10^{-5}$	$(4.0 \pm 0.38) \times 10^{-4}$
1000:1	$(1.5 \pm 0.09) \times 10^{-4}$	$(0.7 \pm 0.05) \times 10^{-5}$	$(4.9 \pm 0.15) \times 10^{-4}$

^a $[alkene]_0:[CCl_4]_0:[AIBN]_0 = 1:4:0.05$, $[alkene]_0 = 0.95M$, solvent= CH_3CN , $T=60$ °C. Errors are given at 95% confidence limits.

In the case of 1-octene, a ten time decrease in the concentration of $[Cu^{II}(TPMA)Cl][Cl]$ resulted in only slight decrease in the observed rate constant ($k_{obs}=(2.1\pm 0.09)\times 10^{-4} s^{-1}$ (100:1) and $(1.5\pm 0.09)\times 10^{-4} s^{-1}$ (1000:1)). Similar results were also observed for methyl acrylate ($k_{obs}=(3.2\pm 0.28)\times 10^{-4} s^{-1}$ (100:1) and $(4.9\pm 0.15)\times 10^{-4}$ (1000:1)). Relatively small variations in k_{obs} values are consistent with Eq. 3.1, which predicts that the rate of alkene consumption should be independent on catalyst concentration. On the other hand, a more pronounced effect of the $[Cu^{II}(TPMA)Cl][Cl]$ concentration was observed for styrene. Increasing styrene to copper(II) ratio from 100:1 to 1000:1 resulted in approximately five times decrease in the observed rate constant ($(3.8\pm 0.20)\times 10^{-5} s^{-1}$ to $(0.7\pm 0.05)\times 10^{-5} s^{-1}$). The origin of this decrease in the rate of styrene consumption is presently not clear. One possibility could include the coordination of styrene radicals to the copper(I) center, which would be more pronounced at higher catalyst loadings. Additionally, the reaction kinetics could be more complicated by the generation of radicals from thermal decomposition of styrene.⁹

Eq. 3.1 predicts that the rate of alkene consumption in copper catalyzed ATRA in the presence of free-radical diazo initiator as reducing agent should also depend on the ratio of equilibrium constants $K_{ATRA,RX}$ and $K_{ATRA,AIBN}$. In order to examine the effect of the nature of copper catalyst, several different complexing ligands, namely tris(2-pyridylmethyl)amine (TPMA), tris[2-(*N,N*-dimethylamino)ethyl]amine (Me_6TREN), *N,N,N',N'',N''*-pentamethyldiethylenetriamine (PMDETA), and 2,2'-bipyridine (bpy) were utilized in ATRA studies. K_{ATRA} values for copper(I) complexes with these ligands in CH_3CN at 35 °C have been shown to span more than four orders of magnitude (e.g. K_{ATRA} (ethyl 2-bromoisobutyrate)= 1.54×10^{-4} (Me_6TREN), 9.65×10^{-6} (TPMA), 7.46×10^{-8} (PMDETA) and 3.93×10^{-9} (bpy)).^{10,11} First- order kinetic plots for the ATRA of CCl_4 to methyl acrylate in the presence of different copper(II) catalysts and AIBN are shown in Figure 3.2a.

Linearity was observed for all complexes investigated, indicating constant radical concentration in each reaction system. The observed rate constants (k_{obs} , Table 3.) were found not to be very dependent on the nature of the catalyst.

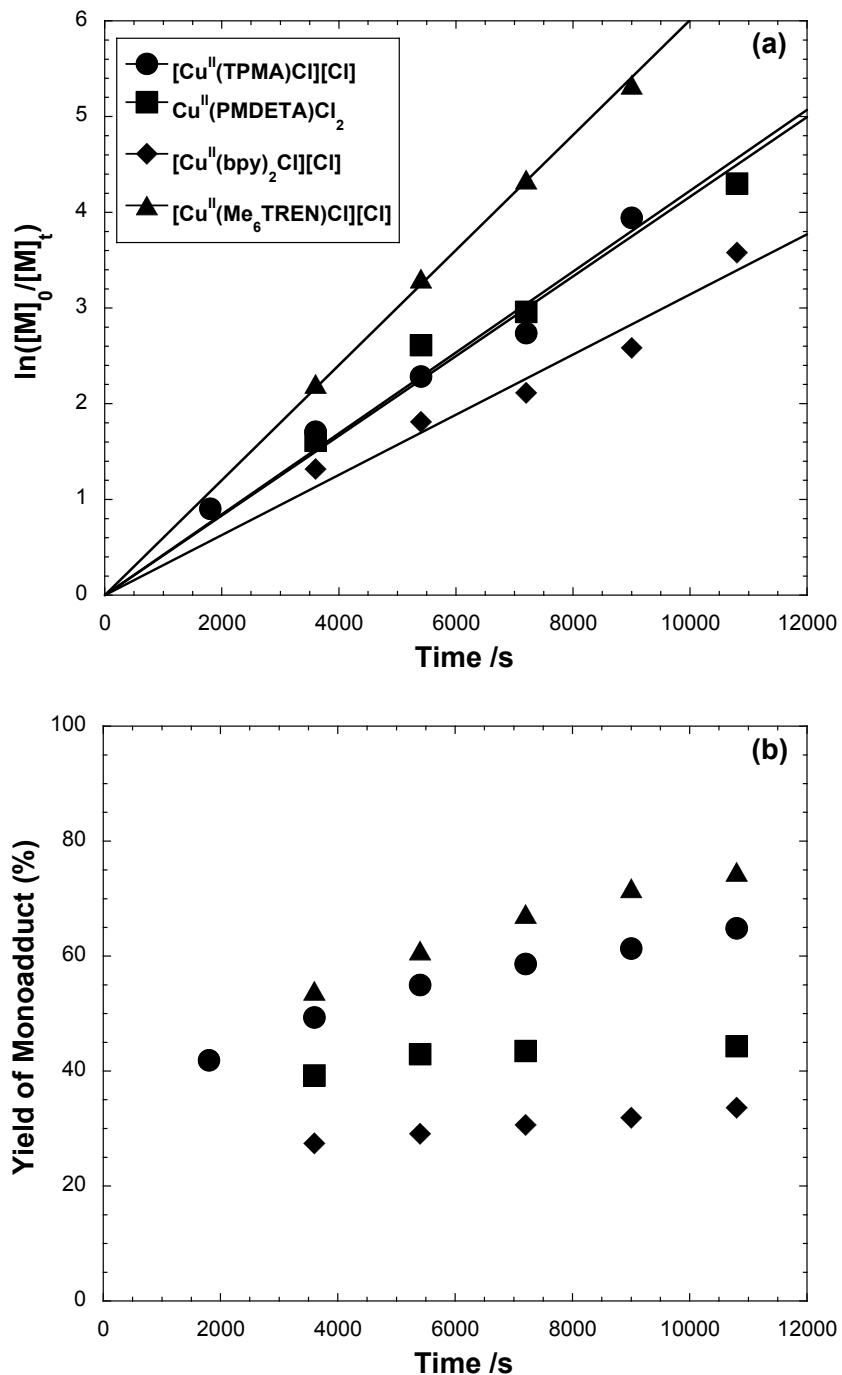


Figure 3.2. Plots of (a) $\ln([M]_0/[M]_t)$ and (b) Percent Yield of Monoadduct Versus Time for the ATRA of CCl₄ to Methyl Acrylate Catalyzed by Copper(II) Complexes with TPMA, PMDETA, bpy, and Me₆TREN Ligands. Experimental conditions: $[MA]_0:[Cu^{II}]_0:[CCl_4]_0:[AIBN]_0 = 500:1:2000:25$, $[MA]_0 = 0.95M$, solvent = CH₃CN, T = 60°C.

Table 3.2. Values of k_{obs} (s^{-1}) for the ATRA of CCl_4 to Styrene and Methyl Acrylate Catalyzed by Different Copper(II) Complexes^a

Cu ^{II} complex	styrene	methyl acrylate
[Cu ^{II} (Me ₆ TREN)Cl][Cl]	$(1.24 \pm 0.17) \times 10^{-5}$	$(5.80 \pm 0.11) \times 10^{-4}$
[Cu ^{II} (TPMA)Cl][Cl]	$(1.28 \pm 0.09) \times 10^{-5}$	$(4.00 \pm 0.38) \times 10^{-4}$
[Cu ^{II} (PMDETA)Cl][Cl]	$(1.26 \pm 0.26) \times 10^{-5}$	$(3.60 \pm 0.36) \times 10^{-4}$
[Cu ^{II} (bpy) ₂ Cl][Cl]	$(1.20 \pm 0.23) \times 10^{-5}$	$(3.40 \pm 0.64) \times 10^{-4}$

^a[alkene]:[Cu^{II}]:[CCl₄]:[AIBN] = 500:1:2000:25, [alkene]₀ = 0.95M, solvent=CH₃CN, T=60 °C. Errors are given at 95% confidence limits.

For styrene, the value for k_{obs} was approximately $1.2 \times 10^{-5} s^{-1}$, and for methyl acrylate it was found to differ by less than a factor of 2 ($3.0-5.0 \times 10^{-4} s^{-1}$). Similar results were also obtained from kinetic modeling of mechanistically similar ICAR (initiators for continuous activator regeneration) ATRP.⁹ These results indicate that regardless of the choice of catalyst, the ratio of equilibrium constants $K_{ATRA,RX}/K_{ATRA,AIBN}$ should remain nearly constant, which is consistent with the rate law derived in Eq. 3.1. Since we have demonstrated that the rate of alkene consumption in copper catalyzed ATRA in the presence of free-radical diazo initiators is independent on the nature of the catalyst, one question that remains to be answered is whether any copper complex could be used in this catalytic system. In order to answer this question, product selectivity needs to be taken into account. The concentration of deactivator (copper(II) complex) and the deactivation rate constant ($k_{d,2}$, Scheme 3.1) play a crucial role. Monoadduct in ATRA will be formed in high yield only if the rate of radical trapping ($k_{d,2}[Cu^{II}][R-CH_2-CHR'^{\bullet}]$) is much higher than the rate of radical polymerization ($k_p[alkene][R-CH_2-CHR'^{\bullet}]$). Since the deactivation rate constant in ATRA is catalyst dependent^{10,12,13} and the amount of

copper(II) in the system is governed by both $k_{d,AIBN}$ and $k_{a,AIBN}$, the yield of monoadduct must depend on the nature of the catalyst. As evident from Figure 3.2b, this was indeed observed. For highly active catalysts such as $[Cu^{II}(Me_6TREN)Cl][Cl]$ and $[Cu^{II}(TPMA)Cl][Cl]$, 65-75% yield of the monoadduct was obtained after 3 h. Catalysts with smaller values of K_{ATRA} such as $Cu^{II}(PMDETA)Cl_2$ and $[Cu^{II}(bpy)_2Cl][Cl]$ only yielded 40 and 30% of the monoadduct, respectively.

3.4 Effect of AIBN Concentration of Observed Rate Constant (k_{obs})

Similar experiments were also conducted with AIBN in order to examine the concentration effect on the reaction rates. For ATRA of CCl_4 to 1-octene catalyzed by $[Cu^{II}(TPMA)Cl][Cl]$, the apparent reaction order was 0.38 with respect to AIBN, which is close to 0.5 predicted from the above derived rate law (Eq. 3.1). Similarly, the reaction order with respect to AIBN was found to be 0.38 and 0.50 in the case of styrene and methyl acrylate, respectively. Furthermore, the rate of consumption of 1-octene, styrene and methyl acrylate was found to increase as the concentration of alkene or CCl_4 increased. Lastly, consistent with Eq. 3.1, the rate decreased as the concentration of I-X (chlorine trapped radicals generated from the decomposition of AIBN, $(CH_3)_2C(CN)Cl$, Scheme 3.1) increased.

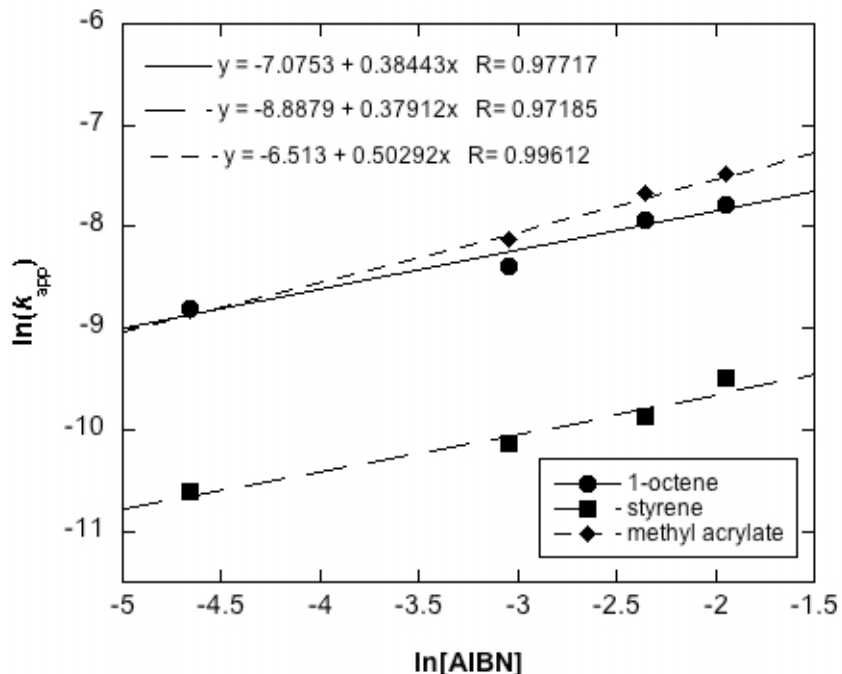


Figure 3.3. Plot of $\ln(k_{app})$ Versus $\ln[AIBN]$. Experimental Conditions: $[alkene]_0:[Cu^{II}]_0:[CCl_4]_0:[AIBN]_0 = 500:1:2000:25$, $[alkene]_0 = 0.95M$, solvent = CH_3CN , $T = 60^\circ C$.

3.5 Reduction of Copper(II) to Copper(I) in the Presence of AIBN

Under typical experimental conditions ($400:1 < [Cu^{II}]_0:[CCl_4]_0 < 10000:1$), we were unable to accurately determine the amount of copper(II) and consequently copper(I) in the ATRA reactions containing AIBN as a reducing agent. The principal reason was that the large amount of CCl_4 resulted in the shift of the equilibrium constant for atom transfer, favoring copper(II) complex. In order to demonstrate that the amount of copper(II) in the reaction is also governed by both $k_{d,AIBN}$ and $k_{a,AIBN}$, UV-Vis experiments were performed at $60^\circ C$ for a model system containing only the copper(II) complex and AIBN. As shown in Figure 3.4, gradual conversion of $[Cu^{II}(bpy)_2Cl][Cl]$ to $[Cu^I(bpy)_2][Cl]$ was observed in the presence of AIBN.

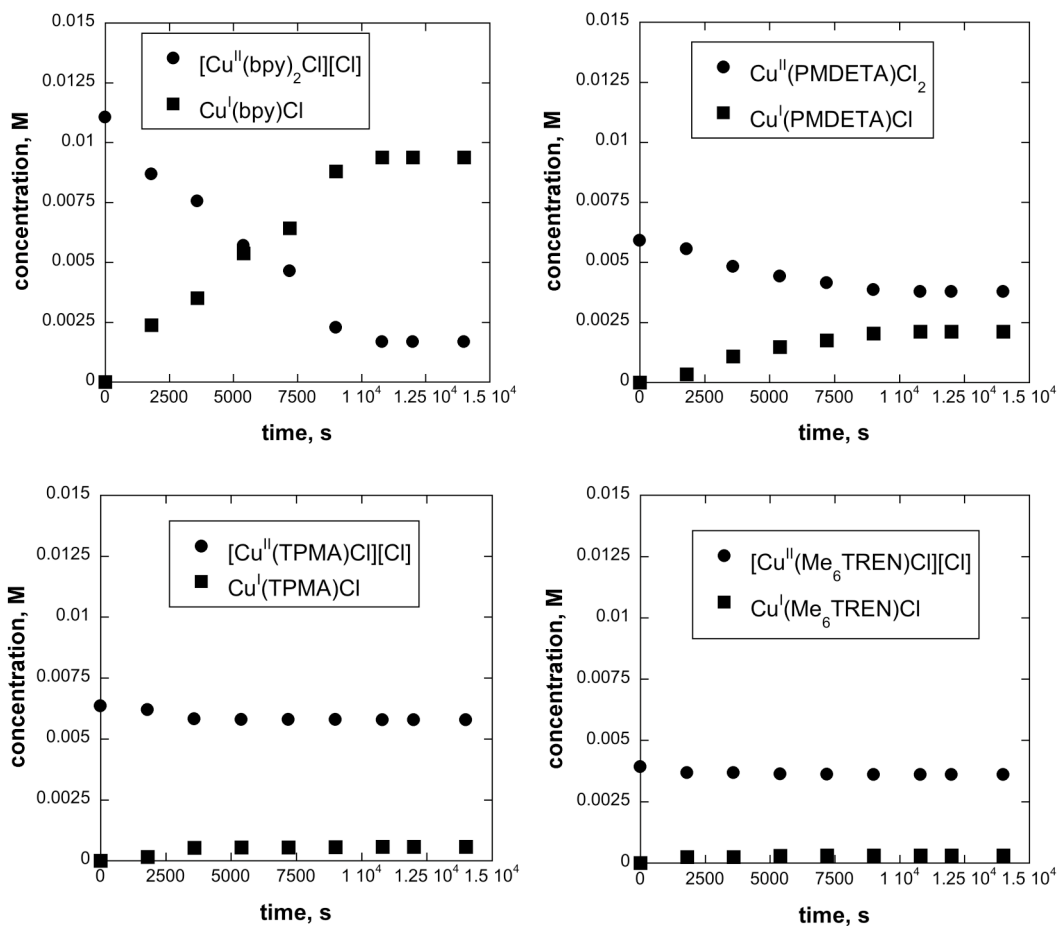


Figure 3.4. Reduction of Copper(II) Complexes with bpy, PMDETA, TPMA and Me₆TREN Ligands in the Presence of AIBN as a Reducing agent in CH₃OH at 60 °C, [Cu^{II}]₀: [AIBN]₀ = 1:10.

After 3 hours, the original amount of copper(II) complex decreased nearly 85% and remained constant, indicating that the ATRA equilibrium ($\text{Cu}^{\text{II}} + \text{I-X} \rightleftharpoons \text{X-Cu}^{\text{I}} + \text{I}^{\cdot}$, I[·] denotes radicals formed from the decomposition of AIBN, Scheme 3.1) had been established. The addition of large excess of CCl₄ (200 equiv.) to the reaction mixture shifted the equilibrium back to $[\text{Cu}^{\text{II}}(\text{bpy})_2\text{Cl}][\text{Cl}]$, confirming that the corresponding $[\text{Cu}^{\text{I}}(\text{bpy})_2][\text{Cl}]$ was indeed generated in the system. This could also be visually observed in the change of the reaction color from dark red

([Cu^I(bpy)₂][Cl]) to green ([Cu^{II}(bpy)₂Cl][Cl]). The ATRA equilibrium should in theory persist for as long as there is a constant source of radicals in the system generated from the decomposition of AIBN (approximately 5 days for 99% conversion, assuming $k_{dc}(\text{AIBN})=1.0\times 10^{-5} \text{ s}^{-1}$). After AIBN has been depleted, [Cu^I(bpy)₂][Cl] will slowly convert to [Cu^{II}(bpy)₂Cl][Cl] complex (as a result of unavoidable radical-radical termination reactions). The kinetics of this process is governed by the persistent radical effect,¹⁰ originally developed by Fischer¹⁴⁻¹⁸ and Fukuda.¹⁹

A decrease in the copper(II) concentration was also observed for complexes with PMDETA, TPMA and Me₆TREN ligands (Figure 3.4), although the extent of the change differed significantly. After 3 hours, the concentration of Cu^{II}(PMDETA)Cl₂ decreased 36%, while only 10% and 15% change was observed for [Cu^{II}(TPMA)Cl][Cl] and [Cu^{II}(Me₆TREN)Cl][Cl] complexes, respectively. These results further confirm that the amounts of copper(II) and copper(I) complexes in ATRA containing AIBN are governed by both $k_{d,\text{AIBN}}$ and $k_{a,\text{AIBN}}$. Further mechanistic studies of this novel catalytic system are subject to future investigation in our laboratories.

3.6 Conclusions

In summary, kinetic features of ATRA of CCl_4 to 1-octene, styrene and methyl acrylate catalyzed by $[\text{Cu}^{\text{II}}(\text{TPMA})\text{Cl}][\text{Cl}]$ in the presence of free-radical diazo initiator (AIBN) as a reducing agent were investigated. The amounts of copper(II) and copper(I) complexes in ATRA in the presence of AIBN were found to be governed by both $k_{\text{d,AIBN}}$ and $k_{\text{a,AIBN}}$. Kinetic studies of the ATRA process revealed that the rate of alkene consumption was dependent on the concentration and rate of decomposition of free-radical diazo initiator, but independent on the nature and concentration of copper catalyst. However, the percent yield of the monoadduct ultimately depended on the nature of the catalyst.

References

- (1) Odian, G., *Principles of Polymerization*, 4th ed., John Wiley & Sons, Hoboken, **2004**.
- (2) Pintauer, T.; Matyjaszewski, K. Atom Transfer Radical Addition and Polymerization Reactions Catalyzed by ppm Amounts of Copper Complexes. *Chem. Soc. Rev.* **2008**, *37*, 1087-1097.
- (3) Tyeklar, Z.; Jacobson, R. R.; Wei, N.; Murthy, N. N.; Zubieta, J.; Karlin, K. D. Reversible Reaction of Dioxygen (and Carbon Monoxide) with a Copper(I) Complex. X-Ray Structures of Relevant Mononuclear Cu(I) Precursor Adducts and the Trans-(μ -1,2-peroxo)dicopper(II) Product. *J. Am. Chem. Soc.* **1993**, *115*(7), 2677-2689.
- (4) Ciampolini, M.; Nardi, N. Five-Coordinated High-Spin Complexes of Bivalent Cobalt, Nickel, and Copper with Tris(2-dimethylaminoethyl)amine. *Inorg. Chem.* **1966**, *5*(1), 41-44.
- (5) Eckenhoff, W. T.; Garrity, S. T.; Pintauer, T. Highly Efficient Copper-Mediated Atom-Transfer Radical Addition (ATRA) in the Presence of Reducing Agent. *Eur. J. Inorg. Chem.* **2008**(4), 563-571.
- (6) Barbucci, R.; Mastroianni, A.; Campbell, M. J. M. The Effect of N-Alkylation on the Properties of Five-Coordinate Copper(II) Complexes of Tetraamine Ligands. *Inorg. Chim. Acta.* **1978**, *27*(1), 109-114.
- (7) Margraf, G.; Bats, J. W.; Wagner, M.; Lerner, H.-W. Copper(II) PMDETA and copper(II) TMEDA Complexes: Precursors for the Synthesis of Dinuclear Dicationic Copper(II) Complexes. *Inorg. Chim. Acta.* **2005**, *358*(4), 1193-1203.
- (8) Stephens, F. S.; Tucker, P. A. Crystal and Molecular Structure of Chloro Bis(2,2'-bipyridyl)copper(II) Chloride Hexahydrate. *J. Chem. Soc., Dalton Trans.* **1973**, *21*, 2293-2297.
- (9) Matyjaszewski, K.; Jakubowski, W.; Min, K.; Tang, W.; Huang, J.; Braunecker, W. A.; Tsarevsky, N. V. Diminishing Catalyst Concentration in Atom Transfer Radical Polymerization with Reducing Agents. *Proc. Natl. Acad. Sci. U.S.A.* **2006**, *103*, 15309-15314.

- (10) Tang, W.; Tsarevsky, N. V.; Matyjaszewski, K. Determination of Equilibrium Constants for Atom Transfer Radical Polymerization. *J. Am. Chem. Soc.* **2006**, *128*(5), 1598-1604.
- (11) Tang, W.; Kwak, Y.; Braunecker, W.; Tsarevsky, N. V.; Coote, M. L.; Matyjaszewski, K. Understanding Atom Transfer Radical Polymerization: Effect of Ligand and Initiator Structures on the Equilibrium Constants. *J. Am. Chem. Soc.* **2008**, *130*(32), 10702-10713.
- (12) Matyjaszewski, K.; Gobelt, B.; Paik, H.-j.; Horwitz, C. P. Tridentate Nitrogen-Based Ligands in Cu-Based ATRP: A Structure-Activity Study. *Macromolecules.* **2001**, *34*(3), 430-440.
- (13) Matyjaszewski, K.; Paik, H.-j.; Zhou, P.; Diamanti, S. J. Determination of Activation and Deactivation Rate Constants of Model Compounds in Atom Transfer Radical Polymerization. *Macromolecules.* **2001**, *34*(15), 5125-5131.
- (14) Fischer, H. Unusual Selectivities of Radical Reactions by Internal Suppression of Fast Modes. *J. Am. Chem. Soc.* **1986**, *108*, 3925-3927.
- (15) Fischer, H. The persistent radical effect in controlled radical polymerizations. *J. Polym. Sci. Part A: Polym. Chem.* **1999**, *37*(13), 1885-1901.
- (16) Fischer, H. The Persistent Radical Effect: A Principle for Selective Radical Reactions and Living Radical Polymerizations. *Chem. Rev.* **2001**, *101*(12), 3581-3610.
- (17) Fischer, H.; Radom, L. Factors Controlling the Addition of Carbon-Centered Radicals to Alkenes – An Experimental and Theoretical Perspective. *Angew. Chem. Int. Ed.* **2001**, *40*, 1340-1371.
- (18) Fischer, H.; Radom, L. Factors Controlling the Addition of Carbon-Centered Radicals to Alkenes. *Macromol. Symp.* **2002**, *182*, 1-14.
- (19) Goto, A.; Fukuda, T. Kinetics of Living Radical Polymerization. *Prog. Polym. Sci.* **2004**, *29*, 329-385.

Chapter 4

Determination of Kinetic Parameters for Catalyst Regeneration in Atom Transfer Radical Addition in the Presence of a Reducing Agent: An Experimental and Theoretical Approach

The kinetic parameters for the regeneration of catalyst in atom transfer radical addition in the presence of a free-radical diazo initiator (AIBN) as a reducing agent were determined using both experimental and theoretical techniques. The rate of decomposition of AIBN (k_{dc}) in various solvents and additives was determined at 60°C using UV-Vis spectroscopy. Rate of deactivation ($k_{d,AIBN}$) of various Cu^{II} complexes by radicals generated from the decomposition of AIBN were measured using TEMPO-trapping method in a competitive reaction along with ¹H NMR spectroscopy. Activation rate constants ($k_{a,AIBN}$) were finally determined utilizing the rates of decomposition of AIBN (k_{dc}), deactivation rate constants ($k_{d,AIBN}$) and kinetic modeling. The effect of $k_{a,AIBN}$, $k_{d,AIBN}$, k_{dc} , and initial AIBN concentration on the overall Cu^I and Cu^{II} concentrations in the initiation step of an ATRA process were also evaluated through kinetic modeling.

4.1 Introduction

Transition metal catalyzed atom transfer radical addition (TMC ATRA) is a very useful synthetic tool for carbon-carbon bond formation.¹⁻⁴ It has been successfully employed on a variety of halogenated alkanes^{2,5-10} and alkenes¹¹⁻¹⁴ in both intermolecular and intramolecular manner using various metal complexes such as those of copper,^{1,7,15,16} ruthenium,¹⁷⁻²¹ iron,^{7,22-25} and nickel²⁶⁻²⁸ as catalysts. Until recently, the major drawback of this versatile tool remained the large amounts of metal catalysts required (as high as 30 mol% relative to alkene) to achieve quantitative yields and high selectivity towards the desired monoadduct.^{1,15,29-31} The reason for this was the inevitable accumulation of the higher-oxidation-state metal complex that is present as a persistent radical, as a result of unavoidable radical termination reactions. Research has been geared towards finding alternative methods in making atom transfer radical reactions more economically and environmentally friendly processes.³²⁻⁴⁰ One methodology for catalyst regeneration, which has been originally developed for the mechanistically similar atom transfer radical polymerization (ATRP), is termed as initiators for continuous activator regeneration (ICAR),⁴¹⁻⁴³ in which radicals formed from the decomposition of free radical initiators such as 2,2'-azobisisobutyronitrile (AIBN) continuously regenerate the catalytically active lower oxidation state transition metal complex (activator) by the abstraction of a halogen atom from the higher oxidation state complex (deactivator) (Scheme 3.1). This technique has been successfully adopted for ATRA reactions which greatly reduced the amount of metal catalyst used to ppm levels.^{34,38,39,44}

In the previous chapter, a rate law for ATRA in the presence of AIBN was derived.³⁷ In deriving the kinetic rate law, the reaction steps involving the free radical

initiator (AIBN), which are the decomposition of AIBN (k_{dc}), the reduction of Cu^{II} to Cu^{I} in the presence of AIBN ($k_{a,\text{AIBN}}$ and $k_{d,\text{AIBN}}$), and the AIBN-initiated free radical polymerization reaction ($k_{p,\text{AIBN}}$) were taken into account (Scheme 3.1). The rate of alkene consumption was then found to be dependent on the initial concentration of the radical initiator and its decomposition and termination rate constants (Eq. 4.1) but not on the concentrations of Cu^{I} and Cu^{II} , which is contrary to the derived rate law for copper-catalyzed ATRA in the absence of a reducing agent (Eq. 4.2).³⁴

$$-\frac{d[\text{alkene}]}{dt} = \sqrt{\frac{k_{dc}}{k_t}} [\text{AIBN}] \left(k_{add} \frac{K_{\text{ATRA},\text{Rx}}}{K_{\text{ATRA},\text{AIBN}}} \frac{[\text{R}-\text{X}]}{[\text{I}-\text{X}]} - + k_p \right) [\text{alkene}] \quad (4.1)$$

$$-\frac{d[\text{alkene}]}{dt} = k_{add} K_{\text{ATRA}} [\text{R}-\text{X}] \frac{[\text{Cu}^{\text{I}}\text{LX}]}{[\text{Cu}^{\text{II}}\text{LX}_2]} [\text{alkene}] \quad (4.2)$$

Kinetic experiments have confirmed that the observed rate of ATRA (k_{obs}) was indeed not dependent on the concentration and nature of the catalyst and the apparent order of the reaction with respect to AIBN was determined to be close to 0.5, which strongly supports the newly derived rate law (Eq. 4.1). However, product selectivity was found to be highly dependent on the nature of the catalyst, i.e. active catalysts with higher equilibrium constants (K_{ATRA}) (where K_{ATRA} is the ratio between the activation (k_a) and deactivation (k_d) rate constants) such as $[\text{Cu}^{\text{II}}(\text{Me}_6\text{TREN})\text{Cl}][\text{Cl}]$ ($\text{Me}_6\text{TREN}=\text{tris}[2-(N,N\text{-dimethylamino})\text{ethyl}]\text{amine}$) and $[\text{Cu}^{\text{II}}(\text{TPMA})\text{Cl}][\text{Cl}]$ ($\text{TPMA}=\text{tris}(2\text{-pyridylmethyl})\text{amine}$) produced higher yields of the monoadduct compared to the less active catalyst such as $[\text{Cu}^{\text{II}}(\text{PMDETA})\text{Cl}_2]$ ($\text{PMDETA}=\text{tris}(2\text{-pyridylmethyl})\text{amine}$).

pentamethyldiethylenetriamine) and $[\text{Cu}^{\text{II}}(\text{bpy})_2\text{Cl}][\text{Cl}]$ (bpy=2,2'-bipyridine). Results from UV-Vis experiments of model reaction systems containing only AIBN and a Cu^{II} complex also revealed that the amount of Cu^{II} is governed by $k_{\text{d,AIBN}}$ and $k_{\text{a,AIBN}}$ and that the highly active catalysts $[\text{Cu}^{\text{II}}(\text{TPMA})\text{Cl}][\text{Cl}]$ and $[\text{Cu}^{\text{II}}(\text{Me}_6\text{TREN})\text{Cl}][\text{Cl}]$ have higher overall Cu^{II} concentration than the less active $[\text{Cu}^{\text{II}}(\text{bpy})_2\text{Cl}][\text{Cl}]$ and $[\text{Cu}^{\text{II}}(\text{PMDETA})\text{Cl}_2]$ catalysts. Determination of the kinetic parameters for the reduction of the deactivator species in copper-catalyzed ATRA in the presence of AIBN is therefore highly crucial in the quantification of the efficiency of various copper(II) catalysts in the reaction systems. Several research groups have extensively studied and measured the k_{a} and k_{d} values for a number of $\text{Cu}^{\text{I}}/\text{Cu}^{\text{II}}$ complexes coupled with various radical initiators using different techniques and methods.⁴⁵⁻⁵³ However, to the best of our knowledge, the k_{a} and k_{d} values of copper-catalyzed ATRA systems using highly active alkyl halides (e.g. 2-chloro-2-methylpropanenitrile or AIBN-Cl) have not yet been determined. In this paper, we measured the rate constants of the initiation steps in copper-catalyzed ATRA in the presence of AIBN as reducing agent, such as the rate of decomposition of the radical initiator (k_{dc}), deactivation rate constants ($k_{\text{d,AIBN}}$) and estimated activation rate constants ($k_{\text{a,AIBN}}$) and equilibrium constant (K_{ATRA}) using a combination of spectroscopic and theoretical methods.

4.2 Experimental

4.2.1 General Procedures

All reagents were obtained from commercial sources. 2,2'-Azobis(isobutyronitrile) (AIBN) was recrystallized from cold methanol and dried at room temperature under vacuum. Solvents (acetonitrile and methanol) were degassed and deoxygenated using Innovative Technology solvent purifier. Tris(2-pyridylmethyl)amine (TPMA),⁵⁴ tris[2-(*N,N*-dimethylamino)ethyl]amine (Me₆TREN)⁵⁵ and copper(II) complexes [Cu^{II}(TPMA)Cl][Cl],⁵⁶ [Cu^{II}(Me₆TREN)Cl][Cl],⁵⁷ Cu^{II}(PMDETA)Cl₂⁵⁸ (PMDETA=*N,N,N',N'',N''*-pentamethyldiethylenetriamine) and [Cu^{II}(bpy)₂Cl][Cl]⁵⁹ (bpy=2,2'-bipyridine) were synthesized according to published procedures. All other reagents were used as received. Manipulations were performed under argon in a dry box (<1.0 ppm of O₂ and <0.5 ppm of H₂O) or using standard Schlenk line techniques unless specified otherwise. ¹H NMR spectra were obtained at room temperature on a Bruker Avance 400 MHz spectrometer with chemical shifts given in ppm relative to the residual solvent peak (CDCl₃, 7.26 ppm). UV-Vis spectra were recorded using Beckman DU-530 spectrometer. Kinetic modelling was performed using Chemical Kinetics Simulator (IBM's Almaden Research Center).⁶⁰

4.2.2 Measurement of the Rate of Decomposition of AIBN

AIBN solutions (0.08 M) were prepared by dissolving AIBN (39.5 mg, 0.24 mmol) in 3.0 mL of acetonitrile or methanol (UV-Vis) or d-acetonitrile (¹H NMR). Anisole (26 μL, 0.24 mmol) and *p*-dimethoxybenzene (33.0 mg, 0.24 mmol) were then added to two separate vials with the CD₃CN solution of AIBN. The solutions were then placed in an airtight 10 mm quartz cell (UV-Vis) or a Schlenk flask (¹H NMR), purged

with argon, capped, and heated at 60°C in an oil bath. Samples were taken at timed intervals and the absorbance of AIBN at λ_{max} 345 nm and the ^1H NMR peak at 1.65 ppm were monitored. The concentration of AIBN in the case of UV-Vis measurements was determined using the extinction coefficient value calculated from Beer-Lambert's law ($\epsilon=11.956 \text{ L mol}^{-1} \text{ cm}^{-1}$).

4.2.3 Measurement of Deactivation Rate Constant

A stock solution of AIBN (17.0 mg, 0.10 mmol) and TEMPO (47.6 mg, 0.3 mmol) was prepared in methanol. Copper(II) catalyst solutions (0.025 M) were prepared *in situ* by dissolving the appropriate ligand in a CuCl_2 solution in methanol. The desired amount of copper(II) catalyst was then added to 0.15 mL of the AIBN/ TEMPO stock solution and the reaction mixture was stirred at 40°C for 5 days. The solution was then passed through basic alumina to remove the Cu^{II} complex and the solvent was evaporated using a rotavap. The amounts of AIBN-Cl and AIBN-TEMPO were monitored using ^1H NMR. ^1H NMR [CDCl_3 , 400 MHz, RT]: $\delta = 1.72$ (s, AIBN-Cl), 1.52 (s, AIBN-TEMPO), 1.23 (b, AIBN-TEMPO), 0.85 (t, AIBN-TEMPO).

4.2.4 Reduction of Copper(II) Complexes in the Presence of AIBN

Copper(II) solutions were prepared with the following initial concentrations using methanol as solvent: $[\text{Cu}^{\text{II}}(\text{Me}_6\text{TREN})\text{Cl}][\text{Cl}]_0=0.0028 \text{ M}$, $[\text{Cu}^{\text{II}}(\text{TPMA})\text{Cl}][\text{Cl}]_0=0.0045 \text{ M}$, $[\text{Cu}^{\text{II}}(\text{PMDETA})\text{Cl}_2]_0=0.0045 \text{ M}$ and $[\text{Cu}^{\text{II}}(\text{bpy})_2\text{Cl}][\text{Cl}]_0=0.01 \text{ M}$. Catalyst solution (3 mL) and AIBN (10 eq. relative to copper(II) complex) were placed in airtight 10 mm quartz cell. The reaction mixture

was heated at 60°C for 3 h and the absorbance at λ_{\max} ($[\text{Cu}^{\text{II}}(\text{Me}_6\text{TREN})\text{Cl}][\text{Cl}]=938$ nm, $[\text{Cu}^{\text{II}}(\text{TPMA})\text{Cl}][\text{Cl}]=967$ nm, $\text{Cu}^{\text{II}}(\text{PMDETA})\text{Cl}_2=698$ nm and $[\text{Cu}^{\text{II}}(\text{bpy})_2\text{Cl}][\text{Cl}]=736$ nm) monitored at timed intervals. The concentration of Cu^{II} was determined using extinction coefficient values calculated from Beer-Lambert's law: $\epsilon([\text{Cu}^{\text{II}}(\text{Me}_6\text{TREN})\text{Cl}][\text{Cl}])=413.9 \text{ Lmol}^{-1}\text{cm}^{-1}$, $\epsilon([\text{Cu}^{\text{II}}(\text{TPMA})\text{Cl}][\text{Cl}])= 192.1 \text{ Lmol}^{-1}\text{cm}^{-1}$, $\epsilon(\text{Cu}^{\text{II}}(\text{PMDETA})\text{Cl}_2)= 214.3 \text{ Lmol}^{-1}\text{cm}^{-1}$ and $\epsilon([\text{Cu}^{\text{II}}(\text{bpy})_2\text{Cl}][\text{Cl}])= 179.0 \text{ Lmol}^{-1}\text{cm}^{-1}$.

4.3 Results and Discussion

4.3.1 Measurement of the Rate of Decomposition of AIBN

The thermal decomposition of AIBN in various solvents has been widely studied and is found to follow first-order kinetics.⁶¹⁻⁶³ The rate of AIBN decomposition has been measured employing different techniques such as monitoring the consumption of the azo initiator using spectroscopic analysis, volumetric determination of the nitrogen liberated during the reaction and radical trapping methods. Several authors have also reported that the decomposition rate constant of AIBN at a given temperature depends on the nature of the reaction medium due to cage effect.⁶³⁻⁶⁵

In this study, the rate of decomposition of AIBN (k_{dc}) at 60°C was determined using acetonitrile and methanol as solvent and also in the presence of additives such as anisole and *p*-dimethoxybenzene (commonly used internal standards for ATRA reactions). The consumption of AIBN was then monitored using ^1H NMR and UV spectroscopy. The absorption of the N=N bond in the UV region at 345 nm allows for the determination of

the concentration of AIBN over a period of time. The consumption of AIBN was then plotted as a function of time and from the slope of the linear regression, the rate constant of decomposition, k_{dc} , of AIBN was determined and are summarized in Table 4.1.

Table 4.1. Decomposition Rate Constant of AIBN at 60°C^a

Solvent/Additive	k_{dc} (s ⁻¹)
d-acetonitrile/anisole ^b	1.2×10^{-5}
d-acetonitrile/ <i>p</i> -dimethoxybenzene ^b	1.2×10^{-5}
acetonitrile ^c	3.8×10^{-6}
methanol ^c	2.7×10^{-6}

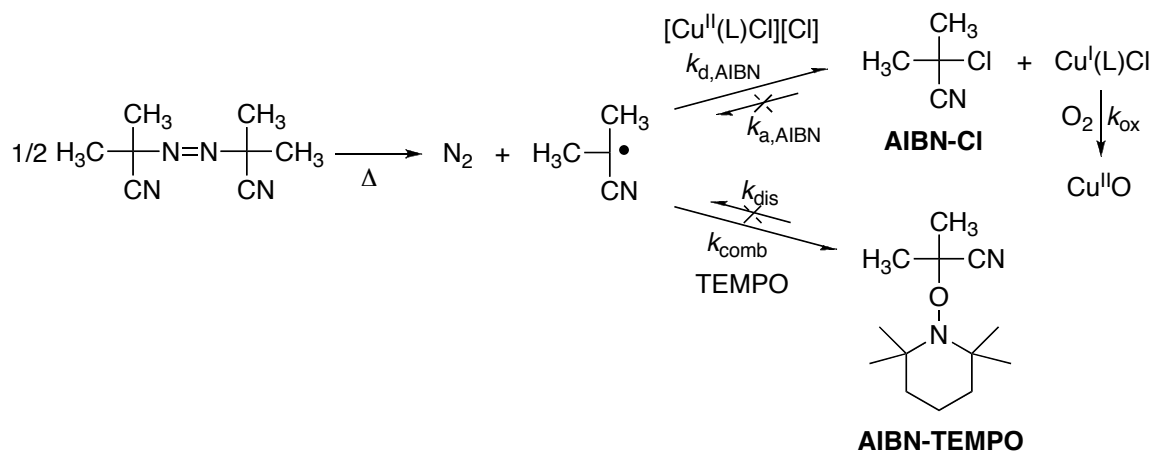
^a[AIBN]₀=0.80 M; ^b[AIBN]₀: [additive]₀ = 1:1, ¹H NMR; ^cUV-Vis

As shown in Table 4.1, the values for the rate of decomposition of AIBN in acetonitrile and methanol is $\sim 3.0 \times 10^{-6} \text{ s}^{-1}$. This is in good agreement with other literature values of k_{dc} of AIBN at 60°C in various solvents, which range from 2.0×10^{-6} to $1.0 \times 10^{-5} \text{ s}^{-1}$.^{63,66} Addition of additives such as anisole and *p*-dimethoxybenzene increased the decomposition rate constant of AIBN by approximately a factor of 2. The presence of additives disrupts the solvent cage, which minimizes the cage effect and, consequently, allows for relatively faster thermal decomposition. AIBN decomposition rate constants in an ATRA reaction system is difficult to determine due to the overlapping peaks in both ¹H NMR and UV-Vis spectra when other compounds, such as the Cu^{II} catalyst, alkenes, alkyl halides, etc. are present in the system. However, these results clearly show that the rate of decomposition of AIBN is not only influenced by the solvent media used but also by the presence of other compounds in the reaction system.

4.3.2 Determination of Deactivation Rate Constant

Determination of the deactivation rate constants are typically performed using a competitive kinetic experiment with formation of a TEMPO adduct in a clock reaction.^{52,67,68} However, this can only be applied to model reaction systems and can be difficult for reactions with low deactivation rate constants, i.e. radical coupling with TEMPO is much faster than the trapping of radical by Cu^{II}. In such cases, deactivation rate constants are determined from the activation rate constant and equilibrium constant ($k_d=k_a/K_e$), provided that both k_a and K_e are known, or by a reverse ATRA procedure⁶⁸ in which the generated Cu^I complex is reacted quickly with O₂ to form stable μ -oxo and/or μ -peroxo Cu^{II} complexes and thus, preventing the reactivation of the halogenated products.

In this study, we employed a combination of the clock reaction and the O₂-trapping of the Cu^I to determine the deactivation rate constants of [Cu^{II}(Me₆TREN)Cl][Cl], [Cu^{II}(TPMA)Cl][Cl], [Cu^{II}(PMDETA)Cl₂], [Cu^{II}(bpy)₂Cl][Cl] with AIBN. In the “radical-clock” methodology^{43,52,69-71}, stable nitroxides such as 2,2,6,6-tetramethylpiperidin-1-oxyl (TEMPO) trap the alkyl radical generated from the decomposition of AIBN to produce an AIBN-TEMPO adduct. In a competitive reaction, the presence of a copper(II) complex in the reaction system also forms an AIBN-Cl complex (Scheme 4.1).



Scheme 4.1. Model Reaction for Deactivation Rate Constant ($k_{\text{d,AIBN}}$) Measurements

Thermal decomposition of AIBN generates tertiary radicals, which do not recombine with N_2 gas to form AIBN, eliminating its interference with the trapping reactions. Dissociation rate constants of TEMPO complexes are typically very low (10^{-4} - $10^{-7} \text{ M}^{-1}\text{s}^{-1}$)⁷² compared to the combination rate constants ($\sim 10^7$ - $10^8 \text{ M}^{-1}\text{s}^{-1}$)^{70,71,73} but, nevertheless, an excess of TEMPO (3 mol equivalents relative to AIBN) was used to prevent the dissociation of the AIBN-TEMPO adduct. An excess of the Cu^{II} complex (6-10 mol equivalents relative to AIBN) was also used to ensure formation of the AIBN-Cl compound and to suppress the consumption of AIBN-Cl by the activation process with the Cu^{I} complex, the reaction was performed in the presence of air to continuously oxidize the reduced catalyst.

By determining the ratio of AIBN-Cl to AIBN-TEMPO produced at various copper(II)-to-TEMPO ratios, the deactivation rate constant can then be calculated from Eq. 4.3 using the combination rate constant, k_{comb} , of a similar *O*-substituted hydroxylamine (1-(2'-cyano-2'-propoxy)-4-oxo-2,2,6,6-tetramethylpiperidine), which is approximately $4.0 \times 10^8 \text{ M}^{-1} \text{ s}^{-1}$.⁷²

$$\frac{d[\text{AIBN} - \text{Cl}]}{d[\text{AIBN} - \text{TEMPO}]} = \frac{k_{d,\text{AIBN}}}{k_{\text{comb}}} \frac{[\text{Cu}^{\text{II}}][\text{AIBN}\cdot]}{[\text{TEMPO}][\text{AIBN}\cdot]} \quad (4.3)$$

The formation of AIBN-Cl and AIBN-TEMPO at 40°C was then monitored using ¹H NMR. Figure 4.1 shows the ¹H NMR spectra of various TEMPO trapping experiments: (a) AIBN peak at time zero, (b) formation of the AIBN-TEMPO complex (c) formation of AIBN-Cl and AIBN-TEMPO. In Figure 4.2, the peak for the AIBN-Cl product at 1.72 ppm is shown to increase at higher [Cu^{II}]₀:[TEMPO]₀ ratios.

The mole ratio of [AIBN-Cl]/[AIBN-TEMPO] versus the ratio of [Cu^{II}]₀/[TEMPO]₀ was then plotted and shown in Figure 4.3. As evident on the plot, the mole ratio of the two reaction products increased linearly with the ratio of copper-to-TEMPO. The deactivation rate constant was then determined from the slope of the plot and the known value of *k*_{comb} (4.0 x 10⁸ M⁻¹s⁻¹) and the results are shown in Table 4.2.

Table 4.2. Deactivation Rate Constants of Various [Cu^{II}(L)Cl][Cl] (L=Ligand) with AIBN^a

Ligand	<i>k</i> _{d,AIBN} (M ⁻¹ s ⁻¹)
Me ₆ TREN	5.3 x 10 ⁷
TPMA	5.4 x 10 ⁷
PMDETA	7.3 x 10 ⁷
bpy	1.1 x 10 ⁸

^a[AIBN]₀ = 0.05 M; ^b[AIBN]₀:[TEMPO]₀ = 1:3; solvent = MeOH, T = 40°C, t = 5 days

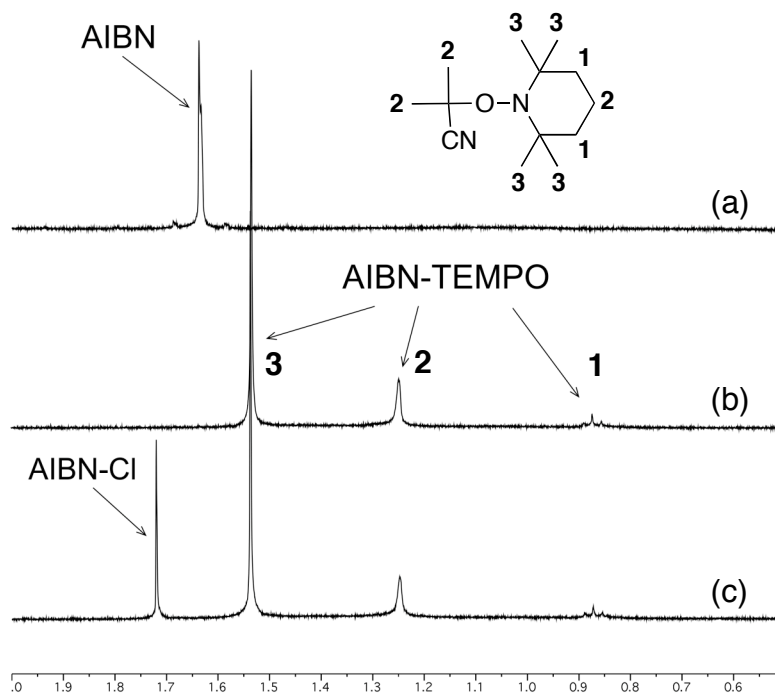


Figure 4.1. ¹H NMR Spectra of TEMPO-Trapping Experiments showing (a) AIBN Peak at Time = 0, (b) Formation of AIBN-TEMPO Adduct, (c) Formation of AIBN-Cl and AIBN-TEMPO Adducts

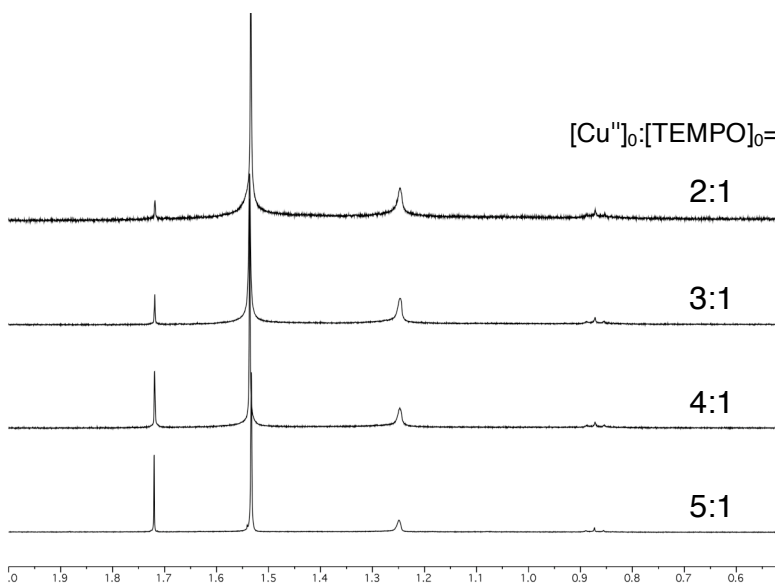


Figure 4.2. ¹H NMR Spectra showing Increasing AIBN-Cl Formation with Increasing [Cu^{II}(TPMA)Cl][Cl]-to-[TEMPO] Ratios

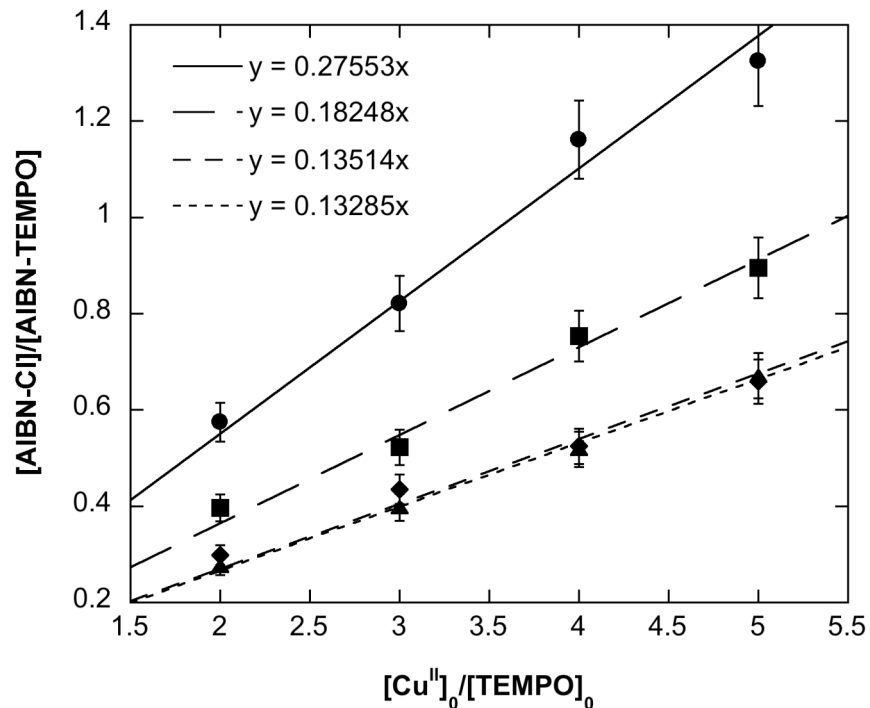
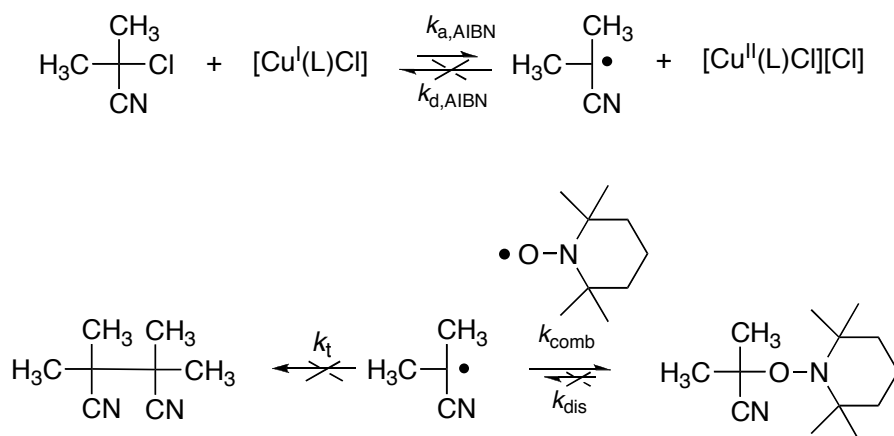


Figure 4.3. Plot of Mole Ratio of [AIBN-Cl]/[AIBN-TEMPO] versus Initial Concentration Ratio of [Cu^{II}]₀/[TEMPO]₀ at 40°C in Methanol: [Cu^{II}(bpy)₂Cl][Cl](●), [Cu^{II}(PMDETA)Cl₂](■), [Cu^{II}(TPMA)Cl][Cl](◆), [Cu^{II}(Me₆TREN)Cl][Cl](▲)

4.3.3 Determination of Activation Rate Constant and Equilibrium Constant

The activation step in atom transfer radical processes is known to be controlled by a number of factors, such as the structure of the radical initiator or alkyl halide, nature of the ligand on the metal complex, reaction temperature, etc. The k_a values for primary, secondary, and tertiary alkyl halides are known to follow the order of $3^\circ > 2^\circ > 1^\circ$.^{45,47} Alkyl bromides are generally more active than alkyl chlorides because C-Br bond is much weaker than C-Cl bond.^{45,47} The general order of activities of copper complexes with N-based ligands is as follows: tetradentate (cyclic-bridged) > tetradentate (branched) > tetradentate (cyclic) > tridentate > tetradentate (linear) > bidentate ligands.^{45,46} Also,

the nature of the N atoms on the ligand is important and usually follows the order alkylamine \approx pyridine $>$ alkylimine $>$ arylimine $>$ arylamine.^{45,46} Knowledge of such important factors is highly crucial in achieving high success in ATRA reactions and, thus, determination of the activation rate constants is essential in choosing the right type of radical initiator to be used as a reducing agent that would not compete with the activation of an alkyl halide to be used in an ATRA reaction.



Scheme 4.2. Model Reaction for Activation Rate Constant ($k_{a,AIBN}$) Measurement

Activation rate constants are typically determined from model studies (Scheme 4.2) in which the activation process is kinetically isolated from the deactivation step by trapping the generated radical with a radical scavenger, such as TEMPO.^{50,52,53,74} As shown in Scheme 4.3, a Cu^{I} complex homolytically cleaves the alkyl halide C-X bond generating a radical and a Cu^{II} complex. In the presence of excess TEMPO, the radical generated after an atom transfer process will be exclusively trapped, yielding an alkoxyamine (R-TEMPO). Addition of excess Cu^{I} complex with respect to R-X provides

first-order kinetic conditions and the disappearance of R-X is then monitored over time to determine the activation rate constant (Eq. 4.4):

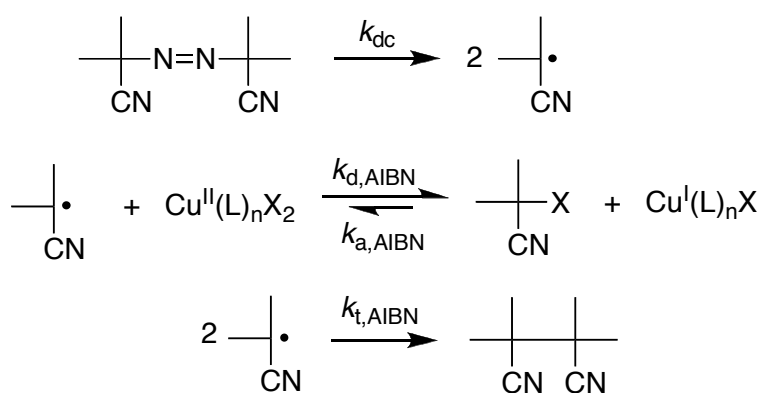
$$-\frac{d[R - X]}{dt} = k_{act}[Cu^I(L)_n X][R - X] = k_{obs}[R - X] \quad (4.4)$$

This method has been widely used in the determination of activation rate constants of various radical initiators and Cu^I catalysts in ATRP in which NMR spectroscopy, HPLC and GC were employed in monitoring the disappearance of R-X.^{46,47,53,75} However, this method is limited in measuring fast activation rate constants with the maximum upper limit of approximately 2 M⁻¹s⁻¹. Other methods, such as the stopped-flow technique, were successfully employed for measuring very fast activations constants (as high as 10² M⁻¹s⁻¹).⁵⁰ In this technique, an excess of alkyl halide and TEMPO was used and the activation rate constant was determined by monitoring the change in concentration of the Cu^I complex according to $\ln([Cu^I(L)_n Cl]_0/[Cu^I(L)_n Cl]_t) = k_{obs} t = -k_a[RX]_0 t$. Activation rate constants greater than 10³ M⁻¹s⁻¹ had to be measured under second order conditions, i.e. stoichiometric amounts of Cu^I catalyst and alkyl halide were used.⁵⁰

Kinetic parameter estimation through computer simulations is also a widely popular alternative method in examining very fast and complicated kinetic reactions.⁷⁶⁻⁷⁹ In Chapter 3, we reported UV-Vis experiments performed at 60°C for model reaction systems containing only a Cu^{II} catalyst and AIBN. The amount of Cu^{II} in the reaction was found to be governed by $k_{a,AIBN}$ and $k_{d,AIBN}$, with active catalysts such as $[Cu^{II}(TPMA)Cl][Cl]$ and $[Cu^{II}(Me_6TREN)Cl][Cl]$ having high amounts of Cu^{II} at

equilibrium compared to the less active catalyst $[\text{Cu}^{\text{II}}(\text{PMDETA})\text{Cl}_2]$ and $[\text{Cu}^{\text{II}}(\text{bpy})_2\text{Cl}][\text{Cl}]$. By using the experimentally determined values of the deactivation rate constants and rates for AIBN decomposition, we employed a combination of UV-Vis experiments and kinetic modeling to determine the activation rate constants of $[\text{Cu}^{\text{II}}(\text{Me}_6\text{TREN})\text{Cl}][\text{Cl}]$, $[\text{Cu}^{\text{II}}(\text{TPMA})\text{Cl}][\text{Cl}]$, $[\text{Cu}^{\text{II}}(\text{PMDETA})\text{Cl}_2]$, $[\text{Cu}^{\text{II}}(\text{bpy})_2\text{Cl}][\text{Cl}]$ with AIBN.

Kinetic simulations of model reaction systems of a Cu^{II} catalyst and AIBN (Scheme 4.3) were performed using Chemical Kinetics Simulator (IBM's Almaden Research Center).⁶⁰ Included in the model system are the following reactions and rate constants: (a) decomposition of the radical initiator in the presence of heat generating 2 equiv of free radical species (k_{dc}), (b) deactivation ($k_{\text{d,AIBN}}$) and activation ($k_{\text{a,AIBN}}$) processes (c) radical termination reaction ($k_{\text{t,AIBN}}$). The values of the rate constants and the initial concentrations of AIBN and Cu^{II} catalysts are summarized in Table 4.3.



Scheme 4.3. Model Reactions for $k_{\text{a,AIBN}}$ Estimation through Kinetic Modeling

Table 4.3. Values of Parameters Used in Kinetic Modeling

Ligand	k_{dc} (s^{-1})	$k_{d,AIBN}$ ($M^{-1}s^{-1}$)	$k_{t,AIBN}$ ($M^{-1}s^{-1}$)	$[AIBN]_0$ (M)	$[Cu^{II}(L)_nX_2]_0$ (M)
Me ₆ TREN	3.0×10^{-6}	5.3×10^7	2.0×10^9	0.039167	0.0039167
TPMA	3.0×10^{-6}	5.4×10^7	2.0×10^9	0.063443	0.0063443
PMDETA	3.0×10^{-6}	7.3×10^7	2.0×10^9	0.059018	0.0059018
bpy	4.5×10^{-6}	1.1×10^8	2.0×10^9	0.11065	0.011065

Simulations were done systematically by varying the activation rate constants and using the previously determined decomposition rate constant (k_{dc}) for AIBN and deactivation rate constants ($k_{d,AIBN}$) and the values for the initial concentrations of AIBN and Cu^{II} catalyst were also based on the previous UV-Vis experiments. The k_{dc} value used for the $[Cu^{II}(bpy)_2Cl][Cl]/AIBN$ system was $4.5 \times 10^{-6} s^{-1}$ as opposed to $3.0 \times 10^{-6} s^{-1}$ in order to obtain a better fit of the kinetic plots. The change in Cu^I and Cu^{II} concentrations were then plotted versus time and the plots were compared to the corresponding plots obtained from UV-Vis experiments of model reactions containing only Cu^{II} and AIBN. The kinetic plots are shown in Figure 4.4 and the activation rate constants and equilibrium constants are summarized in Table 4.4.

The trends obtained for $k_{a,AIBN}$ and K_{ATRA} are in good agreement with previously reported values using NMR, HPLC, GC measurements ($[Cu^{II}(bpy)_2Cl][Cl] < [Cu^{II}(PMDETA)Cl_2] < [Cu^{II}(TPMA)Cl][Cl] < [Cu^{II}(Me_6TREN)Cl][Cl]$).⁴⁵⁻⁴⁸ Kinetic modeling proved to be an effective technique in determining very fast rate constants that would be difficult to measure using current experimental methods.

Table 4.4. Activation Rate Constants and Equilibrium Constants of Various $[\text{Cu}^{\text{II}}(\text{L})\text{Cl}][\text{Cl}]$ Complexes using AIBN as Initiator

Cu^{II} Catalyst	$k_{a,\text{AIBN}} (\text{M}^{-1}\text{s}^{-1})$	K_{ATRA}
$[\text{Cu}^{\text{II}}(\text{Me}_6\text{TREN})\text{Cl}][\text{Cl}]$	6.0×10^4	1.1×10^{-3}
$[\text{Cu}^{\text{II}}(\text{TPMA})\text{Cl}][\text{Cl}]$	5.8×10^4	1.0×10^{-3}
$[\text{Cu}^{\text{II}}(\text{PMDETA})\text{Cl}_2]$	5.0×10^3	6.9×10^{-5}
$[\text{Cu}^{\text{II}}(\text{bpy})_2\text{Cl}][\text{Cl}]$	3.0×10^2	2.8×10^{-6}

$[\text{Cu}^{\text{II}}]_0 : [\text{AIBN}]_0 = 1 : 10$; $T = 60^\circ\text{C}$

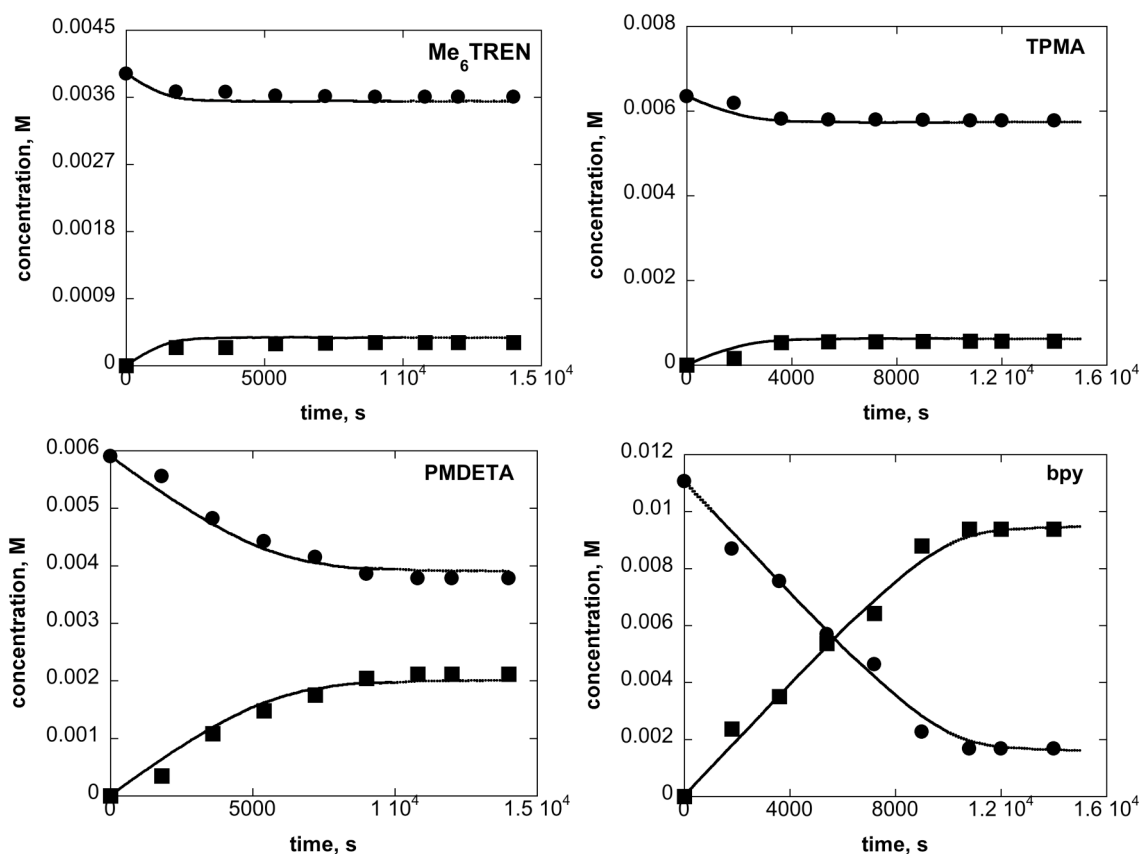


Figure 4.4. Kinetic Plots for Determination of Activation Rate Constants: Data Points (\bullet for Cu^{II} and \blacksquare for Cu^{I}) show Experimental Copper Concentrations Over Time from UV-Vis Data and Solid Lines (—) are Plotted from Kinetic Modeling

4.3.4 Kinetic Modeling of the Initiation Step in Copper-Catalyzed Atom Transfer Radical Addition in the Presence of Reducing Agents

To further understand the role of a reducing agent in a copper-catalyzed ATRA process, kinetic modeling of the reduction of Cu^{II} to Cu^{I} in the presence of AIBN as a reducing agent was performed using Chemical Kinetics Simulator (IBM's Almaden Research Center).⁶⁰ In particular, the effect of the activation ($k_{\text{a,AIBN}}$) and deactivation ($k_{\text{d,AIBN}}$) rate constants, rate of AIBN decomposition (k_{dc}) and initial AIBN concentration on the concentrations of Cu^{I} and Cu^{II} was investigated. Simulations on the model reactions outlined in Scheme 4.3 were done systematically by varying the rate constants $k_{\text{a,AIBN}}$, $k_{\text{d,AIBN}}$, k_{dc} and the initial AIBN concentration in order to evaluate their effects on the concentrations of Cu^{I} and Cu^{II} . The values of the parameters used in the simulations are summarized in Table 4.5.

Table 4.5. Parameters and Reaction Conditions Used in Kinetic Simulation of the Reduction of Cu^{II} to Cu^{I} in Copper-Catalyzed ATRA in the Presence of AIBN

Figure	Varied Parameter	Constant Parameters				
4.5A	k_{dc}	$k_{\text{a,AIBN}}(\text{M}^{-1}\text{s}^{-1})$ 1.0 x 10 ⁻¹	$k_{\text{d,AIBN}}(\text{M}^{-1}\text{s}^{-1})$ 1.0 x 10 ⁸	$k_{\text{t,AIBN}}(\text{M}^{-1}\text{s}^{-1})$ 2.0 x 10 ⁹	$[\text{Cu}]_0(\text{M})$ 0.01	$[\text{AIBN}]_0(\text{M})$ 0.1
4.5B	k_{dc}	$k_{\text{a,AIBN}}(\text{M}^{-1}\text{s}^{-1})$ 1.0 x 10 ²	$k_{\text{d,AIBN}}(\text{M}^{-1}\text{s}^{-1})$ 1.0 x 10 ⁸	$k_{\text{t,AIBN}}(\text{M}^{-1}\text{s}^{-1})$ 2.0 x 10 ⁹	$[\text{Cu}]_0(\text{M})$ 0.01	$[\text{AIBN}]_0(\text{M})$ 0.1
4.6A	$[\text{AIBN}]_0$	$k_{\text{dc}}(\text{M}^{-1}\text{s}^{-1})$ 3.0 x 10 ⁻⁶	$k_{\text{a,AIBN}}(\text{M}^{-1}\text{s}^{-1})$ 1.0 x 10 ²	$k_{\text{d,AIBN}}(\text{M}^{-1}\text{s}^{-1})$ 1.0 x 10 ⁸	$k_{\text{t,AIBN}}(\text{M}^{-1}\text{s}^{-1})$ 2.0 x 10 ⁹	$[\text{Cu}]_0(\text{M})$ 0.01
4.6B	$[\text{AIBN}]_0$	$k_{\text{dc}}(\text{M}^{-1}\text{s}^{-1})$ 3.0 x 10 ⁻⁶	$k_{\text{a,AIBN}}(\text{M}^{-1}\text{s}^{-1})$ 1.0 x 10 ⁴	$k_{\text{d,AIBN}}(\text{M}^{-1}\text{s}^{-1})$ 1.0 x 10 ⁷	$k_{\text{t,AIBN}}(\text{M}^{-1}\text{s}^{-1})$ 2.0 x 10 ⁹	$[\text{Cu}]_0(\text{M})$ 0.01
4.7A	$k_{\text{a,AIBN}}$	$k_{\text{dc}}(\text{M}^{-1}\text{s}^{-1})$ 3.0 x 10 ⁻⁶	$k_{\text{d,AIBN}}(\text{M}^{-1}\text{s}^{-1})$ 1.0 x 10 ⁸	$k_{\text{t,AIBN}}(\text{M}^{-1}\text{s}^{-1})$ 2.0 x 10 ⁹	$[\text{Cu}]_0(\text{M})$ 0.01	$[\text{AIBN}]_0(\text{M})$ 0.1
4.7B	$k_{\text{d,AIBN}}$	$k_{\text{dc}}(\text{M}^{-1}\text{s}^{-1})$ 3.0 x 10 ⁻⁶	$k_{\text{a,AIBN}}(\text{M}^{-1}\text{s}^{-1})$ 1.0 x 10 ²	$k_{\text{t,AIBN}}(\text{M}^{-1}\text{s}^{-1})$ 2.0 x 10 ⁹	$[\text{Cu}]_0(\text{M})$ 0.01	$[\text{AIBN}]_0(\text{M})$ 0.1

To evaluate the effect of the decomposition rate constant of AIBN on the Cu^I and Cu^{II} concentrations, values ranging from 3.5-6.5 x 10⁻⁶ s⁻¹ were used in the kinetic modeling. In addition, its effect at varying catalyst activity (differed by 3 orders of magnitudes) was also investigated, i.e. $k_{a,AIBN}$ and $k_{d,AIBN}$ values of 10⁻¹ M⁻¹s⁻¹ and 1.0 x 10⁸ M⁻¹s⁻¹, respectively, were used in Figure 4.5A and $k_{a,AIBN}$ and $k_{d,AIBN}$ values of 10² M⁻¹s⁻¹ and 1.0 x 10⁸ M⁻¹s⁻¹, respectively, were used in Figure 4.5B.

It is evident in the kinetic plots shown in Figure 4.5 that the decomposition rate constant of AIBN does not have an effect on the extent of Cu^I regeneration and, thus, does not control the concentrations of Cu^I and Cu^{II} at equilibrium, even if the activity of the Cu^{II} catalyst differ by 3 orders of magnitude. However, in both plots, the rate constant of AIBN decomposition controls the time at which the ATRA quasi-equilibrium is being established. Increasing the decomposition rate constant by a factor of 2 reduced the time to establish quasi-equilibrium by half. Thus, the use of radical initiators with faster rate of decomposition as reducing agents would decrease the time it would take to reach ATRA equilibrium.

Kinetic simulation of the effect of the radical initiator concentration relative to the alkene on the concentrations of Cu^I and Cu^{II} in the reaction is shown in Figure 4.6. The values of the concentration of the radical initiator were ranged from 1 mol% to 20 mol% with respect to the alkene. In the same manner, the effect of the radical initiator concentration at varying catalyst activity was investigated. As shown in Figure 4.6A, where $k_{a,AIBN}$ and $k_{d,AIBN}$ values of 10² M⁻¹s⁻¹ and 1.0 x 10⁸ M⁻¹s⁻¹, respectively, were used increasing the relative concentration of AIBN from 1 mol% to 20 mol% allowed for the equilibrium to be reached in a smaller time span. However, the difference between 5, 10,

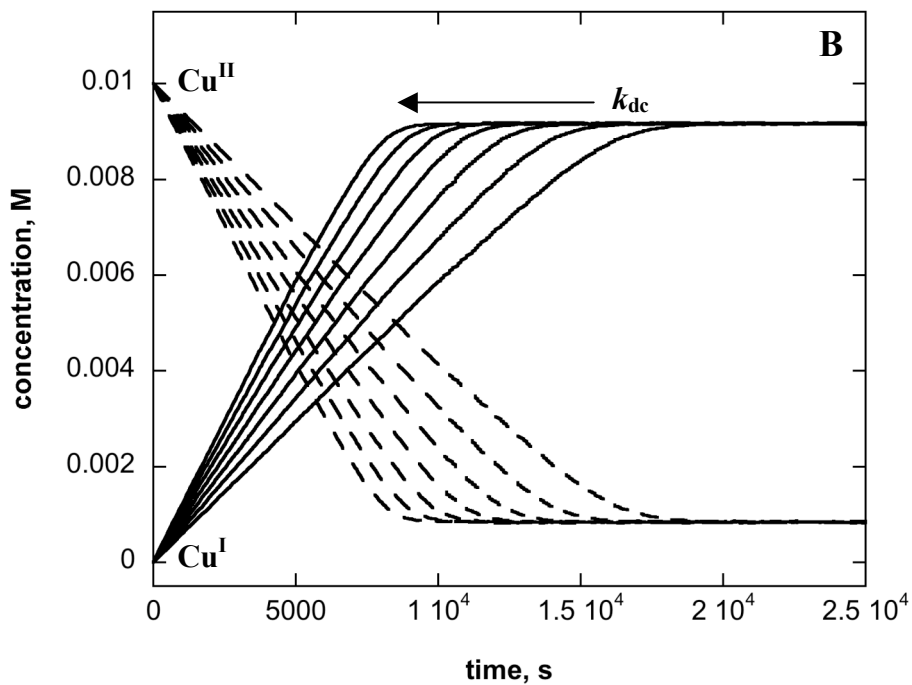
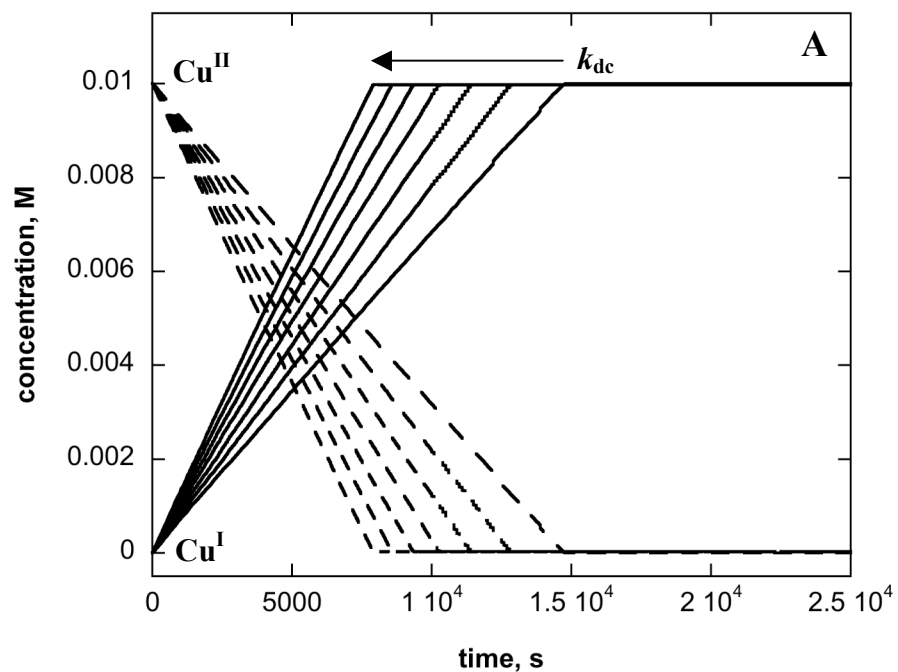


Figure 4.5. Simulation of Kinetic Plots for the Regeneration of Cu^{I} from Cu^{II} in the Presence of AIBN: k_{dc} Values Ranging from $3.5\text{-}6.5 \times 10^{-6} \text{ s}^{-1}$ at (A) $10^{-1} \text{ M}^{-1}\text{s}^{-1}$ ($k_{\text{a,AIBN}}$) and $10^8 \text{ M}^{-1}\text{s}^{-1}$ ($k_{\text{d,AIBN}}$); (B) $10^2 \text{ M}^{-1}\text{s}^{-1}$ ($k_{\text{a,AIBN}}$) and $10^8 \text{ M}^{-1}\text{s}^{-1}$ ($k_{\text{d,AIBN}}$).

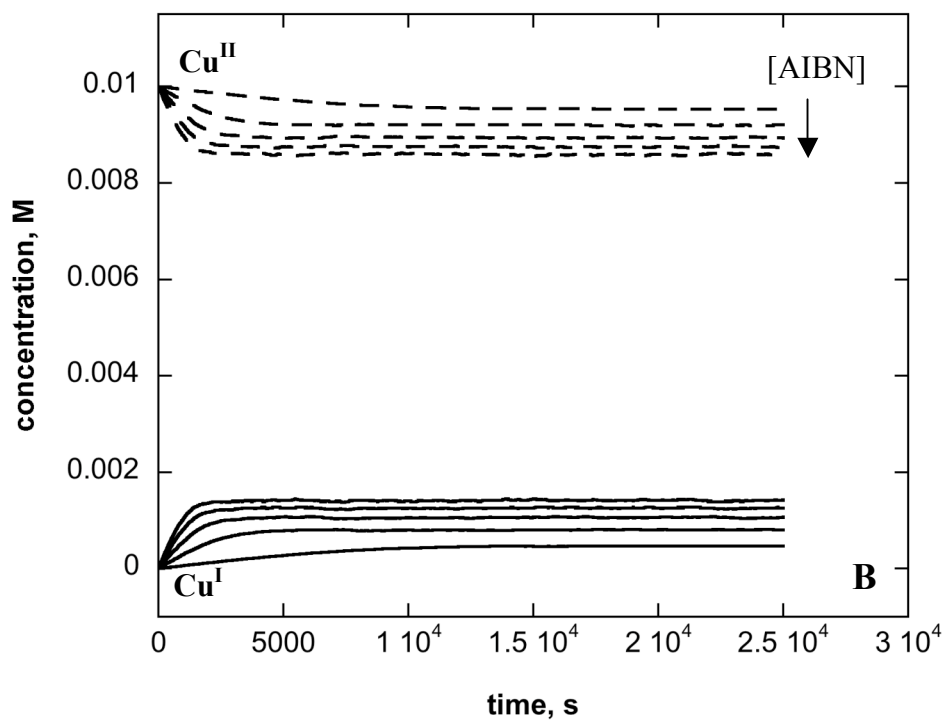
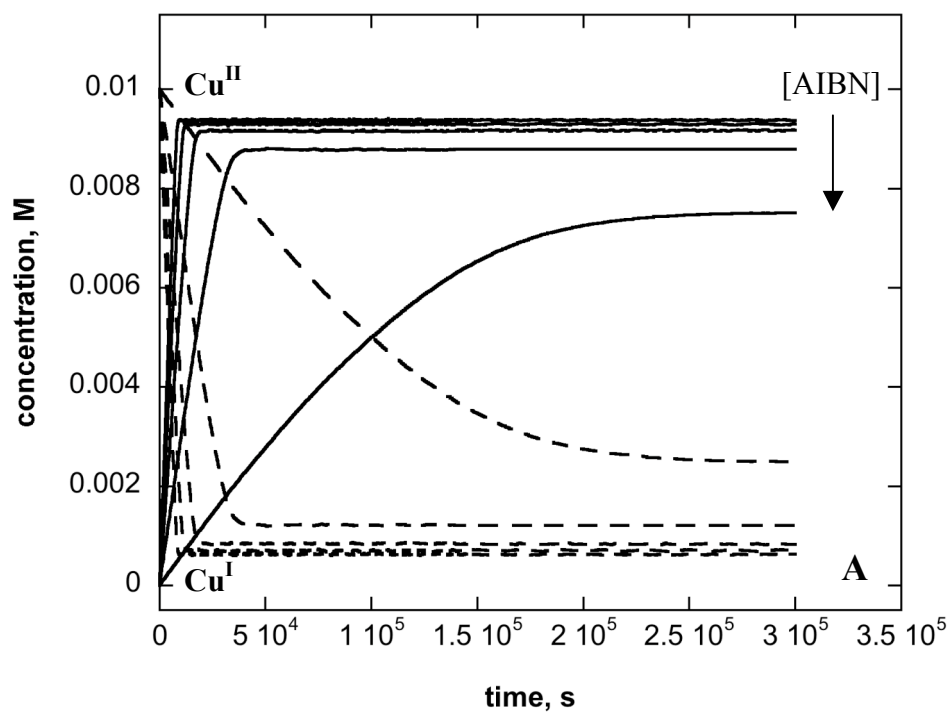


Figure 4.6. Simulation of Kinetic Plots for the Regeneration of Cu^{I} from Cu^{II} in the Presence of AIBN: AIBN Concentration Ranging from 1-20 mol% Relative to Alkene at (A) $10^2 \text{ M}^{-1}\text{s}^{-1}$ ($k_{\text{a,AIBN}}$) and $10^8 \text{ M}^{-1}\text{s}^{-1}$ ($k_{\text{d,AIBN}}$); (B) $10^4 \text{ M}^{-1}\text{s}^{-1}$ ($k_{\text{a,AIBN}}$) and $10^7 \text{ M}^{-1}\text{s}^{-1}$ ($k_{\text{d,AIBN}}$)

15 and 20 mol% is not significant, which is in good agreement with our previous experiments wherein the optimum alkene conversion is achieved at 5 mol% AIBN. Also, the extent of Cu^{II} reduction was affected by the concentration of AIBN. At 1 mol% AIBN relative to the alkene, approximately 70% of Cu^{II} was reduced to Cu^I. This number increased at higher mol% of AIBN with as much as 95% Cu^I generated from Cu^{II} at 20 mol% AIBN.

However, the concentration of AIBN did not significantly affect the extent of Cu^I regeneration from Cu^{II} when the kinetic parameters for an active catalyst with $k_{a,AIBN}$ and $k_{d,AIBN}$ values of $10^4 \text{ M}^{-1}\text{s}^{-1}$ and $1.0 \times 10^7 \text{ M}^{-1}\text{s}^{-1}$ was used. An increase in the concentration of AIBN from 1 mol% to 20 mol% only showed a slight variation in the concentrations of Cu^I and Cu^{II} at equilibrium. These results show that when less active catalysts are used in ATRA reactions, varying the concentration of the radical initiator/reducing agent will greatly affect the overall Cu^I and Cu^{II} concentration in the reaction.

The effect of $k_{a,AIBN}$ on the Cu^I and Cu^{II} concentrations was then evaluated by systematically varying the values for $k_{a,AIBN}$ from 1.0×10^{-3} to $5.0 \times 10^4 \text{ M}^{-1}\text{s}^{-1}$ while the other kinetic parameters and reaction conditions were kept constant. As seen on the simulated kinetic plot in Figure 4.7A, $k_{a,AIBN}$ values of 10^{-3} to $10 \text{ M}^{-1}\text{s}^{-1}$ completely reduced Cu^{II} to Cu^I after $1.5 \times 10^4 \text{ s}$, at which time ATRA quasi-equilibrium ($k_a[\text{Cu}^I][\text{RX}] \approx k_d[\text{Cu}^{II}][\text{R}\cdot]$) is established. Increasing the activation rate constant to $100 \text{ M}^{-1}\text{s}^{-1}$ allowed only 95% of Cu^{II} to be reduced. At $k_{a,AIBN}$ value of $1000 \text{ M}^{-1}\text{s}^{-1}$, only 70% of Cu^{II} was reduced before ATRA quasi-equilibrium is established. A $k_{a,AIBN}$ value of

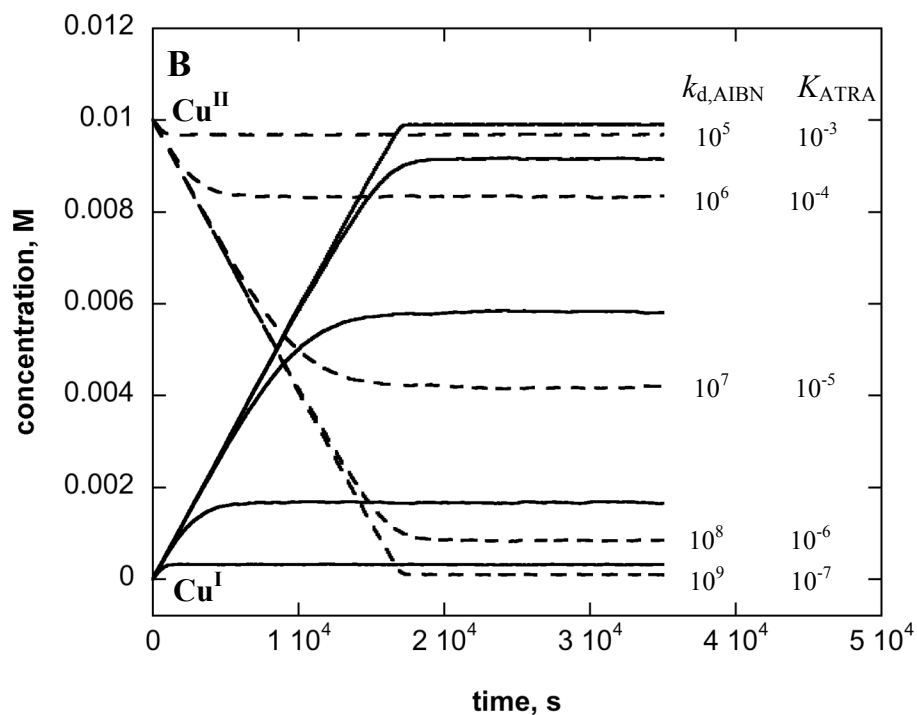
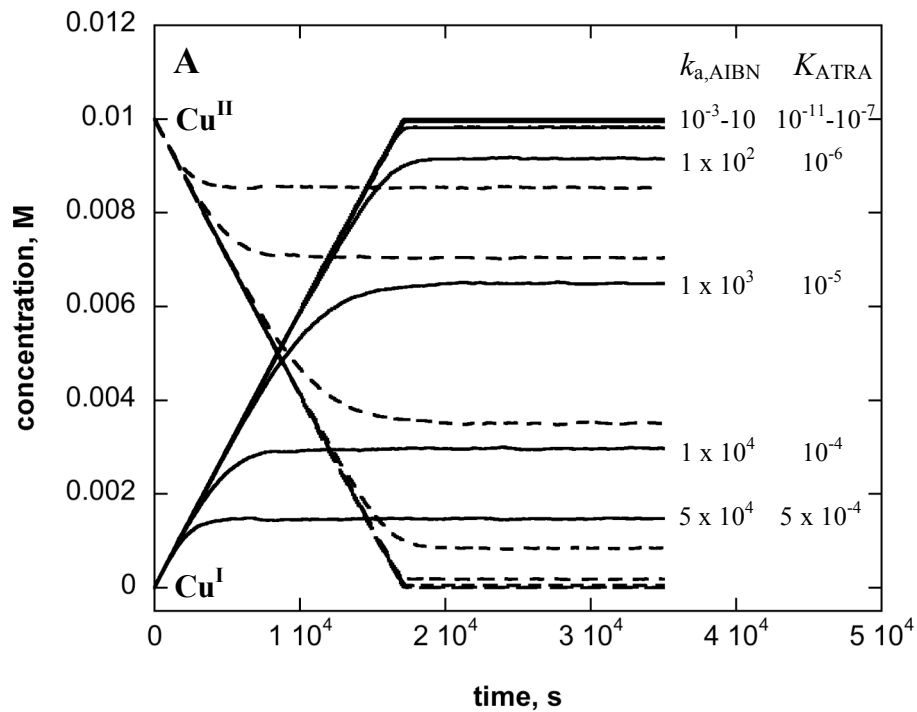


Figure 4.7. Simulation of Kinetic Plots for the Regeneration of Cu^{I} from Cu^{II} in the Presence of AIBN: (A)= $k_{a,AIBN}$ Values Ranging from 0.001 to $5.0 \times 10^5 \text{ M}^{-1}\text{s}^{-1}$ ($k_{d,AIBN}=10^8 \text{ M}^{-1}\text{s}^{-1}$) and (B)= $k_{d,AIBN}$ Values Ranging from 10^5 to $10^9 \text{ M}^{-1}\text{s}^{-1}$ ($k_{a,AIBN}=10^2 \text{ M}^{-1}\text{s}^{-1}$)

$5.0 \times 10^4 \text{ M}^{-1}\text{s}^{-1}$ showed only 15% regeneration of Cu^{I} , which is consistent with our previous activation rate constant measurements. The active copper(II) catalysts such as $[\text{Cu}^{\text{II}}(\text{Me}_6\text{TREN})\text{Cl}][\text{Cl}]$ and $[\text{Cu}^{\text{II}}(\text{TPMA})\text{Cl}][\text{Cl}]$ were found to have very high activation rate constants ($10^4 \text{ M}^{-1}\text{s}^{-1}$) and exhibited high Cu^{II} concentrations at equilibrium.

In the same manner, the effect of $k_{\text{d,AIBN}}$ on the concentrations of Cu^{I} and Cu^{II} was studied by systematically varying the values of $k_{\text{d,AIBN}}$ from 10^5 to $10^9 \text{ M}^{-1}\text{s}^{-1}$ in the kinetic modeling. As shown in Figure 4.7B, decreasing the deactivation rate constant significantly lowers the amount of Cu^{I} generated from Cu^{II} . A $k_{\text{d,AIBN}}$ value of $10^9 \text{ M}^{-1}\text{s}^{-1}$ allows for the complete regeneration of the Cu^{I} . Lowering the deactivation rate constant to $10^5 \text{ M}^{-1}\text{s}^{-1}$ resulted in the reduction of only less than 5% of Cu^{II} to Cu^{I} . These results clearly show that the reduction of Cu^{II} to Cu^{I} in an ATRA process greatly depends on the activation and deactivation rate constants, which can be controlled through ligand design and the choice of the radical initiator.

4.4 Conclusions

In summary, the decomposition rate constant of AIBN and activation and deactivation rate constants of various $\text{Cu}^{\text{II}}/\text{AIBN}$ systems were determined using a combination of spectroscopic and kinetic modeling methods. The decomposition rate constant of AIBN at 60°C was measured to be approximately $3.0 \times 10^{-6} \text{ s}^{-1}$. Deactivation rate constants were successfully measured using the TEMPO-trapping method along with ^1H NMR spectroscopy, however, activation rate constants were too high to be determined using experimental techniques. Kinetic modeling was shown to be an effective technique in the estimation of large activation rate constants and also for evaluating the effects of various kinetic parameters on the reduction Cu^{II} in a copper-catalyzed ATRA process. Activation ($k_{\text{a,AIBN}}$) and deactivation rate constants ($k_{\text{d,AIBN}}$) greatly affected the extent of the reduction of Cu^{II} to Cu^{I} , showing higher concentrations of Cu^{I} and, consequently, lower concentration of Cu^{II} at equilibrium at lower $k_{\text{a,AIBN}}$ and higher $k_{\text{d,AIBN}}$ values. Rate of AIBN decomposition only controlled the time to establish equilibrium but did not affect the concentrations of Cu^{I} and Cu^{II} . ATRA equilibrium was reached faster at higher mol% AIBN relative to Cu^{II} , however, the Cu^{I} and Cu^{II} concentrations at varying AIBN concentration was only greatly affected when a less active catalyst (higher $k_{\text{d,AIBN}}$ and lower $k_{\text{a,AIBN}}$) was modeled.

References

- (1) Clark, A. J. Atom transfer radical cyclisation reactions mediated by copper complexes. *Chem. Soc. Rev.* **2002**, *31*, 1-11.
- (2) Minisci, F. Free-radical addition to olefins in the presence of redox systems. *Acc. Chem. Res.* **1975**, *8*, 165-171.
- (3) Curran, D. P. The design and application of free radical chain reactions in organic synthesis. Part 1. *Synthesis.* **1988**, *6*, 417-439.
- (4) Curran, D. P. The design and application of free radical chain reactions in organic synthesis. Part 2. *Synthesis.* **1988**, *7*, 489-513.
- (5) Baban, J. A.; Roberts, B. P. An electron spin resonance study of alkyl radical addition to diethyl vinylphosphonate. *J. Chem. Soc., Perkin Trans. 2.* **1981**, *1*, 161-166.
- (6) Caronna, T.; Citterio, A.; Ghirardini, M.; Minisci, F. Nucleophilic character of alkyl radicals—XIII: Absolute rate constants for the addition of alkyl radicals to acrylonitrile and methyl acrylate. *Tetrahedron.* **1977**, *33*, 793-796.
- (7) Asscher, M.; Vofsi, D. Chlorine activation by redox-transfer. Part I. The reaction between aliphatic amines and carbon tetrachloride. *J. Chem. Soc.* **1961**, 2261-2264.
- (8) Truce, W. E.; Wolf, G. C. Adducts of sulfonyl iodides with acetylenes. *J. Org. Chem.* **1971**, *36*, 1727-1732.
- (9) Freidlina, R. K.; Velichko, F. K. Synthetic applications of homolytic addition and telomerization reactions of bromine-containing addends with unsaturated compounds containing electron-withdrawing substituents. *Synthesis.* **1977**, *3*, 145-154.
- (10) Julia, M.; Sasussine, L.; Thuillier, G. I. Addition du chloracetate de methyle sur les olefines. *J. Organomet. Chem.* **1979**, *174*, 359-366.
- (11) Imoto, J.; Sato, A.; Yorimitsu, H.; Oshima, K. Atom-transfer Radical Addition of α -Iodo Esters to 1-Alkynyl Sulfides. *Chem. Lett.* **2009**, *38*(5), 462-463.

- (12) Yorimitsu, H.; Shinokubo, H.; Matsubara, S.; Oshima, K.; Omoto, K.; Fujimoto, H. Triethylborane-Induced Bromine Atom-Transfer Radical Addition in Aqueous Media: Study of the Solvent Effect on Radical Addition Reactions. *J. Org. Chem.* **2001**, *66*(23), 7776-7785.
- (13) Riva, R.; Lenoir, S.; Jerome, R.; Lecomte, P. Functionalization of poly(ϵ -caprolactone) by pendant hydroxyl, carboxylic acid and epoxide groups by atom transfer radical addition. *Polymer.* **2005**, *46*(19), 8511-8518.
- (14) Opstal, T.; Verpoort, F. From atom transfer radical addition to atom transfer radical polymerization of vinyl monomers mediated by ruthenium indenylidene complexes. *New J. Chem.* **2003**, *27*(2), 257-262.
- (15) Clark, A. J.; Battle, G. M.; Bridge, A. Efficient β -lactam synthesis via 4-exo atom transfer radical cyclisation using CuBr(triipyridylamine) complex. *Tetrahedron Letters.* **2001**, *42*, 4409-4412.
- (16) Udding, J. H.; Tuijpp, K. C. J. M.; van Zanden, M. N. A.; Hiemstra, H.; Speckamp, W. N. Transition Metal-Catalyzed, Chlorine-Transfer Radical Cyclizations of 2-(3-Alkne-1-oxy)-2-Chloroacetates. Formal Total Synthesis of Avenaciolide and Isoavenaciolide. *J. Org. Chem.* **1994**, *59*(8), 1993-2003.
- (17) Bland, W. J.; Davis, R.; Durrant, J. L. A. The Mechanism of the Addition of Tetrachloromethane to Alkenes in the Presence of $[\text{Cr}(\text{CO})_3(\eta^6\text{-C}_{10}\text{H}_8)]$. *J. Organomet. Chem.* **1984**, *260*(3), C75-C77.
- (18) Matsumoto, H.; Nakano, T.; Nagai, Y. Radical reactions in the coordination sphere I. Addition of carbon tetrachloride and chloroform to 1-olefins catalyzed by ruthenium(II) complexes. *Tetrahedron Lett.* **1973**, *14*(51), 5147-5150.
- (19) Simal, F.; Sebillé, S.; Demonceau, A.; Noels, A. F.; Nunez, R.; Abad, M.; Teixidor, F.; Vinas, C. Radical reactions catalysed by ruthenium(II) complexes with anionic carborane phosphine ligands: Kharasch addition to olefins and controlled polymerisation. *Tetrahedron Letters.* **2000**, *41*(28), 5347-5351.
- (20) Simal, F.; Wlodarczak, L.; Demonceau, A.; Noels, A. F. Highly efficient Kharasch addition catalysed by $\text{RuCl}(\text{Cp}^*)(\text{PPh}_3)_2$. *Tetrahedron Letters.* **2000**, *41*(32), 6071-6074.
- (21) Severin, K. Ruthenium catalysts for the Kharasch reaction. *Curr. Org. Chem.* **2006**, *10*(2), 217-224.

- (22) Benedetti, M.; Forti, L.; Ghelfi, F.; Pagnoni, U. M.; Ronzoni, R. Halogen atom transfer radical cyclization of *N*-allyl-*N*-benzyl-2,2-dihaloamides to 2-pyrrolidinones, promoted by Fe⁰-FeCl₃ or CuCl-TMEDA. *Tetrahedron*. **1997**, *53*(41), 14031-14042.
- (23) Bellesia, F.; Forti, L.; Gallini, E.; Ghelfi, F.; Libertini, E.; Pagnoni, U. M. Telechelic oligomers by halogen atom transfer radical addition. *Tetrahedron*. **1998**, *54*(27), 7849-7856.
- (24) Forti, L.; Ghelfi, F.; Libertini, E.; Pagnoni, U. M.; Soragni, E. Halogen Atom Transfer Radical Addition of α -Polychloroesters to Olefins Promoted by Fe⁰ Filings. *Tetrahedron*. **1997**, *53*(52), 17761-17768.
- (25) Forti, L.; Ghelfi, F.; Pagnoni, U. M. Fe⁰ Initiated Halogen Atom Transfer Radical Addition of Methyl 2-Br-2-Cl-Carboxylates to Olefins. *Tetrahedron Letters*. **1996**, *37*(12), 2077-2078.
- (26) Kleij, A. W.; Gossage, R. A.; Gebbink, R. J. M.; Brinkmann, N.; Reijerse, E. J.; Kragl, U.; Lutz, M.; Spek, A. L.; van Koten, G. A "Dendritic Effect" in Homogeneous Catalysis with Carbosilane-Supported Arylnickel(II) Catalysts: Observation of Active-Site Proximity Effects in Atom-Transfer Radical Addition. *J. Am. Chem. Soc.* **2000**, *122*(49), 12112-12124.
- (27) Kleij, A. W.; Gossage, R. A.; Jastrzebski, J. T. B. H.; Boersma, J.; van Koten, G. The "Dendritic Effect" in Homogenous Catalysts with Carbosilane-Supported Arylnickel(II) Catalysts: Observation of Active-Site Proximity Effects in Atom-Transfer Radical Addition. *Angew. Chem. Int. Ed.* **2000**, *39*(1), 176-178.
- (28) van de Kuil, L. A.; Grove, D. M.; Gossage, R. A.; Zwikker, J. W.; Jennekens, L. W.; Drenth, W.; van Koten, G. Mechanistic Aspects of the Kharasch Addition Reaction Catalyzed by Organonickel(II) Complexes Containing the Monoanionic Terdentate Aryldiamine Ligand System [C₆H₂(CH₂NMe₂)₂-2,6-R-4]. *Organometallics*. **1997**, *16*(23), 4985-4994.
- (29) Clark, A. J.; Dell, C. P.; Ellard, J. M.; Hunt, N. A.; McDonagh, J. P. Efficient room temperature copper(I) mediated 5-*endo* radical cyclisations. *Tetrahedron Letters*. **1999**, *40*(49), 8619-8623.
- (30) Clark, A. J.; Filik, R. P.; Thomas, G. H. Ligand Geometry Effects in Copper Mediated Atom Transfer Radical Cyclisations. *Tetrahedron Letters*. **1999**, *40*, 4885-4888.

- (31) De Campo, F.; Lastecoueres, D.; Verlhac, J.-B. New and Improved Catalysts for Transition Metal Catalyzed Radical Reactions. *Chem. Commun.* **1998**, 2117-2118.
- (32) Pintauer, T.; Eckenhoff, W. T.; Ricardo, C.; Balili, M. N. C.; Biernesser, A.; Noonan, S.; Taylor, M. Highly efficient ambient-temperature copper-catalyzed atom transfer radical addition (ATRA) in the presence of free-radical initiator (V70) as a reducing agent. *Chem. Eur. J.* **2009**, *15*, 38-41.
- (33) Pintauer, T. "Greening" of copper catalyzed atom transfer radical addition (ATRA) and cyclization (ATRC) reactions. *ACS Symp. Ser.* **2009**, *1023*, 63-84.
- (34) Pintauer, T.; Matyjaszewski, K. Atom transfer radical addition and polymerization reactions catalyzed by ppm amounts of copper complexes. *Chem. Soc. Rev.* **2008**, *37*, 1087-1097.
- (35) Tsarevsky, N. V.; Matyjaszewski, K. "Green" Atom Transfer Radical Polymerization: From Process Design to Preparation of Well-Defined Environmentally Friendly Polymeric Materials. *Chem. Rev.* **2007**, *107*, 2270-2299.
- (36) Oh, J. K.; Dong, H.; Zhang, R.; Matyjaszewski, K. Preparation of Nanoparticles of Double-Hydrophilic PEO-PHEMA block copolymers by AGET ATRP in inverse miniemulsion. *J. Polym. Sci. Part A: Polym. Chem.* **2007**, *45*, 4764-4772.
- (37) Balili, M. N. C.; Pintauer, T. Persistent Radical Effect in Action: Kinetic Studies of Copper-Catalyzed Atom Transfer Radical Addition in the Presence of Free-Radical Diazo Initiators as Reducing Agents. *Inorg. Chem.* **2009**, *48*, 9018-9026.
- (38) Eckenhoff, W. T.; Garrity, S. T.; Pintauer, T. Highly Efficient Copper-Mediated Atom-Transfer Radical Addition (ATRA) in the Presence of Reducing Agent. *Eur. J. Inorg. Chem.* **2008**(4), 563-571.
- (39) Eckenhoff, W. T.; Pintauer, T. Atom Transfer Radical Addition in the Presence of Catalytic Amounts of Copper(I/II) Complexes with Tris(2-pyridylmethyl)amine. *Inorg. Chem.* **2007**, *46*, 5844-5846.
- (40) Ricardo, C.; Pintauer, T. Copper catalyzed atom transfer radical cascade reactions in the presence of free-radical diazo initiators as reducing agents. *Chem. Commun.* **2009**, *21*, 3029-3031.

- (41) Matyjaszewski, K.; Jakubowski, W.; Min, K.; Tang, W.; Huang, J.; Braunecker, W. A.; Tsarevsky, N. V. Diminishing catalyst concentration in atom transfer radical polymerization with reducing agents. *Proc. Natl. Acad. Sci. USA.* **2006**, *103*, 15309-15314.
- (42) Dong, H.; Tang, W.; Matyjaszewski, K. Well-Defined High-Molecular-Weight Polyacrylonitrile via Activators Regenerated by Electron Transfer ATRP. *Macromolecules.* **2007**, *40(9)*, 2974-2977.
- (43) Mueller, L.; Jakubowski, W.; Tang, W.; Matyjaszewski, K. Successful Chain Extension of Polyacrylate and Polystyrene Macroinitiators with Methacrylates in an ARGET and ICAR ATRP. *Macromolecules.* **2007**, *40(18)*, 6464-6472.
- (44) Quebatte, L.; Thommes, K.; Severin, K. Highly Efficient Atom Transfer Radical Addition Reactions with a Ru^{III} Complex as a Catalyst Precursor. *J. Am. Chem. Soc.* **2006**, *128*, 7440-7441.
- (45) Tang, W.; Kwak, Y.; Braunecker, W.; Tsarevsky, N. V.; Coote, M. L.; Matyjaszewski, K. Understanding Atom Transfer Radical Polymerization: Effect of Ligand and Initiator Structures on the Equilibrium Constants. *J. Am. Chem. Soc.* **2008**, *130(32)*, 10702-10713.
- (46) Tang, W.; Matyjaszewski, K. Effect of Ligand Structure on Activation Rate Constants in ATRP. *Macromolecules.* **2006**, *39(15)*, 4953-4959.
- (47) Tang, W.; Matyjaszewski, K. Effects of Initiator Structure on Activation Rate Constants in ATRP. *Macromolecules.* **2007**, *40(6)*, 1858-1863.
- (48) Tang, W.; Tsarevsky, N. V.; Matyjaszewski, K. Determination of Equilibrium Constants for Atom Transfer Radical Polymerization. *J. Am. Chem. Soc.* **2006**, *128(5)*, 1598-1604.
- (49) Seeliger, F.; Matyjaszewski, K. Temperature Effect on Activation Rate Constants in ATRP: New Mechanistic Insights into the Activation Process. *Macromolecules.* **2009**, *42*, 6050-6055.
- (50) Pintauer, T.; Braunecker, W.; Collange, E.; Poli, R.; Matyjaszewski, K. Determination of Rate Constants for the Activation Step in Atom Transfer Radical Polymerization Using the Stopped-Flow Technique. *Macromolecules.* **2004**, *37(8)*, 2679-2682.

- (51) Matyjaszewski, K.; Nanda, A. K.; Tang, W. Effect of [CuII] on the Rate of Activation in ATRP. *Macromolecules*. **2005**, *38*(5), 2015-2018.
- (52) Matyjaszewski, K.; Paik, H.-j.; Zhou, P.; Diamanti, S. J. Determination of Activation and Deactivation Rate Constants of Model Compounds in Atom Transfer Radical Polymerization. *Macromolecules*. **2001**, *34*(15), 5125-5131.
- (53) Goto, A.; Fukuda, T. Determination of the activation rate constants of alkyl halides initiators for atom transfer radical polymerization. *Macromol. Rapid Commun.* **1999**, *20*, 633-636.
- (54) Tyeklar, Z.; Jacobson, R. R.; Wei, N.; Murthy, N. N.; Zubieta, J.; Karlin, K. D. Reversible Reaction of Dioxygen (and Carbon Monoxide) with a Copper(I) Complex. X-Ray Structures of Relevant Mononuclear Cu(I) Precursor Adducts and the Trans-(μ -1,2-peroxy)dicopper(II) Product. *J. Am. Chem. Soc.* **1993**, *115*(7), 2677-2689.
- (55) Ciampolini, M.; Nardi, N. Five-Coordinated High-Spin Complexes of Bivalent Cobalt, Nickel, and Copper with Tris(2-dimethylaminoethyl)amine. *Inorg. Chem.* **1966**, *5*(1), 41-44.
- (56) Eckenhoff, W. T.; Pintauer, T. Atom Transfer Radical Addition in the Presence of Catalytic Amounts of Copper(I/II) Complexes with Tris(2-pyridylmethyl)amine. *Inorg. Chem.* **2007**, *46*(15), 5844-5846.
- (57) Barbucci, R.; Mastroianni, A.; Campbell, M. J. M. The Effect of N-Alkylation on the Properties of Five-Coordinate Copper(II) Complexes of Tetraamine Ligands. *Inorg. Chim. Acta.* **1978**, *27*(1), 109-114.
- (58) Margraf, G.; Bats, J. W.; Wagner, M.; Lerner, H.-W. Copper(II) PMDETA and copper(II) TMEDA Complexes: Precursors for the Synthesis of Dinuclear Dicationic Copper(II) Complexes. *Inorg. Chim. Acta.* **2005**, *358*(4), 1193-1203.
- (59) Stephens, F. S.; Tucker, P. A. Crystal and Molecular Structure of Chloro Bis(2,2'-bipyridyl)copper(II) Chloride Hexahydrate. *J. Chem. Soc., Dalton Trans.* **1973**, *21*, 2293-2297.
- (60) Hinsberg, W. D.; Houle, F. A., Chemical Kinetics Simulator Program, v1.0, IBM Corporation, **1995**. available for a no-cost license from <http://www.almaden.ibm.com/st/msim>.

- (61) Moroni, A. F. Effect of Solvent in Thermal Decomposition of Azobisisobutyronitrile. *Makromol. Chem.* **1967**, *105(1)*, 43-49.
- (62) Talat-Erben, M.; Bywater, S. The Thermal Decomposition of 2,2'-Azo-bis-isobutyronitrile. Part II. Kinetics of the Reactions. *J. Am. Chem. Soc.* **1955**, *77*, 3712-3713.
- (63) Tabka, M. T.; Chenal, J.; Widmaier, J. Effect of stannous octoate on the thermal decomposition of 2,2'-azobis(isobutyronitrile). *Polym Int.* **2000**, *49*, 412-416.
- (64) Hammond, G. S.; Wu, C. S.; Trapp, O. D.; Warkentin, J.; Keys, R. T. The Mechanism of Decomposition of Azo Compounds. II. Cage Effects in the Decomposition of α,α -Azobisisobutyronitrile and Related Compounds. *J. Am. Chem. Soc.* **1960**, *82*, 5394-5399.
- (65) Szafko, J.; Feist, W. Solvation effect in thermal decomposition of 2,2'-azobisisobutyronitrile. *J. Polym. Sci. Part A: Polym. Chem.* **1995**, *33*, 1643-1655.
- (66) Van Hook, J. P.; Tobolsky, A. V. The Thermal Decomposition of 2,2'-Azo-bis-isobutyronitrile. *J. Am. Chem. Soc.* **1958**, *80*, 779-782.
- (67) Matyjaszewski, K.; Gobelt, B.; Paik, H.-j.; Horwitz, C. P. Tridentate Nitrogen-Based Ligands in Cu-Based ATRP: A Structure-Activity Study. *Macromolecules.* **2001**, *34(3)*, 430-440.
- (68) Gromada, J.; Matyjaszewski, K. Measurement of Initial Degree of Polymerization without Reactivation as a New Method to Estimate Rate Constants of Deactivation in ATRP. *Macromolecules.* **2002**, *35(16)*, 6167-6173.
- (69) Simal, F.; Wlodarczak, L.; Demonceau, A.; Noels, A. F. New, Highly Efficient Catalyst Precursors for Kharasch Additions – $[\text{RuCl}(\text{Cp}^*)(\text{PPh}_3)_2]$ and $[\text{RuCl}(\text{Ind})(\text{PPh}_3)_2]$. *Eur. J. Org. Chem.* **2001**, 2689-2695.
- (70) Beckwith, A. L. J.; Bowry, V. W.; Ingold, K. U. Kinetics of nitroxide radical trapping. 1. Solvent effects. *J. Am. Chem. Soc.* **1992**, *114(13)*, 4983-4992.
- (71) Bowry, V. W.; Ingold, K. U. Kinetics of Nitroxide Radical Trapping. 2. Structural Effects. *J. Am. Chem. Soc.* **1992**, *114*, 4992-4996.

- (72) Grattan, D. W.; Carlsson, D. J.; Howard, J. A.; Wiles, D. M. The thermal decomposition of 1-(2'-cyano-2'-propoxy)-4-oxo-2,2,6,6-tetramethylpiperidine. *Can. J. Chem.* **1979**, *57*, 2834-2842.
- (73) Skene, W. G.; Scaiano, J. C.; Listigovers, N. A.; Kazmaier, P. M.; Georges, M. K. Rate Constants for the Trapping of Various Carbon-Centered Radicals by Nitroxides: Unimolecular Initiators for Living Free Radical Polymerization. *Macromolecules*. **2000**, *33*, 5065-5072.
- (74) Nanda, A. K.; Matyjaszewski, K. Effect of Penultimate Unit on the Activation Process in ATRP. *Macromolecules*. **2003**, *36*, 8222-8224.
- (75) Chambard, G.; Klumperman, B.; German, A. L. Effect of Solvent on the Activation Rate Parameters for Polystyrene and Poly(butyl acrylate) Macroinitiators in Atom Transfer Radical Polymerization. *Macromolecules*. **2000**, *33*(12), 4417-4421.
- (76) Kwark, Y.-J.; Novak, B. M. Determination of the Kinetic Parameters of Atom Transfer Radical Polymerizations. *Macromolecules*. **2004**, *37*(25), 9395-9401.
- (77) Shipp, D. A.; Matyjaszewski, K. Kinetic Analysis of Controlled/"Living" Radical Polymerizations by Simulations. 1. The Importance of Diffusion-Controlled Reactions. *Macromolecules*. **1999**, *32*(9), 2948-2955.
- (78) Al-Harthi, M.; Soares, J. B. P.; Simon, L. Modeling of atom transfer radical polymerization with bifunctional initiators: diffusion effects and case studies. *Macromol. Chem. Phys.* **2006**, *207*(5), 469-483.
- (79) Tang, W.; Matyjaszewski, K. Kinetic Modeling of Normal ATRP, Normal ATRP with $[\text{Cu}^{\text{II}}]_0$, Reverse ATRP and SR & NI ATRP. *Macromol. Theory Simul.* **2008**, *17*, 359-375.

Chapter 5

Photoinitiated Ambient Temperature Copper-Catalyzed Atom Transfer Radical Addition and Cyclization Reactions in the Presence of AIBN as Reducing Agent

5.1 Introduction

Transition metal catalyzed Kharasch addition or atom transfer radical addition (TMC ATRA), is an effective tool for C-C bond formation and has gained considerable interest in organic synthesis.¹⁻⁵ With the discovery of transition metal complexes, such as those of Cu,⁶⁻⁸ Ru,⁹⁻¹⁴ Fe¹⁵⁻¹⁸ or Ni¹⁹⁻²⁴, as potential catalysts for ATRA, diminished polymerization has been achieved and selectivity towards the formation of single addition adducts has dramatically improved. However, the large amounts of metal catalysts needed to achieve quantitative yields and high selectivity towards the desired product made TMC ATRA an expensive and environmentally unfriendly process.²⁵⁻²⁸ The use of free radical initiators, such as the diazo compound 2,2'-azobis(isobutyronitrile) or AIBN, as reducing agents has significantly reduced the amount of metal catalysts required for such reactions.²⁹⁻³⁴ The thermal decomposition of AIBN yields two isobutyronitrile radicals, which constantly regenerate the active catalyst species (metal complex in lower oxidation state), preventing the accumulation of the deactivator species (higher oxidation state metal complex) (for the mechanism, see Scheme 3.1). Since such regeneration

compensates for the unavoidable radical termination reactions, the amount of catalysts used has been greatly reduced to ppm levels. However, these free-radical-initiated processes have been plagued by side reactions (namely radical-initiated polymerization) especially when highly reactive monomers are involved. The elevated temperatures used in these ATRA reactions, which is necessary for faster decomposition of AIBN, increase the propagation rate constant of the monomers and the target products are often contaminated by oligomers/polymers formed by direct initiation from the free radical initiator.

In our recent work,³⁵ we reported ATRA reactions of various alkyl halides and alkenes using a free radical initiator (2,2'-azobis(4-methoxy-2,4-dimethylvaleronitrile) or V70) that readily decomposes at room temperature. The use of a low temperature radical initiator allowed the reactions to be performed at ambient temperature, which also lowered the propagation rate constants of the highly active monomers (Table 5.1). Impressive results were obtained in the addition of CCl₄ and CBr₄ to various alkenes, with TONs as high as 12500 for CBr₄ and [Cu^{II}(TPMA)Br][Br].³⁵ Indeed, a lower reaction temperature enabled the selective formation of the single addition adducts, as can be seen in the comparison of the results obtained at 60°C (Table 5.2).

Table 5.1. Propagation Rate Constants of Highly Active Alkenes³⁶

Alkene	k_p (M ⁻¹ s ⁻¹)	
	60°C	25°C
methyl acrylate	2090	883
methyl methacrylate	515	190
vinyl acetate	2300	1000
acrylonitrile	1960	930
styrene	165	--

Table 5.2. ATRA of CCl₄ to Highly Active Alkenes at 60°C and Ambient Temperature^a

Alkene	[Alk] ₀ : [Cu ^{II}] ₀	%Product	
		AIBN (60°C) ^b	V70 (room T) ^c
styrene	500:1	66	94
styrene	1000:1	61	94
styrene	2000:1	60	100
methyl acrylate	1000:1	47	84
methyl acrylate	2000:1	30	62
methyl methacrylate	1000:1	46 ^d	66
methyl methacrylate	2000:1	32 ^d	51
vinyl acetate	1000:1	90 ^d	98
vinyl acetate	2000:1	78 ^d	88
acrylonitrile	1000:1	53 ^d	68 ^d
acrylonitrile	2000:1	38 ^d	62 ^d

^a catalyst = [Cu^{II}(TPMA)Cl][Cl], solvent = CH₃CN, time = 24 h.

^b [alkene]₀: [CCl₄]₀: [AIBN]₀ = 1:4:0.05; for reference, see [37].

^c [alkene]₀: [CCl₄]₀: [V70]₀ = 1:1:0.05; for reference, see [35].

^d unpublished results

In spite of the promising ATRA results with V70, the use of this low temperature free radical initiator is not practical on a large scale because of the high cost involved in its shipment (V70 decomposes at room temperature and, thus, requires special handling during shipping). We, therefore, explored other ways to perform the reactions at a lower temperature using the cheaper radical initiator (AIBN). One possible alternative to generate the isobutyronitrile radicals from AIBN without the use of heat is through UV irradiation. Commonly used thermal radical initiators, including azo and peroxide compounds, are also known to be capable of photoinitiation.³⁸ The light-induced decomposition of AIBN is established to be first-order with a rate of $k=1.23 \times 10^{-4} \text{ s}^{-1}$ at 80°C.³⁸ Additionally, organohalogen derivatives with weak C-X bonds (where

X=halogen) can also undergo photolysis. Alkyl chlorides absorb in the vacuum UV region ($\lambda=10-200$ nm) while alkyl bromides and iodides absorb at longer wavelengths ($\lambda=200-350$ nm).³⁹ Indeed, light has been successfully used by Kharasch in the 1940's in the addition of polyhalogenated alkanes (CBr₄, CCl₄, CBr₃Cl, CCl₃Br) to alkenes.⁴⁰⁻⁴³ Thus, the advantage of employing UV irradiation in ATRA is two-fold. First, ATRA reactions can now be carried out at lower temperatures, which will consequently lower the propagation rate constants of highly polymerizable monomers and allow selective formation of the desired monoadduct. Second, it could increase the yield of monoadduct as a result of the contribution of the addition of radical generated from the photolytic cleavage of the carbon-halogen bond.

In this chapter, photoinitiated ATRA reactions involving alkenes that are highly active in free radical polymerization, such as methyl acrylate, methyl methacrylate, vinyl acetate, acrylonitrile and styrene are presented. Various polyhalogenated (carbon tetrabromide (CBr₄), carbon tetrachloride (CCl₄), bromoform (CHBr₃), chloroform (CHCl₃), ethyl trichloroacetate (EtOCOCl₃)) and monohalogenated compounds (benzyl bromide (BzBr) and benzyl chloride (BzCl)) were used in the ATRA reactions. Atom transfer radical cascade reactions initiated by the photodecomposition of AIBN, which results in the formation of interesting *5-exo-trig* cyclic compounds, were also explored.

5.2 Experimental

5.2.1 General Procedures

All reagents were obtained from commercial sources. 2,2'-Azobis(2-methylpropionitrile) (AIBN) was recrystallized from cold methanol and dried at room temperature under vacuum. Solvents (acetonitrile and toluene) were degassed and deoxygenated using Innovative Technology solvent purifier. Tris(2-pyridylmethyl)amine (TPMA)⁴⁴ and copper(II) complexes $[\text{Cu}^{\text{II}}(\text{TPMA})\text{Cl}][\text{Cl}]^{\text{30}}$ and $[\text{Cu}^{\text{II}}(\text{TPMA})\text{Br}][\text{Br}]^{\text{30}}$ were synthesized according to published procedures. All other reagents were used as received. UV-irradiation was carried out using a high-intensity UV curing lamp (Spectroline model SB-100PC, Spectronics Corporation, Westbury, NY, long wave UV (365 nm)), which is equipped with a 2F100C clear filter that reduces transmission of medium wave (UV-B) and short wave (UV-C) radiation to safe levels, while emitting a UV intensity of 27,000 $\mu\text{W}/\text{cm}^2$ at 6-inch (15 cm). ¹H NMR spectra were obtained at room temperature on a Bruker Avance 400 MHz spectrometer with chemical shifts given in ppm relative to the residual solvent peak (CDCl_3 , 7.26 ppm).

5.2.2 Kharasch Addition of Halogenated Compounds to Alkenes

A stock solution containing an alkene, AIBN, and an internal standard (toluene or *p*-dimethoxybenzene for methyl acrylate and methyl methacrylate; anisole for vinyl acetate, acrylonitrile, styrene) was prepared ($[\text{alkene}]_0:[\text{AIBN}]_0 = 1:0.05$). The desired amount of alkyl halide was added to 0.3 ml of the stock solution. The total volume was adjusted by adding acetonitrile to obtain consistent alkene concentration in each reaction system ($[\text{alkene}]_0 = 0.75\text{M}$). The resulting solution was then placed in an NMR tube,

purged with argon for 1 min, capped and sealed with Teflon tape. The NMR tubes were then placed in a water bath and under a UV lamp for 24 hr.

5.2.3 Copper-Catalyzed ATRA of Halogenated Compounds to Alkenes

The corresponding alkene, alkyl halide, AIBN (for CCl_4 , CBr_4 , CHCl_3 , CHBr_3 , EtOCOCl_3 : $[\text{alkene}]_0:[\text{RX}]_0:[\text{AIBN}]_0=1:1.25:0.05$; for BzCl and BzBr : $[\text{alkene}]_0:[\text{RX}]_0:[\text{AIBN}]_0=1:4:0.05$) and an internal standard (toluene or *p*-dimethoxybenzene for methyl acrylate and methyl methacrylate; anisole for vinyl acetate, acrylonitrile, styrene) was dissolved in acetonitrile to make up a stock solution ($[\text{alkene}]_0=1.1\text{M}$). The desired amount of Cu^{II} catalyst ($[\text{Cu}^{\text{II}}(\text{TPMA})\text{Cl}][\text{Cl}]$ for alkyl chlorides, $[\text{Cu}^{\text{II}}(\text{TPMA})\text{Br}][\text{Br}]$ for alkyl bromides, $[\text{Cu}^{\text{II}}]_0=0.025\text{ M}$) was added to 0.3 ml of the stock solution in an NMR tube. The total volume was adjusted by adding acetonitrile to obtain consistent alkene concentration in each reaction system ($[\text{alkene}]_0=0.75\text{M}$). After purging the solution with argon for 1 min, the NMR tube was capped and sealed with Teflon tape. The NMR tubes were then placed in a water bath to maintain an ambient reaction temperature and irradiated under a UV lamp for 24 hr.

5.2.4 Kinetic Studies

The desired amount of $[\text{Cu}^{\text{II}}(\text{TPMA})\text{Cl}][\text{Cl}]$ (440 μL , 0.025 M solution in acetonitrile) was added to 1.0 mL of the acetonitrile solution containing CCl_4 , alkene, AIBN, and the internal standard ($[\text{CCl}_4]_0:[\text{alkene}]_0:[\text{AIBN}]_0 = 1.25:1:0.05$, $[\text{alkene}]_0=0.75\text{ M}$). A 0.3 ml aliquot of the reaction mixture was then placed in separate NMR tubes. The reaction mixture was purged for 1 min with argon, capped, sealed with Teflon tape, and placed under a UV lamp. A water bath was used to maintain the reaction temperature at

23 ± 2 °C. An NMR tube containing an aliquot of the reaction mixture was quenched at timed intervals and analyzed using ¹H NMR spectroscopy.

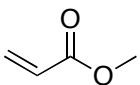
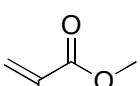
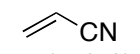
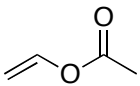
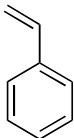
5.3 Results and Discussion

5.3.1 Kharasch Addition of Halogenated Compounds to Highly Active Alkenes

In the first set of experiments, the non-metal catalyzed Kharasch addition of halogenated alkanes to monomers that are highly active in free radical polymerization was initiated by free radicals generated from the photodecomposition of AIBN. As shown in Table 5.3 (entries 3 and 5), addition of polybrominated compounds (CBr₄ and CHBr₃) to methyl acrylate at ambient temperature resulted to low yields of the monoadduct (30-38%). Polymerization side reactions were evident in the high conversion of the alkene. Addition of CCl₄ resulted to a much lower monoadduct yield (2%) with a high percent conversion, again indicating the formation of AIBN-initiated polymers. Nearly quantitative conversions of methyl acrylate were also observed for the other less active alkyl halides with no formation of the monoadduct. These results were consistent with those of Kharasch, in which the addition of alkyl halides to highly active alkenes in the presence of free radical initiators only led to the formation of polymers initiated by the free radicals.

Similarly, low yields of the alkyl halide-vinyl acetate adduct were obtained in the Kharasch addition of polyhalogenated alkanes CCl₄ and CBr₂ (entries 26 and 27). However, the percent conversion of vinyl acetate was also low, which suggests insignificant polymer formation. The selective formation of the monoadduct is expected with vinyl acetate since it has a high chain transfer constant ($k_{tr}/k_p = 1.04$ for CCl₄).³⁶

Table 5.3. Photoinitiated Kharasch Addition of Polyhalogenated Compounds to Highly Active Alkenes at Ambient Temperature^a

Entry	Alkene	Alkyl Halide	[Alk] ₀ : [RX] ₀	%Conv	%Product	%Yield ^b
1		none	1:0	86	0	0
2		CCl ₄	1:1.25	93	2	2
3		CBr ₄	1:1.25	95	40	38
4		CHCl ₃	1:1.25	79	0	0
5	methyl acrylate	CHBr ₃	1:1.25	48	61	30
6		EtOCOCl ₃	1:1.25	84	0	0
7		BzCl	1:4	87	0	0
8		BzBr	1:4	88	0	0
9		none	1:0	80	0	0
10		CCl ₄	1:1.25	85	5	4
11		CBr ₄	1:1.25	93	10	9
12		CHCl ₃	1:1.25	83	0	0
13	methyl methacrylate	CHBr ₃	1:1.25	84	4	3
14		EtOCOCl ₃	1:1.25	85	0	0
15		BzCl	1:4	83	0	0
16		BzBr	1:4	86	0	0
17		none	1:0	33	0	0
18		CCl ₄	1:1.25	38	0	0
19		CBr ₄	1:1.25	42	25	11
20		CHCl ₃	1:1.25	34	0	0
21	acrylonitrile	CHBr ₃	1:1.25	36	0	0
22		EtOCOCl ₃	1:1.25	34	0	0
23		BzCl	1:4	33	0	0
24		BzBr	1:4	33	0	0
25		none	1:0	0	0	0
26		CCl ₄	1:1.25	26	76	20
27		CBr ₄	1:1.25	32	87	28
28		CHCl ₃	1:1.25	9	0	0
29	vinyl acetate	CHBr ₃	1:1.25	14	9	1
30		EtOCOCl ₃	1:1.25	7	0	0
31		BzCl	1:4	0	0	0
32		BzBr	1:4	2	0	0
33		none	1:0	10	0	0
34		CCl ₄	1:1.25	12	0	0
35		CBr ₄	1:1.25	27	42	11
36		CHCl ₃	1:1.25	11	0	0
37		CHBr ₃	1:1.25	26	0	0
38	styrene	EtOCOCl ₃	1:1.25	10	0	0
39		BzCl	1:4	11	0	0
40		BzBr	1:4	10	0	0

^aAll reactions were performed in CH₃CN in the presence of light for 24 h. Reaction temperature was maintained at 23 ± 2 °C using a water bath. [alkene]₀: [AIBN]₀ = 1:0.05, [alkene]₀ = 0.75M, ^bYield is based on the formation of monoadduct and was determined by ¹H NMR spectroscopy (relative errors are ± 10%).

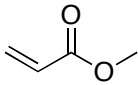
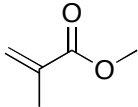

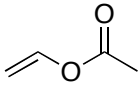
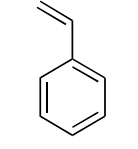
The desired monoadduct was not obtained in the addition of the other halogenated compounds to vinyl acetate (entries 28-32). However, free-radical initiated polymerization was also negligible, which is evident in the low conversion of the alkene.

Kharasch addition of halogenated compounds to other highly active monomers such as methyl methacrylate (entries 10-16), acrylonitrile (entries 18-24), and styrene (entries 34-40) was also conducted without a Cu catalyst. In all three alkenes, very low yields of the CBr₄ monoadduct were obtained and the competing polymerization reaction led to a high conversion of the alkene. Monoadduct formation was negligible or was not observed for the less active alkyl halides. These results clearly show that the halogenated compounds are ineffective as chain transfer agents for these highly active alkenes in the presence of free radical initiators.

5.3.2 Photoinitiated Copper Catalyzed ATRA of CCl₄ and CBr₄ to Highly Active Alkenes

The [Cu^{II}(TPMA)X][X] (X = Cl or Br) complex was then used as a catalyst in the ATRA of CCl₄ and CBr₄ to the highly active alkenes at ambient temperature. Transition metal catalysts were shown to be very efficient chain-transfer agents in radical addition reactions and the yield of monoadduct was expected to increase in the presence of a metal catalyst. As evident from Table 5.4 (entry 2), total conversion of methyl acrylate to the CCl₄-methyl acrylate monoadduct was observed in the presence of 1 mol% of the [Cu^{II}(TPMA)Cl][Cl] catalyst. Nearly quantitative yields were also obtained even at lower catalyst loadings (up to 0.05 mol% of the catalyst, entries 3-5). Even more impressive

Table 5.4. Photoinitiated Copper-Catalyzed ATRA of CCl₄ and CBr₄ to Highly Active Alkenes at Ambient Temperature^a

Entry	Alkene	Alkyl Halide	[Alk] ₀ : [Cu ^{II}] ₀	%Conv	%Product	%Yield ^d
1	 methyl acrylate	CCl ₄ ^b	1000:1	100	47	47
2		CCl ₄	100:1	100	100	100
3		CCl ₄	500:1	100	99	99
4		CCl ₄	1000:1	100	94	94
5		CCl ₄	2000:1	100	85	85
6		CBr ₄ ^c	500:1	100	100	100
7		CBr ₄ ^c	10000:1	100	79	79
8	 methyl methacrylate	CCl ₄ ^b	1000:1	100	46	46
9		CCl ₄	100:1	100	100	100
10		CCl ₄	500:1	100	99	99
11		CCl ₄	1000:1	95	96	91
12		CCl ₄	2000:1	90	90	81
13		CBr ₄ ^c	500:1	100	100	100
14		CBr ₄ ^c	10000:1	100	73	73
15	 acrylonitrile	CCl ₄ ^b	1000:1	100	48	48
16		CCl ₄	100:1	100	98	98
17		CCl ₄	500:1	100	84	84
18		CCl ₄	1000:1	100	75	75
19		CCl ₄	2000:1	96	68	65
20		CBr ₄ ^c	500:1	100	96	96
21		CBr ₄ ^c	1000:1	95	92	87
22	 vinyl acetate	CCl ₄ ^b	1000:1	99	90	88
23		CCl ₄	100:1	99	100	99
24		CCl ₄	500:1	98	100	98
25		CCl ₄	1000:1	96	99	95
26		CCl ₄	2000:1	95	97	92
27		CBr ₄ ^c	500:1	99	100	99
28		CBr ₄ ^c	5000:1	78	95	74
29	 styrene	CCl ₄ ^b	1000:1	65	58	38
30		CCl ₄	100:1	99	97	96
31		CCl ₄	500:1	50	92	46
32		CCl ₄	1000:1	32	90	29
33		CCl ₄	2000:1	27	82	22
34		CBr ₄ ^c	500:1	77	98	75
35		CBr ₄ ^c	2000:1	60	85	51

^aAll reactions were performed in CH₃CN in the presence of light for 24 h. Reaction temperature was maintained at 23 ± 2 °C using a water bath. [alkene]₀: [AIBN]₀ = 1:0.05, [alkene]₀ = 0.75M, catalyst = [Cu^{II}(TPMA)Cl][Cl]. ^bAIBN decomposition by heating at 60°C; ^ccatalyst = [Cu^{II}(TPMA)Br][Br]. ^dYield is based on the formation of monoadduct and was determined by ¹H NMR spectroscopy (relative errors are ± 10%).

results were obtained in the ATRA of CBr_4 to methyl acrylate using as low as 0.01 mol% of the $[\text{Cu}^{\text{II}}(\text{TPMA})\text{Br}][\text{Br}]$ catalyst (entry 7). Also, lowering the reaction temperature does, indeed, promote the selective formation of the target monoadduct, as can be seen in the ATRA results at 60°C (entry 1) and at ambient temperature (entry 4), which were done at the same alkene-to-catalyst ratio. Similar results were also obtained in the ATRA reactions involving methyl methacrylate. The CCl_4 -methyl methacrylate monoadduct was formed in excellent yields using 0.05-1 mol% of the copper catalyst (entries 9-12). In the ATRA of CBr_4 to methyl methacrylate (entries 13-14), high yields of the monoadduct were observed even at very low catalyst loadings (0.01 mol% relative to the alkene). At an alkene-to-catalyst ratio of 1000:1, the amount of monoadduct formed at ambient temperature (entry 11) was again approximately two times higher than at 60°C (entry 8). The ATRA of CCl_4 and CBr_4 to acrylonitrile, vinyl acetate and styrene also showed high selectivity towards monoadduct formation (entries 16-21, 23-28, 30-35). However, conversion of styrene was significantly lower than the other alkenes, which was due to the slower rate of addition at ambient temperature and will be further discussed in section 5.3.4 in this chapter.

These promising results, which are similar to our previous findings in ATRA reactions in the presence of V70,³⁵ show that generation of free radicals from the photolysis of AIBN is as efficient as the decomposition of V70 at room temperature and can be successfully applied in catalyst regeneration for ambient temperature ATRA reactions. With the exception of styrene, the ambient temperature ATRA reactions still proceeded at a reasonable rate to allow quantitative consumption of the alkene at a reasonable amount of time. Encouraged by these results, we then investigated ATRA of

less active alkyl halides such as CHBr_3 , CHCl_3 , EtOCOCl_3 , BzBr , and BzCl to reactive alkenes (methyl acrylate, methyl methacrylate, acrylonitrile, vinyl acetate, and styrene).

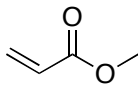
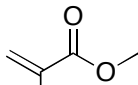
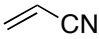
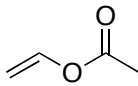
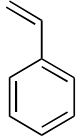
5.3.3 Photoinitiated Copper-Catalyzed ATRA of CHBr_3 , CHCl_3 , EtOCOCl_3 , BzBr and BzCl to Highly Active Alkenes

Alkyl halides with less number of halogen atoms on the carbon radical center typically have lower activation rate constants⁴⁵ and are, thus, less reactive towards addition to an alkene and often requires harsher reaction conditions, high catalyst loadings, and a huge excess of the alkyl halide to achieve reasonable yields of the monoadduct. For instance, Snapper *et. al.* reported quantitative yields of the monoadduct in the ATRA of CHCl_3 to styrene using 10 equivalents of the alkyl halide relative to the alkene (alkyl halides used are typically 4 equivalents or less relative to the alkene) at an alkene-to-catalyst ratio of 40:1.²⁸ ATRA reactions involving monohalogenated compounds are far less common which is unfortunate since monoadducts with a single functional group are easier to manipulate in subsequent chemical transformations.

We investigated the TMC ATRA of less active alkyl halides to alkenes in the presence of light. Kharasch *et. al.* previously reported that the halogenation of various alkanes and alkenes were greatly accelerated by UV light.^{42,43,46-49} Thus, the use of UV irradiation in our reactions will not only promote the photodecomposition of AIBN at ambient temperature but will also induce the photolytic cleavage of the carbon-halogen bonds of the alkyl halide and allow the addition to the alkenes to proceed more efficiently.

As indicated in Table 5.5 (entries 1 to 3), addition of polyhalogenated compounds CHBr_3 , CHCl_3 and EtOCOCl_3 to methyl acrylate proceeded with reasonable yields.

Table 5.5. Photoinitiated Copper Catalyzed ATRA of CHBr_3 , CHCl_3 , EtOCOCl_3 , BzBr and BzCl to Highly Active Alkenes at Ambient Temperature^a

Entry	Alkene	Alkyl Halide	[Alk] ₀ : [RX] ₀	%Conv	%Prod	%Yield ^b
1		CHBr_3	1:1.25	70	90	63
2		CHCl_3	1:1.25	51	90	46
3		EtOCOCl_3	1:1.25	55	89	49
4		BzBr	1:4	42	78	33
5		BzCl	1:4	35	74	26
6		CHBr_3	1:1.25	98	32	31
7		CHCl_3	1:1.25	80	25	20
8		EtOCOCl_3	1:1.25	86	33	28
9		BzBr	1:4	70	17	12
10		BzCl	1:4	59	12	7
11		CHBr_3	1:1.25	69	70	48
12		CHCl_3	1:1.25	55	64	35
13		EtOCOCl_3	1:1.25	50	80	40
14		BzBr	1:4	49	42	21
15		BzCl	1:4	47	35	16
16		CHBr_3	1:1.25	10	95	9
17		CHCl_3	1:1.25	5	95	5
18		EtOCOCl_3	1:1.25	10	99	10
19		BzBr	1:4	3	0	0
20		BzCl	1:4	0	0	0
21		CHBr_3	1:1.25	89	88	78
22		CHCl_3	1:1.25	61	80	49
23		EtOCOCl_3	1:1.25	68	90	61
24		BzBr	1:4	40	84	34
25		BzCl	1:4	29	79	23

^aAll reactions were performed in CH_3CN in the presence of light for 24 h. Reaction temperature was maintained at 23 ± 2 °C using a water bath. $[\text{alkene}]_0: [\text{Cu}^{\text{II}}]_0: [\text{AIBN}]_0 = 100:1:5$, $[\text{alkene}]_0 = 0.75\text{M}$, catalyst = $[\text{Cu}^{\text{II}}(\text{TPMA})\text{Cl}][\text{Cl}]$ for alkyl chlorides, $[\text{Cu}^{\text{II}}(\text{TPMA})\text{Br}][\text{Br}]$ for alkyl bromides. ^bYield is based on the formation of monoadduct and was determined by ^1H NMR spectroscopy (relative errors are $\pm 10\%$).

However, the monoadduct was formed in lower yields for the monohalogenated alkyl halides even with 4 equivalents of BzBr or BzCl with respect to methyl acrylate (entries 4 and 5), which were attributed incomplete alkene conversion. For methyl methacrylate (entries 6 to 10) and vinyl acetate (entries 16 to 18), monoadduct was

obtained in significantly lower yields than with methyl acrylate. In the case of methyl methacrylate, the low yields were not mainly due to incomplete alkene conversion but rather due to the faster rate of propagation relative to the rate of addition of the alkyl halides, leading to the formation of large amounts of polymers even at lower temperatures. Additionally, BzBr and BzCl were quite inactive alkyl halides in copper-catalyzed ATRA of vinyl acetate (entries 19 and 20). Monoadduct formation was observed in the ATRA reactions involving acrylonitrile (entries 11 to 15) and styrene (entries 21 to 25), albeit in lower yields. Furthermore, the conversions of the alkene were also significantly lower in the ATRA of monohalogenated compounds as compared to the conversions using trisubstituted alkyl halides. For all alkenes, the discrepancies between the conversion and the yield were attributed to the competing free radical polymerization.

Despite the unfavorable yields obtained in the copper-catalyzed ATRA of BzBr and BzCl to alkenes, to the best of our knowledge, these are the first ever reported ATRA reactions involving these monohalogenated compounds. The monoadduct yields can be improved by performing the reactions at longer reaction times, running reactions neat, increasing the concentrations of the catalyst and alkyl halide relative to the alkene, or by using a more active transition metal catalyst.

5.3.4 Kinetic Studies of Copper-Catalyzed ATRA of CCl₄ to Highly Active Alkenes at Ambient Temperature

The consumption of the alkene over time in the ATRA of CCl₄ to the highly active alkenes at ambient temperature using 0.2 mol% of the [Cu^I(TPMA)Cl][Cl] catalyst and 5 mol% of AIBN was monitored and the pseudo-first order kinetic plot is shown in Figure 5.1. All of the alkenes exhibited linear plots, which indicates a constant

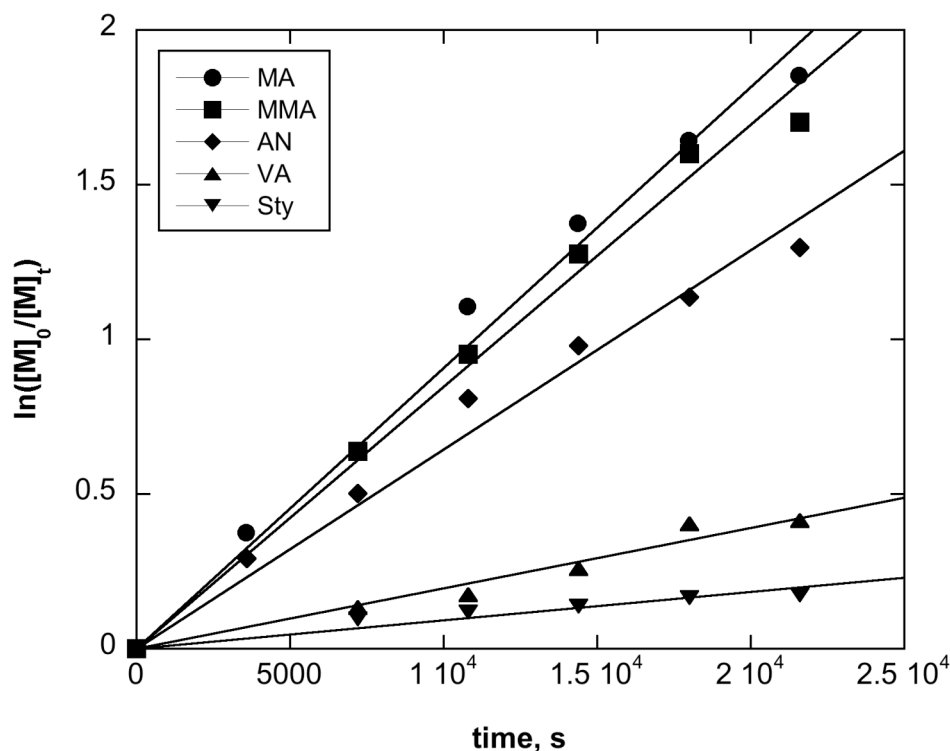


Figure 5.1. Pseudofirst-Order Kinetic Plot for the Photoinitiated ATRA of CCl_4 to Methyl Acrylate (MA), Methyl Methacrylate (MMA), Acrylonitrile (AN), Vinyl Acetate (VA), and Styrene (Sty) using $[\text{Cu}^{\text{II}}(\text{TPMA})\text{Cl}][\text{Cl}]$ as Catalyst and AIBN as Reducing Agent. Experimental Conditions: $[\text{alkene}]_0:[\text{Cu}^{\text{II}}]_0:[\text{CCl}_4]_0:[\text{AIBN}]_0 = 500:1:625:25$, $[\text{alkene}]_0 = 0.75 \text{ M}$, solvent = CH_3CN .

Table 5.6. Values of k_{obs} (s^{-1}) for the Photoinitiated ATRA of CCl_4 to Highly Active Alkenes using $[\text{Cu}^{\text{II}}(\text{TPMA})\text{Cl}][\text{Cl}]$ as Catalyst and AIBN as Reducing Agent^a

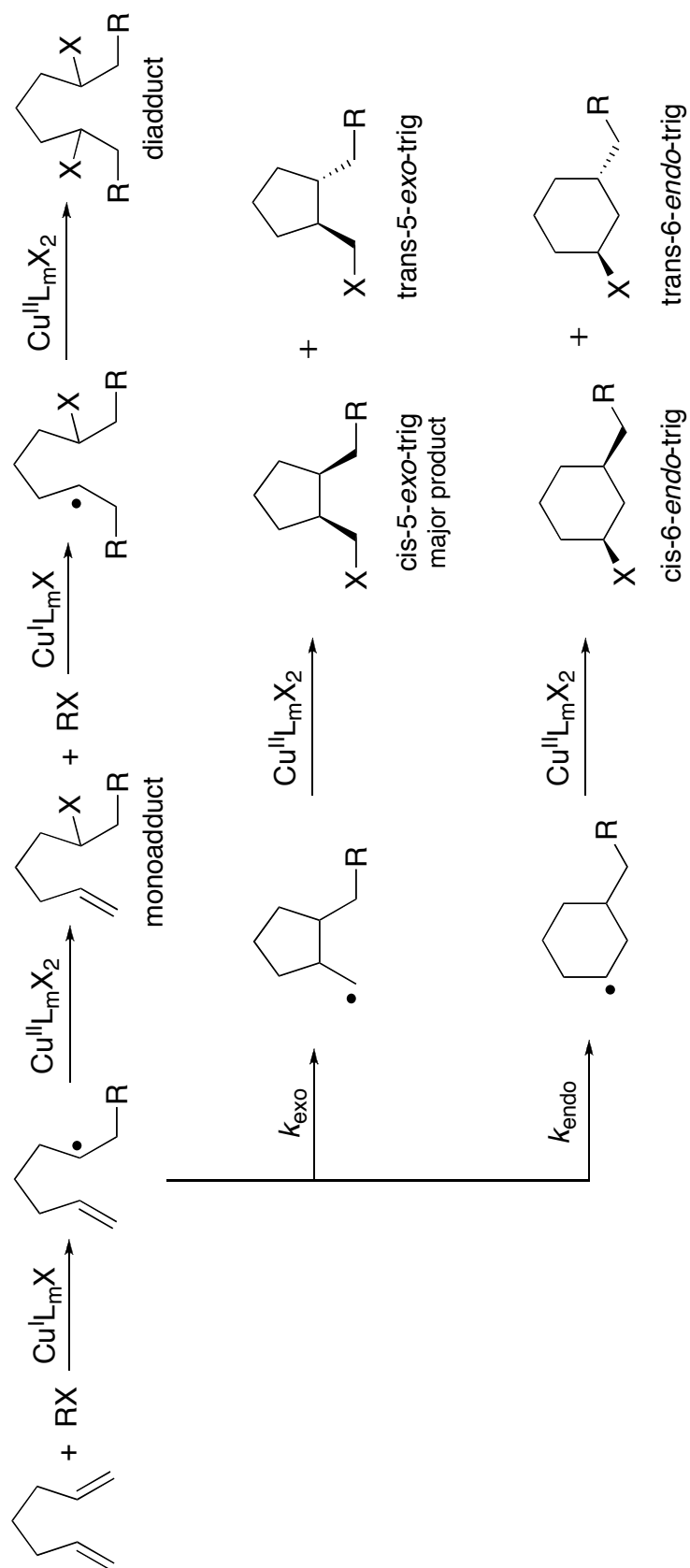
Alkene	k_{obs}
methyl acrylate	$(9.08 \pm 0.05) \times 10^{-5}$
methyl methacrylate	$(8.47 \pm 0.06) \times 10^{-5}$
acrylonitrile	$(6.44 \pm 0.04) \times 10^{-5}$
vinyl acetate	$(1.95 \pm 0.03) \times 10^{-5}$
styrene	$(8.35 \pm 0.02) \times 10^{-6}$

^a $[\text{alkene}]_0:[\text{Cu}^{\text{II}}]_0:[\text{CCl}_4]_0:[\text{AIBN}]_0=500:1:625:25$, $[\text{alkene}]_0=0.75 \text{ M}$, solvent= CH_3CN . Errors are given at 95% confidence limits.

concentration of radicals. The observed rate constants (k_{obs}) were determined from the slopes and are listed in Table 5.6. The sequence of the k_{obs} values was as follows: methyl acrylate > methyl methacrylate > acrylonitrile > vinyl acetate > styrene, and is in good agreement with the results shown in Table 5.4. ATRA of CCl_4 to methyl acrylate, methyl methacrylate and acrylonitrile displayed the highest k_{obs} values (methyl acrylate = $(9.08 \pm 0.05) \times 10^{-5} \text{ s}^{-1}$, methyl methacrylate = $(8.47 \pm 0.06) \times 10^{-5} \text{ s}^{-1}$, acrylonitrile = $(6.44 \pm 0.04) \times 10^{-5} \text{ s}^{-1}$) and all three alkenes were completely consumed after 24 hours, as shown in Table 5.4 (entries 3, 10, 17). Nearly quantitative conversion of vinyl acetate was observed at 24 hours in the ATRA reaction with CCl_4 at an alkene-to-catalyst ratio of 500:1 (Table 5.4, entry 24), which corresponds to the lower k_{obs} value for vinyl acetate ($(1.95 \pm 0.03) \times 10^{-5} \text{ s}^{-1}$). Furthermore, the k_{obs} value obtained for styrene is $(8.35 \pm 0.02) \times 10^{-6} \text{ s}^{-1}$ and the half-life was determined to be 23 hours, which is in good agreement with the result in Table 5.4 (entry 31) wherein 50% conversion of the alkene was observed at 24 hours.

5.3.5 Photoinitiated Atom Transfer Radical Cascade Reactions

In order to expand the synthetic applications of photoinitiated Cu-catalyzed ATRA, atom transfer radical cascade reactions of various 1,6-dienes using $[\text{Cu}^{\text{II}}(\text{TPMA})\text{Cl}][\text{Cl}]$ as catalyst and AIBN as reducing agent were investigated. In cascade reactions, the sequential addition of the alkyl halide to a diene and ring closure via intramolecular attack of the generated radical to the second double bond of the diene



Scheme 5.1. Reaction Pathways in the Atom Transfer Radical Cascade Reaction of Halogenated Compounds to 1,6-Dienes Catalyzed by Copper Complexes (X=Halogen, Pseudohalogen)

substrate leads to the formation of functionalized cyclic compounds. This type of cyclization reaction is particularly attractive since the nature and number of functional groups on the cyclic end product can be controlled by using the appropriate alkyl halide to obtain the desired ring compound.

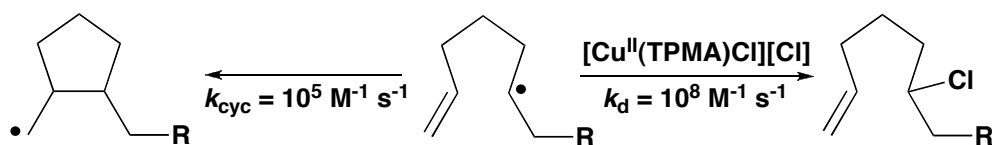
The addition of an alkyl halide to 1,6-diene results in the formation of a 5-hexenyl radical, which generally prefers the formation of a 5-*exo-trig* product ($k_{\text{exo-trig}} \approx 10^5 \text{ s}^{-1}$, $k_{\text{exo-trig}}/k_{\text{endo-trig}} \approx 100$).⁵⁰ Furthermore, cascade reactions of 1,6-dienes typically afford a mixture of the *cis*- and *trans*-isomer with preferential formation of the *cis* cyclic compound (Scheme 5.1).⁵¹⁻⁵⁵ For some substrates, formation of the linear addition products from the direct addition of the alkyl halide to the two unsaturated moiety is also observed.⁵⁴

In this section, the copper-catalyzed atom transfer radical cascade reactions of CCl_4 to various 1,6-dienes in the presence of AIBN as reducing agent and light are reported. As displayed in Table 5.7 (entries 1, 4, 7, 10), cyclization did not occur for all dienes in the absence of a copper catalyst. In contrast, impressive results were observed when the $[\text{Cu}^{\text{II}}(\text{TPMA})\text{Cl}][\text{Cl}]$ catalyst was used in conjunction with AIBN. Nearly quantitative yields of the 5-*exo-trig* products were obtained even at low catalyst loadings (0.05 mol% relative to the diene). Interestingly, the diastereoselectivity of the cyclization reactions was independent on the nature of the substituents on the diene. All four 1,6-dienes resulted only in the formation a 5-*exo-trig* cyclopentane derivative with a *cis:trans* ratio of approximately 80:20. Formation of the 6-*endo-trig* and linear addition products was not observed in all of the cascade reactions. Furthermore, yields of the cyclic products were slightly higher at lower catalyst loadings. At lower Cu^{II} catalyst

Table 5.7. Photoinitiated Copper Catalyzed Atom Transfer Radical Cascade Reactions at Ambient Temperature^a

Entry	1,6-Diene	Product	[Diene] ₀ : [Cu ^{II}] ₀	%Conv	%Yield ^b	Cis: Trans
1			100:0	0	0	0
2			100:1	100	85	82:18
3			2000:1	100	96	80:20
4			100:0	0	0	0
5			100:1	100	92	80:20
6			2000:1	100	97	79:21
7			100:0	0	0	0
8			100:1	88	86	85:15
9			2000:1	92	93	83:17
10			100:0	0	0	0
11			100:1	87	84	85:15
12			2000:1	90	90	85:15

^aAll reactions were performed in methanol in the presence of light for 24 h. Reaction temperature was maintained at 23 ± 2 °C using a water bath. [diene]₀: [CCl₄]₀: [AIBN]₀ = 1:1.25:0.05, catalyst=[Cu^{II}(TPMA)Cl][Cl]. ^bYield is based on the formation of 5-*exo-trig* product and was determined by ¹H NMR spectroscopy using *p*-dimethoxybenzene as internal standard (relative errors are $\pm 10\%$)



Scheme 5.2. Cyclization and Radical Trapping Pathways of the 5-Hexenyl Radical

concentrations, the rate of cyclization will approach the rate of trapping (k_d) resulting in halogen terminated open chain products (for Cu^{II} complexes with the TPMA ligand, $k_d \approx 10^8 \text{ M}^{-1}\text{s}^{-1}$), thus, promoting the cyclization of the 5-hexenyl radical (Scheme 5.2).

Additionally, results in Table 5.7 show similar diastereoselectivities regardless of the catalysts loadings. These findings are in good agreement with the works of Muñoz-Molina and coworkers in which they proposed that the copper complex is not involved in the cyclization steps but rather only in the formation and trapping of the radical.⁵⁴

5.4 Conclusions

We have described the use of UV light in copper-catalyzed atom transfer radical reactions of various halogenated compounds to highly active alkenes in the presence of AIBN as reducing agent. Generation of radicals from the photodecomposition of AIBN efficiently regenerated the copper catalyst at ambient temperature in the ATRA of CCl_4 and CBr_4 , dramatically increasing the yield of monoadduct at very low catalyst loadings. The desired monoadduct was obtained in lower yields in the ATRA of less active alkyl halides, which was mostly due to incomplete alkene conversion. Kinetics studies of the ATRA of CCl_4 to the highly active alkenes using $[\text{Cu}^{\text{II}}(\text{TPMA})\text{Cl}][\text{Cl}]$ as catalyst has shown that the order for the k_{obs} values was as follows: methyl acrylate > methyl methacrylate > acrylonitrile > vinyl acetate > styrene.

Ambient temperature atom transfer radical cascade reactions of CCl_4 to various 1,6-dienes were also performed in the presence of light using $[\text{Cu}^{\text{II}}(\text{TPMA})\text{Cl}][\text{Cl}]$ as catalyst and AIBN as reducing agent. High yields of the 5-*exo-trig* cyclic product were obtained for all 1,6-dienes with preferential formation of the *cis* isomer. Linear addition products and the 6-*endo-trig* cyclopentane derivative were not obtained from the cascade reactions. The ratio of *cis:trans* cyclic isomers was found to be independent on the nature of the substituents on the diene and on catalyst loadings. Yields of cyclic products slightly increased at higher alkene-to-catalyst ratio due to the slower rate of trapping of the 5-hexenyl radical as a result of lower Cu^{II} catalyst concentration.

References

- (1) Severin, K. Ruthenium catalysts for the Kharasch reaction. *Curr. Org. Chem.* **2006**, *10*(2), 217-224.
- (2) Iqbal, J.; Bhatia, B.; Nayyar, K. Transition Metal-Promoted Free-Radical Reactions in Organic Synthesis: The Formation of Carbon-Carbon Bonds. *Chem. Rev.* **1994**, *94*, 519-564.
- (3) Minisci, F. Free-radical addition to olefins in the presence of redox systems. *Acc. Chem. Res.* **1975**, *8*, 165-171.
- (4) Curran, D. P. The design and application of free radical chain reactions in organic synthesis. Part 1. *Synthesis.* **1988**, *6*, 417-439.
- (5) Curran, D. P. The design and application of free radical chain reactions in organic synthesis. Part 2. *Synthesis.* **1988**, *7*, 489-513.
- (6) Munoz-Molina, J. M.; Caballero, A.; Diaz-Requejo, M. M.; Trofimenko, S.; Belderrain, T. R.; Perez, P. J. Copper-Homoscorpionate Complexes as Active Catalysts for Atom Transfer Radical Addition to Olefins. *Inorg. Chem.* **2007**, *46*(19), 7725-7730.
- (7) Munoz-Molina, J. M.; Belderrain, T. R.; Perez, P. J. An Efficient, Selective and Reducing Agent-Free Copper Catalyst for the Atom-Transfer Radical Addition of Halo Compounds to Activated Olefins. *Inorg. Chem.* **2010**.
- (8) Eckenhoff, W. T.; Pintauer, T. Atom Transfer Radical Addition in the Presence of Catalytic Amounts of Copper(I/II) Complexes with Tris(2-pyridylmethyl)amine. *Inorg. Chem.* **2007**, *46*, 5844-5846.
- (9) Borguet, Y.; Richel, A.; Delfosse, S.; Leclerc, A.; Delaude, L.; Demonceau, A. Microwave-enhanced ruthenium-catalysed atom transfer radical additions. *Tetrahedron Letters.* **2007**, *48*(36), 6334-6338.
- (10) De Clercq, B.; Verpoort, F. Synthesis and evaluation of a new class of ruthenium-based catalytic systems for atom transfer radical addition and enol ester synthesis. *J. Organomet. Chem.* **2003**, *672*, 11-16.

- (11) Lundgren, R. J.; Rankin, M. A.; McDonald, R.; Stradiotto, M. Neutral, Cationic, and Zwitterionic Ruthenium(II) Atom Transfer Radical Addition Catalysts Supported by P,N-Substituted Indene or Indenide Ligands. *Organometallics*. **2008**, *27*(2), 254-258.
- (12) Opstal, T.; Verpoort, F. From atom transfer radical addition to atom transfer radical polymerization of vinyl monomers mediated by ruthenium indenylidene complexes. *New J. Chem.* **2003**, *27*(2), 257-262.
- (13) Richel, A.; Delfosse, S.; Cremasco, C.; Delaude, L.; Demonceau, A.; Noels, A. F. Ruthenium catalysts bearing N-heterocyclic carbene ligands in atom transfer radical reactions. **2003**, *44*, 6011-6015.
- (14) Richel, A.; Demonceau, A.; Noels, A. F. Electrochemistry as a correlation tool with the catalytic activities in [Ru(Cl₂(p-cymene)(PAR₃)]-catalyzed Kharasch additions. *Tetrahedron Lett.* **2006**, *47*, 2077-2081.
- (15) Bach, T.; Schlummer, B.; Harms, K. Intramolecular Iron(II)-catalyzed Nitrogen Transfer Reactions of Unsaturated Alkoxy carbonyl Oxides: A Facile and Stereoselective Route to 4,5-Disubstituted Oxazolidinones. *Chem. Eur. J.* **2001**, *7*(12), 2581-2594.
- (16) Bellesia, F.; Forti, L.; Gallini, E.; Ghelfi, F.; Libertini, E.; Pagnoni, U. M. Telechelic oligomers by halogen atom transfer radical addition. *Tetrahedron*. **1998**, *54*(27), 7849-7856.
- (17) Forti, L.; Ghelfi, F.; Libertini, E.; Pagnoni, U. M.; Soragni, E. Halogen Atom Transfer Radical Addition of α -Polychloroesters to Olefins Promoted by Fe⁰ Filings. *Tetrahedron*. **1997**, *53*(52), 17761-17768.
- (18) Forti, L.; Ghelfi, F.; Pagnoni, U. M. Fe⁰ Initiated Halogen Atom Transfer Radical Addition of Methyl 2-Br-2-Cl-Carboxylates to Olefins. *Tetrahedron Letters*. **1996**, *37*(12), 2077-2078.
- (19) Granel, C.; Dubois, P.; Jerome, R.; Teyssie, P. Controlled Radical Polymerization of Methacrylic Monomers in the Presence of a Bis(ortho-chelated) Arylnickel(II) Complex and Different Activated Alkyl Halides. *Macromolecules*. **1996**, *29*(27), 8576-8582.
- (20) Kleij, A. W.; Gossage, R. A.; Gebbink, R. J. M.; Brinkmann, N.; Reijerse, E. J.; Kragl, U.; Lutz, M.; Spek, A. L.; van Koten, G. A "Dendritic Effect" in Homogeneous Catalysis with Carbosilane-Supported Arylnickel(II) Catalysts: Observation of Active-

Site Proximity Effects in Atom-Transfer Radical Addition. *J. Am. Chem. Soc.* **2000**, *122*(49), 12112-12124.

(21) Kleij, A. W.; Gossage, R. A.; Jastrzebski, J. T. B. H.; Boersma, J.; van Koten, G. The "Dendritic Effect" in Homogenous Catalysts with Carbosilane-Supported Arylnickel(II) Catalysts: Observation of Active-Site Proximity Effects in Atom-Transfer Radical Addition. *Angew. Chem. Int. Ed.* **2000**, *39*(1), 176-178.

(22) Kleijn, H.; Jastrzebski, J. T. B. H.; Gossage, R. A.; Kooijman, H.; Spek, A. L.; van Koten, G. *Ortho*-bis(amino)arylnickel(II) Halide Complexes Containing Perfluoroalkyl Chains as Model Catalyst Precursors for Use in Fluorous Biphasic Systems. *Tetrahedron.* **1998**, *54*, 1145-1152.

(23) Spasyuk, D. M.; Zargarian, D.; van der Est, A. New POCN-Type Pincer Complexes of Nickel(II) and Nickel(III). *Organometallics.* **2009**, *28*, 6531-6540.

(24) van de Kuil, L. A.; Grove, D. M.; Gossage, R. A.; Zwikker, J. W.; Jenneskens, L. W.; Drenth, W.; van Koten, G. Mechanistic Aspects of the Kharasch Addition Reaction Catalyzed by Organonickel(II) Complexes Containing the Monoanionic Terdentate Aryldiamine Ligand System [C₆H₂(CH₂NMe₂)₂-2,6-R-4]. *Organometallics.* **1997**, *16*(23), 4985-4994.

(25) Clark, A. J. Atom transfer radical cyclisation reactions mediated by copper complexes. *Chem. Soc. Rev.* **2002**, *31*, 1-11.

(26) Clark, A. J.; Battle, G. M.; Bridge, A. Efficient β -lactam synthesis via 4-exo atom transfer radical cyclisation using CuBr(tripyridylamine) complex. *Tetrahedron Letters.* **2001**, *42*, 4409-4412.

(27) Clark, A. J.; Filik, R. P.; Thomas, G. H. Ligand Geometry Effects in Copper Mediated Atom Transfer Radical Cyclisations. *Tetrahedron Letters.* **1999**, *40*, 4885-4888.

(28) Tallarico, J. A.; Malnick, L. M.; Snapper, M. L. New Reactivity from (PCy₃)₂Cl₂Ru=CHPh: A Mild Catalyst for Kharasch Additions. *J. Org. Chem.* **1999**, *64*, 344-345.

(29) Pintauer, T.; Matyjaszewski, K. Atom transfer radical addition and polymerization reactions catalyzed by ppm amounts of copper complexes. *Chem. Soc. Rev.* **2008**, *37*, 1087-1097.

- (30) Eckenhoff, W. T.; Garrity, S. T.; Pintauer, T. Highly Efficient Copper-Mediated Atom-Transfer Radical Addition (ATRA) in the Presence of Reducing Agent. *Eur. J. Inorg. Chem.* **2008**(4), 563-571.
- (31) Quebatte, L.; Thommes, K.; Severin, K. Highly Efficient Atom Transfer Radical Addition Reactions with a Ru^{III} Complex as a Catalyst Precursor. *J. Am. Chem. Soc.* **2006**, *128*, 7440-7441.
- (32) Pintauer, T. "Greening" of copper catalyzed atom transfer radical addition (ATRA) and cyclization (ATRC) reactions. *ACS Symp. Ser.* **2009**, *1023*, 63-84.
- (33) Eckenhoff, W. T.; Pintauer, T. Copper catalyzed atom transfer radical addition (ATRA) and cyclization (ATRC) reactions in the presence of reducing agents. *Catalysis Reviews.* **2010**, *52*(1), 1-59.
- (34) Clark, A. J.; Wilson, P. Copper mediated atom transfer radical cyclisations with AIBN. *Tetrahedron Letters.* **2008**, *49*, 4848-4850.
- (35) Pintauer, T.; Eckenhoff, W. T.; Ricardo, C.; Balili, M. N. C.; Biernesser, A.; Noonan, S.; Taylor, M. Highly efficient ambient-temperature copper-catalyzed atom transfer radical addition (ATRA) in the presence of free-radical initiator (V70) as a reducing agent. *Chem. Eur. J.* **2009**, *15*, 38-41.
- (36) Odian, G., *Principles of Polymerization*, 4th ed., Wiley, New York, **2004**.
- (37) Balili, M. N. C.; Pintauer, T. Persistent Radical Effect in Action: Kinetic Studies of Copper-Catalyzed Atom Transfer Radical Addition in the Presence of Free-Radical Diazo Initiators as Reducing Agents. *Inorg. Chem.* **2009**, *48*, 9018-9026.
- (38) Sirbiladze, K. J.; Rusznák, I.; Víg, A. The impact of UV irradiation on the radical initiating capacity of dissolved dyes. *Radiation Physics and Chemistry.* **2003**, *67*, 331-334.
- (39) Parsons, A. F., *An Introduction to Free Radical Chemistry*. Blackwell Science Ltd., Oxford, UK, **2000**.
- (40) Kharasch, M. S.; Jensen, E. V.; Urry, W. H. Addition of carbon tetrachloride and chloroform to olefins. *Science.* **1945**, *102*, 128.

- (41) Kharasch, M. S.; Jensen, E. V.; Urry, W. H. Addition of derivatives of chlorinated acetic acids to olefins. *J. Am. Chem. Soc.* **1945**, *67*, 1626.
- (42) Kharasch, M. S.; White, P. C.; Mayo, F. R. Factors affecting the addition of bromine to phenanthrene. *J. Org. Chem.* **1938**, *2*, 574-576.
- (43) Kharasch, M. S.; Berkman, M. G. Effect of organic peroxides in chlorination reactions. *J. Org. Chem.* **1941**, *6*, 810-817.
- (44) Tyeklar, Z.; Jacobson, R. R.; Wei, N.; Murthy, N. N.; Zubieta, J.; Karlin, K. D. Reversible Reaction of Dioxygen (and Carbon Monoxide) with a Copper(I) Complex. X-Ray Structures of Relevant Mononuclear Cu(I) Precursor Adducts and the Trans-(μ -1,2-peroxo)dicopper(II) Product. *J. Am. Chem. Soc.* **1993**, *115*(7), 2677-2689.
- (45) Tang, W.; Matyjaszewski, K. Effects of Initiator Structure on Activation Rate Constants in ATRP. *Macromolecules.* **2007**, *40*(6), 1858-1863.
- (46) Kharasch, M. S.; Rossin, E. H.; Fields, E. K. The Peroxide Effect in the Addition of Halogen Acids to Olefins. XXVI. The Addition of Halogen Acids to Trichloromethylethylene. *J. Am. Chem. Soc.* **1941**, *63*, 2558-2560.
- (47) Kharasch, M. S.; M., H. L. The bromination of aliphatic acids and their acyl derivatives. *J. Org. Chem.* **1941**, *6*, 705-712.
- (48) Kharasch, M. S.; Hered, W.; Mayo, F. R. The bromination of cyclihexane, methylcyclohexane and isobutane. *J. Org. Chem.* **1941**, *6*, 818-829.
- (49) Kharasch, M. S.; Fineman, M. Z. The Oxygen Effect in the Reaction of Bromine with Neopentane, *t*-Butylbenzene and Trimethylacetic Acid. *J. Am. Chem. Soc.* **1941**, *63*, 2776-2779.
- (50) Togo, H., *Advanced Free Radical Reactions for Organic Synthesis*. Elsevier, Oxford, UK, **2004**.
- (51) Diaz-Alvarez, A. E.; Crochet, P.; Zablocka, M.; Duhayon, C.; Cadierno, V.; Majoral, J. P. Developing the Kharasch Reaction in Aqueous Media: Dinuclear Group 8 and 9 Catalysts Containing the Bridging Cage Ligand Tris(1,2-dimethylhydrazino)diphosphane. *Eur. J. Inorg. Chem.* **2008**, 786-794.

- (52) Gilbert, B. C.; Kalz, W.; Lindsay, C. I.; McGrail, P. T.; Parsons, A. F.; Whittaker, D. T. E. Initiation of radical cyclisation reactions using dimanganese decacarbonyl. A flexible approach to preparing 5-membered rings. *J. Chem. Soc., Perkin Trans. 1.* **2000**, 1187-1194.
- (53) Huther, N.; McGrail, P. T.; Parsons, A. F. Radical Reactions Using Decacarbonyldimanganese under Biphasic Conditions. *Eur. J. Org. Chem.* **2004**, 1740-1749.
- (54) Muñoz-Molina, J. M.; Belderrain, T. R.; Perez, P. J. Copper-Catalyzed Synthesis of 1,2-Disubstituted cyclopentanes from 1,6-Dienes by Ring-Closing Kharasch Addition of Carbon Tetrachloride. *Adv. Synth. Catal.* **2008**, 350, 2365-2372.
- (55) Nakamura, T.; Yorimitsu, H.; Shinokubo, H.; Oshima, K. Triethylborane-Induced Radical Addition of Halogenated Compounds to Alkenes and Alkynes in Water. *Synlett.* **1998**, 1351-1352.

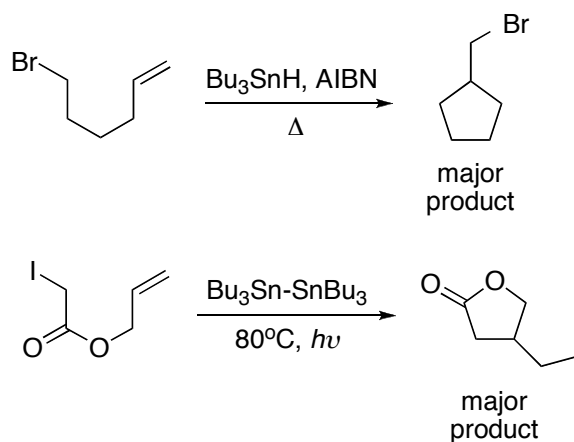
Chapter 6

Copper-Catalyzed Free Radical and Atom Transfer Radical Cyclization Processes

6.1 Introduction

Radical addition reactions are becoming an increasingly popular technique in the rapidly developing field of free radical chemistry.^{1,2} The formation of new carbon-carbon bonds under mild reaction conditions in which a broad range of functional groups is compatible makes radical addition processes highly useful and versatile in organic syntheses. In particular, generation of a radical in a compound that contains a double or a triple bond presents an opportunity for cyclization. Radical cyclization, which is a powerful method for the production of polycyclic compounds, is of great interest because of its wide application in the syntheses of natural products.³⁻⁶ A number of groups have reported successful radical cyclization of polyhaloacetates and amides, leading to the formation of lactones, lactams, and indoles, which are commonly found in basic skeletons of many biologically active natural products.⁷⁻¹³

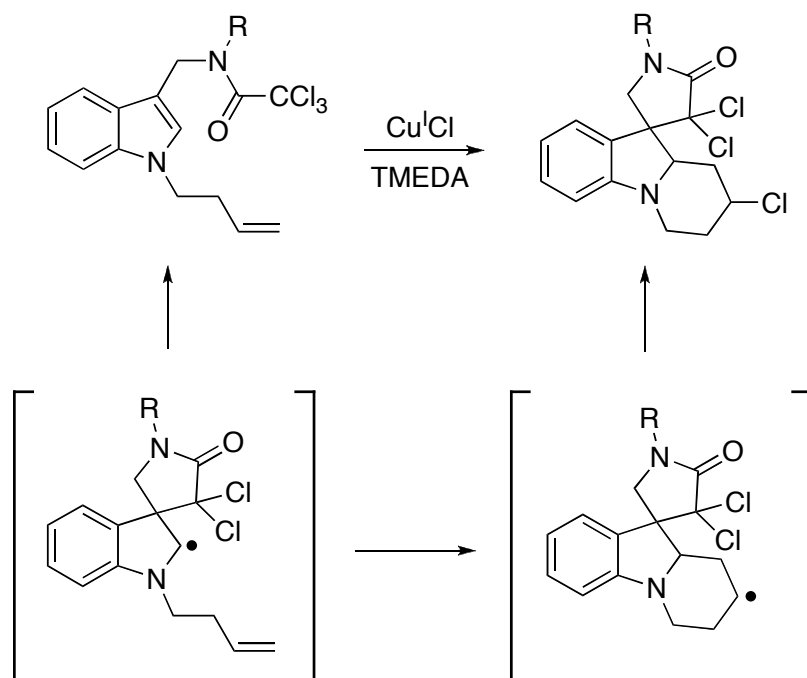
Several methods have been developed to carry out radical cyclization reactions, including the standard tributylstannane method² and the halogen atom transfer method¹⁴⁻¹⁸ using bis(tributyltin) or triethylborane (Scheme 6.1). The latter, which was developed



Scheme 6.1. Tributylstannane (Bu_3SnH) and Halogen Atom Transfer Method

by Curran *et al.*, is particularly attractive since the termination of the radical center after cyclization with a halogen instead of a hydrogen atom generates a product with a reactive center, which can be used for further chemical transformations. Indeed, it has been shown to be very effective in the synthesis of polycyclic spiro-indoles,^{13,19} in which the sequential activation of the functionalized moiety and ring closure via electrophilic attack of the radical center to a double bond led to the formation of multi-ring systems (Scheme 6.2).

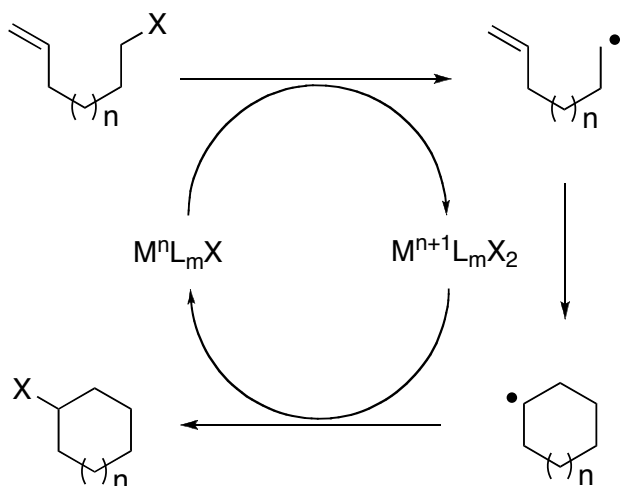
In the last decade, research has been geared towards developing safer and more environmentally friendly techniques for radical cyclization than the commonly used method using tributyltin hydride. In particular, the use of transition metal complexes, such as those of Cu, Ru and Fe,^{9,20-28} as catalysts in atom transfer radical cyclization (ATRC) reactions provides a useful alternative to the more widely used tin hydride variants of these cyclization processes. The Bu_3SnH -mediated reaction has two main disadvantages. First, the reduction of the cyclized radicals by the addition of a hydrogen



Scheme 6.2. Synthesis of Spiro-Indoles via Sequential Radical Cyclization

atom from the mediating reagent greatly limits the synthetic use of the cyclic products due to the loss of the functional groups. Second, the presence of toxic organotin complexes in the reaction mixture necessitates additional purification procedures to remove the tin compounds, often leading to a decrease in product yield. In contrast, transition metal complexes only act as halogen transfer agents and, thus, preserve the functionalized moiety of the cyclization products. Additionally, the design of solid-supported metal catalysts^{29,30} and the use of reducing agents,^{22,31} such as AIBN, to continuously regenerate the active catalyst species greatly lowered the amount of metal catalyst required in the reaction and eliminated the need for tedious purification steps.

Scheme 6.3 outlines the proposed mechanism for ATRC in the presence of a transition metal complex. The carbon-halogen bond of a halogenated substrate is

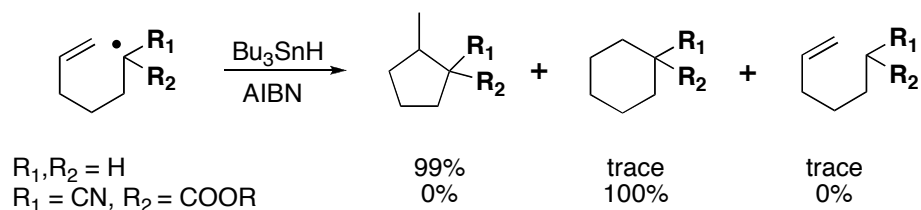


Scheme 6.3. Proposed Mechanism for Transition Metal-Catalyzed Atom Transfer Radical Cyclization (TMC ATRC) (L = Ligand, X = Halogen)

homolytically cleaved by a lower oxidation state metal complex, forming a carbon-centered radical species and a metal complex in a higher oxidation state. Subsequent intramolecular addition of the radical center to the unsaturated moiety generates a cyclic radical species, which is then deactivated by the higher oxidation state metal complex through halogen transfer. ATRC has been successfully applied in the syntheses of γ - and δ -lactones and lactams^{7,25,32-35} and was also extended to the construction of macrocyclic systems²⁸ (ring structures with 8 or more atoms), which was difficult to achieve using the tin hydride method, leading only to the formation of reduced products and oligomers.

This chapter explores both Bu_3SnH -mediated free radical cyclization and atom transfer radical cyclization reactions in the presence of different copper catalysts. Copper(I)-tris(pyrazolyl)borate ($TpCu^I$) compounds are used as catalysts for the free radical cyclization of 6-bromo-1-hexene. Cyclization of 5-hexenyl radicals are known to be kinetically controlled which generally results in the formation of cyclopentane derivatives via a predominant 5-*exo* mode of closure (Scheme 6.4).³⁶⁻³⁸ Substituted 5-

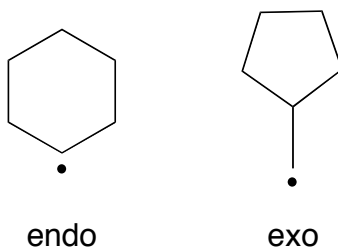
hexenyl derivatives, however, are found to form both 5- and 6-membered ring products.³⁹⁻⁴³ The formation of the 6-*endo* cyclic product has been attributed to the stereoelectronic effects of the substituents on the 5-hexenyl radical. This prompted us to investigate whether the electronic nature of the unsaturated moiety of the 5-hexenyl radical can also be manipulated through copper-olefin coordination. Thus, Cu^I complexes with different substituted Tp ligands were examined as potential catalysts for the free radical cyclization of 6-bromo-1-hexene.



Scheme 6.4. Bu₃SnH-Mediated Free Radical Cyclization of 5-Hexenyl Radicals

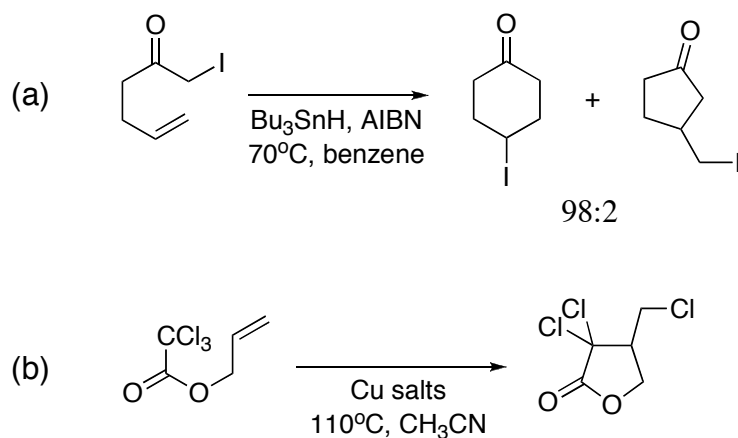
Atom transfer radical cyclization of alkenyl bromoacetates and trichloroacetates in the presence of [Cu^{II}(TPMA)Br][Br]/[Cu^{II}(TPMA)Cl][Cl] and AIBN were also examined. Cyclization of haloacetates yields γ - and δ -lactones and the regioselectivity of the cyclic products can be predicted through the application of Baldwin's rules. These rules are general guidelines for predicting favorable conformations of three- to seven-membered rings produced from various cyclization reactions and are based on both kinetic and thermodynamic factors.⁴⁴ The Baldwin's rules predict two types of ring closure, depending on whether the bond broken during the ring closure is inside (*endo*) or outside (*exo*) the new ring formed (Scheme 6.5). Oftentimes, for unsubstituted alkenyl radicals containing up to eight carbons, the preferred mode of cyclization is *exo*.^{2,45} These

reactions were shown to be kinetically controlled wherein the major product is the one that forms faster. However, the *endo* product usually predominates for substituted alkenyl radicals, which is due to the steric hindrance that is observed in the formation of the *exo* product (thermodynamically controlled).³⁹



Scheme 6.5. *Endo* and *Exo* Mode of Cyclization

Nevertheless, some radical cyclization reactions still deviate from the predicted mode of cyclization. For instance, Clive and Cheshire reported the formation of 6-*endo* products over the preferred 5-*exo* cyclic compounds in the intramolecular radical addition of acyl-substituted radicals (Scheme 6.6a).⁴⁶ However, in similar radical cyclization reactions involving alkenyl acetate radicals, there was a marked preference for the formation of the 5-*exo* products (Scheme 6.6b).⁴⁷ It is clear that both thermodynamic and kinetic factors play a significant role in determining the conformation of the resulting cyclic products.



Scheme 6.6. Radical Cyclization of (a) Acyl-Substituted Radicals and (b) Alkenyl Acetate Radicals

6.2 Experimental

6.2.1 General Procedures

All chemicals were purchased from commercial sources and used as received, unless otherwise noted. Solvents (toluene, dichloromethane and acetonitrile) were deoxygenated using Innovative Technology solvent purifier prior to use. 1,2-Dichloroethane was degassed by bubbling argon for 30 min before use. Tris(2-pyridylmethyl)amine (TPMA)⁴⁸, [Cu^{II}(TPMA)Cl][Cl]⁴⁹ and [Cu^{II}(TPMA)Br][Br]⁵⁰ were synthesized according to published procedures. Standard glovebox and Schlenk line techniques were employed in the handling of air-sensitive complexes. ¹H NMR spectra were obtained at room temperature on a Bruker Avance 300 and 400 MHz spectrometer with chemical shifts given in ppm relative to the residual solvent peak (CDCl₃, 7.26 ppm; C₆D₆, 7.16 ppm) and shown in Appendix A. X-ray analysis was performed using a Bruker SMART APEXII diffractometer and GC analysis was carried out using a

Shimadzu GC-14A gas chromatogram. ^1H NMR spectra and X-ray crystal data are shown in Appendix A and B, respectively.

6.2.2 Synthesis of Copper(I) Hydrotris(pyrazolyl)borate Complexes

[(Hydrotris(1-pyrazolyl)borato)copper(I)]₂ or [TpCu^I]₂

Copper(I) bromide (100 mg, 0.7 mmol) and potassium hydrotris(1-pyrazolyl)borate or KTp (173 mg, 0.7 mmol) were dissolved in 10 mL of (1:1) $\text{CH}_2\text{Cl}_2/\text{CH}_3\text{CN}$ in a Schlenk flask. Degassed deionized water (8 mL) was then added to the reaction mixture using a purged syringe. The mixture was stirred at room temperature under argon atmosphere for 1 h. The $\text{CH}_2\text{Cl}_2/\text{CH}_3\text{CN}$ layer was then transferred to another Schlenk flask with MgSO_4 using a cannula. The mixture was then filtered and dried under vacuum. A white powder was obtained in 38% yield. ^1H NMR (300 Hz, C_6D_6 , RT): $\delta = 7.59$ (d, $J = 2.0$ Hz, 6H), 7.11 (d, $J = 2.0$ Hz, 6H), 5.97 (t, $J = 2.0$ Hz, 6H).

[(Hydrotris(3,5-dimethyl-1-pyrazolyl)borato)copper(I)]₂ or [Tp^{CH₃}Cu^I]₂

[Tp^{CH₃}Cu]₂ was prepared according to the previous procedure using potassium hydrotris(3,5-dimethyl-1-pyrazolyl)borate or KTp^{CH₃}. A pale green powder was obtained 40% yield. ^1H NMR (300 Hz, C_6D_6 , RT): $\delta = 5.76$ (s, 1H), 2.29 (s, 3H), 1.85 (s, 3H).

[(Hydrotris(3,5-trifluoromethyl-1-pyrazolyl)borato](acetonitrile)copper(I) or Tp^{CF₃}Cu^I(CH₃CN)

Sodium [hydrotris(3,5-trifluoromethyl-1-pyrazolyl)borato] or Tp^{CF₃}Na(H₂O) was synthesized from sodium borohydride and 3,5-bis(trifluoromethyl)pyrazole according to published procedures.^{51,52} [Cu^I(CF₃SO₃)₂·C₆H₅CH₃ (25.4 g, 0.05 mmol) and

$\text{Tp}^{\text{CF}_3}\text{Na}(\text{H}_2\text{O})$ (72.5 mg, 0.10 mmol) were placed in a Schlenk flask with 10 mL CH_2Cl_2 . Dry and degassed acetonitrile (5 mL) was added to the mixture. The reaction mixture was stirred overnight at room temperature under argon atmosphere, filtered, and the solvent was evaporated under vacuum. A white powder was obtained in 46% yield. ^1H NMR (300 Hz, CDCl_3 , RT): δ = 6.34 (s, 3H), 0.80 (s, 3H); FT-IR (solid): $\nu(\text{B-H}) = 2623 \text{ cm}^{-1}$, $\nu(\text{C}\equiv\text{N}) = 2279 \text{ cm}^{-1}$, $\nu(\text{C}=\text{C}) = 1556 \text{ cm}^{-1}$. X-ray quality crystals were obtained by slow evaporation of a dichloromethane solution at room temperature.

[Hydrotris(1-pyrazolyl)borato](6-bromo-1-hexene)copper(I) or TpCu^{I} (6-bromo-1-hexene)

Copper(I) bromide (100 mg, 0.70 mmol) and 6-bromo-1-hexene (94 μL , 0.70 mmol) were dissolved in 5 mL CH_2Cl_2 in a Schlenk flask. In another Schlenk flask, potassium hydrotris(1-pyrazolyl)borate or KTp (173 mg, 0.70 mmol) was dissolved in 5 mL CH_2Cl_2 . The KTp mixture was then slowly added to the CuBr/6-bromo-1-hexene mixture over 1 h. Degassed deionized water (8 mL) was added to the mixture using a purged syringe. The reaction mixture was then stirred at room temperature under argon atmosphere for 2 h. The CH_2Cl_2 layer was then transferred to another Schlenk flask containing MgSO_4 using a cannula. The mixture was then filtered and dried under vacuum. A light blue powder was obtained in 40% yield. ^1H NMR (300 Hz, C_6D_6 , RT): δ = 7.57 (d, $J = 3.0$ Hz, 3H), 7.16 (d, $J = 3.0$ Hz, 3H), 5.98 (t, $J = 3.0$ Hz, 3H), 5.25-5.35 (m, 1H), 4.59 (dd, $J = 18, 9$ Hz, 2H), 2.88 (t, $J = 9$ Hz, 2H), 1.74-1.81 (m, 2H), 1.40-1.47 (m, 2H), 1.20-1.24 (m, 2H).

6.2.3 Synthesis of Alkenyl Bromoacetates

Allyl Bromoacetate

Allyl alcohol (2.9 mL, 42.5 mmol) was dissolved in 15 mL CH₂Cl₂ in a Schlenk flask and cooled to -40°C. Degassed bromoacetyl bromide (3.7 mL, 42.5 mmol) was slowly added over 1 h using a purged syringe. The temperature was allowed to rise to room temperature and the mixture was stirred overnight under argon atmosphere. The reaction mixture was then treated with saturated NaHCO₃ solution (25 mL). The organic layer was washed with water, dried over MgSO₄, filtered and the solvent was evaporated in vacuo. A pale yellow liquid was obtained in 74% yield. ¹H NMR (300 Hz, CDCl₃, RT): δ = 5.85-5.98 (m, 1H), 5.31 (dd, *J* = 18, 9 Hz, 2H), 4.66 (d, *J* = 6 Hz, 2H), 3.85 (s, 2H).

4-Pentenyl Bromoacetate

4-Pentenyl bromoacetate was prepared according to the previous procedure using 4-penten-1-ol. A viscous, pale yellow liquid was obtained 55% yield. ¹H NMR (300 Hz, CDCl₃, RT): δ = 5.78-5.90 (m, 1H), 5.07 (dd, *J* = 15, 12 Hz, 2H), 4.25 (t, *J* = 6 Hz, 2H), 3.83 (s, 2H), 2.17-2.24 (m, 2H), 1.88-1.79 (m, 2H).

6.2.4 Synthesis of Alkenyl Trichloroacetates

General Procedure

Trichloroacetyl chloride (2.88 mL, 25.8 mmol) was dissolved in 30 mL CH₂Cl₂ in a Schlenk flask and was cooled to 0°C. Degassed alkenol (23.5 mmol) was slowly added to the mixture using a purged syringe. Triethylamine (6.5 mL, 46.6 mmol) in 15 mL

CH₂Cl₂ was then added dropwise to the reaction mixture and stirred under argon at 0°C for 3 h. A 2M solution of hydrochloric acid (18 mL) was then poured into the reaction flask (cloudy solution then turns clear). The organic phase was separated, washed with saturated NaHCO₃ solution and water until the pH reached 7. After drying with MgSO₄, the solvent was then evaporated in vacuo. The resulting crude product was purified on a silica gel column (petroleum ether:ethyl acetate= 90:10) and the solvent was again evaporated under vacuum.

Allyl Trichloroacetate. (Yield 63%) ¹H NMR (400 Hz, CDCl₃, RT): δ = 5.93-6.02 (m, 1H), 5.42 (dd, *J* = 16, 12 Hz, 2H), 4.84 (d, *J* = 8 Hz, 2H).

Allyl-3-Ethyl Trichloroacetate. (Yield 39%) ¹H NMR (400 Hz, CDCl₃, RT): δ = 5.79-5.87 (m, 1H), 5.34 (dd, *J* = 16, 12 Hz, 2H), 5.27-5.28 (m, 1H), 1.78-1.82 (m, 2H), 0.984 (t, *J* = 8 Hz, 3H).

Allyl-3-Phenyl Trichloroacetate. (Yield 42%) ¹H NMR (400 Hz, CDCl₃, RT): δ = 7.30-7.44 (m, 6H, Ph), 6.79 (d, *J* = 16 Hz, 1H), 6.29-6.37 (m, 1H), 5.00 (d, *J* = 4 Hz, 2H).

Allyl-1-Methyl Trichloroacetate. (Yield 34%) ¹H NMR (400 Hz, CDCl₃, RT): δ = 5.90-5.96 (m, 1H), 5.61-5.65 (m, 1H), 4.75 (d, *J* = 4 Hz, 2H), 1.75 (d, *J* = 4 Hz, 3H).

4-Pentenyl Trichloroacetate. (Yield 70%) ^1H NMR (400 Hz, CDCl_3 , RT): $\delta = 5.75\text{-}5.85$ (m, 1H), 5.04 (dd, $J = 16, 12$ Hz, 2H), 4.38 (t, $J = 4$ Hz, 2H), 2.17-2.23 (m, 2H), 1.84-1.91 (m, 2H).

6.2.5 Free Radical Cyclization of 6-Bromo-1-Hexene

Cyclization reactions were carried out in airtight Schlenk flasks containing 6-bromo-1-hexene (50 μL , 0.4 mmol), AIBN (10 mg, 0.06 mmol) and the appropriate amounts of Bu_3SnH and TpCu^{I} complex. The reaction was run at 70°C under argon atmosphere for 6 h using toluene as solvent. Product analyses were performed by gas chromatography using benzene as internal standard.

6.2.6 ATRC of Alkenyl Haloacetates

A stock solution containing an alkenyl bromoacetate or trichloroacetate, AIBN, and an internal standard (*p*-dimethoxybenzene) was prepared ($[\text{haloacetate}]_0/[\text{AIBN}]_0 = 100:5$) using 1,2-dichloroethane as solvent. The desired amount of $[\text{Cu}^{\text{II}}(\text{TPMA})\text{Cl}][\text{Cl}]$ was added to 0.30 ml of the stock solution in an NMR tube. The total volume was adjusted by adding 1,2-dichloroethane to obtain consistent haloacetate concentration in each reaction system ($[\text{haloacetate}]_0 = 0.20\text{M}$). The resulting solution was then purged with argon and the NMR tube was capped and sealed with Teflon tape. The reactions were run at 80°C for 24 hours and the product were analyzed using ^1H NMR.

6.2.7 Modeling of *s-cis* and *s-trans* Isomers of Alkenyl Trichloroacetates

Calculations of *cis*- and *trans*-isomers of various alkenyl trichloroacetate radicals was performed using the Spartan software package (version 4.1.0, Wavefunction, Inc.,

Irvine).⁵³ Structures of various analogs of the allyl trichloroacetate radical were optimized with Becke's three parameter hybrid exchange functional and the Lee-Yang-Parr correlation functional (B3LYP) and the 6-31G* basis set and also at the unrestricted Hartree-Fock (UHF/6-31G*) level. Output files are shown in Appendix C.

6.3 Results and Discussion

6.3.1 Synthesis and Characterization of Copper(I) Homoscorpionate Complexes

Homoscorpionate complexes, which have a tridentate ligand bound to the metal center in a *fac* manner, are attractive candidates for investigating stereoelectronic effects on metal-monomer coordination.⁵⁴⁻⁵⁶ In particular, the tris(pyrazolyl)hydroborate family of ligands (Tp), which is the most popular type of homoscorpionate ligand, is also extensively used as ligands in metal-mediated organic reactions because the properties of the resulting metal complexes can be dramatically altered depending on the steric and electronic nature of the substituents on the ligand framework.⁵⁴⁻⁵⁹ Furthermore, modification of the Tp ligand can also influence the volatility, solubility, and oxidation resistance of the metal complexes.⁵⁹⁻⁶¹ For instance, Tp ligands bearing fluorinated substituents are highly useful for applications in fluorous biphasic media and in supercritical carbon dioxide^{57,60-62} while metal complexes with electron-donating Tp ligands are of great interest in modeling studies of dioxygen binding in oxygen transport proteins.^{54,63}

A comparison of the differences in the CO stretching frequency of copper(I)-carbonyl adducts bearing various Tp ligands gives an insight on the electronic nature of the ligands. Copper(I) carbonyl complexes are stabilized by back-donation of copper *d*

electrons to the antibonding C≡O orbital and the $\nu(\text{C}\equiv\text{O})$ value is a sensitive indicator of the extent of back donation and, thus, the electron density at the copper center. The IR spectrum of the Cu-CO adduct with trifluoromethylated Tp ligand⁶² showed a relatively strong absorption band at 2137 cm^{-1} corresponding to the CO stretching frequency as compared to the $\nu(\text{C}\equiv\text{O})$ value for the Cu-CO adduct with methylated Tp ligand. This high ν_{CO} value of the fluorinated Cu-CO adducts indicates a poor electron density at the copper center, which is expected due to the highly electron-withdrawing nature of the trifluoromethylated Tp ligand. As pyrazolyl substituents become more electron-donating from CF_3 to alkyl, the increased electron density on the Cu^{I} ion from the methylated Tp ligands leads to greater π -backbonding, which is evident in the $\nu(\text{C}\equiv\text{O})$ value of 2066 cm^{-1} for Tp^{CH_3} .⁶⁴ The electron density at the copper center for various $\text{TpCu}^{\text{I}}(\text{CO})$ complexes found in the literature increases in the following order: $\text{Tp}^{i\text{-Pr},i\text{-Pr}}$ (2056 cm^{-1})⁶³ $\approx \text{Tp}^{t\text{-Bu},i\text{-Pr}}$ (2057 cm^{-1})⁵⁹ $> \text{Tp}^{t\text{-Bu},\text{CH}_3}$ (2059 cm^{-1})⁶⁵ $> \text{Tp}^{\text{CH}_3,\text{CH}_3}$ (2066 cm^{-1})⁶⁶ $> \text{Tp}^{t\text{-Bu}}$ (2069 cm^{-1})⁶⁷ $> \text{Tp}$ (2083 cm^{-1})⁶⁸ $> \text{Tp}^{\text{Ph},\text{Ph}}$ (2086 cm^{-1})⁶⁵ $> \text{Tp}^{\text{CF}_3}$ (2100 cm^{-1})⁶⁰ $> \text{Tp}^{\text{C}_2\text{F}_5}$ (2102 cm^{-1})⁶¹ $> \text{Tp}^{\text{C}_2\text{F}_7}$ (2110 cm^{-1})⁶¹ $> \text{Tp}^{\text{CF}_3,\text{CF}_3}$ (2137 cm^{-1}).⁶²

To investigate the effects of the electronic nature of the Tp ligand on metal-monomer coordination, copper(I)-acetonitrile complexes with the parent tris(pyrazolyl)borate (Tp) ligand and two alkyl-substituted analogs, one bearing electron-donating methyl groups on the 3- and 5- positions on the pyrazolyl ring (Tp^{CH_3}) and another with electron-withdrawing trifluoromethyl groups on the same positions of the ring (Tp^{CF_3}) were synthesized. Acetonitrile is fairly labile in nature and in the presence of other stronger coordinating ligands and monomers, such as triphenylphosphine and ethylene, is easily displaced from the metal center.^{57,69} Unfortunately, attempts to

synthesize $\text{TpCu}^{\text{I}}(\text{CH}_3\text{CN})$ and $\text{Tp}^{\text{CH}_3}\text{Cu}^{\text{I}}(\text{CH}_3\text{CN})$ were unsuccessful and only led to dimerization of the Cu^{I} complex. Other derivatives of the $\text{TpCu}^{\text{I}}(\text{CH}_3\text{CN})$ found in literature have bulky groups on the 3-position of the pyrazolyl moiety, such as $\text{Tp}^{3\text{-CF}_3,5\text{-CH}_3}\text{Cu}(\text{CH}_3\text{CN})$,^{56,70} $\text{Tp}^{3\text{-CF}_3}\text{Cu}(\text{CH}_3\text{CN})$,⁶⁰ $\text{Tp}^{3\text{-p-tBuPh},5\text{-CH}_3}\text{Cu}(\text{CH}_3\text{CN})$ ⁵⁸ and $\text{Tp}^{4\text{-Br},5\text{-CH}_3,3\text{-Ph}}\text{Cu}(\text{CH}_3\text{CN})$,⁷¹ and this steric crowding prevented the dimerization of the complex.

A copper(I)-Tp complex with 6-bromo-1-hexene bound to the fourth coordination site through an η^2 fashion was also synthesized. These TpCu^{I} complexes will then be used in the succeeding free radical cyclization reactions.

$[\text{TpCu}^{\text{I}}]_2$ and $[\text{Tp}^{\text{CH}_3}\text{Cu}^{\text{I}}]_2$

Synthesis of $\text{TpCu}^{\text{I}}(\text{CH}_3\text{CN})$ and $\text{Tp}^{\text{CH}_3}\text{Cu}^{\text{I}}(\text{CH}_3\text{CN})$ were attempted by treatment of $\text{Cu}^{\text{I}}\text{Br}$ with potassium hydrotris(1-pyrazolyl)borate or KTp and potassium hydrotris(3,5-dimethyl-1-pyrazolyl)borate or KTp^{CH_3} , respectively, in a large excess of acetonitrile under argon atmosphere. However, ^1H NMR analysis of the $\text{TpCu}(\text{CH}_3\text{CN})$ product showed no resonance peak corresponding to the acetonitrile ligand, indicating that acetonitrile did not bind to the Cu center. Indeed, the solid state structure of the compound (shown in Figure 6.1), which crystallizes in the triclinic space group P1, revealed a neutral dimeric Cu complex with each of the Tp moiety bound to two Cu centers through the nitrogen atom of a terminal pyrazole with another pyrazole ring bridging both Cu atoms.

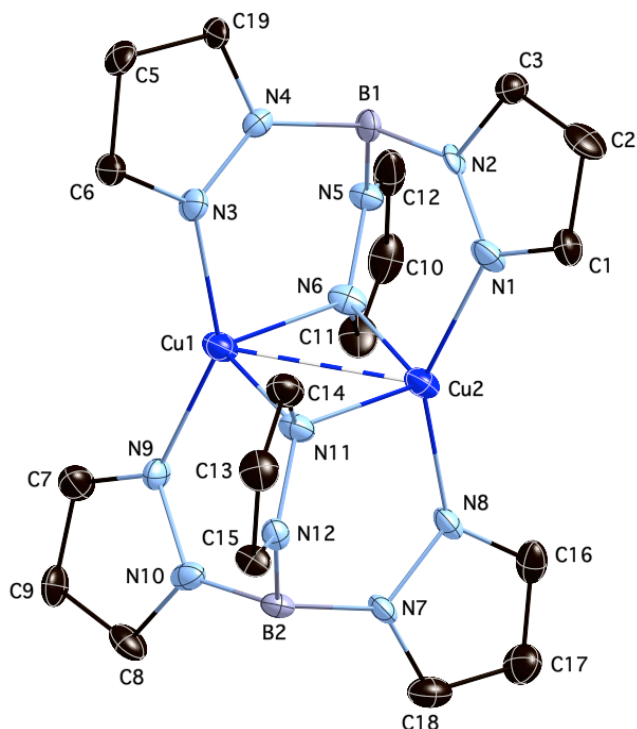


Figure 6.1. Molecular Structure of $[\text{TpCu}]_2$ Showing the Atom-Labeling Scheme. Thermal ellipsoids are drawn at the 50% probability level. Hydrogen atoms are omitted for clarity.

Selected intramolecular bond distances and angles are summarized in Table 6.1. The coordination arrangement of each copper atom is best described as distorted tetrahedral, with six N–Cu–N angles of 145.0 (2), 108.7 (2), 95.0 (2), 93.80 (19), 104.2 (2), 105.9 (2), 108.17 (15) $^\circ$. The Cu–Cu bond distance within the dimeric unit is 2.6544 (3) Å, which is typical for binuclear Cu complexes with two ligands bridging each Cu atom.^{64,72,73} The terminal pyrazole Cu–N bond lengths are 1.960 (5), 1.955 (6), 1.942 (6) and 1.939 (5) Å while the bridging Cu–N distances are considerably longer at 2.239 (5) and 2.236 (5) Å.

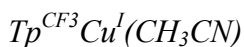
Table 6.1. Selected Bond Distances (Å) and Angles (deg) for [TpCu^I]₂

Cu(1) – N(3)	1.955 (6)	N(9) – Cu(1) – N(3)	145.0 (2)
Cu(1) – N(6)	2.209 (5)	N(9) – Cu(1) – N(6)	108.7 (2)
Cu(1) – N(9)	1.939 (5)	N(3) – Cu(1) – N(6)	95.0 (2)
Cu(1) – N(11)	2.236 (5)	N(9) – Cu(1) – N(11)	93.80 (19)
Cu(2) – N(1)	1.960 (5)	N(3) – Cu(1) – N(11)	104.2 (2)
Cu(2) – N(6)	2.239 (5)	N(6) – Cu(1) – N(11)	105.9 (2)
Cu(2) – N(8)	1.942 (6)	N(8) – Cu(2) – N(1)	144.2 (2)
Cu(2) – N(11)	2.178 (6)	N(8) – Cu(2) – N(11)	95.9 (2)
Cu(1) – Cu(2)	2.6544 (3)	N(1) – Cu(2) – N(11)	108.5 (2)
		N(8) – Cu(2) – N(6)	103.98 (19)
		N(1) – Cu(2) – N(6)	93.8 (2)
		N(11) – Cu(2) – N(6)	106.9 (2)

Internal bond distances and angles within the pyrazole moiety as well as the B–N distances do not differ significantly from Tp ligands in monomeric Cu^I complexes.^{54,68} However, there is a slight distortion in the boron valence angles in the dimeric structure. The N–B–N angles for [TpCu^I]₂ range between 110.7 (5) – 113.4 (5)°, which is slightly larger than the average N–B–N angle of 108.5 (6)° for other monomeric TpCu^I complexes.^{54,68} If a plane of best fit for the three nitrogen atoms bound to boron is determined, the boron atom in the binuclear Cu complex was found to deviate 0.456 Å from the plane while those of monomeric complexes are typically 0.53 Å from the plane. These distortions are evidently caused by the bridging of the Tp ligand on two copper atoms.

Attempts to obtain X-ray quality crystals of Tp^{CH₃}Cu^I(CH₃CN) were unsuccessful. However, the ¹H NMR spectra of the compound also showed no resonance peak corresponding to the acetonitrile ligand (Appendix A, Figure A2), indicating

coordination of the ligand to the copper center did not take place leading to the formation of dimeric complex.



Treatment of $NaTp^{CF_3}(H_2O)$ with $[Cu^I(CF_3SO_3)]_2.C_6H_5CH_3$ under argon atmosphere in the presence of excess acetonitrile yielded $Tp^{CF_3}Cu^I(CH_3CN)$. This compound was found to be air stable both in the solid state and in solution. The molecular structure of $Tp^{CF_3}Cu^I(CH_3CN)$ shows that the Cu^I atom is in a distorted tetrahedral environment, bound to the three pyrazole nitrogen atoms and the nitrogen atom from the acetonitrile ligand (Figure 6.2 and Table 6.2). Furthermore, in the solid state structure, Cu1, N1, C1, C2, B1 lie on a crystallographic threefold rotation axis.

There are two sets of angles about the copper center, which are typical of tetrahedral Tp complexes.^{58,64,69} The bond angle between any two coordinated pyrazole nitrogen atoms at copper is $89.79(5)^\circ$ and a larger angle of $125.41(3)^\circ$ is observed for the corresponding pyrazole N atoms, Cu and N from the CH_3CN ligand. The three Cu-N bond distances in the fluorinated Tp ligand are equal ($2.0992(12) \text{ \AA}$) and are longer than the Cu-NCCH₃ bond distance ($1.888(3) \text{ \AA}$). The Cu-N bond distance in the coordinated acetonitrile is in agreement with other previously characterized tetrahedral copper(I)-acetonitrile complexes.^{56,74,75}

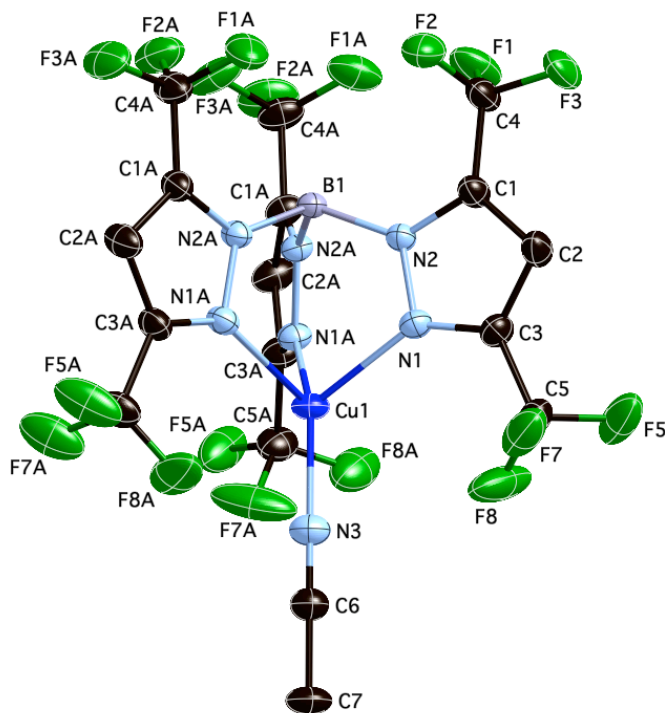


Figure 6.2. Molecular Structure of $\text{Tp}^{\text{CF}_3}\text{Cu}^{\text{I}}(\text{CH}_3\text{CN})$ Showing the Atom-Labeling Scheme. Thermal ellipsoids are drawn at the 50% probability level. Hydrogen atoms are omitted for clarity.

Table 6.2. Selected Bond Distances (Å) and Angles (deg) for $\text{Tp}^{\text{CF}_3}\text{Cu}^{\text{I}}(\text{CH}_3\text{CN})$

Cu(1) – N(3)	1.891 (9)	N(3) – Cu(1) – N(1)	125.91 (12)
Cu(1) – N(1)	2.104 (4)	N(3) – Cu(I) – N(1A)#1	125.91 (12)
Cu(1) – N(1A)#1	2.104 (4)	N(3) – Cu(I) – N(1A)#2	125.91 (12)
Cu(1) – N(1A)#2	2.104 (4)	N(1) – Cu(I) – N(1A)#1	89.08 (17)
		N(1) – Cu(I) – N(1A)#2	89.08 (17)
		N(1A)#1 – Cu(I) – N(1A)#2	89.08 (17)

The acetonitrile ligand, lying on a threefold rotation axis, is exactly linear. The nitrile C-N bond distance is 1.140 (5) Å, which falls within the range (1.11-1.15 Å) observed for other transition metal-acetonitrile complexes.⁵⁸

TpCu^I(6-bromo-1-hexene)

TpCu^I(6-bromo-1-hexene) was prepared by the slow addition of the Tp ligand to a solution of CuBr and 6-bromo-1-hexene in dichloromethane. The slow addition of the ligand is crucial as it prevents the dimerization of the copper(I) complex. The compound was then analyzed by ¹H NMR in C₆D₆ and the spectrum is shown in Figure 6.3. Coordination of 6-bromo-1-hexene to the Cu^I center is evident in the upfield shift of the resonance peaks for the olefinic protons, which is attributed to the increased shielding caused by the copper-to-olefin π -backdonation.

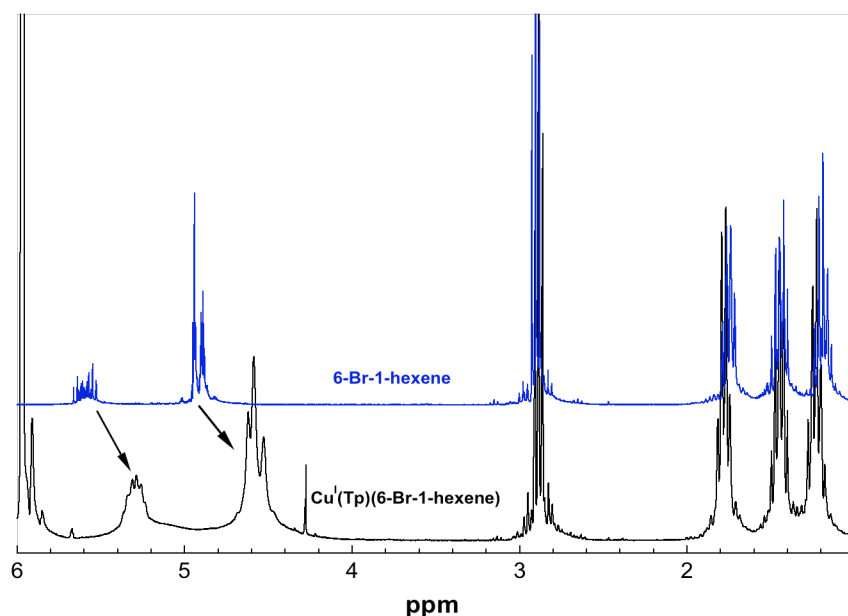


Figure 6.3. ¹H NMR Spectra of 6-bromo-1-hexene and CuTp(6-bromo-1-hexene) Showing Shielding of Olefinic Protons

TpCu^I(6-bromo-1-hexene) was also characterized by X-ray crystallography and the molecular structure is illustrated in Figure 6.4. The Cu^I atom adopts a pseudo-tetrahedral geometry and is coordinated to a nitrogen atom from each of the three pyrazole rings in the Tp ligand and to the two olefinic carbon atoms of 6-bromo-1-hexene

via an η^2 fashion. Disregarding the olefinic ligand, the compound has a C_{3v} symmetry along the Cu–B axis. Selected bond distances and angles are summarized in Table 6.3. The Cu–N bond lengths and angles are in the range typically found for analogs of the TpCu complex.^{54,55,68} The Cu–C bond distances are also comparable to those previously reported for Cu^I-olefin complexes.⁷⁶⁻⁷⁸ The C=C bond of the coordinated 6-bromo-1-hexene also shown no notable changes compared to the free ethylene molecule, which is consistent with other TpCu^I-olefin complexes.^{57,78}

Table 6.3. Selected Bond Distances (Å) and Angles (deg) for TpCu^I(6-bromo-1-hexene)

Cu(1) – N(1)	1.999 (6)	N(1) – Cu(1) – N(5)	93.8 (3)
Cu(1) – N(5)	2.031 (6)	N(1) – Cu(I) – N(3)	87.6 (2)
Cu(1) – N(3)	2.207 (6)	N(3) – Cu(I) – N(5)	87.7 (2)
Cu(1) – C(10)	2.011 (8)	N(1) – Cu(I) – C(10)	141.7 (3)
Cu(1) – C(11)	2.035 (8)	N(1) – Cu(I) – C(11)	105.4 (3)
C(10) – C(11)	1.307 (13)	N(3) – Cu(I) – C(10)	119.2 (4)
		N(3) – Cu(I) – C(11)	123.9 (3)
		N(5) – Cu(I) – C(10)	112.8 (4)
		N(5) – Cu(I) – C(11)	142.9 (3)

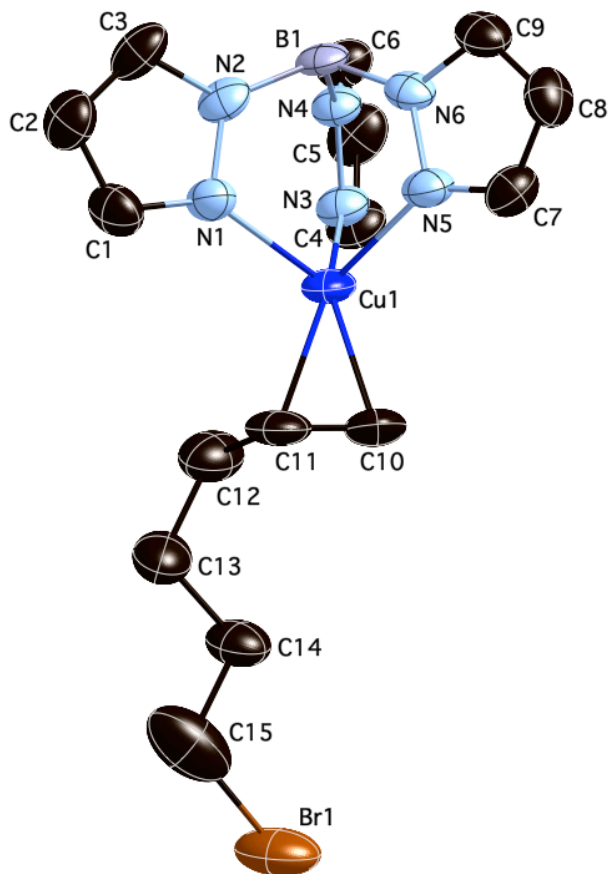


Figure 6.4. Molecular Structure of TpCu^{I} (6-bromo-1-hexene) Showing the Atom-Labeling Scheme. Thermal ellipsoids are drawn at the 50% probability level. Hydrogen atoms are omitted for clarity.

6.3.2 Free Radical Cyclization Reactions in the presence of TpCu^{I} Complexes

One of the most common strategies applied in radical cyclization processes is the use of a reducing agent, which plays a significant role as a chain carrying species.^{2,36-39,79,80} Organotin hydrides are very efficient H-donors due to the relatively weak, nonionic bond between tin and hydrogen ($\sim 74 \text{ kcal/mol}$)⁸¹ that can easily cleave homolytically under the right conditions. However, tin hydrides are also H-donor agents

and one of the major drawbacks in using reductive conditions is the possibility for reduction of the radical prior to cyclization.

Tributyltin hydride/AIBN-initiated cyclization of 5-hexenyl radicals is a popular reaction for free radical cyclization processes.^{36-39,80} Unsubstituted 5-hexenyl radicals are known to undergo very fast and selective 5-*exo*-trig cyclization ($k_{\text{exo-trig}} = 10^5 \text{ s}^{-1}$, $k_{\text{exo-trig}} / k_{\text{endo-trig}} \approx 100$),² however, regioselectivity of substituted 5-hexenyl radicals have been found to be dictated by both the relative position of the substituent and the stereochemistry of the stereocenter.³⁹⁻⁴² Indeed, exclusive formation of the thermodynamically favored cyclohexane product has been observed in cyclization processes involving cyano ester 5-hexenyl radicals.³⁹ This 6-*endo* selectivity promoted by stereoelectronic contributions prompted us to develop other ways to control the regioselectivity of these cyclization reactions.

One possible approach is to induce stereoelectronic control through copper-olefin coordination. The nature of the coordination between an olefin and a copper center can be generally described qualitatively by the Dewar-Chatt-Duncanson model,^{82,83} as shown in Figure 6.5, which includes both contributions of the filled π -MO of the olefin which donates a σ -electron to an empty d orbital of the metal and a $d\pi$ - $p\pi$ back donation of an electron from a filled valence d -orbital on the metal to an empty π^* MO on the alkene.

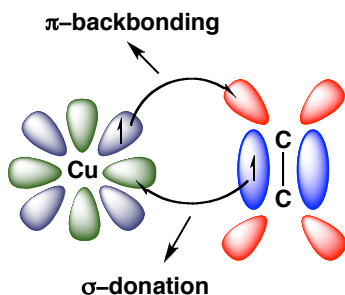
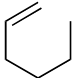
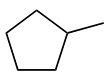
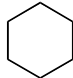


Figure 6.5. Dewar-Chatt-Duncanson Model of Copper-Olefin Binding

Chemical and physical properties and reactivities of copper(I)-olefin complexes are greatly manipulated by varying the nature of the ligand on the copper center.⁸⁴

The TpCu^{I} complexes synthesized and described in the previous section were utilized in Bu_3SnH -mediated free radical cyclization reactions of 6-bromo-1-hexene. Reactions were run for 6 hours at 70°C in sealed, degassed Schlenk flasks using toluene as solvent and AIBN as radical initiator. Equivalent molar concentrations of 6-bromo-1-hexene and TpCu^{I} complex were used while molar concentrations of Bu_3SnH were varied. Actual yields of yields of cyclized and uncyclized products were determined by gas chromatography and the results are summarized in Table 6.4.

Table 6.4. Bu_3SnH -Mediated Free Radical Cyclization of 6-bromo-1-hexene in the Presence of TpCu^{I} Complexes

Entry	TpCu^{I}	$[\text{Bu}_3\text{SnH}]_0$	%Conv	Product Distribution		
						
1	None	0.025	49	0	100	0
2	None	0.0375	46	25	75	0
3	None	0.50	42	43	57	0
4	$[\text{TpCu}^{\text{I}}]_2$	0.0375	52	21	79	0
5	$[\text{Tp}^{\text{CH}_3}\text{Cu}^{\text{I}}]_2$	0.0375	47	18	82	0
6	$\text{Tp}^{\text{CF}_3}\text{Cu}^{\text{I}}(\text{CH}_3\text{CN})$	0.0375	40	20	80	0
7	$\text{TpCu}^{\text{I}}(6\text{-Br-1-Hex})^{\text{b}}$	0.0375	65	0	90	10
8	$\text{TpCu}^{\text{I}}(6\text{-Br-1-Hex})^{\text{b}}$	0.0	0	0	0	0

^a $[\text{6-bromo-1-hexene}]_0:[\text{Cu}^{\text{I}}]_0:[\text{AIBN}]_0 = 1:1:0.15$, $[\text{6-bromo-1-hexene}]_0 = 0.0375 \text{ M}$, $T=70^\circ\text{C}$, $t = 6 \text{ h}$, solvent = toluene, product distribution is determined by GC.

^b6-bromo-1-hexene is already bound to the Cu^{I} catalyst and excess 6-bromo-1-hexene was not added to the reaction mixture

As expected, free radical cyclization of 6-bromo-1-hexene in the absence of a catalyst yielded only the predominant 5-*exo* cyclic product (entry 1, Table 6.4). When the molar concentration of Bu₃SnH relative to 6-bromo-1-hexene was increased, yield of the reduced product dramatically increased (entries 2 and 3, Table 6.4), however, formation of the 6-*endo* cyclic product did not occur.

In the subsequent reactions containing a TpCu^I catalyst, equivalent molar concentrations of Bu₃SnH and 6-bromo-1-hexene were used in order to minimize the H-transfer to the 5-hexenyl radical. Addition of the dimeric TpCu^I complexes (entries 4 and 5, Table 6.4) did not show any effect on the regioselectivity of the cyclization. Formation of cyclohexane was still not observed and the ratio of the reduced and 5-*exo* cyclic products were comparable to the uncatalyzed cyclization reaction (entry 2, Table 6.4). Evidently, the dimer structure of [TpCu^I]₂ and [Tp^{CH₃}Cu^I]₂ was not disrupted and coordination of the olefin to the Cu^I center did not take place.

Similarly, no significant effect on the regioselectivity of the cyclization was observed upon addition of the Tp^{CF₃}Cu^I(CH₃CN). This was surprising since acetonitrile ligand is known to be easily displaced by other stronger coordinating ligands, such as ethylene and triphenylphosphine, and thus, dissociation of the acetonitrile ligand from the Cu^I center was expected in the presence of 6-bromo-1-hexene. However, close examination of the reaction mixture revealed that the Tp^{CF₃}Cu^I(CH₃CN) complex was not completely soluble in nonpolar solvents such as toluene even with vigorous stirring. These poor results was therefore attributed to the heterogeneous nature of the reaction in the presence of Tp^{CF₃}Cu^I(CH₃CN).

When 6-bromo-1-hexene was effectively bound to the Cu^I center, formation of the 6-*endo* cyclic product was observed, albeit to a small extent (entry 7). This indicates that coordination of the olefin to the copper complex does indeed affect the regioselectivity of the cyclization. However, when the reaction was done in the absence of Bu₃SnH (entry 8), homolytic cleavage of the C-Br bond did not occur indicating that the TpCu^I complex alone does not abstract the bromide from the substrate to generate the 5-hexenyl radical.

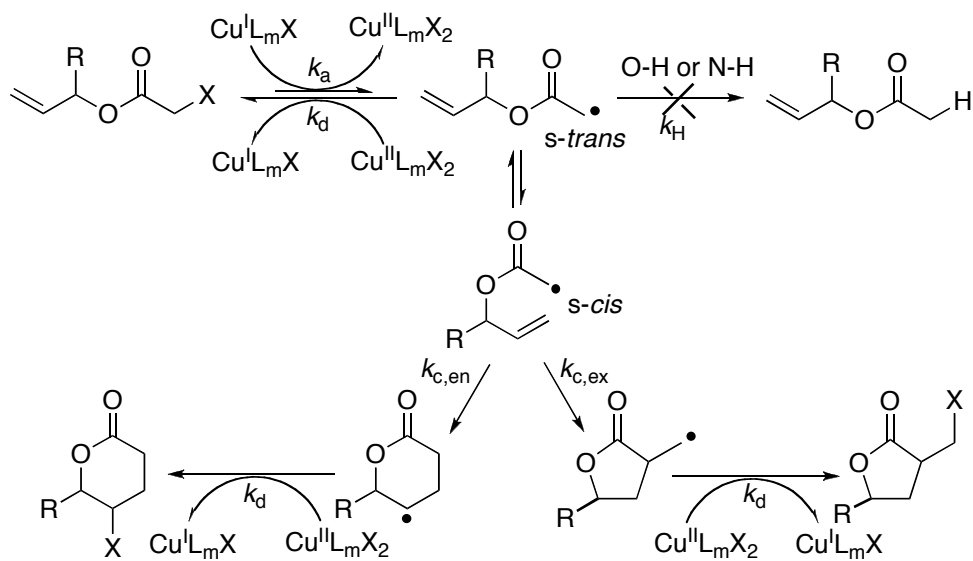
These unfavorable results can be attributed to the labile nature of the copper-olefin interaction,^{57,84,85} which may have caused the 6-bromo-1-hexene to be easily displaced from the copper in solution. Also, the fast reduction or cyclization of the 5-hexenyl radical may have occurred more readily than the olefin coordination to the Cu^I center. These results can be improved by the slow addition of the Bu₃SnH reducing agent, which will minimize the competing reduction processes but still provide a radical source that can cleave the C-Br bond. Additionally, the design of copper catalysts which can homolytically cleave the bromine atom and generate the primary radical will eliminate the need for Bu₃SnH and the subsequent reduction of the 5-hexenyl radical.

6.3.3 Atom Transfer Radical Cyclization of Alkenyl Haloacetates

Transition metal catalyzed atom transfer radical cyclization reactions (TMC ATRC) provide a more useful alternative to the more commonly adopted organotin-mediated variant of this process.^{9,20-28} Aside from preventing the reduction of generated radicals in the presence of an H-donor tin reagent, the use of more environmentally transition metal complexes, such as those of Cu^{9,22} and Fe,^{26,28,86} makes TMC ATRC a far more attractive method for radical cyclization. Furthermore, ATRC reactions are of great

interest in that they generate functionalized adducts, which possess a potentially useful C-halogen bond for further chemical transformations after cyclization has occurred. A number of groups have reported on the successful synthesis of γ - and δ -lactones and lactams via the ATRC of haloacetates and amide precursors^{7,25,32-35} and on the synthesis of polycyclic indole systems via sequential activation and intramolecular addition of the functionalized moiety onto the unsaturated end.^{13,19}

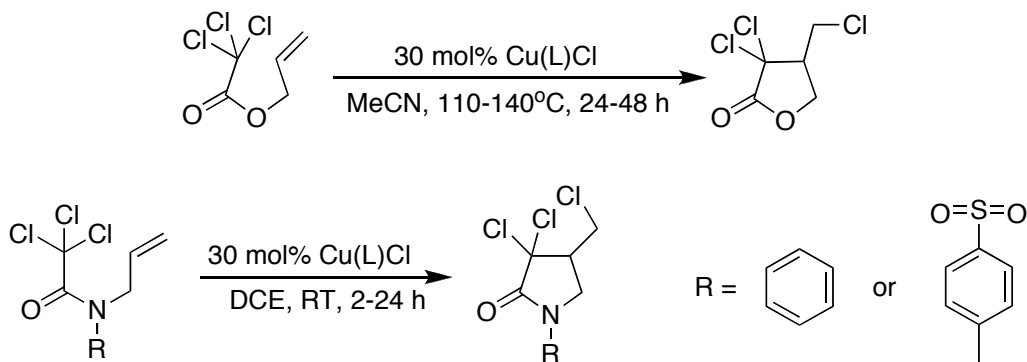
In copper-catalyzed ATRC of haloacetates, cyclization is promoted by the redox couple $\text{Cu}^{\text{I}}/\text{Cu}^{\text{II}}$, whose electrochemical properties are influenced by the chelating ligands. The C-halogen bond of the haloester is homolytically cleaved by a Cu^{I} complex, generating a primary radical and a Cu^{II} compound (Scheme 6.7). In the absence of H-donor agents, the radical can then undergo intramolecular addition to the unsaturated moiety of the substrate, forming a cyclic radical species which is then functionalized via the abstraction of a halide from the Cu^{II} complex.



Scheme 6.7. Proposed Mechanism for Copper-Catalyzed ATRC of Haloacetates

This direct cyclization of haloesters has oftentimes met with variable success due to the high energy barrier of rotation of the ester bond to form the *s-cis* conformer, which is the sole conformer suited for the intramolecular attack, and the instability of the said isomer. Ueno⁸⁷ and Stork⁸⁸ developed an indirect method for synthesis of γ -butyrolactones via an alkoxytetrahydrofuran, which is then converted to the desired lactones using a Jones reagent. However, this indirect method, while successful, is limited to the formation of 5-membered ring systems.

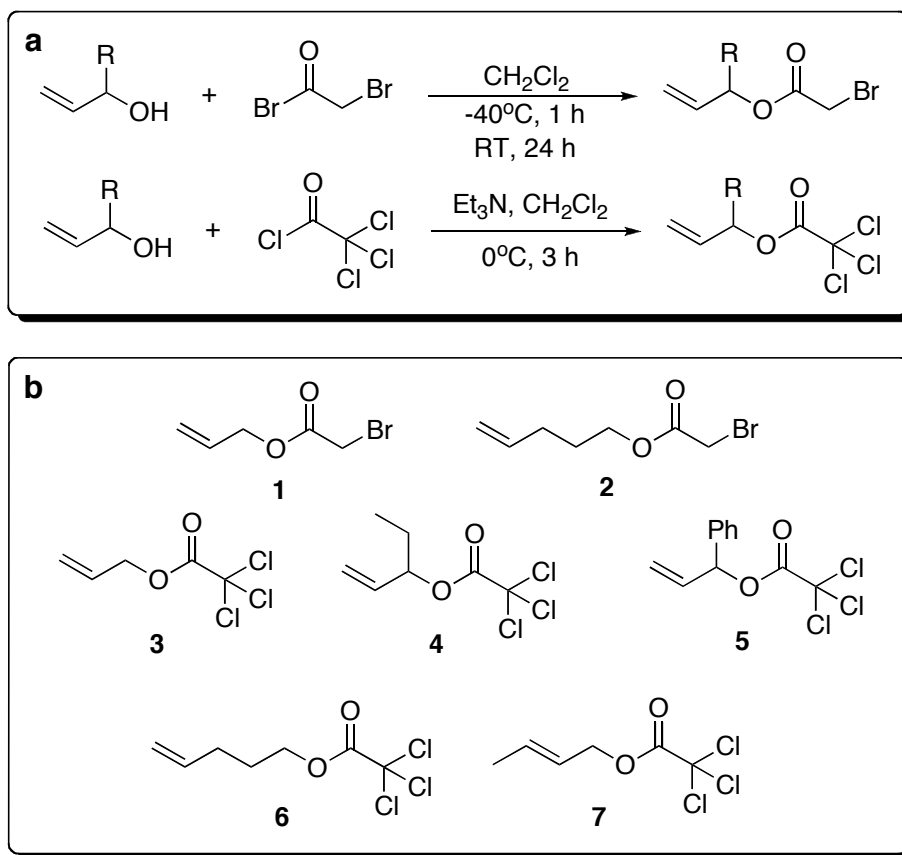
Since the main problem of the direct method for cyclization of haloesters is the rotational requirement of the acetate radical, we tried to develop a strategy that would shift the rotameric population at equilibrium towards the *s-cis* conformer and, thus, allows cyclization. A survey of other radical cyclization reactions brought an interesting detail to our attention. Copper-catalyzed ATRC of trichloroamides²⁵ resulted in nearly quantitative yields of the target lactams under less vigorous reactions conditions (Scheme 6.8). However, ATRC of trichloroacetates⁴⁷ with almost identical structures to the trichloroamides, required higher temperatures and longer reaction times and yielded significantly lesser amounts of the desired lactones. A comparison of the structures of the



Scheme 6.8. Copper-Catalyzed ATRC of Trichloroacetates and Amides

starting materials revealed that the haloamide precursors have highly bulky substituents, such as phenyl and tosyl groups, on the nitrogen atom adjacent to the carbonyl C. The presence of these bulky groups can cause steric crowding in the *s-trans* conformation, making the *s-cis* conformers of the haloamide radical more stable and, thus, promoted cyclization. Since addition of a bulky group could not be made on the acetate moiety, we opted to introduce the substituents on the carbon α to the acetate functional group.

Syntheses of the haloacetate precursors were carried out by treatment of an alkenyl alcohol with bromoacetyl bromide to yield alkenyl bromoacetates and with trichloroacetyl chloride to obtain alkenyl trichloroacetates (Scheme 6.9a).



Scheme 6.9. (a) Synthetic Scheme for Alkenyl Bromoacetates and Trichloroacetates, (b) Haloacetate Precursors for ATRC Reactions

Commercially available C3-substituted alcohols were used to introduce the bulky substituent on the alkenyl trichloroacetates (Scheme 6.9b). Additionally, a substrate with a methyl group on the terminal olefinic carbon was also synthesized in order to investigate the effect of substituents on the double bond on the regioselectivity of the cyclization process.

The ATRC reactions were performed using $[\text{Cu}^{\text{II}}(\text{TPMA})\text{Cl}][\text{Cl}]$ / $[\text{Cu}^{\text{II}}(\text{TPMA})\text{Br}][\text{Br}]$ as catalyst and AIBN as reducing agent under argon atmosphere. Reactions were run at 80°C (preliminary ATRC reactions run at 60°C did not promote cyclization) and the products were analyzed using ^1H NMR spectroscopy with the results shown in Table 6.5.

Table 6.5. Copper-Catalyzed ATRC of Alkenyl Bromoacetates and Trichloroacetates^a

entry	substrate	[substrate] ₀ : $[\text{Cu}^{\text{II}}]$ ₀	solvent	%yield
1	1^b	100:1	CH ₃ CN	0
2	2^b	100:1	CH ₃ CN	0
3	2^b	100:1	MeOH	57 (reduced product)
4	3	100:1	MeOH	40 (reduced product)
5	3	100:1	DCE	10 (5- <i>exo</i> product)
6	3	200:1	DCE	5 (5- <i>exo</i> product)
7	4	100:1	DCE	35 (5- <i>exo</i> product)
8	4	500:1	DCE	14 (5- <i>exo</i> product)
9	5	100:1	DCE	27 (5- <i>exo</i> product)
10	6	100:1	DCE	74 (8- <i>endo</i> product)
11	6	500:1	DCE	66 (8- <i>endo</i> product)
12	6	1000:1	DCE	56 (8- <i>endo</i> product)
13	6	2000:1	DCE	48 (8- <i>endo</i> product)
14	7	100:1	DCE	48 (6- <i>endo</i>); 5 (5- <i>exo</i>)

^a[substrate]₀: $[\text{AIBN}]_0$ = 100:5, [substrate]₀ = 0.20 M, T = 80°C, t=24 h; DCE = 1,2-dichloroethane; yield is based on formation of cyclic or reduced products and was determined by ^1H NMR spectroscopy using anisole or *p*-dimethoxybenzene as internal standards; ^b $[\text{Cu}^{\text{II}}(\text{TPMA})\text{Br}][\text{Br}]$ was used as catalyst instead of $[\text{Cu}^{\text{II}}(\text{TPMA})\text{Cl}][\text{Cl}]$

ATRC of **1** in acetonitrile revealed no formation of cyclic or reduced products (entry 1, Table 6.5) and the starting precursor was fully obtained at the end of the reaction. Similarly, cyclization of **2**, which is a longer-chain bromoacetate, did not proceed (entry 2, Table 6.5). This was unexpected because longer chain radicals cyclize more readily since both *s-cis* and *s-trans* conformers are amenable for cyclization.²⁸ At first, we thought that the C-Br bond of the substrate was not cleaved by the Cu^I(TPMA)Br complex and, therefore, failed to generate the radical species. However, subsequent reactions in protic solvents such as methanol led to the formation of the reduced product via H-abstraction (entry 3, Table 6.5). The lack of success in the cyclization was therefore not due to failure to generate the radical species but was attributed to the faster rate of deactivation of the radical in the presence of [Cu^{II}(TPMA)Br][Br] (typically 10⁷-10⁸ M⁻¹s⁻¹) as compared to the rate of cyclization (~10⁵-10⁶ M⁻¹s⁻¹).

ATRC of **3** in protic solvents also led to the formation of reduced products (entry 4, Table 6.5). When an aprotic solvent (1,2-dichloroethane or DCE) was used, formation of the 5-*exo* lactone was finally observed, albeit in very low yields (entry 6, Table 6.5). The presence of two electronegative Cl atoms on the radical moiety produces a more electrophilic radical species, which can readily attack the electron-rich double bond. However, the low yield still indicates that the halide abstraction of the radical occurs faster than the cyclization. An increase in catalyst loading caused a slight increase in the yield of lactone (entry 5, Table 6.5).

The presence of substituents on the carbon atom adjacent to the acetate moiety did promote cyclization as expected, which is evident on the ATRC results of **4** and **5** (entries

7-9, Table 6.5). The yield of 5-*exo* cyclic product increased three-fold when bulky groups were introduced to the substrates. Dramatic improvements were also observed in the ATRC of the longer-chain trichloroacetate **6** with 74% yield of the 8-*endo* lactone at higher catalyst loadings (entry 10, Table 6.5) and a decrease in catalyst loadings still afforded considerable amounts of the lactone (entries 11-13, Table 6.5).

The terminal carbon-substituted alkenyl trichloroacetate **7** exhibited a preference for the 6-*endo* mode of closure over the kinetically favored 5-*exo* cyclization, yielding 10 times more of the δ -lactone (entry 14, Table 6.5). This type of influence on the regiochemistry of the cyclization was first noted in the free radical cyclization of 5-hexenyl radicals. Julia³⁹ reported that the introduction of electron-withdrawing substituents on the radical moiety induced the attack on the terminal olefinic carbon, leading to the exclusive formation of the 6-*endo* cyclohexane product. In our case, the presence of an electron-donating alkyl group on the terminal olefinic carbon made it susceptible to the electrophilic attack of the electron-deficient radical end. This further proves that modifying the electronic contributions on both the radical moiety and the unsaturated end of the cyclization precursor can control the regioselectivity of these cyclization reactions.

6.3.4 Theoretical Elucidation of Thermodynamic Control in Radical Cyclization Regioselectivity

To further confirm the effects of the internal alkyl substituents on the stability of the *s-cis* conformer and, consequently, on the overall cyclization process, the relative energies of both *s-cis* and *s-trans* conformers of various derivatives of the allyl trichloroacetate radical were calculated. All calculations were carried out using the

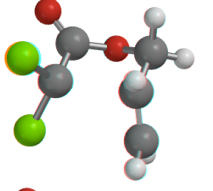
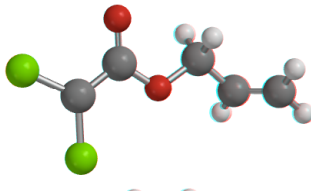
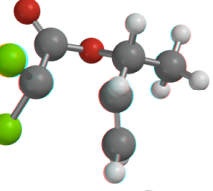
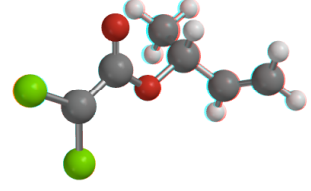
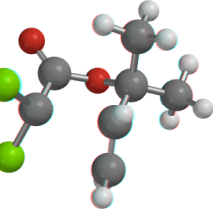
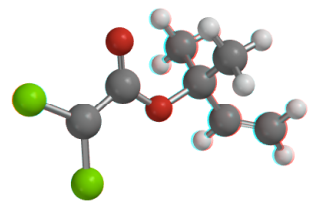
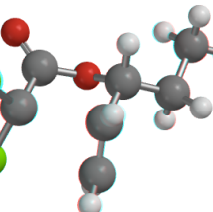
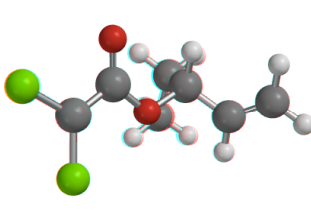
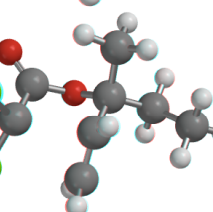
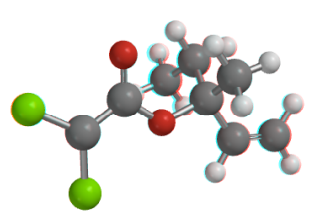
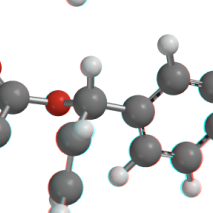
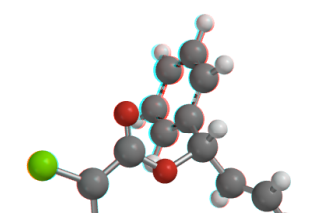
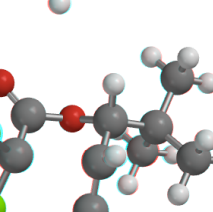
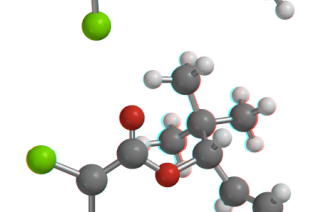
Spartan software package (version 4.1.0, Wavefunction, Inc., Irvine).⁵³ The structures of the *s-cis* and *s-trans* conformers were optimized with Becke's three parameter hybrid exchange functional and the Lee-Yang-Parr correlation functional (B3LYP)^{89,90} and the 6-31G* basis set. Additionally, structures of various derivatives of the allyl trichloroacetate radical bearing larger substituents at the nonterminal position were optimized at the unrestricted Hartree-Fock (UHF/6-31G*) level. The electron density surfaces of the radicals were also mapped and the dipole moments were then determined.

The *s-cis* radical intermediate is known to adopt the chair conformation, which is more stable than its boat counterpart (chair conformation is usually ~2 kcal/mol lower in energy).⁹¹ This is true for both the *5-exo* and the *6-endo* configurations. Thus, in the calculation of the *s-cis* radical, the chair conformation was applied. The structures and the relative energies of the *s-cis* and *s-trans* conformers of various C3-substituted allyl trichloroacetate radicals are summarized in Table 6.6.

The *s-trans* conformer of the parent allyl trichloroacetate radical was found to be 8.6 kcal/mol more stable than its *s-cis* counterpart. This supports the experimental observations where cyclizations of unsubstituted allyl haloacetates formed very small amounts of the target lactone due to preference of the generated radical to the *s-trans* conformation. Substitution of the C3 atom with a methyl group lowered the energy difference between the two isomers to ~6 kcal/mol, however, the *s-trans* conformer was still found to be more stable.

With the substitution of two methyl groups on the C3 atom, the *s-cis* conformer became the more stable isomer (2.9 kcal/mol lower in energy). Apart from the steric

Table 6.6. Calculated Relative Energies of *s-cis* and *s-trans* Conformers of Various C3-Substituted Allyl Trichloroacetate Radicals

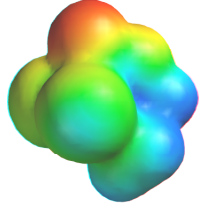
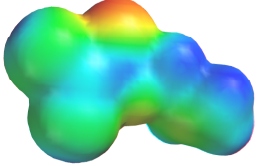
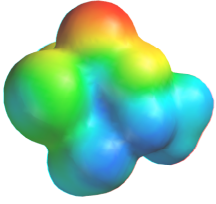
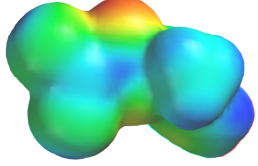
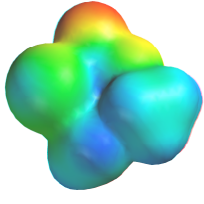
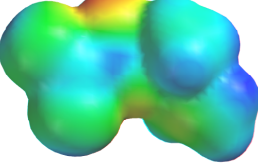
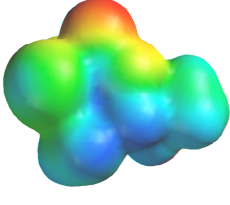
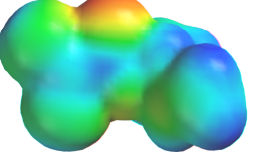
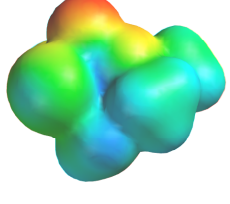
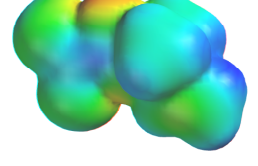
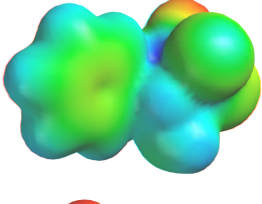
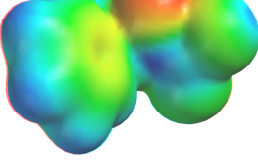
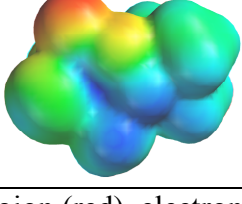
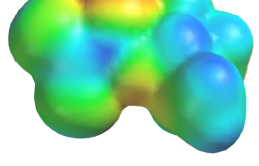
Substituent	Structures		Relative Energy kcal/ mol ($\Delta E = E_{cis} - E_{trans}$)
	<i>s-cis</i>	<i>s-trans</i>	
none			8.6
methyl			6.5
dimethyl			-2.9
ethyl			-1.8
ethyl, methyl			-5.2
phenyl			-4.5
t-butyl			-6.0

crowding, rotation to the *s-cis* conformation was also induced due to Thorpe-Ingold effect.⁹² Apparently, the introduction of two alkyl groups on the C3 atom was more effective in stabilizing the *s-cis* conformer. The substitution of an ethyl group only resulted to a 1.8 kcal/mol energy difference as compared to the 2.9 kcal/mol energy difference when two methyl groups are on the C3 atom. Also, substitution of a methyl and an ethyl group greatly stabilized the *s-cis* conformer (5.2 kcal/mol lower in energy) while a phenyl group on the C3 atom only resulted to a 4.5 kcal/mol energy difference.

The substitution of a *tert*-butyl group proved to be the most effective in stabilizing the *s-cis* conformer. An energy difference of 6.0 kcal/mol (*s-cis* is lower in energy) was calculated for the *tert*-butyl substituted radical. Unfortunately, this could not be supported with actual experimental results since ATRC of the allyl-3-*tert*-butyl trichloroacetate was not performed. The synthesis of allyl-3-*tert*-butyl trichloroacetate could not be carried out due to the unavailability of the alcohol precursor from commercial sources. Synthesis of the alcohol precursor also involved numerous reaction steps and could not be performed due to time constraints.

The dipole moment of the isomers is also an important factor to consider because the use of an appropriate solvent could stabilize one conformer over the other. A molecule with a larger dipole moment is more stabilized in a polar solvent and vice versa. The dipole moments of the various substituted allyl trichloroacetate radicals were calculated from the electron density surface maps and the results are summarized in Table 6.7.

Table 6.7. Electron Density Maps and Dipole Moments (Debye) of *s-cis* and *s-trans* Conformers of Various C3-Substituted Allyl Trichloroacetate Radicals^a

Substituent	Electron Density Map		μ , Debye	
	<i>s-cis</i>	<i>s-trans</i>	<i>s-cis</i>	<i>s-trans</i>
none			5.05	2.07
methyl			5.14	2.15
dimethyl			5.19	2.23
ethyl			5.17	2.19
ethyl, methyl			5.60	2.27
phenyl			5.66	2.86
t-butyl			5.60	2.83

^aelectron-rich region (red), electron-poor region (blue)

As evident in the results shown in Table 6.7, the *s-cis* conformers have consistently higher dipole moments than the *s-trans* radicals. This means that the *s-cis* radical conformation would be more stabilized in polar solvents. The solvents used in the ATRC reactions are relatively polar and, thus, had contributed to promote the overall cyclization reaction. These calculations are also consistent with previously reported ATRC reactions where cyclization of allyl acetate radicals occurred more readily in highly polar solvents, such as water, as compared to ATRC reactions done in nonpolar solvents such as benzene or toluene.^{93,94}

6.4 Conclusions

In summary, free radical cyclization and atom transfer radical cyclization reactions in the presence of copper catalysts were reported. As expected, the Bu_3SnH -mediated cyclization of 6-bromo-1-hexene predominantly resulted in the formation of the kinetically favored 5-*exo* cyclic product. An increase in Bu_3SnH concentration led to the reduction of the 5-hexenyl radical. The $[\text{TpCu}^{\text{I}}]_2$ and $[\text{Tp}^{\text{CH}_3}\text{Cu}^{\text{I}}]_2$ catalysts were found to be catalytically inactive since Cu^{I} -olefin complexation did not take place due to the lack of coordination site in the dimeric structure. Similarly, the $\text{Tp}^{\text{CF}_3}\text{Cu}^{\text{I}}(\text{CH}_3\text{CN})$ complex did not affect the regiochemistry of the cyclization reaction, which was probably due to the heterogeneous nature of the reaction mixture. When 6-bromo-1-hexene was effectively bound to the Cu^{I} center, as with the case of the $\text{TpCu}^{\text{I}}(6\text{-bromo-1-hexene})$ complex, formation of the cyclohexane product was observed, albeit to a small degree. In the absence of Bu_3SnH , free radical cyclization did not proceed, indicating that the TpCu^{I} complex does not initiate the formation of the 5-hexenyl radical.

Atom transfer radical cyclization of alkenyl bromoacetates in the presence of $[\text{Cu}^{\text{II}}(\text{TPMA})\text{Cl}][\text{Cl}]$ was also unsuccessful due to the fast deactivation of the acetate radical. When carried out in protic solvents, reduction products were formed, indicating that cleavage of the C-Br did occur, however, the faster deactivation and H-transfer steps prevented the intramolecular addition of the radical center to the unsaturated moiety. Clearly, a copper catalyst with a lower deactivation rate constant (preferably $\sim 10^5 \text{ M}^{-1}\text{s}^{-1}$) is ideal for these cyclization reactions. ATRC of alkenyl trichloroacetates were more successful and the substitution of the C3 atom resulted in higher yields of the desired lactones. Calculations of the *s-cis* and *s-trans* structures confirmed that the presence of

alkyl groups on the C3 atom stabilizes the *s-cis* conformer, which is essential for the cyclization to proceed.

References

- (1) Matyjaszewski, K.; Davis, T. P., eds. *Handbook of Radical Polymerization*. 2002, John Wiley and Sons, Inc.: Hoboken.
- (2) Togo, H., *Advanced Free Radical Reactions for Organic Synthesis*. Elsevier, Oxford, UK, **2004**.
- (3) Lee, E.; Choi, S. J. Radical Cyclization of β -Alkoxy methacrylates: Expedient Synthesis of (+)-Methyl Nonactate. *Org. Lett.* **1999**, *1*(7), 1127-1128.
- (4) Stork, G.; Sher, P. M.; Chen, H. L. Radical cyclization-trapping in the synthesis of natural products. A simple, stereocontrolled route to prostaglandin F_{2 α} . *J. Am. Chem. Soc.* **1986**, *108*, 6384-6385.
- (5) Snider, B. B. Manganese(III)-Based Oxidative Free-Radical Cyclizations. *Chem. Rev.* **1996**, *96*, 339-363.
- (6) Parsons, P. J.; Penkett, C. S.; Shell, A. J. Tandem Reactions in Organic Synthesis: Novel Strategies for Natural Product Elaboration and the Development of New Synthetic Methodology. *Chem. Rev.* **1996**, *96*, 195-206.
- (7) Ghelfi, F.; Roncaglia, F.; Pattarozzi, M.; Giangiordano, V.; Petrillo, G.; Sancassan, F.; Parsons, A. F. Atom transfer radical cyclization of *O*-allyl-2,2-dichlorohemiacetal acetates: an expedient method to dichloro- γ -lactones. *Tetrahedron*. **2009**, *65*, 10323-10333.
- (8) Wetter, C.; Studer, A. Microwave-assisted free radical chemistry using the persistent radical effect. *Chem. Commun.* **2004**, 174-174.
- (9) Clark, A. J. Atom transfer radical cyclisation reactions mediated by copper complexes. *Chem. Soc. Rev.* **2002**, *31*, 1-11.
- (10) Iwamatsu, S. I.; Matsubara, K.; Nagashima, H. Synthetic Studies of *cis*-3a-Aryloctahydroindole Derivatives by Copper-Catalyzed Cyclization of *N*-Allyltrichloroacetamides: Facile Construction of Benzylic Quaternary Carbons by Carbon-Carbon Bond-Forming Reactions. *J. Org. Chem.* **1999**, *64*, 9625-9631.

- (11) Yoshimitsu, T.; Nakajima, H.; Nagaoka, H. Synthesis of the CD ring system of paclitaxel by atom-transfer radical annulation reaction. *Tetrahedron Lett.* **2002**, *43*, 8587-8590.
- (12) Yanada, R.; Koh, Y.; Nishimori, N.; Matsumara, A.; Obika, S.; Mitsuya, H.; Fujii, N.; Takemoto, Y. Indium-Mediated Atom-Transfer and Reductive Radical Cyclizations of Iodoalkynes: Synthesis and Biological Evaluation of HIV-Protease Inhibitors. *J. Org. Chem.* **2004**, *69*, 2417-2422.
- (13) Stevens, C. V.; Meenen, E. V.; Eeckhout, Y.; Vanderhoydonck, B.; Hooghe, W. Synthesis of highly functionalized spiro-indoles by a halogen atom transfer radical cyclization. *Chem. Commun.* **2005**, 4827-4829.
- (14) Curran, D. P. The design and application of free radical chain reactions in organic synthesis. Part 1. *Synthesis.* **1988**, *6*, 417-439.
- (15) Curran, D. P. The design and application of free radical chain reactions in organic synthesis. Part 2. *Synthesis.* **1988**, *7*, 489-513.
- (16) Curran, D. P.; Chang, C. T. Atom transfer cyclization reactions of α -iodo carbonyls. *Tetrahedron Lett.* **1987**, *28*, 2477-2480.
- (17) Curran, D. P.; Chang, C. T. Evidence that palladium(0)-promoted cyclizations of unsaturated α -iodocarbonyls occur by an atom transfer mechanism. *Tetrahedron Lett.* **1990**, *31*, 933-936.
- (18) Curran, D. P.; Tamine, J. Effects of Temperature on Atom Transfer Radical Cyclization Reactions of Allylic α -Iodo Esters and Amides. *J. Org. Chem.* **1991**, *56*, 2746-2750.
- (19) Stevens, C. V.; Meenen, E. V.; Masschelein, K. G. R.; Eeckhout, Y.; Hooghe, W.; D'hondt, B.; Nemykin, V. N.; Zhdankin, V. V. A copper-catalyzed domino radical cyclization route to benzospiro-indolizidinepyrrolidinones. *Tetrahedron Lett.* **2007**, *28*, 7108-7111.
- (20) Thommes, K.; Icli, B.; Scopelliti, R.; Severin, K. Atom-Transfer Radical Addition (ATRA) and Cyclization (ATRC) Reactions Catalyzed by a Mixture of [RuCl₂Cp*(PPh₃)] and Magnesium. *Chem. Eur. J.* **2007**, *13*, 6899-6907.

- (21) Bull, J. A.; Hutchings, M. G.; Lujan, C.; Quayle, P. New reactivity patterns of copper(I) and other transition metal NHC complexes: application to ATRC and related reactions. *Tetrahedron Letters*. **2008**, *49*, 1352-1356.
- (22) Clark, A. J.; Wilson, P. Copper mediated atom transfer radical cyclisations with AIBN. *Tetrahedron Letters*. **2008**, *49*, 4848-4850.
- (23) Clark, A. J.; Filik, R. P.; Thomas, G. H. Ligand Geometry Effects in Copper Mediated Atom Transfer Radical Cyclisations. *Tetrahedron Letters*. **1999**, *40*, 4885-4888.
- (24) Clark, A. J.; Dell, C. P.; Ellard, J. M.; Hunt, N. A.; McDonagh, J. P. Efficient room temperature copper(I) mediated 5-*endo* radical cyclisations. *Tetrahedron Letters*. **1999**, *40*(49), 8619-8623.
- (25) Clark, A. J.; Battle, G. M.; Bridge, A. Efficient β -lactam synthesis via 4-*exo* atom transfer radical cyclisation using CuBr(tripyridylamine) complex. *Tetrahedron Letters*. **2001**, *42*, 4409-4412.
- (26) Benedetti, M.; Forti, L.; Ghelfi, F.; Pagnoni, U. M.; Ronzoni, R. Halogen atom transfer radical cyclization of *N*-allyl-*N*-benzyl-2,2-dihaloamides to 2-pyrrolidinones, promoted by Fe⁰-FeCl₃ or CuCl-TMEDA. *Tetrahedron*. **1997**, *53*(41), 14031-14042.
- (27) Schmidt, B.; Pohler, M. Ruthenium-catalyzed tandem ring closing metathesis (RCM) – atom transfer radical cyclization (ATRC) sequences. *J. Organomet. Chem.* **2005**, *690*, 5552-5555.
- (28) De Campo, F.; Lastecoueres, D.; Verlhac, J.-B. New copper(I) and iron(II) complexes for atom transfer radical macrocyclisation reactions. *J. Chem. Soc., Perkin Trans.* **2000**, *1*, 575-580.
- (29) Clark, A. J.; Geden, J. V.; Thom, S. Solid-Supported Copper Catalysts for Atom-Transfer Radical Cyclizations: Assessment of Support Type and Ligand Structure on Catalyst Performance in the Synthesis of Nitrogen Heterocycles. *J. Org. Chem.* **2006**, *71*(4), 1471-1479.
- (30) Clark, A. J.; Filik, R. P.; Haddleton, D. M.; Radigue, A.; Sanders, C. J.; Thomas, G. H.; Smith, M. E. Solid-Supported Catalysts for Atom-Transfer Radical Cyclization of 2-Haloacetamides. *J. Org. Chem.* **1999**, *64*, 8954-8957.

- (31) Ricardo, C.; Pintauer, T. Copper catalyzed atom transfer radical cascade reactions in the presence of free-radical diazo initiators as reducing agents. *Chem. Commun.* **2009**, *21*, 3029-3031.
- (32) Edlin, C.; Faulkner, J.; Helliwell, M.; Knight, C. K.; Parker, J.; Quayle, P.; Raftery, J. Atom transfer radical cyclization reactions (ATRC): synthetic applications. *Tetrahedron.* **2006**, *62*, 3004-3015.
- (33) Felluga, F.; Forzato, C.; Ghelfi, F.; Nitti, P.; Pitacco, G.; Pagnoni, U. M.; Roncaglia, F. Atom transfer radical cyclization (ATRC) applied to a chemoenzymatic synthesis of Quercus lactones. *Tetrahedron: Assymetry.* **2007**, *18*, 527-536.
- (34) Yang, D.; Yan, Y.; Zheng, B.; Gao, Q.; Zhu, N. Copper(I)-Catalyzed Chlorine Atom Transfer Radical Cyclization Reactions of Unsaturated α -Chloro β -Keto Esters. *Organic Letters.* **2006**, *8*, 5757-5760.
- (35) Pattarozzi, M.; Roncaglia, F.; Accorsi, L.; Parsons, A. F.; Ghelfi, F. Functional rearrangement of 3-Cl or 3,3-diCl- γ -lactams bearing a secondary 1-chloroalkyl substituent at C-4. *Tetrahedron.* **2010**, *66*, 1357-1364.
- (36) Julia, M.; Maumy, M. Free radical cyclizations. *Pure Appl. Chem.* **1967**, *15*, 167-183.
- (37) Walling, C.; Cioffari, A. Cyclization of 5-Hexenyl Radicals. *J. Am. Chem. Soc.* **1972**, *94*, 6059-6064.
- (38) Walling, C.; Cioffari, A. Interconversion of 1-Phenyl-5-hexenyl, 2-Phenylcyclopentylmethyl, and 3-Phenylcyclohexyl Radicals. *J. Am. Chem. Soc.* **1972**, *94*, 6064-6069.
- (39) Julia, M. Free-Radical Cyclization. *Acc. Chem. Res.* **1971**, *4*, 386-392.
- (40) Padwa, A.; Nimmegern, H.; Wong, G. S. K. Synthesis of the Pyrrolidine Ring System by Radical Cyclization. *J. Org. Chem.* **1985**, *50*, 5620-5627.
- (41) Knapp, S.; Gibson, F. S.; Choe, Y. H. Radical based annulations of iodo lactams. *Tetrahedron Lett.* **1990**, *31*, 5397-5400.

- (42) Cassayre, J.; Gagosz, F.; Zard, S. Z. A Short Synthesis of (\pm)-13-Deoxyserratine. *Angew. Chem. Int. Ed.* **2002**, *41*, 1783-1785.
- (43) Gómez, A. M.; Company, M. D.; Uriel, C.; Valverde, S.; López, J. C. 6-endo Versus 5-*exo* radical cyclization: streamlined syntheses of carbahexopyranoses and derivatives by 6-endo-*trig* radical cyclization. *Tetrahedron.* **2007**, *48*, 1645-1649.
- (44) Baldwin, J. E. Rules for ring closure. *J. Chem. Soc., Chem. Commun.* **1976**, 734-746.
- (45) Thebtaranonth, C.; Thebtaranonth, C., *Cyclization Reactions*. CRC Press, Inc., Boca Raton, FL, **1994**.
- (46) Clive, D. L. J.; Cheshire, D. R. On Baldwin's Kinetic Barrier against 5-(enol-*endo*)-*exo*-Trigonal Closures: a Comparison of Ionic and Analogous Radical Reactions, and a New Synthesis of Cyclopentanones. *J. Chem. Soc., Chem. Commun.* **1987**, 1520-1523.
- (47) Nagashima, H.; Seki, K.; Ozaki, N.; Wakamatsu, H.; Itoh, K.; Tomo, Y.; Tsuji, J. Transition-Metal-Catalyzed Radical Cyclization: Copper-Catalyzed Cyclization of Allyl Trichloroacetates to Trichlorinated γ -Lactones. *J. Org. Chem.* **1990**, *55*, 985-990.
- (48) Tyeklar, Z.; Jacobson, R. R.; Wei, N.; Murthy, N. N.; Zubieta, J.; Karlin, K. D. Reversible Reaction of Dioxygen (and Carbon Monoxide) with a Copper(I) Complex. X-Ray Structures of Relevant Mononuclear Cu(I) Precursor Adducts and the Trans-(μ -1,2-peroxo)dicopper(II) Product. *J. Am. Chem. Soc.* **1993**, *115*(7), 2677-2689.
- (49) Eckenhoff, W. T.; Pintauer, T. Atom Transfer Radical Addition in the Presence of Catalytic Amounts of Copper(I/II) Complexes with Tris(2-pyridylmethyl)amine. *Inorg. Chem.* **2007**, *46*(15), 5844-5846.
- (50) Eckenhoff, W. T.; Garrity, S. T.; Pintauer, T. Highly Efficient Copper-Mediated Atom-Transfer Radical Addition (ATRA) in the Presence of Reducing Agent. *Eur. J. Inorg. Chem.* **2008**(4), 563-571.
- (51) Claire, P. P. K.; Coe, P. L.; Jones, C. J.; McCleverty, J. A. 3,5-Bis(trifluoromethyl)pyrazole and some N-substituted derivatives. *J. Fluorine Chem.* **1991**, *51*, 283-289.

- (52) Rasika Dias, H. V.; Jin, W.; Kim, H.; Lu, H. Polyfluorinated Tris(pyrazolyl)borates. Syntheses and Spectroscopic and Structural Characterization of Group I and Group II Metal Complexes of $[\text{HB}(3,5\text{-(CF}_3)_2\text{Pz)}_3]^-$ and $[\text{HB}(3\text{-(CF}_3)\text{Pz)}_3]^-$. *Inorg. Chem.* **1996**, *35*, 2317-2328.
- (53) Wavefunction, SPARTAN, 4.1.0 ed., Inc., 18401 Von Karman Ave., Ste. 370, Irvine, CA 92612 (USA), **1997**.
- (54) Aullon, G.; Gorun, S. M.; Alvarez, S. Effects of Tris(pyrazolyl)borato Ligand Substituents on Dioxygen Activation and Stabilization by Copper Compounds. *Inorg. Chem.* **2006**, *45*, 3594-3601.
- (55) Mairena, M. A.; Urbano, J.; Carbajo, J.; Maraver, J. J.; Alvarez, E.; Diaz-Requejo, M. M.; Perez, P. J. Effects of the Substituents in the Tp^xCu Activation of Dioxygen: An Experimental Study. *Inorg. Chem.* **2007**, *46*, 7428-7435.
- (56) Schneider, J. L.; Carrier, S. M.; Ruggiero, C. E.; Young, V. G.; Tolman, W. B. Influences of Ligand Environment on the Spectroscopic Properties and Disproportionation Reactivity of Copper-Nitrosyl Complexes. *J. Am. Chem. Soc.* **1998**, *120*, 11408-11418.
- (57) Rasika Dias, H. V.; Lu, H.; Kim, H.; Polach, S. A.; Goh, T.; Browning, R. G.; Lovely, C. J. Copper(I) Ethylene Adducts and Aziridination Catalysts Based on Fluorinated Tris(pyrazolyl)borates $[\text{HB}(3\text{-CF}_3)_2,5\text{-(R)Pz)}_3]^-$ (where R = CF_3 , C_6H_5 , H; Pz = pyrazolyl). *Organometallics.* **2002**, *21*, 1466-1473.
- (58) Conry, R. R.; Ji, G.; Tipton, A. A. Synthesis and Characterization of Copper(I) Complexes with a Fairly Bulky Tris(pyrazolyl)hydroborate Ligand. Probing the Flexibility of the Metal-Containing Pocket Formed by the Ligand. *Inorg. Chem.* **1999**, *38*, 906-913.
- (59) Fujisawa, K.; Ono, T.; Ishikawa, Y.; Amir, N.; Miyashita, Y.; Okamoto, K.; Lehnert, N. Structural and Electronic Differences of Copper(I) Complexes with Tris(pyrazolyl)methane and Hydrotris(pyrazolyl)borate Ligands. *Inorg. Chem.* **2006**, *45*, 1698-1713.
- (60) Rasika Dias, H. V.; Kim, H.; Lu, H.; Rajeshwar, K.; Tacconi, N.; Derecskei-Kovacs, A.; Marynick, D. S. Investigation of the Electronic and Geometric Effects of Trifluoromethyl Substituents on Tris(pyrazolyl)borate Ligands Using Manganese(I) and Copper(I) Complexes. *Organometallics.* **1996**, *15*, 2994-3003.

- (61) Rasika Dias, H. V.; Kim, H. Novel Tris(pyrazolyl)borates Bearing Perfluoroalkyl Pigtailes. Syntheses and Characterization of the Sodium and Copper(I) Complexes of [HB(3-(R)Pz)₃]⁻ (R = C₂F₂, C₃F₇; Pz = Pyrazolyl). *Organometallics*. **1996**, *15*, 5374-5379.
- (62) Rasika Dias, H. V.; Lu, H. Copper(I) Carbonyl Complex of a Trifluoromethylated Tris(pyrazolyl)borate Ligand. *Inorg. Chem.* **1995**, *34*, 5380-5382.
- (63) Kitajima, N.; Fujisawa, K.; Fujimoto, C.; Moro-oka, Y.; Hashimoto, S.; Kitagawa, T.; Toriumi, K.; Tatsumi, K.; Makamura, A. A New Model for Dioxygen Binding in Hemocyanin. Synthesis, Characterization, and Molecular Structure of the μ - η^2 : η^2 Peroxo Dinuclear Copper(II) Complexes, [Cu(HB(3,5-R₂pz)₃)₂(O₂)] (R = *i*-Pr and Ph). *J. Am. Chem. Soc.* **1992**, *114*, 1277-1291.
- (64) Mealli, C.; Arcus, C. S.; Wilkinson, J. L.; Marks, T. J.; Ibers, J. A. Structural Studies of Copper(I) Binding by Hydrotris(1-pyrazolyl)borate and Hydrotris(3,5-dimethyl-1-pyrazolyl)borate in the Solid State and in Solution. *J. Am. Chem. Soc.* **1976**, *98*, 711-718.
- (65) Imai, S.; Fujisawa, K.; Kobayashi, T.; Shirasawa, N.; Fujii, H.; Yoshimura, T.; Kitajima, N.; Moro-oka, Y. ⁶³Cu NMR Study of Copper(I) Carbonyl Complexes with Various Hydrotris(pyrazolyl)borates: Correlation between ⁶³Cu Chemical Shifts and CO Stretching Vibrations. *Inorg. Chem.* **1998**, *37*, 3066-3070.
- (66) Bruce, M. I. Carbonyl chemistry of the group IB metals. *J. Organomet. Chem.* **1972**, *44*, 209-226.
- (67) Ruggiero, C. E.; Carrier, S. M.; Antholine, W. E.; Whittaker, J. W.; Cramer, C. J.; Tolman, W. B. Synthesis and Structural and Spectroscopic Characterization of Mononuclear Copper Nitrosyl Complexes: Models for Nitric Oxide Adducts of Copper Proteins and Copper-Exchanged Zeolites. *J. Am. Chem. Soc.* **1993**, *115*, 11285-11298.
- (68) Churchill, M. R.; G., d. B.; Rotella, F. J.; Salah, O.; Bruce, M. Determination of the Crystal Structure and Molecular Geometry of [Hydrotris(1-pyrazolyl)borato]copper(I) Carbonyl. A Unique Structural Investigation of a Copper-Carbonyl Linkage. *Inorg. Chem.* **1975**, *14*, 2051-2056.
- (69) Lobbia, G. C.; Pettinari, C.; Marchetti, F. Synthesis and Characterization of Copper(I) Derivatives with N-Donor Ligands. III. Hydrotris(1H-pyrazol-1-yl)borate. The X-ray Crystal Structure of [HB-(μ -pz)₃-Cu(PPh₃)]. *Polyhedron*. **1996**, *15*, 881-890.

- (70) Hu, Z.; Williams, R. D.; Tran, D.; Spiro, T. G.; Gorun, S. M. Re-engineering Enzyme-Model Active Sites: Reversible Binding of Dioxygen at Ambient Conditions by a Bioinspired Copper Complex. *J. Am. Chem. Soc.* **2000**, *122*, 3556-3557.
- (71) Yap, G. P. A.; Jove, F.; Urbano, J.; Alvarez, E.; Trofimenko, S.; Diaz-Requejo, M. M.; Perez, P. J. Unusual Polybrominated Polypyrazolylborates and Their Copper(I) Complexes: Synthesis, Characterization, and Catalytic Activity. *Inorg. Chem.* **2007**, *46*, 780.
- (72) Valach, F.; Tokarcik, M.; Melnik, M. Distortion Isomerism and Plasticity of the Coordination Sphere of Binuclear Cu(II) Complexes: Crystal Structure of the Monoclinic Isomer of [Cu₂(2-bromopropionato)₄(caffeine)₄]. *J. Coord. Chem.* **2009**, *62*, 225-233.
- (73) Jezierska, J.; Glowiak, T.; Ozarowski, A.; Yablokov, Y. V.; Rzaczynzka, Z. Crystal Structure, EPR, and Magnetic Susceptibility Studies of Tetrakis[μ-(β-alanine)-O-O']dichlorodicopper(II) dichloro monohydrate. *Inorg. Chim. Acta.* **1998**, *275-276(1,2)*, 28-36.
- (74) Blake, A. J.; Gould, R. O.; Holder, A. J.; Lavery, A. J.; Schroder, M. Copper Thioether Chemistry: The Synthesis and Single Crystal X-ray Structures of [Cu₂([18]aneS₆)(NCMe)₂](ClO₄)₂ and [Cu([9]aneS₃)(AsPPh₃)](ClO₄). *Polyhedron.* **1990**, *9*, 2919-2924.
- (75) Karlin, K. D.; Hayes, J. C.; Hutchinson, J. P.; Zubieta, J. Synthesis and Characterization of a Novel Dicopper(I) Complex of a Thiaether containing *meta*-xylyl binucleating ligand. *Inorg. Chim. Acta.* **1983**, *79*, L45-L46.
- (76) Adams, H.; Batten, S. R.; Davies, G. M.; Duriska, M. B.; Jeffery, J. C.; Jensen, P.; Jinzhen, L.; Motson, G.; Coles, S. J.; Hursthouse, M. B.; Ward, M. D. New bis-, tris- and tetrakis(pyrazolyl)borate ligands with 3-pyridyl and 4-pyridyl substituents: synthesis and coordination chemistry. *Dalton Trans.* **2005**, 1910-1923.
- (77) Diaz-Requejo, M. M.; Caballero, A.; Belderrain, T. R.; Nicasio, M. C.; Trofimenko, S.; Perez, P. J. Copper(I)-Homoscorpionate Catalysts for the Preferential, Kinetically Controlled Cis Cyclopropanation of α-Olefins with Ethyl Diazoacetate. *J. Am. Chem. Soc.* **2002**, *124*, 978-983.
- (78) Thompson, J. S.; Harlow, R. L.; Whitney, J. F. Copper(I)-Olefin Complexes. Support for the Proposed Role of Copper in the Ethylene Effect in Plants. *J. Am. Chem. Soc.* **1983**, *105*, 3522-3527.

- (79) Lee, E.; Yoon, C. H.; Lee, T. H.; Kim, S. Y.; J., H. T.; Sung, Y.; Park, S.; Lee, S. 8-Endo Cyclization of (Alkoxy carbonyl)methyl Radicals: Radical Ways for Preparation of Eight-Membered-Ring Lactones. *J. Am. Chem. Soc.* **1998**, *120*, 7469-7478.
- (80) Julia, M.; Sasussine, L.; Thuillier, G. I. Addition du chloracetate de methyle sur les olefines. *J. Organomet. Chem.* **1979**, *174*, 359-366.
- (81) Burkey, T. J.; Majewski, M.; Griller, D. Heats of Formation of Radical and Molecules by a Photoacoustic Technique. *J. Am. Chem. Soc.* **1986**, *108*, 2218-2221.
- (82) Dewar, M. J. S. A review of the n-complex theory. *Bull. Soc. Chim. Fr.* **1951**, *18*, C71-C79.
- (83) Chatt, L.; Duncanson, A. Olefin co-ordination compounds. Part III. Infra-red spectra and structure: attempted preparation of acetylene complexes. *J. Chem. Soc.* **1953**, 2939-2947.
- (84) Wang, X.; Zhao, H.; Li, Y.; Xiong, R.; You, X. Olefin-copper(I) complexes and their properties. *Topics in Catalysis.* **2005**, *35*, 43-61.
- (85) Mairena, M. A.; Diaz-Requejo, M. M.; Belderrain, T. R.; Nicasio, M. C.; Trofimenko, S.; Perez, P. J. Copper-Homoscorpionate Complexes as Very Active Catalysts for the Olefin Aziridination Reaction. *Organometallics.* **2004**, *23*, 253-256.
- (86) Bach, T.; Schlummer, B.; Harms, K. Intramolecular Iron(II)-catalyzed Nitrogen Transfer Reactions of Unsaturated Alkoxy carbonyl Oxides: A Facile and Stereoselective Route to 4,5-Disubstituted Oxazolidinones. *Chem. Eur. J.* **2001**, *7(12)*, 2581-2594.
- (87) Ueno, Y.; Chino, K.; Watanabe, M.; Moriya, O.; Okawara, M. Homolytic Carbocyclization by use of a Heterogeneous Supported Organotin Catalyst. A New Synthetic Route to 2-Alkoxytetrahydrofurans and γ -Butyrolactones. *J. Am. Chem. Soc.* **1982**, *104*, 5564-5566.
- (88) Stork, G.; Mook, R.; Biller, S. A.; Rychnovsky, S. D. Free-radical Cyclization of Bromo Acetals. Use in the Construction of Bicyclic Acetals and Lactones. *J. Am. Chem. Soc.* **1983**, *105*, 3741-3742.
- (89) Becke, A. D. Density-Functional Exchange-Energy Approximation with Correct Asymptotic Behavior. *Phys. Rev. A.* **1988**, *38*, 3098-3100.

- (90) Lee, C.; Yang, W.; Parr, R. G. Development of the Colle-Salvetti Correlation-Energy Formula into a Functional of the Electron Density. *Phys. Rev. B.* **1988**, *37*, 785-789.
- (91) Leach, A. G.; Wang, R.; Wohlhietter, G. E.; Khan, S. I.; Jung, M. E.; Houk, K. N. Theoretical Elucidation of Kinetic and Thermodynamic Control of Radical Addition Regioselectivity. *J. Am. Chem. Soc.* **2003**, *125*, 4271-4278.
- (92) Beesley, R. M.; Ingold, K. U.; Thorpe, J. F. Formation and Stability of Spiro-Compounds. I. Spiro-Compounds from Cyclohexano. *J. Chem. Soc.* **1915**, *107*, 1080-1106.
- (93) Yorimitsu, H.; Nakamura, T.; Shinokubo, H.; Oshima, K.; Omoto, K.; Fujimoto, H. Powerful Solvent Effect of Water in Radical Reaction: Triethylborane-Induced Atom-Transfer Radical Cyclization in Water. *J. Am. Chem. Soc.* **2000**, *122*(45), 11041-11047.
- (94) Yorimitsu, H.; Shinokubo, H.; Matsubara, S.; Oshima, K.; Omoto, K.; Fujimoto, H. Triethylborane-Induced Bromine Atom-Transfer Radical Addition in Aqueous Media: Study of the Solvent Effect on Radical Addition Reactions. *J. Org. Chem.* **2001**, *66*(23), 7776-7785.

FUTURE DIRECTIONS

Monoadducts with only one functional group are easier to manipulate in further chemical transformations and, thus, would have more applications in organic synthesis. However, reports on ATRA reactions involving less active alkyl halides, especially monohalogenated compounds, which would result in the formation of singly functionalized monoadducts, are far less common than those of the polyhalogenated alkyl halides. This is because monohalogenated alkyl halides, which have lower activation rate constants, are less prone to add to alkenes and often require harsh reaction conditions to achieve high yields of the desired single addition adduct.

The photoinitiated ATRA reactions using less active alkyl halides discussed in Chapter 5 resulted in low yields of the desired monoadduct. These results can be further improved by increasing the molar concentration of the alkyl halide relative to the alkene. This can also be done by running the ATRA reactions in neat alkyl halides. Solubility of the copper catalysts might pose a problem when the reactions are run neat, however, this can be remedied by preparing concentrated solutions (as high as 2M) of the catalysts in an appropriate solvents such as acetonitrile or methanol so that the volume of the catalyst that will be added into the reaction mixture will be minute relative to the total volume of the alkyl halide.

In the determination of the activation rate constant ($k_{a,AIBN}$) for $[Cu^I(bpy)_2Cl]$ with AIBN (Chapter 4), the AIBN decomposition rate constant used in the kinetic modeling was adjusted to $4.5 \times 10^{-6} \text{ s}^{-1}$ instead of $3.0 \times 10^{-6} \text{ s}^{-1}$ in order to obtain a better fit of the kinetic modeling plot with the experimental UV-Vis data. It is possible that an interaction between $[Cu^I(bpy)_2Cl]$ and AIBN caused the decomposition of AIBN to proceed faster.

Thus, the decomposition rate constant of AIBN in the presence of $[\text{Cu}^{\text{I}}(\text{bpy})_2\text{Cl}]$ needs to be further investigated. Also, temperature fluctuations might have led to inaccurate measurement of the AIBN decomposition rate constant. This can be prevented by running several aliquots of the AIBN solution in separate flasks instead of having a single flask containing the AIBN solution and an aliquot can be quenched and analyzed at timed intervals while the remaining aliquots are kept at 60°C .

The effect of $k_{\text{a,AIBN}}$ (at constant $k_{\text{d,AIBN}}$) and $k_{\text{d,AIBN}}$ (at constant $k_{\text{a,AIBN}}$) on the concentrations of Cu^{I} and Cu^{II} at equilibrium was also investigated via kinetic modeling (Chapter 4). However, a closer examination of the kinetic modeling plots revealed varying concentrations of Cu^{I} and Cu^{II} at similar K_{ATRA} values, depending on the values of $k_{\text{a,AIBN}}$ and $k_{\text{d,AIBN}}$ used. It would also be interesting to perform kinetic modeling to investigate the effect of varying $k_{\text{a,AIBN}}$ and $k_{\text{d,AIBN}}$ at constant K_{ATRA} values on the equilibrium concentrations of Cu^{I} and Cu^{II} .

APPENDIX A. ^1H NMR Spectra

This appendix contains ^1H NMR spectra of all synthesized complexes described in Chapter 6.

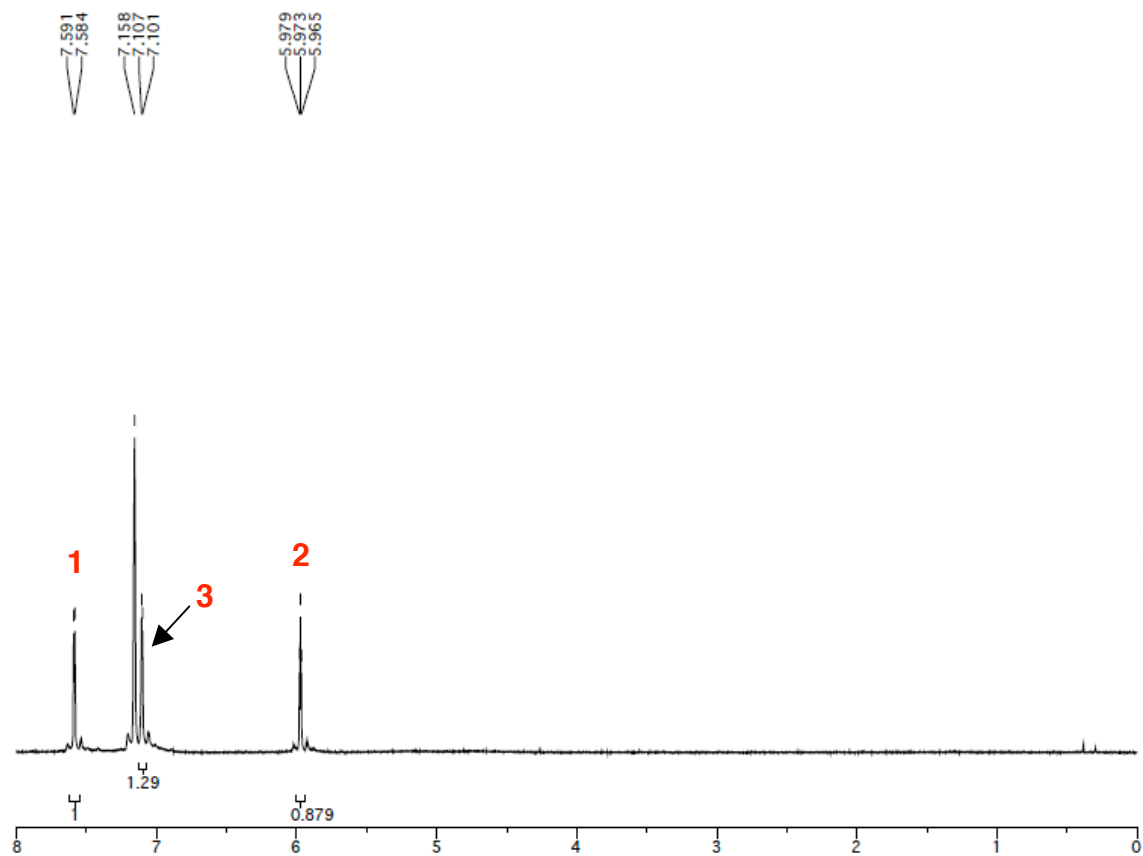
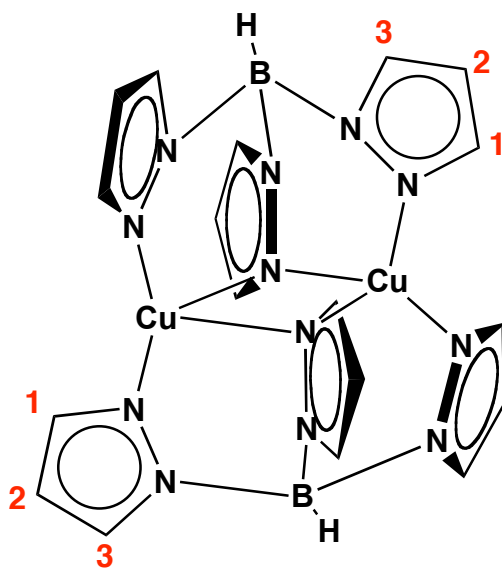


Figure A1. ^1H NMR Spectrum of $[(\text{hydrotris}(1\text{-pyrazolyl})\text{borato})\text{copper}(\text{I})]_2$ or $[\text{TpCu}^{\text{I}}]_2$ (300 Hz, C_6D_6 , RT)



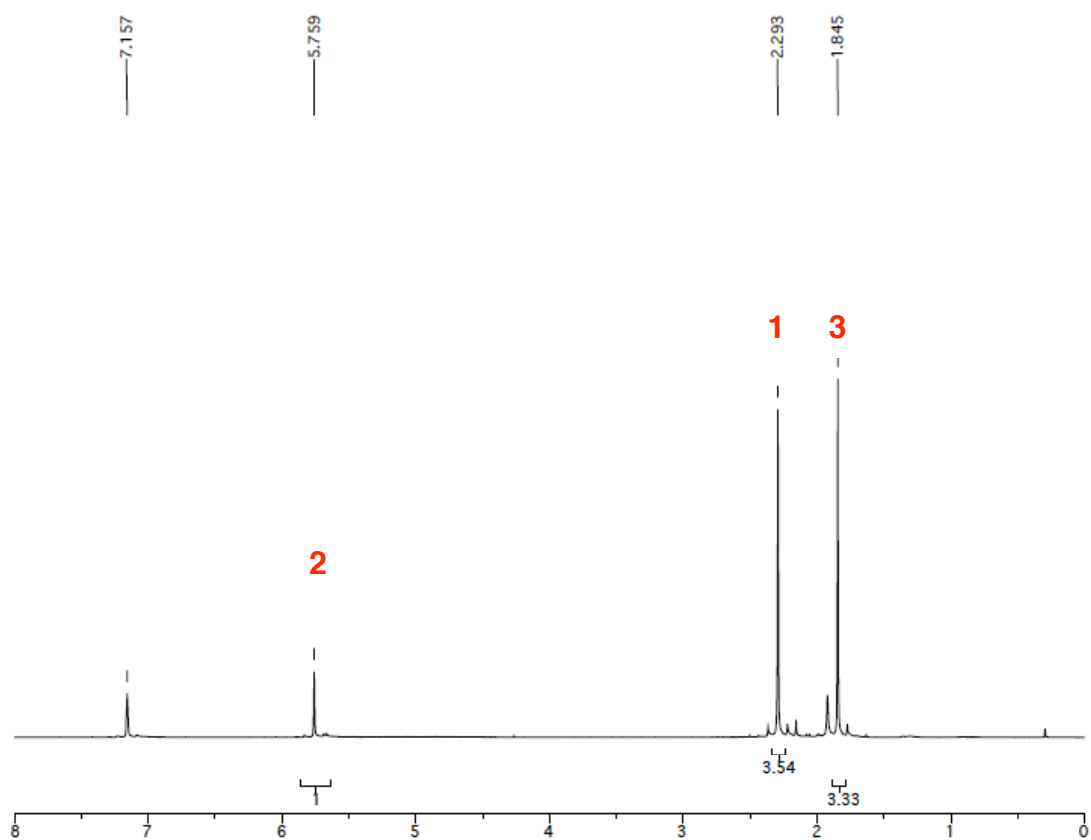
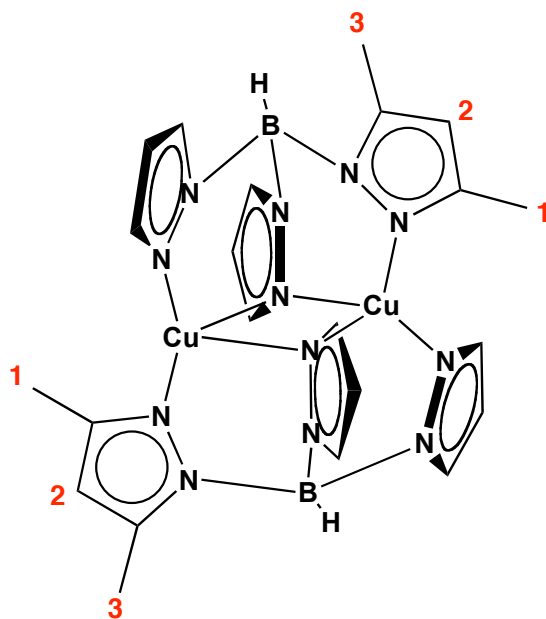


Figure A2. ^1H NMR Spectrum of [(hydrotris(3,5-dimethyl-1-pyrazolyl)borato)copper(I)]₂ or [Tp^{CH₃}Cu]₂ (300 Hz, C₆D₆, RT)



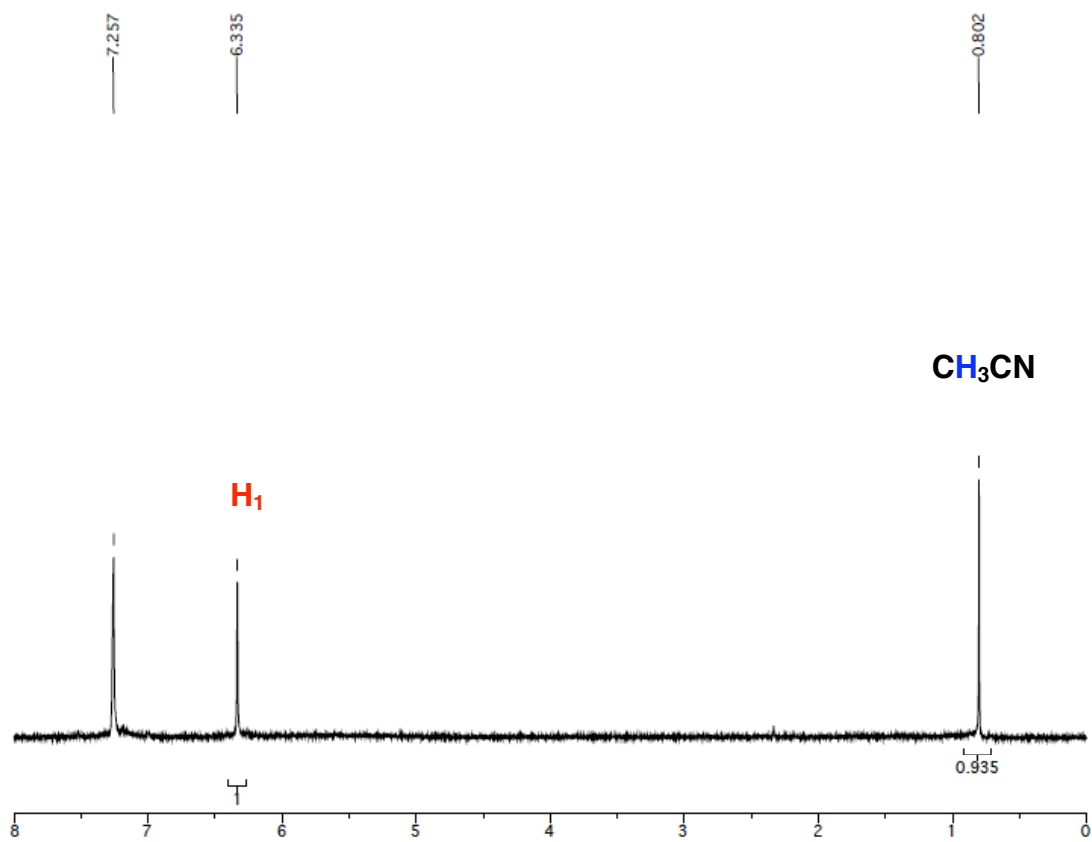
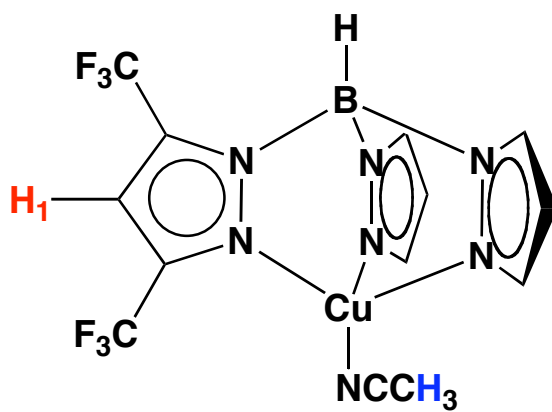


Figure A3. ^1H NMR Spectra of [hydrotris(3,5-trifluoromethyl-1-pyrazolyl)borato](acetonitrile)copper(I) or $\text{Tp}^{\text{CF}_3}\text{Cu}^{\text{I}}(\text{CH}_3\text{CN})$ (300 Hz, CDCl_3 , RT)



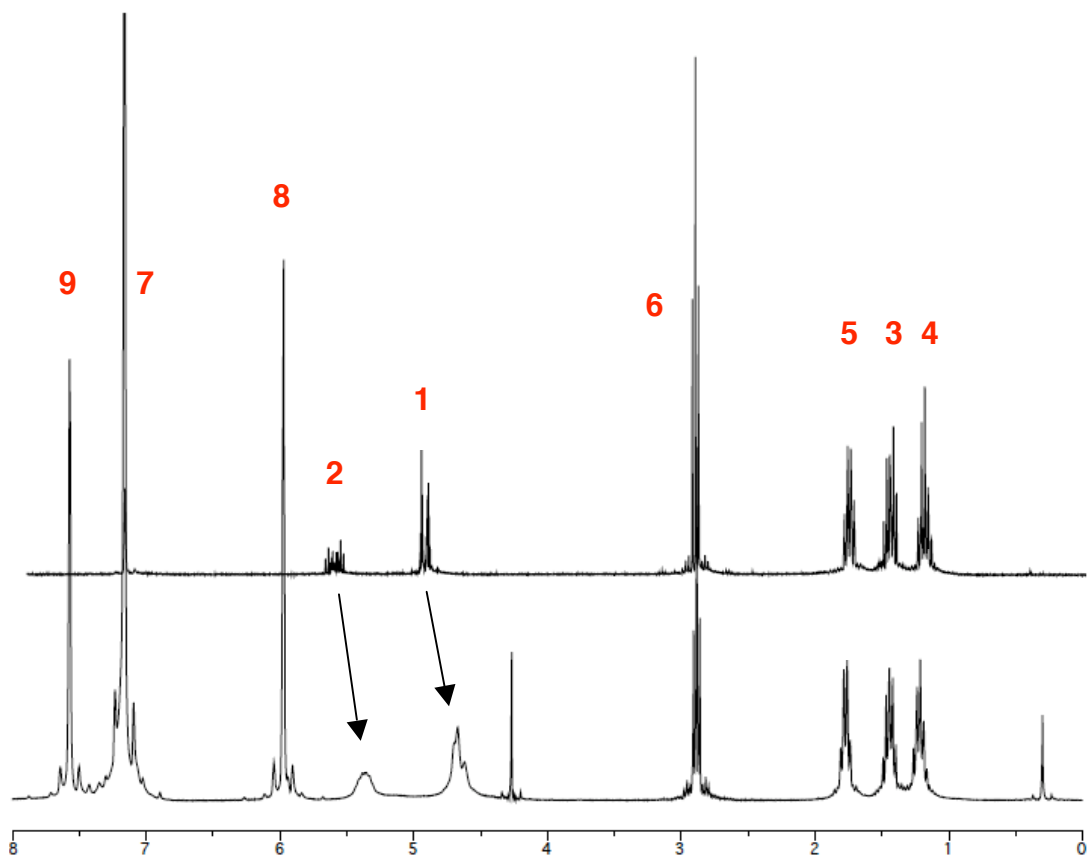
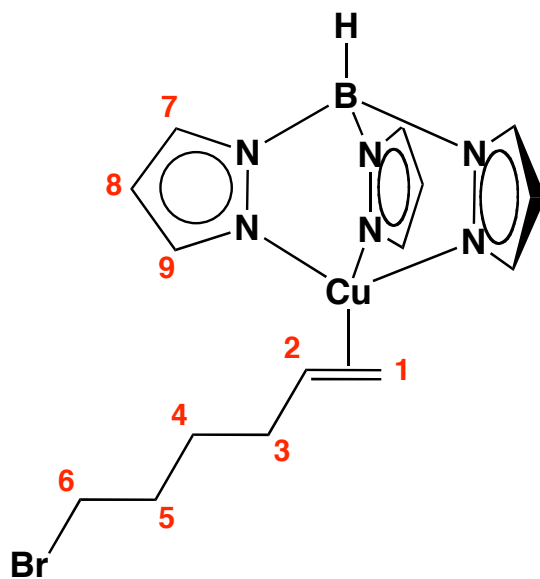


Figure A4. ^1H NMR Spectra of (a) [hydrotris(1-pyrazolyl)borato](6-bromo-1-hexene)copper(I) or TpCu^{I} (6-bromo-1-hexene) and (b) free 6-bromo-1-hexene (300 Hz, C_6D_6 , RT)



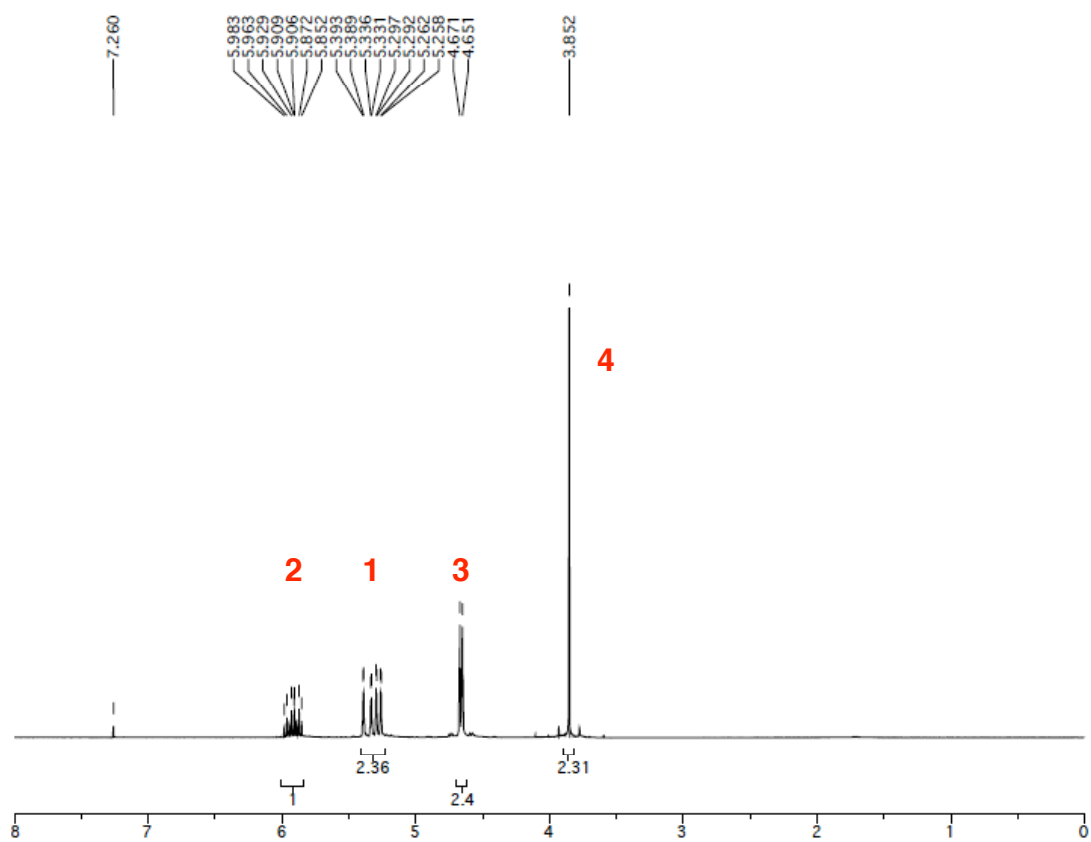
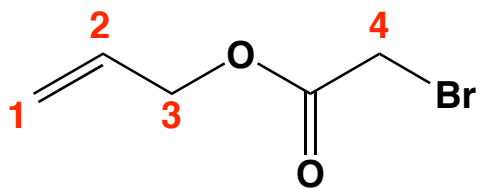


Figure A5. ^1H NMR Spectrum of Allyl Bromoacetate (300 Hz, CDCl_3 , RT)



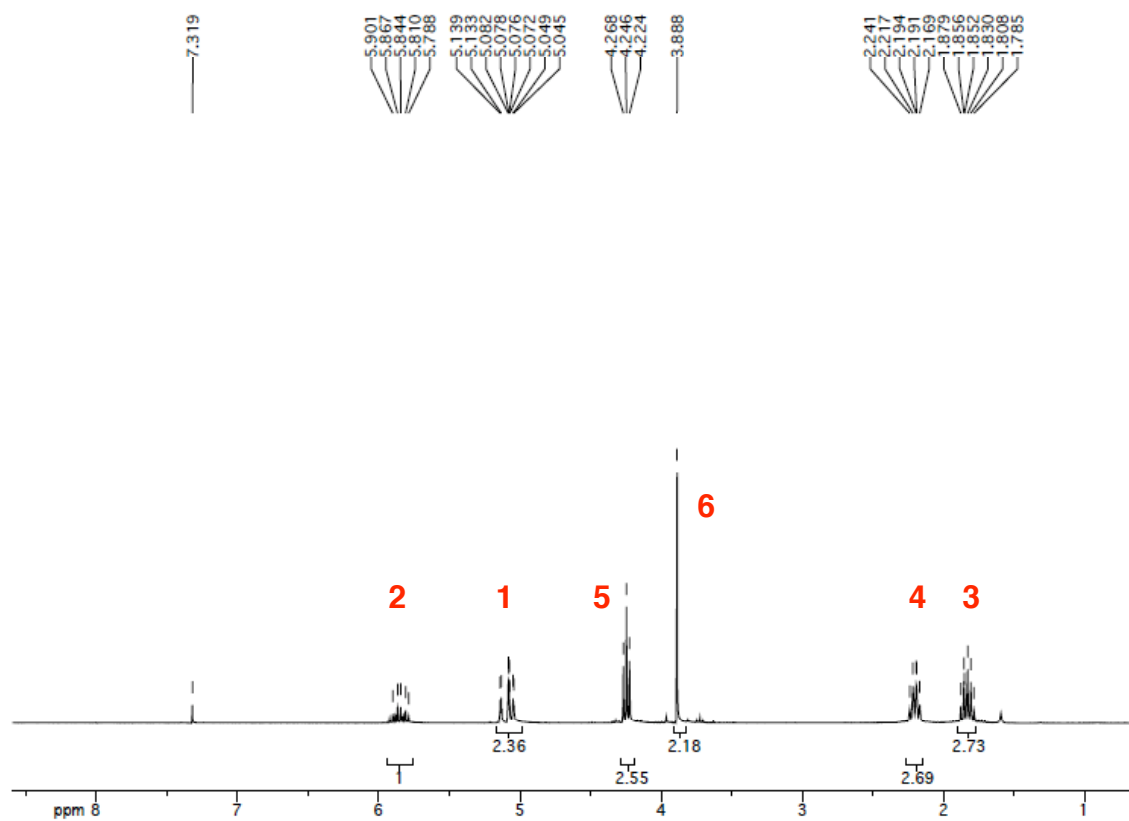
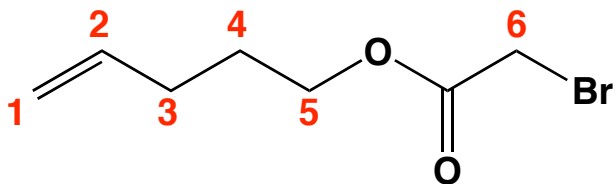


Figure A6. ^1H NMR Spectrum of 4-Pentenyl Bromoacetate (300 Hz, CDCl_3 , RT)



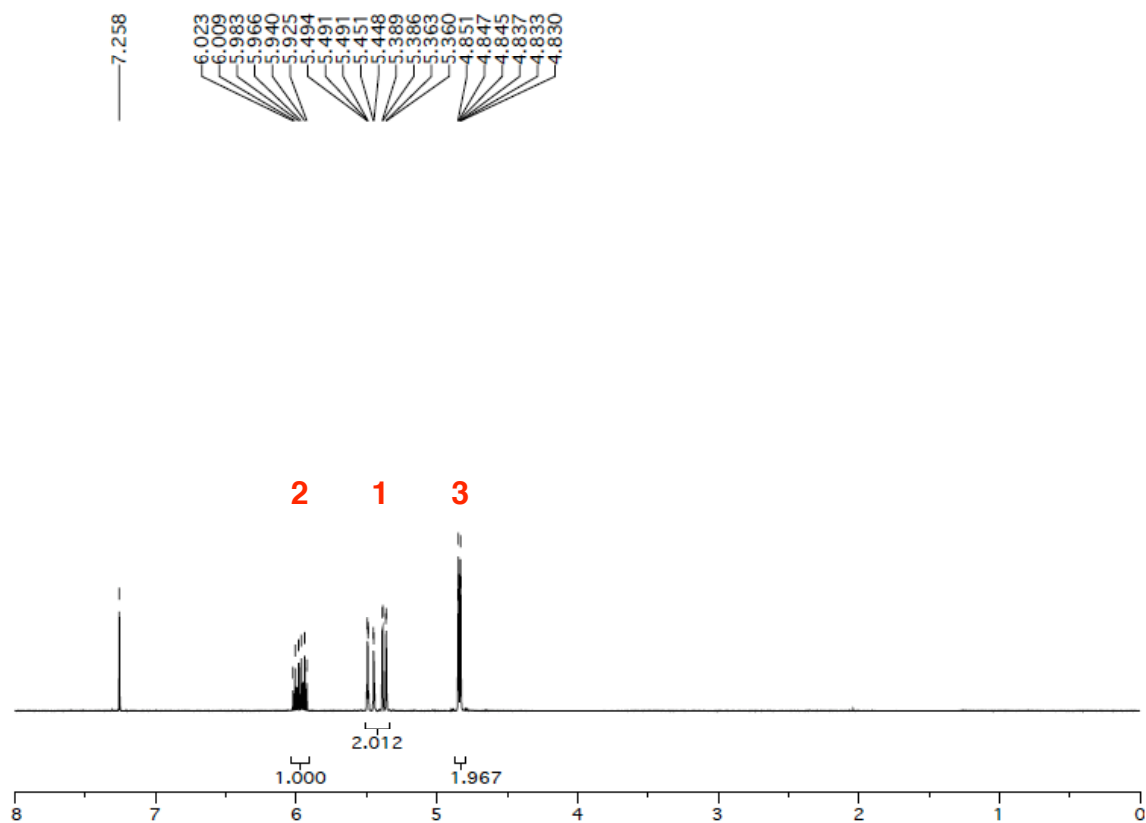
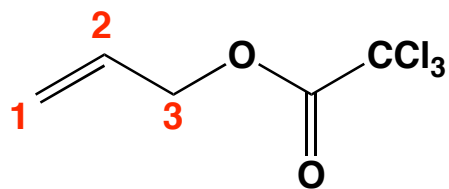


Figure A7. ^1H NMR Spectrum of Allyl Trichloroacetate (400 Hz, CDCl_3 , RT)



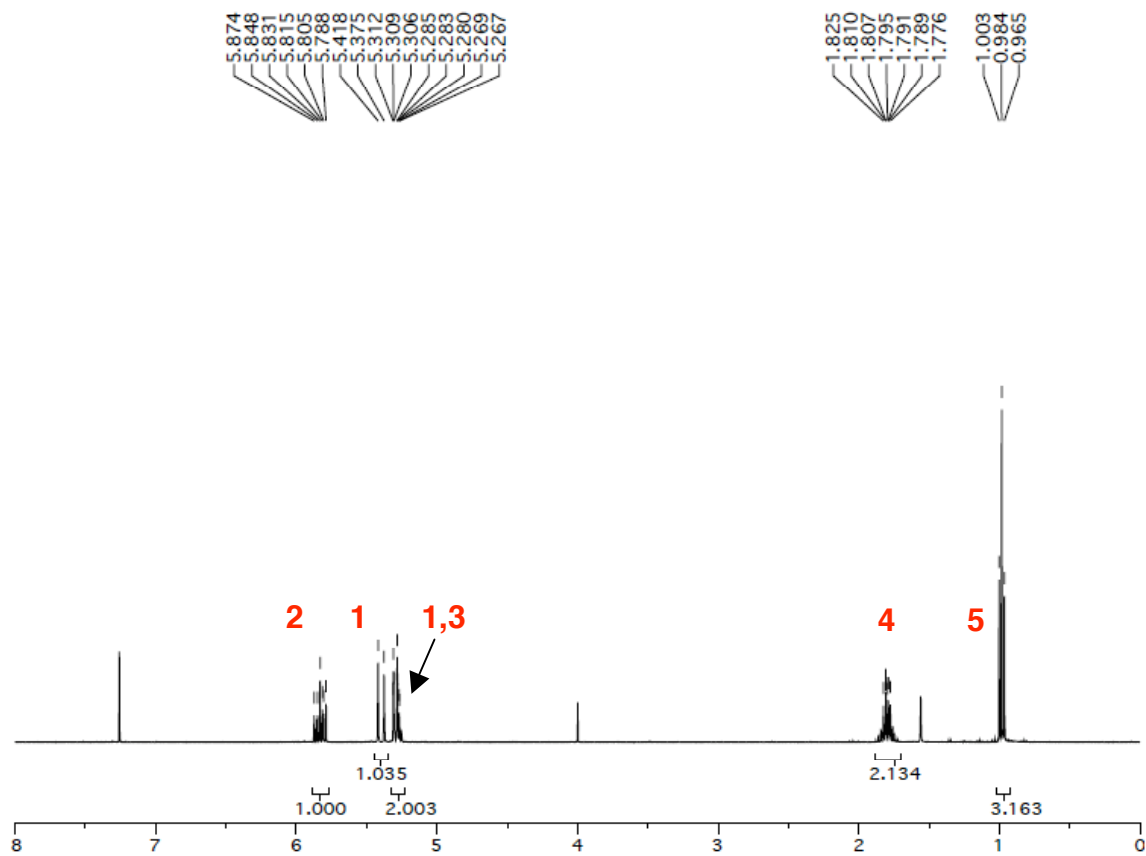
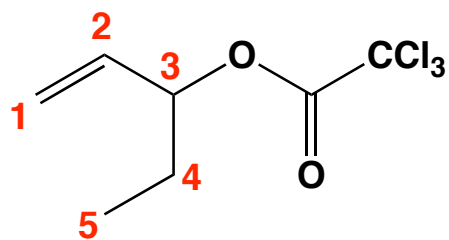


Figure A8. ^1H NMR Spectrum of Allyl-3-Ethyl Trichloroacetate (400 Hz, CDCl_3 , RT)



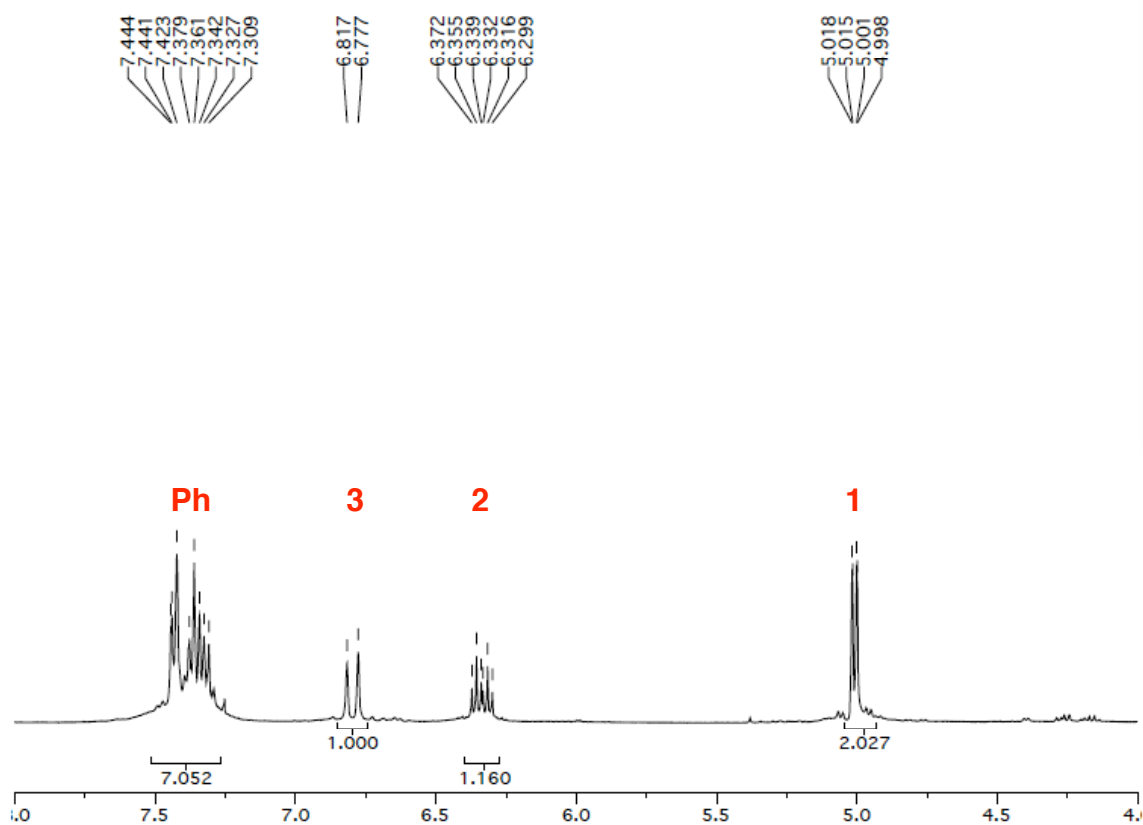
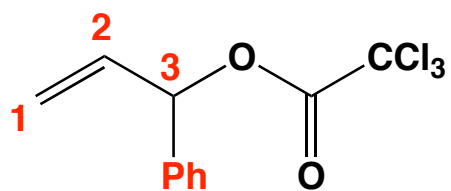


Figure A9. ^1H NMR Spectrum of Allyl-3-Phenyl Trichloroacetate (400 Hz, CDCl_3 , RT)



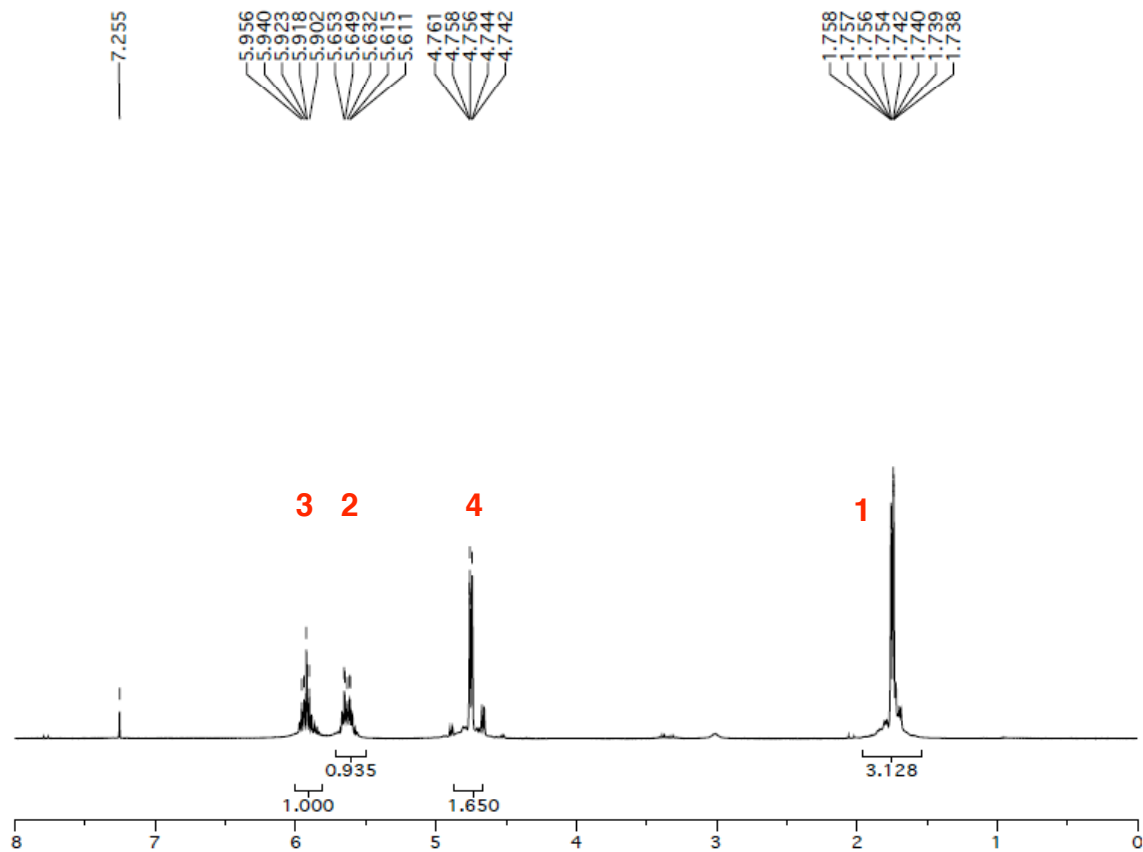
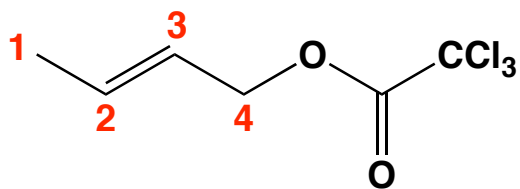


Figure A10. ^1H NMR Spectrum of Allyl-1-Methyl Trichloroacetate (400 Hz, CDCl_3 , RT)



APPENDIX B. X-RAY Crystal Data

This appendix contains X-ray crystal data for the TpCu^{I} complexes described in Chapter 6, namely $[(\text{hydrotris}(1\text{-pyrazolyl})\text{borato})\text{copper}(\text{I})]_2$ or $[\text{TpCu}^{\text{I}}]_2$, $[\text{hydrotris}(3,5\text{-trifluoromethyl-1-pyrazolyl})\text{borato}](\text{acetonitrile})\text{copper}(\text{I})$ or $\text{Tp}^{\text{CF}_3}\text{Cu}^{\text{I}}(\text{CH}_3\text{CN})$, and $[\text{hydrotris}(1\text{-pyrazolyl})\text{borato}](6\text{-bromo-1-hexene})\text{copper}(\text{I})$ or $\text{TpCu}^{\text{I}}(6\text{-bromo-1-hexene})$.

Table B1. Crystal Data and Structure Refinement for [TpCu¹]₂

Identification code	[TpCu] ₂
Empirical formula	C11 H13 B Cu N7
Formula weight	317.63
Temperature	150(1) K
Wavelength	0.71073 Å
Crystal system, space group	Triclinic, P1
Unit cell dimensions	a = 7.5843(4) Å alpha = 78.5630(10) deg. b = 8.0628(4) Å beta = 89.0260(10) deg. c = 9.1979(7) Å gamma = 87.4240(10) deg.
Volume	550.71(6) Å ³
Z, Calculated density	1, 0.958 Mg/m ³
Absorption coefficient	0.991 mm ⁻¹
F(000)	162
Crystal size	0.17 x 0.098 x 0.047 mm
Theta range for data collection	2.26 to 32.96 deg.
Limiting indices	-11 ≤ h ≤ 11, -12 ≤ k ≤ 12, -13 ≤ l ≤ 13
Reflections collected / unique	7419 / 6617 [R(int) = 0.0093]
Completeness to theta = 32.96	91.2 %
Refinement method	Full-matrix least-squares on F ²
Data / restraints / parameters	6617 / 3 / 352
Goodness-of-fit on F ²	0.790
Final R indices [I > 2σ(I)]	R1 = 0.0289, wR2 = 0.0907
R indices (all data)	R1 = 0.0349, wR2 = 0.1002
Absolute structure parameter	0.50(2)
Largest diff. peak and hole	0.514 and -0.284 e.Å ⁻³

Table B2. Atomic Coordinates ($\times 10^4$) and Equivalent Isotropic Displacement Parameters ($\text{\AA}^2 \times 10^3$) for $[\text{TpCu}^{\text{I}}]_2$.

U(eq) is Defined as One Third of the Trace of the Orthogonalized U_{ij} Tensor.

	x	y	z	U(eq)
Cu(1)	4653(1)	5157(1)	1415(1)	19(1)
Cu(2)	1617(1)	6510(1)	2202(1)	19(1)
N(2)	1893(7)	4282(7)	5108(5)	13(1)
N(7)	1412(7)	8702(7)	-796(6)	16(1)
N(10)	4366(7)	7473(7)	-1545(6)	18(1)
N(4)	4868(7)	2977(7)	4370(6)	14(1)
N(12)	4215(7)	9049(6)	589(5)	15(1)
N(5)	2045(7)	2636(6)	3010(5)	16(1)
N(6)	2122(7)	3879(6)	1803(5)	17(1)
N(11)	4114(8)	7767(6)	1843(6)	20(1)
N(8)	523(7)	7721(6)	381(6)	17(1)
N(3)	5749(7)	3914(6)	3241(6)	18(1)
N(9)	4981(7)	5934(6)	-703(6)	16(1)
N(1)	1252(8)	5754(7)	4342(6)	21(1)
B(1)	2802(8)	2784(8)	4494(7)	16(1)
B(2)	3389(9)	8889(7)	-892(6)	15(1)
C(18)	209(9)	9400(8)	-1799(7)	24(1)
C(19)	6000(7)	2211(8)	5470(6)	16(1)
C(11)	1226(9)	3299(9)	732(6)	23(1)
C(3)	1508(8)	4150(8)	6555(7)	18(1)
C(8)	4767(10)	7481(9)	-2990(6)	22(1)
C(12)	1113(8)	1364(8)	2668(8)	30(1)
C(6)	7453(9)	3783(8)	3605(7)	21(1)
C(14)	4986(9)	8267(8)	2873(7)	22(1)
C(16)	-1187(8)	7918(7)	4(7)	22(1)
C(2)	613(10)	5624(9)	6738(6)	26(1)
C(15)	5125(7)	10325(6)	888(5)	14(1)
C(1)	459(10)	6595(8)	5298(7)	21(1)
C(10)	571(9)	1760(9)	1267(8)	27(1)
C(7)	5772(10)	5095(9)	-1675(8)	25(1)
C(5)	7684(8)	2652(9)	5021(7)	20(1)
C(9)	5692(9)	6003(7)	-3111(7)	23(1)
C(13)	5647(9)	9904(8)	2365(7)	23(1)
C(17)	-1434(9)	8898(9)	-1341(8)	26(1)

Table B3. Bond Lengths [\AA] and Angles [deg] for $[\text{TpCu}^{\text{I}}]_2$.

Cu(1)-N(9)	1.939(5)
Cu(1)-N(3)	1.955(6)
Cu(1)-N(6)	2.209(5)
Cu(1)-N(11)	2.236(5)
Cu(1)-Cu(2)	2.6544(3)
Cu(2)-N(8)	1.942(6)
Cu(2)-N(1)	1.960(5)
Cu(2)-N(11)	2.178(6)
Cu(2)-N(6)	2.239(5)
N(2)-N(1)	1.330(8)
N(2)-C(3)	1.342(8)
N(2)-B(1)	1.561(8)
N(7)-C(18)	1.333(8)
N(7)-N(8)	1.391(7)
N(7)-B(2)	1.513(9)
N(10)-C(8)	1.357(8)
N(10)-N(9)	1.392(8)
N(10)-B(2)	1.547(8)
N(4)-N(3)	1.344(8)
N(4)-C(19)	1.369(8)
N(4)-B(1)	1.581(9)
N(12)-C(15)	1.340(6)
N(12)-N(11)	1.391(7)
N(12)-B(2)	1.540(8)
N(5)-N(6)	1.343(7)
N(5)-C(12)	1.360(8)
N(5)-B(1)	1.518(8)
N(6)-C(11)	1.373(7)
N(11)-C(14)	1.301(8)
N(8)-C(16)	1.343(8)
N(3)-C(6)	1.335(8)
N(9)-C(7)	1.342(8)
N(1)-C(1)	1.333(8)
C(18)-C(17)	1.361(10)
C(19)-C(5)	1.376(9)
C(11)-C(10)	1.354(11)
C(3)-C(2)	1.380(9)
C(8)-C(9)	1.378(9)
C(12)-C(10)	1.332(10)
C(6)-C(5)	1.443(9)
C(14)-C(13)	1.421(10)
C(16)-C(17)	1.341(10)
C(2)-C(1)	1.402(9)

C(15)-C(13)	1.393(7)
C(7)-C(9)	1.378(10)
N(9)-Cu(1)-N(3)	145.0(2)
N(9)-Cu(1)-N(6)	108.7(2)
N(3)-Cu(1)-N(6)	95.0(2)
N(9)-Cu(1)-N(11)	93.80(19)
N(3)-Cu(1)-N(11)	104.2(2)
N(6)-Cu(1)-N(11)	105.9(2)
N(9)-Cu(1)-Cu(2)	108.17(15)
N(3)-Cu(1)-Cu(2)	106.61(16)
N(6)-Cu(1)-Cu(2)	53.87(13)
N(11)-Cu(1)-Cu(2)	52.04(15)
N(8)-Cu(2)-N(1)	144.2(2)
N(8)-Cu(2)-N(11)	95.9(2)
N(1)-Cu(2)-N(11)	108.5(2)
N(8)-Cu(2)-N(6)	103.98(19)
N(1)-Cu(2)-N(6)	93.8(2)
N(11)-Cu(2)-N(6)	106.9(2)
N(8)-Cu(2)-Cu(1)	106.37(14)
N(1)-Cu(2)-Cu(1)	109.12(17)
N(11)-Cu(2)-Cu(1)	54.03(14)
N(6)-Cu(2)-Cu(1)	52.85(14)
N(1)-N(2)-C(3)	110.2(5)
N(1)-N(2)-B(1)	127.9(5)
C(3)-N(2)-B(1)	121.7(5)
C(18)-N(7)-N(8)	107.4(6)
C(18)-N(7)-B(2)	127.6(5)
N(8)-N(7)-B(2)	125.0(5)
C(8)-N(10)-N(9)	108.2(5)
C(8)-N(10)-B(2)	127.6(6)
N(9)-N(10)-B(2)	124.2(5)
N(3)-N(4)-C(19)	110.9(6)
N(3)-N(4)-B(1)	126.4(5)
C(19)-N(4)-B(1)	122.6(5)
C(15)-N(12)-N(11)	110.2(5)
C(15)-N(12)-B(2)	128.2(5)
N(11)-N(12)-B(2)	121.6(5)
N(6)-N(5)-C(12)	108.5(5)
N(6)-N(5)-B(1)	122.7(5)
C(12)-N(5)-B(1)	128.8(6)
N(5)-N(6)-C(11)	104.8(5)
N(5)-N(6)-Cu(1)	115.9(4)
C(11)-N(6)-Cu(1)	124.2(4)
N(5)-N(6)-Cu(2)	115.6(4)
C(11)-N(6)-Cu(2)	121.3(4)

Cu(1)-N(6)-Cu(2)	73.28(14)
C(14)-N(11)-N(12)	106.2(5)
C(14)-N(11)-Cu(2)	124.4(4)
N(12)-N(11)-Cu(2)	116.0(4)
C(14)-N(11)-Cu(1)	119.4(4)
N(12)-N(11)-Cu(1)	114.4(4)
Cu(2)-N(11)-Cu(1)	73.93(17)
C(16)-N(8)-N(7)	105.0(5)
C(16)-N(8)-Cu(2)	129.8(4)
N(7)-N(8)-Cu(2)	125.0(4)
N(4)-N(3)-C(6)	107.2(5)
N(4)-N(3)-Cu(1)	124.4(4)
C(6)-N(3)-Cu(1)	128.4(4)
C(7)-N(9)-N(10)	105.4(5)
C(7)-N(9)-Cu(1)	128.0(5)
N(10)-N(9)-Cu(1)	126.5(4)
N(2)-N(1)-C(1)	107.8(5)
N(2)-N(1)-Cu(2)	123.6(4)
C(1)-N(1)-Cu(2)	128.5(5)
N(5)-B(1)-N(4)	110.7(5)
N(5)-B(1)-N(2)	111.7(5)
N(4)-B(1)-N(2)	110.7(5)
N(12)-B(2)-N(10)	110.7(5)
N(12)-B(2)-N(7)	113.4(5)
N(10)-B(2)-N(7)	112.8(5)
C(17)-C(18)-N(7)	110.7(6)
N(4)-C(19)-C(5)	107.8(5)
N(6)-C(11)-C(10)	111.5(6)
N(2)-C(3)-C(2)	108.1(5)
N(10)-C(8)-C(9)	109.9(6)
C(10)-C(12)-N(5)	110.6(6)
N(3)-C(6)-C(5)	109.6(5)
N(11)-C(14)-C(13)	111.7(6)
C(17)-C(16)-N(8)	112.4(6)
C(3)-C(2)-C(1)	104.5(5)
N(12)-C(15)-C(13)	108.2(5)
N(1)-C(1)-C(2)	109.3(6)
C(12)-C(10)-C(11)	104.6(6)
N(9)-C(7)-C(9)	112.5(6)
C(19)-C(5)-C(6)	104.4(5)
C(7)-C(9)-C(8)	104.0(5)
C(15)-C(13)-C(14)	103.8(5)
C(16)-C(17)-C(18)	104.5(6)

Symmetry transformations used to generate equivalent atoms:

Table B4. Anisotropic Displacement Parameters ($\text{\AA}^2 \times 10^3$) for $[\text{TpCu}^{\text{I}}]_2$.

The Anisotropic Displacement Factor Exponent Takes the Form:

$$-2 \pi^2 [h^2 a^{*2} U_{11} + \dots + 2 h k a^* b^* U_{12}]$$

	U11	U22	U33	U23	U13	U12
Cu(1)	21(1)	19(1)	15(1)	1(1)	2(1)	-1(1)
Cu(2)	22(1)	18(1)	16(1)	2(1)	3(1)	-1(1)
N(2)	14(2)	18(2)	8(2)	-5(1)	6(1)	-1(1)
N(7)	16(2)	18(2)	12(2)	1(2)	5(2)	-4(2)
N(10)	16(2)	15(2)	21(2)	5(1)	-5(2)	-2(1)
N(4)	15(2)	13(2)	15(2)	-3(2)	-3(2)	2(2)
N(12)	14(2)	13(2)	17(2)	-4(2)	3(2)	0(2)
N(5)	18(2)	16(2)	14(2)	0(2)	-1(2)	-4(2)
N(6)	24(2)	17(2)	11(2)	-4(2)	-3(2)	-6(2)
N(11)	21(2)	20(2)	17(2)	3(2)	2(2)	0(2)
N(8)	19(2)	16(2)	15(2)	0(2)	7(2)	-2(2)
N(3)	11(2)	20(2)	21(2)	-1(2)	-2(2)	-1(2)
N(9)	16(2)	17(2)	15(2)	-4(2)	2(2)	5(2)
N(1)	24(3)	18(2)	18(2)	3(2)	6(2)	-3(2)
B(1)	9(2)	20(3)	18(2)	-2(2)	1(2)	-1(2)
B(2)	20(3)	12(2)	11(2)	0(2)	0(2)	-2(2)
C(18)	35(3)	19(2)	16(2)	-1(2)	-3(2)	0(2)
C(19)	8(2)	23(2)	16(2)	0(2)	-1(2)	-1(2)
C(11)	23(3)	37(3)	14(2)	-15(2)	-8(2)	1(2)
C(3)	19(2)	18(2)	16(2)	-2(2)	0(2)	2(2)
C(8)	26(3)	30(3)	11(2)	-4(2)	3(2)	-6(2)
C(12)	21(3)	17(2)	50(4)	-5(2)	12(2)	-1(2)
C(6)	13(3)	25(3)	21(2)	3(2)	1(2)	-1(2)
C(14)	26(2)	17(2)	21(2)	-1(2)	3(2)	0(2)
C(16)	16(2)	17(2)	34(3)	-9(2)	4(2)	-3(2)
C(2)	34(3)	35(3)	8(2)	-4(2)	3(2)	-5(2)
C(15)	18(2)	17(2)	10(2)	-6(1)	-4(1)	-6(2)
C(1)	22(3)	21(3)	20(2)	-5(2)	7(2)	1(2)
C(10)	21(3)	28(3)	36(3)	-20(3)	-1(2)	-1(2)
C(7)	29(3)	18(3)	25(3)	-1(2)	7(2)	3(2)
C(5)	13(2)	27(2)	19(2)	-3(2)	-6(2)	4(2)
C(9)	25(3)	19(2)	25(2)	-10(2)	8(2)	5(2)
C(13)	24(3)	27(3)	21(3)	-11(2)	-4(2)	-1(2)
C(17)	20(3)	28(2)	28(3)	-5(2)	-4(2)	-2(2)

Table B5. Crystal Data and Structure Refinement for $\text{Tp}^{\text{CF}_3}\text{Cu}(\text{CH}_3\text{CN})$

Identification code	$\text{Tp}^{\text{CF}_3}\text{Cu}(\text{CH}_3\text{CN})$
Empirical formula	$\text{C}_{17}\text{H}_7\text{B Cu F}_{18}\text{N}_7$
Formula weight	725.66
Temperature	273(2) K
Wavelength	0.71073 Å
Crystal system, space group	Trigonal, R3C
Unit cell dimensions	$a = 13.3106(8)$ Å $\alpha = 90$ deg. $b = 13.3106(8)$ Å $\beta = 90$ deg. $c = 25.695(3)$ Å $\gamma = 120$ deg.
Volume	$3942.6(6)$ Å ³
Z, Calculated density	9, 1.886 Mg/m ³
Absorption coefficient	1.331 mm ⁻¹
F(000)	2214
Crystal size	0.41 x 0.37 x 0.09 mm
Theta range for data collection	2.37 to 26.74 deg.
Limiting indices	$-16 \leq h \leq 16$, $-16 \leq k \leq 16$, $-32 \leq l \leq 32$
Reflections collected / unique	11485 / 1874 [R(int) = 0.1117]
Completeness to theta = 26.74	99.9 %
Refinement method	Full-matrix least-squares on F ²
Data / restraints / parameters	1874 / 1 / 143
Goodness-of-fit on F ²	0.930
Final R indices [I > 2σ(I)]	R1 = 0.0533, wR2 = 0.1477
R indices (all data)	R1 = 0.0811, wR2 = 0.1616
Absolute structure parameter	0.00
Largest diff. peak and hole	0.318 and -0.281 e.Å ⁻³

Table B6. Atomic Coordinates ($\times 10^4$) and Equivalent Isotropic Displacement Parameters ($\text{Å}^2 \times 10^3$) for $\text{Tp}^{\text{CF}_3}\text{Cu}(\text{CH}_3\text{CN})$
 $U(\text{eq})$ is Defined as One Third of the Trace of the Orthogonalized U_{ij} Tensor.

	x	y	z	U(eq)
Cu(1)	0	10000	1205(1)	78(1)
N(1)	1123(4)	9729(4)	1685(1)	68(1)
N(2)	1010(4)	9840(4)	2203(2)	65(1)
B(1)	0	10000	2399(5)	63(3)
C(2)	2553(6)	9635(6)	2099(3)	88(2)
C(3)	2047(5)	9593(5)	1624(2)	71(1)
C(1)	1878(5)	9765(5)	2455(2)	77(1)
C(4)	2060(7)	9877(9)	3022(3)	107(3)
C(5)	2403(6)	9438(7)	1108(3)	83(2)
F(3)	2946(7)	9792(9)	3157(2)	212(4)
F(2)	1155(6)	9087(6)	3294(2)	143(2)
F(1)	2176(6)	10870(6)	3222(2)	145(2)
N(3)	0	10000	469(3)	91(3)
C(6)	0	10000	30(6)	89(4)
C(7)	0	10000	-532(9)	167(14)
F(5)	3367(6)	9461(11)	1105(3)	217(4)
F(7)	2682(11)	10276(9)	798(3)	239(5)
F(8)	1701(6)	8619(8)	867(3)	247(6)

Table B7. Bond Lengths [Å] and Angles [deg] for $\text{Tp}^{\text{CF}_3}\text{Cu}(\text{CH}_3\text{CN})$.

Cu(1)-N(3)	1.891(9)
Cu(1)-N(1)	2.104(4)
Cu(1)-N(1)#1	2.104(4)
Cu(1)-N(1)#2	2.104(4)
N(1)-C(3)	1.339(7)
N(1)-N(2)	1.357(5)
N(2)-C(1)	1.371(7)
N(2)-B(1)	1.545(6)
B(1)-N(2)#1	1.545(7)
B(1)-N(2)#2	1.545(7)
B(1)-H(1)	1.30(13)
C(2)-C(1)	1.351(9)
C(2)-C(3)	1.380(8)
C(2)-H(2)	1.20(6)
C(3)-C(5)	1.458(9)
C(1)-C(4)	1.473(9)
C(4)-F(3)	1.288(9)
C(4)-F(2)	1.333(10)
C(4)-F(1)	1.352(10)
C(5)-F(8)	1.194(8)
C(5)-F(7)	1.265(11)
C(5)-F(5)	1.268(8)
N(3)-C(6)	1.128(17)
C(6)-C(7)	1.44(3)
C(7)-H(3)	0.75(13)
N(3)-Cu(1)-N(1)	125.91(12)
N(3)-Cu(1)-N(1)#1	125.91(12)
N(1)-Cu(1)-N(1)#1	89.08(17)
N(3)-Cu(1)-N(1)#2	125.91(12)
N(1)-Cu(1)-N(1)#2	89.08(17)
N(1)#1-Cu(1)-N(1)#2	89.08(17)
C(3)-N(1)-N(2)	106.8(4)
C(3)-N(1)-Cu(1)	137.3(3)
N(2)-N(1)-Cu(1)	115.5(3)
N(1)-N(2)-C(1)	108.1(4)
N(1)-N(2)-B(1)	119.0(6)
C(1)-N(2)-B(1)	132.9(6)
N(2)-B(1)-N(2)#1	110.0(5)
N(2)-B(1)-N(2)#2	110.0(5)
N(2)#1-B(1)-N(2)#2	110.0(5)
N(2)-B(1)-H(1)	108.9(5)

N(2)#1-B(1)-H(1)	108.9(5)
N(2)#2-B(1)-H(1)	108.9(5)
C(1)-C(2)-C(3)	105.2(5)
C(1)-C(2)-H(2)	134(3)
C(3)-C(2)-H(2)	121(3)
N(1)-C(3)-C(2)	110.7(5)
N(1)-C(3)-C(5)	120.7(5)
C(2)-C(3)-C(5)	128.6(5)
C(2)-C(1)-N(2)	109.2(5)
C(2)-C(1)-C(4)	126.6(6)
N(2)-C(1)-C(4)	124.1(5)
F(3)-C(4)-F(2)	107.2(8)
F(3)-C(4)-F(1)	108.7(8)
F(2)-C(4)-F(1)	100.9(7)
F(3)-C(4)-C(1)	111.7(6)
F(2)-C(4)-C(1)	113.6(6)
F(1)-C(4)-C(1)	114.1(7)
F(8)-C(5)-F(7)	103.3(10)
F(8)-C(5)-F(5)	109.9(8)
F(7)-C(5)-F(5)	97.4(9)
F(8)-C(5)-C(3)	116.1(6)
F(7)-C(5)-C(3)	114.8(6)
F(5)-C(5)-C(3)	113.4(6)
C(6)-N(3)-Cu(1)	180.000(2)
N(3)-C(6)-C(7)	180.000(5)
C(6)-C(7)-H(3)	122(10)

Symmetry transformations used to generate equivalent atoms:

#1 -y+1,x-y+2,z #2 -x+y-1,-x+1,z

Table B8. Anisotropic Displacement Parameters ($\text{Å}^2 \times 10^3$) for $\text{Tp}^{\text{CF}_3}\text{Cu}(\text{CH}_3\text{CN})$
 The Anisotropic Displacement Factor Exponent Takes the Form:
 $-2 \pi^2 [h^2 a^{*2} U_{11} + \dots + 2 h k a^* b^* U_{12}]$

	U11	U22	U33	U23	U13	U12
Cu(1)	97(1)	97(1)	40(1)	0	0	49(1)
N(1)	71(3)	83(3)	43(2)	-11(2)	-5(2)	34(2)
N(2)	76(3)	83(3)	41(2)	-9(2)	-9(2)	44(2)
B(1)	73(5)	73(5)	43(7)	0	0	36(2)
C(2)	81(4)	116(5)	77(4)	-11(3)	-20(3)	58(4)
C(3)	71(3)	92(4)	58(3)	-15(2)	-4(2)	46(3)
C(1)	86(4)	88(4)	67(3)	-14(3)	-15(3)	51(3)
C(4)	106(5)	187(8)	57(4)	-8(5)	-25(4)	95(5)
C(5)	79(4)	108(5)	67(4)	-16(3)	-3(3)	50(3)
F(3)	215(6)	426(11)	87(4)	-37(5)	-59(4)	230(7)
F(2)	201(5)	197(5)	63(2)	14(3)	-10(3)	123(5)
F(1)	183(5)	166(4)	79(3)	-48(3)	-56(3)	82(4)
N(3)	116(5)	116(5)	42(4)	0	0	58(2)
C(6)	111(7)	111(7)	45(8)	0	0	55(3)
C(7)	220(20)	220(20)	63(10)	0	0	109(11)
F(5)	177(6)	405(13)	143(6)	-70(7)	11(5)	202(8)
F(7)	414(15)	227(8)	120(6)	26(5)	125(7)	192(9)
F(8)	150(5)	265(9)	159(6)	-146(7)	59(5)	-21(5)

Table B9. Hydrogen Coordinates ($\times 10^4$) and Isotropic Displacement Parameters ($\text{Å}^2 \times 10^3$) for $\text{Tp}^{\text{CF}_3}\text{Cu}(\text{CH}_3\text{CN})$.

	x	y	z	U(eq)
H(1)	0	10000	2900(50)	70(30)
H(2)	3430(50)	9580(50)	2130(20)	85(17)
H(3)	60(180)	9550(140)	-690(50)	180(60)

Table B10. Crystal Data and Structure Refinement for $\text{TpCu}^{\text{I}}(6\text{-Bromo-1-hexene})$

Identification code	$\text{TpCu}^{\text{I}}(6\text{-Bromo-1-hexene})$
Empirical formula	$\text{C}_{15} \text{H}_{21} \text{Br Cu N}_6$
Formula weight	439.64
Temperature	273(2) K
Wavelength	0.71073 Å
Crystal system, space group	monoclinic, $P2(1)/m$
Unit cell dimensions	$a = 8.4137(10) \text{ Å}$ $\alpha = 90 \text{ deg.}$ $b = 17.795(2) \text{ Å}$ $\beta = 94.932(2) \text{ deg.}$ $c = 12.5165(14) \text{ Å}$ $\gamma = 90 \text{ deg.}$
Volume	$1867.0(4) \text{ Å}^3$
Z, Calculated density	4, 1.564 Mg/m^3
Absorption coefficient	3.319 mm^{-1}
F(000)	888
Crystal size	0.38 x 0.15 x 0.04 mm
Theta range for data collection	1.99 to 25.70 deg.
Limiting indices	$-10 \leq h \leq 10, -21 \leq k \leq 21, -15 \leq l \leq 15$
Reflections collected / unique	15776 / 3543 [$R(\text{int}) = 0.6727$]
Completeness to $\theta = 25.70$	99.8 %
Refinement method	Full-matrix least-squares on F^2
Data / restraints / parameters	3543 / 0 / 223
Goodness-of-fit on F^2	0.762
Final R indices [$I > 2\sigma(I)$]	$R_1 = 0.0926, wR_2 = 0.2352$
R indices (all data)	$R_1 = 0.1485, wR_2 = 0.2943$
Largest diff. peak and hole	1.314 and -1.126 e.Å^{-3}

Table B11. Atomic Coordinates ($\times 10^4$) and Equivalent Isotropic Displacement Parameters ($\text{\AA}^2 \times 10^3$) for TpCu^{I} (6-Bromo-1-hexene).

U(eq) is Defined as One Third of the Trace of the Orthogonalized Uij Tensor.

	x	y	z	U(eq)
B(1)	11711(10)	7759(5)	8908(7)	38(5)
Br(1)	901(1)	4849(1)	6446(1)	91(5)
C(1)	10364(10)	6018(4)	10051(7)	53(5)
Cu(1)	8969(1)	6779(1)	7904(1)	50(5)
N(1)	10291(8)	6545(3)	9268(5)	43(5)
C(2)	11579(11)	6165(4)	10814(7)	57(5)
N(2)	11512(7)	7029(3)	9560(5)	41(5)
C(3)	12290(11)	6803(5)	10492(7)	54(5)
N(3)	8745(7)	7935(3)	8511(5)	42(5)
C(4)	9930(11)	8915(4)	9272(6)	50(5)
N(4)	10155(7)	8228(3)	8916(5)	37(5)
C(5)	8362(12)	9097(5)	9095(7)	60(5)
N(5)	10861(7)	7142(3)	7141(5)	44(5)
C(6)	7645(10)	8468(5)	8618(7)	52(5)
N(6)	11951(7)	7558(3)	7741(5)	38(5)
C(7)	11378(10)	7093(4)	6156(6)	49(5)
C(8)	12753(10)	7493(4)	6116(6)	53(5)
C(9)	13108(9)	7783(4)	7129(7)	50(5)
C(10)	7210(12)	6353(6)	6893(8)	72(6)
C(11)	7167(10)	6013(5)	7815(8)	60(5)
C(12)	5978(11)	6169(6)	8615(8)	68(5)
C(13)	4725(12)	5552(6)	8661(8)	70(6)
C(14)	3599(11)	5516(5)	7624(8)	63(5)
C(15)	2326(17)	4919(6)	7686(12)	104(7)

Table B12. Bond Lengths [\AA] and Angles [deg] for TpCu^{I} (6-Bromo-1-hexene).

B(1)-N(6)	1.534(10)
B(1)-N(2)	1.551(10)
B(1)-N(4)	1.554(10)
B(1)-H(22)	1.00(6)
Br(1)-C(15)	1.882(16)
C(1)-N(1)	1.354(9)
C(1)-C(2)	1.364(12)
C(1)-H(1)	0.9300
Cu(1)-N(1)	1.999(6)
Cu(1)-C(10)	2.011(8)
Cu(1)-N(5)	2.031(6)
Cu(1)-C(11)	2.035(8)
Cu(1)-N(3)	2.207(6)
N(1)-N(2)	1.366(8)
C(2)-C(3)	1.360(12)
C(2)-H(2)	0.9300
N(2)-C(3)	1.349(10)
C(3)-H(3)	0.9300
N(3)-C(6)	1.339(10)
N(3)-N(4)	1.354(8)
C(4)-N(4)	1.320(9)
C(4)-C(5)	1.357(12)
C(4)-H(4)	0.9300
C(5)-C(6)	1.382(12)
C(5)-H(5)	0.9300
N(5)-C(7)	1.345(10)
N(5)-N(6)	1.354(8)
C(6)-H(6)	0.9300
N(6)-C(9)	1.350(10)
C(7)-C(8)	1.363(11)
C(7)-H(7)	0.9300
C(8)-C(9)	1.378(11)
C(8)-H(8)	0.9300
C(9)-H(9)	0.9300
C(10)-C(11)	1.307(13)
C(10)-H(10A)	0.9300
C(10)-H(10B)	0.9300
C(11)-C(12)	1.500(13)
C(11)-H(11)	0.9800
C(12)-C(13)	1.528(13)
C(12)-H(12A)	0.9700
C(12)-H(12B)	0.9700

C(13)-C(14)	1.541(13)
C(13)-H(13A)	0.9700
C(13)-H(13B)	0.9700
C(14)-C(15)	1.514(14)
C(14)-H(14A)	0.9700
C(14)-H(14B)	0.9700
C(15)-H(15A)	0.9700
C(15)-H(15B)	0.9700

N(6)-B(1)-N(2)	109.6(6)
N(6)-B(1)-N(4)	108.1(6)
N(2)-B(1)-N(4)	108.5(6)
N(6)-B(1)-H(22)	111(3)
N(2)-B(1)-H(22)	108(3)
N(4)-B(1)-H(22)	111(3)
N(1)-C(1)-C(2)	111.0(7)
N(1)-C(1)-H(1)	124.5
C(2)-C(1)-H(1)	124.5
N(1)-Cu(1)-C(10)	141.7(3)
N(1)-Cu(1)-N(5)	93.8(3)
C(10)-Cu(1)-N(5)	112.8(4)
N(1)-Cu(1)-C(11)	105.4(3)
C(10)-Cu(1)-C(11)	37.7(4)
N(5)-Cu(1)-C(11)	142.9(3)
N(1)-Cu(1)-N(3)	87.6(2)
C(10)-Cu(1)-N(3)	119.2(4)
N(5)-Cu(1)-N(3)	87.7(2)
C(11)-Cu(1)-N(3)	123.9(3)
C(1)-N(1)-N(2)	104.8(6)
C(1)-N(1)-Cu(1)	138.5(5)
N(2)-N(1)-Cu(1)	116.6(4)
C(3)-C(2)-C(1)	106.0(7)
C(3)-C(2)-H(2)	127.0
C(1)-C(2)-H(2)	127.0
C(3)-N(2)-N(1)	110.0(6)
C(3)-N(2)-B(1)	129.7(7)
N(1)-N(2)-B(1)	119.9(5)
N(2)-C(3)-C(2)	108.2(8)
N(2)-C(3)-H(3)	125.9
C(2)-C(3)-H(3)	125.9
C(6)-N(3)-N(4)	106.3(6)
C(6)-N(3)-Cu(1)	140.8(6)
N(4)-N(3)-Cu(1)	112.9(4)
N(4)-C(4)-C(5)	109.3(7)
N(4)-C(4)-H(4)	125.3
C(5)-C(4)-H(4)	125.3

C(4)-N(4)-N(3)	109.6(6)
C(4)-N(4)-B(1)	130.2(6)
N(3)-N(4)-B(1)	120.1(5)
C(4)-C(5)-C(6)	105.0(7)
C(4)-C(5)-H(5)	127.5
C(6)-C(5)-H(5)	127.5
C(7)-N(5)-N(6)	106.7(6)
C(7)-N(5)-Cu(1)	137.6(6)
N(6)-N(5)-Cu(1)	115.7(5)
N(3)-C(6)-C(5)	109.7(8)
N(3)-C(6)-H(6)	125.2
C(5)-C(6)-H(6)	125.2
C(9)-N(6)-N(5)	109.5(6)
C(9)-N(6)-B(1)	129.2(6)
N(5)-N(6)-B(1)	121.1(6)
N(5)-C(7)-C(8)	110.0(7)
N(5)-C(7)-H(7)	125.0
C(8)-C(7)-H(7)	125.0
C(7)-C(8)-C(9)	106.2(7)
C(7)-C(8)-H(8)	126.9
C(9)-C(8)-H(8)	126.9
N(6)-C(9)-C(8)	107.5(7)
N(6)-C(9)-H(9)	126.2
C(8)-C(9)-H(9)	126.2
C(11)-C(10)-Cu(1)	72.2(5)
C(11)-C(10)-H(10A)	120.0
Cu(1)-C(10)-H(10A)	110.3
C(11)-C(10)-H(10B)	120.0
Cu(1)-C(10)-H(10B)	87.7
H(10A)-C(10)-H(10B)	120.0
C(10)-C(11)-C(12)	125.0(10)
C(10)-C(11)-Cu(1)	70.2(5)
C(12)-C(11)-Cu(1)	112.0(6)
C(10)-C(11)-H(11)	113.9
C(12)-C(11)-H(11)	113.9
Cu(1)-C(11)-H(11)	113.9
C(11)-C(12)-C(13)	113.2(8)
C(11)-C(12)-H(12A)	108.9
C(13)-C(12)-H(12A)	108.9
C(11)-C(12)-H(12B)	109.0
C(13)-C(12)-H(12B)	108.9
H(12A)-C(12)-H(12B)	107.7
C(12)-C(13)-C(14)	112.0(8)
C(12)-C(13)-H(13A)	109.2
C(14)-C(13)-H(13A)	109.2
C(12)-C(13)-H(13B)	109.2

C(14)-C(13)-H(13B)	109.2
H(13A)-C(13)-H(13B)	107.9
C(15)-C(14)-C(13)	111.8(9)
C(15)-C(14)-H(14A)	109.2
C(13)-C(14)-H(14A)	109.3
C(15)-C(14)-H(14B)	109.3
C(13)-C(14)-H(14B)	109.2
H(14A)-C(14)-H(14B)	107.9
C(14)-C(15)-Br(1)	114.0(9)
C(14)-C(15)-H(15A)	108.8
Br(1)-C(15)-H(15A)	108.8
C(14)-C(15)-H(15B)	108.7
Br(1)-C(15)-H(15B)	108.7
H(15A)-C(15)-H(15B)	107.6

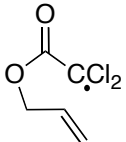
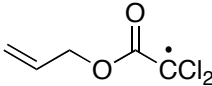
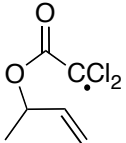
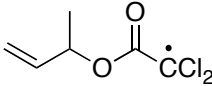
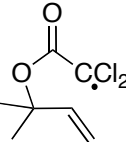
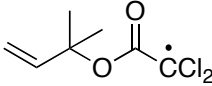
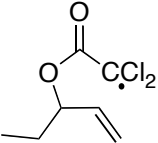
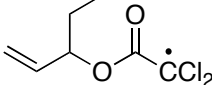
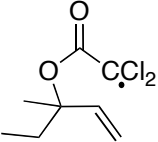
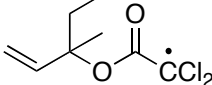
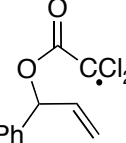
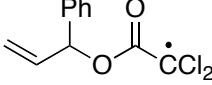
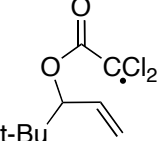
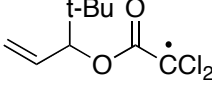
Symmetry transformations used to generate equivalent atoms:

Table B13. Anisotropic Displacement Parameters ($\text{Å}^2 \times 10^3$) for TpCu^{I} (6-Bromo-1-hexene). The Anisotropic Displacement Factor Exponent Takes the Form:
 $-2 \pi^2 [h^2 a^{*2} U_{11} + \dots + 2 h k a^* b^* U_{12}]$

	U11	U22	U33	U23	U13	U12
B(1)	21(6)	43(7)	48(7)	-4(4)	-13(4)	-3(3)
Br(1)	46(5)	83(5)	141(5)	-10(1)	-11(1)	-14(1)
C(1)	51(7)	38(6)	69(7)	9(4)	4(4)	-1(4)
Cu(1)	30(5)	67(5)	51(5)	-1(1)	-8(1)	-17(1)
N(1)	39(6)	42(6)	47(6)	3(3)	-9(3)	-5(3)
C(2)	64(8)	48(7)	57(7)	12(4)	-5(5)	11(4)
N(2)	29(6)	44(6)	46(6)	-2(3)	-11(3)	10(3)
C(3)	47(7)	66(8)	46(7)	-10(4)	-19(4)	14(4)
N(3)	30(6)	44(6)	49(6)	-3(3)	-7(3)	0(3)
C(4)	49(7)	45(7)	52(7)	-8(4)	-7(4)	1(4)
N(4)	26(6)	38(6)	44(6)	-2(3)	-5(3)	2(2)
C(5)	68(8)	49(7)	61(7)	-6(4)	-4(5)	21(4)
N(5)	33(6)	49(6)	49(6)	1(3)	-10(3)	-5(3)
C(6)	34(7)	57(7)	63(7)	-1(4)	-9(4)	11(4)
N(6)	22(6)	40(6)	52(6)	2(3)	-1(3)	0(2)
C(7)	43(7)	58(7)	45(7)	-7(4)	-3(4)	3(4)
C(8)	46(7)	64(7)	50(7)	11(4)	17(4)	1(4)
C(9)	30(7)	53(7)	67(7)	7(4)	-1(4)	-1(3)
C(10)	57(8)	88(8)	66(8)	1(5)	-21(5)	-37(5)
C(11)	35(7)	64(7)	78(8)	-7(5)	-11(4)	-19(4)
C(12)	43(7)	94(8)	68(8)	-11(5)	6(4)	-9(5)
C(13)	44(7)	97(9)	69(8)	10(5)	5(5)	-13(5)
C(14)	38(7)	65(7)	85(8)	3(5)	-1(5)	-8(4)
C(15)	100(12)	71(8)	150(13)	-13(7)	58(9)	-15(6)

APPENDIX C. SPARTAN Output Files

This appendix contains the output files from the simulation of various *cis*- and *trans*- isomers of allyl trichloroacetate derivatives using SPARTAN. The names and the corresponding structures of the allyl trichloroacetate derivatives are shown as follows.

Name	Structure	Name	Structure
<i>cis</i> -allyl trichloroacetate		<i>trans</i> -allyl trichloroacetate	
<i>cis</i> -allyl-3-methyl trichloroacetate		<i>trans</i> -allyl-3-methyl trichloroacetate	
<i>cis</i> -allyl-3,3-dimethyl trichloroacetate		<i>trans</i> -allyl-3,3-dimethyl trichloroacetate	
<i>cis</i> -allyl-3-ethyl trichloroacetate		<i>trans</i> -allyl-3-ethyl trichloroacetate	
<i>cis</i> -allyl-3,3-ethylmethyl trichloroacetate		<i>trans</i> -allyl-3,3-ethylmethyl trichloroacetate	
<i>cis</i> -allyl-3-phenyl trichloroacetate		<i>trans</i> -allyl-3-phenyl trichloroacetate	
<i>cis</i> -allyl-3- <i>t</i> -butyl trichloroacetate		<i>trans</i> -allyl-3- <i>t</i> -butyl trichloroacetate	

SPARTAN Output File for *Cis*-Allyl Trichloroacetate

SPARTAN STUDENT MECHANICS PROGRAM: x86/Darwin 131k

Frequency Calculation

Adjusted 4 (out of 42) low frequency modes

Reason for exit: Successful completion

Mechanics CPU Time: .02

Mechanics Wall Time: .29

SPARTAN STUDENT Quantum Mechanics Program:

(x86/Darwin) build 131kv4

Job type: Geometry optimization.

Method: UB3LYP

Basis set: 6-31G(D)

Number of shells: 48

Number of basis functions: 153

Multiplicity: 2

SCF model: An unrestricted hybrid HF-DFT SCF calculation will be performed using Pulay DIIS + Geometric Direct Minimization

Optimization:

Step	Energy	Max Grad.	Max Dist.
1	-1264.279074	0.079897	0.117168
2	-1264.290651	0.021477	0.089279
3	-1264.292694	0.005277	0.066263
4	-1264.292999	0.002809	0.032853
5	-1264.293050	0.001284	0.135002
6	-1264.292365	0.013231	0.075832
7	-1264.293003	0.004812	0.033267
8	-1264.293066	0.001209	0.149159
9	-1264.292396	0.009262	0.108017
10	-1264.292949	0.006449	0.054929
11	-1264.293050	0.001755	0.172225
12	-1264.269155	0.105526	0.140600
13	-1264.291526	0.029024	0.053180
14	-1264.292776	0.013687	0.124943
15	-1264.292839	0.006881	0.115967
16	-1264.291968	0.027589	0.090263
17	-1264.290204	0.033564	0.212073
18	-1264.274840	0.152840	0.104599
19	-1264.292544	0.020484	0.060725
20	-1264.292949	0.004334	0.060036
21	-1264.292455	0.008912	0.028961
22	-1264.292831	0.008086	0.020486
23	-1264.292950	0.003738	0.018516
24	-1264.293024	0.002727	0.011807
25	-1264.293065	0.001665	0.007111
26	-1264.293068	0.000771	0.003958
27	-1264.293073	0.000544	0.000906
28	-1264.293074	0.000323	0.001403

29	-1264.293074	0.000343	0.000360
30	-1264.293074	0.000155	0.000928

Reason for exit: Successful completion
Quantum Calculation CPU Time : 40:30.48
Quantum Calculation Wall Time: 48:06.54

SPARTAN STUDENT Semi-Empirical Program:
(x86/Darwin) build 131k

Semi-empirical Property Calculation
M0001
Solvation implemented only for closed shell systems
Energy Due to Solvation
Memory Used: 770.36 Kb
Reason for exit: Successful completion
Semi-Empirical Program CPU Time : .00
Semi-Empirical Program Wall Time: .07

SPARTAN PROPERTIES PACKAGE: MAC/P4 build 131
Reason for exit: Successful completion
Properties CPU Time : .51
Properties Wall Time: .65

molecule M0001 terminated normally

End- molecule "M0001" Mon Nov 16 16:16:40 2009

SPARTAN Output File for *Trans*-Allyl Trichloroacetate

SPARTAN STUDENT MECHANICS PROGRAM: x86/Darwin 131k

Frequency Calculation

Adjusted 2 (out of 42) low frequency modes

Reason for exit: Successful completion

Mechanics CPU Time : .02

Mechanics Wall Time: .07

SPARTAN STUDENT Quantum Mechanics Program:

(x86/Darwin) build 131kv4

Job type: Geometry optimization.

Method: UB3LYP

Basis set: 6-31G(D)

Number of shells: 48

Number of basis functions: 153

Multiplicity: 2

SCF model: An unrestricted hybrid HF-DFT SCF calculation will be performed using Pulay DIIS + Geometric Direct Minimization

Optimization:

Step	Energy	Max Grad.	Max Dist.
1	-1264.277581	0.036814	0.173438
2	-1264.288146	0.016868	0.061472
3	-1264.290555	0.003829	0.060522
4	-1264.291136	0.002196	0.126319
5	-1264.291484	0.001554	0.138255
6	-1264.287651	0.022436	0.139842
7	-1264.292283	0.002848	0.170379
8	-1264.293592	0.003483	0.178623
9	-1264.295485	0.003914	0.176774
10	-1264.297817	0.004186	0.172661
11	-1264.300312	0.004217	0.169595
12	-1264.302606	0.003629	0.169271
13	-1264.304382	0.002643	0.170036
14	-1264.305655	0.002029	0.157012
15	-1264.306450	0.002005	0.138676
16	-1264.306705	0.001933	0.024977
17	-1264.306739	0.000509	0.012268
18	-1264.306748	0.000224	0.005289
19	-1264.306748	0.000055	0.002633

Reason for exit: Successful completion

Quantum Calculation CPU Time : 21:09.69

Quantum Calculation Wall Time: 24:57.02

SPARTAN STUDENT Semi-Empirical Program:
(x86/Darwin) build 131k

Semi-empirical Property Calculation
M0001
Solvation implemented only for closed shell systems

Energy Due to Solvation
Memory Used: 770.36 Kb
Reason for exit: Successful completion
Semi-Empirical Program CPU Time : .00
Semi-Empirical Program Wall Time: .05

SPARTAN PROPERTIES PACKAGE: MAC/P4 build 131

Reason for exit: Successful completion
Properties CPU Time : .53
Properties Wall Time: .66

molecule M0001 terminated normally

End- molecule "M0001" Sun Nov 15 18:01:36 2009

SPARTAN Output File for *Cis-Allyl-3-Methyl Trichloroacetate*

SPARTAN STUDENT MECHANICS PROGRAM: x86/Darwin 131k

Frequency Calculation

Adjusted 4 (out of 51) low frequency modes

Reason for exit: Successful completion

Mechanics CPU Time: .02

Mechanics Wall Time: .12

SPARTAN STUDENT Quantum Mechanics Program:

(x86/Darwin) build 131kv4

Job type: Geometry optimization.

Method: UB3LYP

Basis set: 6-31G(D)

Number of shells: 56

Number of basis functions: 172

Multiplicity: 2

SCF model: An unrestricted hybrid HF-DFT SCF calculation will be performed using Pulay DIIS + Geometric Direct Minimization

Optimization:

Step	Energy	Max Grad.	Max Dist.
1	-1303.579916	0.065718	0.120366
2	-1303.595302	0.039768	0.138248
3	-1303.603883	0.030141	0.093066
4	-1303.609617	0.026086	0.078372
5	-1303.611799	0.019726	0.060374
6	-1303.613171	0.008706	0.036111
7	-1303.613634	0.007012	0.098735
8	-1303.613162	0.012624	0.060285
9	-1303.613840	0.004297	0.013894
10	-1303.613885	0.003219	0.027033
11	-1303.613912	0.003026	0.040078
12	-1303.613938	0.001914	0.005654
13	-1303.613947	0.001204	0.022988
14	-1303.613952	0.001267	0.005950
15	-1303.613954	0.000486	0.007571
16	-1303.613955	0.000334	0.000803
17	-1303.613956	0.000274	0.000673

Reason for exit: Successful completion

Quantum Calculation CPU Time : 30:19.63

Quantum Calculation Wall Time: 1:11:45.98

SPARTAN STUDENT Semi-Empirical Program:

(x86/Darwin) build 131k

Semi-empirical Property Calculation
M0001
Solvation implemented only for closed shell systems

Energy Due to Solvation
Memory Used: 1.038 Mb
Reason for exit: Successful completion
Semi-Empirical Program CPU Time : .00
Semi-Empirical Program Wall Time: .06

SPARTAN PROPERTIES PACKAGE: MAC/P4 build 131

Reason for exit: Successful completion
Properties CPU Time : .68
Properties Wall Time: .80

molecule M0001 terminated normally

End- molecule "M0001" Mon Nov 16 17:49:32 2009

SPARTAN Output File for *Trans*-Allyl-3-Methyl
Trichloroacetate

SPARTAN STUDENT MECHANICS PROGRAM: x86/Darwin 131k

Frequency Calculation

Adjusted 2 (out of 51) low frequency modes

Reason for exit: Successful completion

Mechanics CPU Time : .02

Mechanics Wall Time: .08

SPARTAN STUDENT Quantum Mechanics Program:

(x86/Darwin) build 131kv4

Job type: Geometry optimization.

Method: UB3LYP

Basis set: 6-31G(D)

Number of shells: 56

Number of basis functions: 172

Multiplicity: 2

SCF model: An unrestricted hybrid HF-DFT SCF calculation will be
performed using Pulay DIIS + Geometric Direct Minimization

Optimization:

Step	Energy	Max Grad.	Max Dist.
1	-1303.602726	0.016058	0.084653
2	-1303.607448	0.005921	0.108646
3	-1303.608251	0.001681	0.137739
4	-1303.609037	0.002919	0.150496
5	-1303.610632	0.004875	0.103445
6	-1303.602416	0.040918	0.129317
7	-1303.611922	0.013106	0.147087
8	-1303.614783	0.010075	0.148866
9	-1303.617519	0.005806	0.147375
10	-1303.619514	0.005811	0.143378
11	-1303.621254	0.006784	0.148048
12	-1303.622586	0.004990	0.159615
13	-1303.623555	0.004210	0.142766
14	-1303.624169	0.002503	0.059607
15	-1303.624324	0.001056	0.030522
16	-1303.624365	0.000315	0.020777
17	-1303.624372	0.000156	0.005680
18	-1303.624373	0.000087	0.002605

Reason for exit: Successful completion

Quantum Calculation CPU Time : 30:19.44

Quantum Calculation Wall Time: 41:00.30

SPARTAN STUDENT Semi-Empirical Program:

(x86/Darwin) build 131k

Semi-empirical Property Calculation
M0001
Solvation implemented only for closed shell systems

Energy Due to Solvation
Memory Used: 1.038 Mb
Reason for exit: Successful completion
Semi-Empirical Program CPU Time : .00
Semi-Empirical Program Wall Time: .06

SPARTAN PROPERTIES PACKAGE: MAC/P4 build 131
Reason for exit: Successful completion
Properties CPU Time : .70
Properties Wall Time: .86

molecule M0001 terminated normally

End- molecule "M0001" Sun Nov 15 19:35:11 2009

SPARTAN Output File for *Cis-Allyl-3,3-Dimethyl
Trichloroacetate*

SPARTAN STUDENT MECHANICS PROGRAM: x86/Darwin 131k

Frequency Calculation

Adjusted 3 (out of 69) low frequency modes

Reason for exit: Successful completion

Mechanics CPU Time : .03

Mechanics Wall Time: .09

SPARTAN STUDENT Quantum Mechanics Program:

(x86/Darwin) build 131kv4

Job type: Geometry optimization.

Method: UHF

Basis set: 6-31G(D)

Number of shells: 64

Number of basis functions: 191

Multiplicity: 2

SCF model: An unrestricted Hartree-Fock SCF calculation will be performed using Pulay DIIS + Geometric Direct Minimization

Optimization:

Step	Energy	Max Grad.	Max Dist.
1	-1342.957280	0.034301	0.097138
2	-1342.967509	0.010197	0.124681
3	-1342.968787	0.002321	0.150894
4	-1342.969593	0.003498	0.164158
5	-1342.970779	0.004007	0.125084
6	-1342.963012	0.024554	0.109213
7	-1342.972592	0.004435	0.159507
8	-1342.974397	0.003619	0.097290
9	-1342.961096	0.037335	0.129841
10	-1342.974869	0.007934	0.166652
11	-1342.977026	0.005698	0.157665
12	-1342.979063	0.002516	0.164235
13	-1342.980290	0.002826	0.119322
14	-1342.981222	0.003184	0.149683
15	-1342.981702	0.001661	0.115624
16	-1342.981796	0.000893	0.044450
17	-1342.981828	0.000249	0.009011
18	-1342.981833	0.000106	0.008748
19	-1342.981834	0.000073	0.001653
20	-1342.981835	0.000044	0.001432

Reason for exit: Successful completion

Quantum Calculation CPU Time : 33:08.44

Quantum Calculation Wall Time: 37:38.56

SPARTAN STUDENT Semi-Empirical Program:
(x86/Darwin) build 131k

Semi-empirical Property Calculation
M0001
Solvation implemented only for closed shell systems

Energy Due to Solvation

Memory Used: 1.793 Mb

Reason for exit: Successful completion

Semi-Empirical Program CPU Time : .00

Semi-Empirical Program Wall Time: .05

SPARTAN PROPERTIES PACKAGE: MAC/P4 build 131

Reason for exit: Successful completion

Properties CPU Time : 1.10

Properties Wall Time: 1.26

molecule M0001 terminated normally

End- molecule "M0001" Thu Nov 26 17:32:14 2009

SPARTAN Output File for *Trans*-Allyl-3,3-Dimethyl
Trichloroacetate

SPARTAN STUDENT MECHANICS PROGRAM: x86/Darwin 131k

Frequency Calculation

Adjusted 6 (out of 69) low frequency modes

Reason for exit: Successful completion

Mechanics CPU Time : .03

Mechanics Wall Time: .09

SPARTAN STUDENT Quantum Mechanics Program:
(x86/Darwin) build 131kv4

Job type: Geometry optimization.

Method: UHF

Basis set: 6-31G(D)

Number of shells: 64

Number of basis functions: 191

Multiplicity: 2

SCF model: An unrestricted Hartree-Fock SCF calculation will be
performed using Pulay DIIS + Geometric Direct Minimization

Optimization:

Step	Energy	Max Grad.	Max Dist.
1	-1342.927757	0.087187	0.124784
2	-1342.951240	0.050205	0.140798
3	-1342.964364	0.034188	0.128513
4	-1342.972265	0.022508	0.121988
5	-1342.975918	0.014219	0.087710
6	-1342.976789	0.007137	0.103354
7	-1342.976885	0.004297	0.038681
8	-1342.977031	0.002639	0.033127
9	-1342.977087	0.001833	0.044935
10	-1342.977125	0.001274	0.077567
11	-1342.977162	0.002117	0.049581
12	-1342.977189	0.000755	0.024443
13	-1342.977190	0.001596	0.025222
14	-1342.977196	0.000400	0.012510
15	-1342.977197	0.000228	0.002082
16	-1342.977197	0.000098	0.003161

Reason for exit: Successful completion

Quantum Calculation CPU Time : 25:47.90

Quantum Calculation Wall Time: 28:55.35

SPARTAN STUDENT Semi-Empirical Program:
(x86/Darwin) build 131k

Semi-empirical Property Calculation
M0001
Solvation implemented only for closed shell systems

Energy Due to Solvation
Memory Used: 1.793 Mb
Reason for exit: Successful completion
Semi-Empirical Program CPU Time : .00
Semi-Empirical Program Wall Time: .04

SPARTAN PROPERTIES PACKAGE: MAC/P4 build 131

Reason for exit: Successful completion
Properties CPU Time : 1.08
Properties Wall Time: 1.20

molecule M0001 terminated normally

End- molecule "M0001" Thu Nov 26 16:51:38 2009

SPARTAN Output File for *Cis*-Allyl-3-Ethyl Trichloroacetate

SPARTAN STUDENT MECHANICS PROGRAM: x86/Darwin 131k

Frequency Calculation

Adjusted 3 (out of 72) low frequency modes

Reason for exit: Successful completion

Mechanics CPU Time : .03

Mechanics Wall Time: .20

SPARTAN STUDENT Quantum Mechanics Program:

(x86/Darwin) build 131kv4

Job type: Geometry optimization.

Method: UHF

Basis set: 6-31G(D)

Number of shells: 64

Number of basis functions: 191

Multiplicity: 2

SCF model: An unrestricted Hartree-Fock SCF calculation will be performed using Pulay DIIS + Geometric Direct Minimization

Optimization:

Step	Energy	Max Grad.	Max Dist.
1	-1342.393501	0.040491	0.162113
2	-1342.410464	0.016999	0.068258
3	-1342.413553	0.003785	0.051966
4	-1342.414084	0.002341	0.066843
5	-1342.414264	0.001025	0.150263
6	-1342.414559	0.002211	0.129877
7	-1342.412244	0.020655	0.114354
8	-1342.415078	0.001746	0.144361
9	-1342.415698	0.002165	0.148733
10	-1342.416812	0.002438	0.155957
11	-1342.417344	0.002590	0.144283
12	-1342.418222	0.003238	0.131855
13	-1342.418409	0.083559	0.108883
14	-1342.418743	0.007087	0.132574
15	-1342.419047	0.005593	0.136373
16	-1342.419473	0.003062	0.131439
17	-1342.419505	0.001200	0.081188
18	-1342.419521	0.001338	0.018913
19	-1342.419533	0.000880	0.012905
20	-1342.419540	0.000401	0.011414
21	-1342.419549	0.000331	0.003253
22	-1342.419552	0.000170	0.002070
23	-1342.419554	0.000067	0.001034

Reason for exit: Successful completion

Quantum Calculation CPU Time : 1:05:22.25

Quantum Calculation Wall Time: 1:32:04.16

SPARTAN STUDENT Semi-Empirical Program:
(x86/Darwin) build 131k

Semi-empirical Property Calculation
M0001
Solvation implemented only for closed shell systems

Energy Due to Solvation

Memory Used: 2.426 Mb

Reason for exit: Successful completion

Semi-Empirical Program CPU Time : .00

Semi-Empirical Program Wall Time: .10

SPARTAN PROPERTIES PACKAGE: MAC/P4 build 131

Reason for exit: Successful completion

Properties CPU Time : 1.54

Properties Wall Time: 1.77

molecule M0001 terminated normally

End- molecule "M0001" Tue Nov 17 15:54:50 2009

SPARTAN Output File for *Trans*-Allyl-3-Ethyl
Trichloroacetate

SPARTAN STUDENT MECHANICS PROGRAM: x86/Darwin 131k

Frequency Calculation

Adjusted 6 (out of 72) low frequency modes

Reason for exit: Successful completion

Mechanics CPU Time : .03

Mechanics Wall Time: .30

SPARTAN STUDENT Quantum Mechanics Program:

(x86/Darwin) build 131kv4

Job type: Geometry optimization.

Method: UHF

Basis set: 6-31G(D)

Number of shells: 64

Number of basis functions: 191

Multiplicity: 2

SCF model: An unrestricted Hartree-Fock SCF calculation will be
performed using Pulay DIIS + Geometric Direct Minimization

Optimization:

Step	Energy	Max Grad.	Max Dist.
1	-1342.367899	0.080743	0.125044
2	-1342.391313	0.047041	0.136094
3	-1342.404242	0.032439	0.118442
4	-1342.411873	0.021177	0.100818
5	-1342.415356	0.013276	0.089474
6	-1342.416209	0.006665	0.100624
7	-1342.416221	0.004881	0.066863
8	-1342.416289	0.007418	0.039964
9	-1342.416451	0.003922	0.083703
10	-1342.416471	0.007141	0.017821
11	-1342.416544	0.000889	0.047451
12	-1342.416566	0.000654	0.077248
13	-1342.416584	0.002126	0.081350
14	-1342.416616	0.001593	0.098993
15	-1342.416646	0.003335	0.020161
16	-1342.416626	0.000958	0.058411
17	-1342.416635	0.000968	0.013872
18	-1342.416636	0.002096	0.022666
19	-1342.416646	0.001130	0.083752
20	-1342.416651	0.000902	0.024526
21	-1342.416660	0.000317	0.029215
22	-1342.416667	0.000367	0.132115
23	-1342.416680	0.001367	0.101028
24	-1342.416678	0.002963	0.022185
25	-1342.416678	0.002449	0.043455
26	-1342.416689	0.000701	0.039746
27	-1342.416698	0.000308	0.082651
28	-1342.416703	0.000738	0.065457

29	-1342.416710	0.000849	0.121481
30	-1342.416670	0.003518	0.019382
31	-1342.416711	0.001011	0.058742
32	-1342.416705	0.001829	0.022049
33	-1342.416713	0.001838	0.064055
34	-1342.416720	0.001165	0.064235
35	-1342.416725	0.001348	0.046112
36	-1342.416752	0.001131	0.022368
37	-1342.416712	0.001141	0.078581
38	-1342.416708	0.001406	0.057148
39	-1342.416719	0.000598	0.028630
40	-1342.416723	0.000249	0.017883
41	-1342.416724	0.000245	0.054738

Reason for exit: Successful completion
Quantum Calculation CPU Time : 1:39:44.22
Quantum Calculation Wall Time: 1:49:56.82

SPARTAN STUDENT Semi-Empirical Program:
(x86/Darwin) build 131k

Semi-empirical Property Calculation
M0001
Solvation implemented only for closed shell systems

Energy Due to Solvation
Memory Used: 2.426 Mb
Reason for exit: Successful completion
Semi-Empirical Program CPU Time : .00
Semi-Empirical Program Wall Time: .05

SPARTAN PROPERTIES PACKAGE: MAC/P4 build 131

Reason for exit: Successful completion P
roperties CPU Time : 1.52
Properties Wall Time: 1.93

molecule M0001 terminated normally

End- molecule "M0001" Tue Nov 17 15:26:32 2009

SPARTAN Output File for *Cis-Allyl-3,3-EthylMethyl*
Trichloroacetate

SPARTAN STUDENT MECHANICS PROGRAM: x86/Darwin 131k

Frequency Calculation

Adjusted 6 (out of 78) low frequency modes

Reason for exit: Successful completion

Mechanics CPU Time : .03

Mechanics Wall Time: .05

SPARTAN STUDENT Quantum Mechanics Program:

(x86/Darwin) build 131kv4

Job type: Geometry optimization.

Method: UHF

Basis set: 6-31G(D)

Number of shells: 72

Number of basis functions: 210

Multiplicity: 2

SCF model: An unrestricted Hartree-Fock SCF calculation will be performed using Pulay DIIS + Geometric Direct Minimization

Optimization:

Step	Energy	Max Grad.	Max Dist.
1	-1376.961963	0.088161	0.130354
2	-1376.985412	0.050216	0.145653
3	-1376.998487	0.034114	0.132659
4	-1377.006275	0.022102	0.106383
5	-1377.009799	0.013139	0.067817
6	-1377.010657	0.006950	0.080212
7	-1377.010674	0.006328	0.047319
8	-1377.010589	0.006643	0.049448
9	-1377.010840	0.004289	0.059137
10	-1377.010937	0.001184	0.013861
11	-1377.010958	0.000447	0.025300
12	-1377.010966	0.000977	0.026593
13	-1377.010980	0.000714	0.089894
14	-1377.010980	0.001324	0.035718
15	-1377.010988	0.001087	0.011237
16	-1377.010989	0.000756	0.012982
17	-1377.010991	0.000185	0.002987
18	-1377.010991	0.000072	0.001259

Reason for exit: Successful completion

Quantum Calculation CPU Time : 36:02.25

Quantum Calculation Wall Time: 40:17.59

SPARTAN STUDENT Semi-Empirical Program:

(x86/Darwin) build 131k

Semi-empirical Property Calculation
M0001
Solvation implemented only for closed shell systems

Energy Due to Solvation
Memory Used: 2.272 Mb
Reason for exit: Successful completion
Semi-Empirical Program CPU Time : .00
Semi-Empirical Program Wall Time: .01

SPARTAN PROPERTIES PACKAGE: MAC/P4 build 131

Reason for exit: Successful completion
Properties CPU Time : 1.31
Properties Wall Time: 1.43

molecule M0001 terminated normally

End- molecule "M0001" Mon Nov 16 21:13:20 2009

SPARTAN Output File for *Trans-Allyl-3,3-EthylMethyl*
Trichloroacetate

SPARTAN STUDENT MECHANICS PROGRAM: x86/Darwin 131k

Frequency Calculation

Adjusted 4 (out of 78) low frequency modes

Reason for exit: Successful completion

Mechanics CPU Time : .03

Mechanics Wall Time: .15

SPARTAN STUDENT Quantum Mechanics Program:

(x86/Darwin) build 131kv4

Job type: Geometry optimization.

Method: UHF

Basis set: 6-31G(D)

Number of shells: 72

Number of basis functions: 210

Multiplicity: 2

SCF model: An unrestricted Hartree-Fock SCF calculation will be
performed using Pulay DIIS + Geometric Direct Minimization

Optimization:

Step	Energy	Max Grad.	Max Dist.
1	-1377.000036	0.038746	0.132607
2	-1377.002014	0.011514	0.058271
3	-1377.002472	0.001161	0.115442
4	-1377.002512	0.002438	0.068043
5	-1377.002513	0.002540	0.121349
6	-1377.002253	0.006041	0.087100
7	-1377.002533	0.001308	0.121240
8	-1377.002552	0.001549	0.093217
9	-1377.002491	0.004188	0.051455
10	-1377.002559	0.000883	0.138528
11	-1377.002510	0.003678	0.094533
12	-1377.002567	0.000782	0.014298
13	-1377.002570	0.000548	0.007403
14	-1377.002567	0.000846	0.024690
15	-1377.002574	0.000325	0.017013
16	-1377.002576	0.000323	0.015745
17	-1377.002576	0.000266	0.027520

Reason for exit: Successful completion

Quantum Calculation CPU Time : 31:36.08

Quantum Calculation Wall Time: 35:26.31

SPARTAN STUDENT Semi-Empirical Program:

(x86/Darwin) build 131k

Semi-empirical Property Calculation
M0001
Solvation implemented only for closed shell systems

Energy Due to Solvation
Memory Used: 2.272 Mb
Reason for exit: Successful completion
Semi-Empirical Program CPU Time : .00
Semi-Empirical Program Wall Time: .05

SPARTAN PROPERTIES PACKAGE: MAC/P4 build 131
Reason for exit: Successful completion
Properties CPU Time : 1.33
Properties Wall Time: 1.42

molecule M0001 terminated normally

End- molecule "M0001" Sun Nov 15 23:10:06 2009

SPARTAN Output File for *Cis*-Allyl-3-Phenyl Trichloroacetate

SPARTAN STUDENT MECHANICS PROGRAM: x86/Darwin 131k

Frequency Calculation

Adjusted 2 (out of 60) low frequency modes

Reason for exit: Successful completion

Mechanics CPU Time : .02

Mechanics Wall Time: .10

SPARTAN STUDENT Quantum Mechanics Program:

(x86/Darwin) build 131kv4

Job type: Geometry optimization.

Method: UHF

Basis set: 6-31G(D)

Number of shells: 80

Number of basis functions: 251

Multiplicity: 2

SCF model: An unrestricted hybrid HF-DFT SCF calculation will be performed using Pulay DIIS + Geometric Direct Minimization

Optimization:

Step	Energy	Max Grad.	Max Dist.
1	-1490.915647	0.018284	0.109770
2	-1490.920804	0.005430	0.156661
3	-1490.921965	0.002633	0.108761
4	-1490.914401	0.025773	0.134900
5	-1490.922225	0.005112	0.168806
6	-1490.923982	0.004094	0.128534
7	-1490.907106	0.062847	0.114607
8	-1490.924608	0.005786	0.170551
9	-1490.926802	0.004426	0.154473
10	-1490.918963	0.040776	0.135200
11	-1490.929414	0.009703	0.165285
12	-1490.931899	0.006252	0.169114
13	-1490.934069	0.003903	0.166615
14	-1490.935675	0.001966	0.158172
15	-1490.936690	0.001394	0.150057
16	-1490.937119	0.001571	0.053017
17	-1490.937193	0.001134	0.022925
18	-1490.937219	0.000372	0.013714
19	-1490.937225	0.000120	0.002383
20	-1490.937226	0.000048	0.003290

Reason for exit: Successful completion

Quantum Calculation CPU Time : 45:59.31

Quantum Calculation Wall Time: 53:39.75

SPARTAN STUDENT Semi-Empirical Program:

(x86/Darwin) build 131k

Semi-empirical Property Calculation
M0001
Solvation implemented only for closed shell systems

Energy Due to Solvation
Memory Used: 1.384 Mb
Reason for exit: Successful completion
Semi-Empirical Program CPU Time : .00
Semi-Empirical Program Wall Time: .09

SPARTAN PROPERTIES PACKAGE: MAC/P4 build 131
Reason for exit: Successful completion
Properties CPU Time : .88
Properties Wall Time: 1.04

molecule M0001 terminated normally

End- molecule "M0001" Sun Nov 15 20:54:51 2009

SPARTAN Output File for *Trans*-Allyl-3-Phenyl
Trichloroacetate

SPARTAN STUDENT MECHANICS PROGRAM: x86/Darwin 131k

Frequency Calculation

Adjusted 5 (out of 60) low frequency modes

Reason for exit: Successful completion

Mechanics CPU Time : .02

Mechanics Wall Time: .11

SPARTAN STUDENT Quantum Mechanics Program:

(x86/Darwin) build 131kv4

Job type: Geometry optimization.

Method: UHF

Basis set: 6-31G(D)

Number of shells: 80

Number of basis functions: 251

Multiplicity: 2

SCF model: An unrestricted hybrid HF-DFT SCF calculation will be
performed using Pulay DIIS + Geometric Direct Minimization

Optimization:

Step	Energy	Max Grad.	Max Dist.
1	-1490.875313	0.023466	0.136405
2	-1490.883950	0.013442	0.143784
3	-1490.888418	0.009049	0.137834
4	-1490.890416	0.005659	0.125979
5	-1490.891090	0.006491	0.090606
6	-1490.891511	0.004626	0.087885
7	-1490.891758	0.005927	0.090133
8	-1490.892051	0.003723	0.086543
9	-1490.892254	0.004279	0.091472
10	-1490.892453	0.002806	0.088446
11	-1490.892638	0.002840	0.095670
12	-1490.892796	0.003382	0.095193
13	-1490.892940	0.002360	0.090732
14	-1490.893121	0.003293	0.148525
15	-1490.855609	0.213543	0.132883
16	-1490.892446	0.015984	0.066384
17	-1490.893098	0.005737	0.090484
18	-1490.893343	0.002952	0.093251
19	-1490.893484	0.004235	0.094266
20	-1490.893629	0.005587	0.050574
21	-1490.891674	0.017562	0.076524
22	-1490.892142	0.015617	0.039375
23	-1490.893471	0.007476	0.104416
24	-1490.894080	0.003739	0.091080
25	-1490.894304	0.003526	0.090959
26	-1490.892242	0.012321	0.090781
27	-1490.894273	0.011046	0.088312
28	-1490.894831	0.003266	0.088266

29	-1490.895052	0.004658	0.077841
30	-1490.895262	0.004603	0.072903
31	-1490.895861	0.004679	0.082639
32	-1490.896391	0.005887	0.081380
33	-1490.892417	0.033071	0.096806
34	-1490.897353	0.005804	0.102628
35	-1490.898331	0.010414	0.103668
36	-1490.899318	0.012268	0.099785
37	-1490.900692	0.015573	0.099774
38	-1490.901907	0.025965	0.100629
39	-1490.903895	0.027954	0.148642
40	-1490.898751	0.063692	0.126729
41	-1490.912253	0.042037	0.100810
42	-1490.916997	0.023212	0.169285
43	-1490.920515	0.012526	0.127319
44	-1490.922159	0.017069	0.100641
45	-1490.923316	0.022605	0.106781
46	-1490.924811	0.017267	0.161392
47	-1490.926639	0.011130	0.110594
48	-1490.927902	0.007480	0.098377
49	-1490.928856	0.009562	0.094789
50	-1490.930046	0.009227	0.087516

Reason for exit: Successful completion
Quantum Calculation CPU Time : 55:47.03
Quantum Calculation Wall Time: 59:21.32

SPARTAN STUDENT Semi-Empirical Program:
(x86/Darwin) build 131k

Semi-empirical Property Calculation
M0001
Solvation implemented only for closed shell systems

Energy Due to Solvation
Memory Used: 2.834 Mb
Reason for exit: Successful completion
Semi-Empirical Program CPU Time : .00
Semi-Empirical Program Wall Time: .08

SPARTAN PROPERTIES PACKAGE: MAC/P4 build 131
Reason for exit: Successful completion
Properties CPU Time : 1.48
Properties Wall Time: 2.71

molecule M0001 terminated normally

End- molecule "M0001" Sun Nov 15 20:54:51 2009

SPARTAN Output File for *Cis-Allyl-3-t-Butyl*
Trichloroacetate

SPARTAN STUDENT MECHANICS PROGRAM: x86/Darwin 131k

Frequency Calculation

Adjusted 3 (out of 60) low frequency modes

Reason for exit: Successful completion

Mechanics CPU Time : .02

Mechanics Wall Time: .11

SPARTAN STUDENT Quantum Mechanics Program:

(x86/Darwin) build 131kv4

Job type: Geometry optimization.

Method: UHF

Basis set: 6-31G(D)

Number of shells: 80

Number of basis functions: 229

Multiplicity: 2

SCF model: An unrestricted hybrid HF-DFT SCF calculation will be performed using Pulay DIIS + Geometric Direct Minimization

Optimization:

Step	Energy	Max Grad.	Max Dist.
1	-1417.916449	0.020765	0.107938
2	-1417.921255	0.005757	0.108591
3	-1417.922016	0.001215	0.149924
4	-1417.922911	0.004573	0.146846
5	-1417.924766	0.003574	0.150987
6	-1417.926711	0.006387	0.157918
7	-1417.921249	0.025502	0.140725
8	-1417.927974	0.013395	0.151620
9	-1417.931442	0.007260	0.148315
10	-1417.933825	0.004878	0.148369
11	-1417.935826	0.002311	0.146708
12	-1417.936939	0.003341	0.165134
13	-1417.937549	0.004249	0.124923
14	-1417.937878	0.000604	0.029779
15	-1417.937908	0.000404	0.031648
16	-1417.937920	0.000215	0.006548
17	-1417.937921	0.000066	0.001764
18	-1417.937922	0.000029	0.000779

Reason for exit: Successful completion

Quantum Calculation CPU Time : 37:46.40

Quantum Calculation Wall Time: 44:01.76

SPARTAN STUDENT Semi-Empirical Program:

(x86/Darwin) build 131k

Semi-empirical Property Calculation

M0001

Solvation implemented only for closed shell systems

Energy Due to Solvation

Memory Used: 1.384 Mb

Reason for exit: Successful completion

Semi-Empirical Program CPU Time : .00

Semi-Empirical Program Wall Time: .05

SPARTAN PROPERTIES PACKAGE: MAC/P4

build 131

Reason for exit: Successful completion

Properties CPU Time : .88

Properties Wall Time: 1.01

molecule M0001 terminated normally

End- molecule "M0001" Sun Nov 15 21:40:50 2009

SPARTAN Output File for *Trans-Allyl-3-t-Butyl*
Trichloroacetate

SPARTAN STUDENT MECHANICS PROGRAM: x86/Darwin 131k

Frequency Calculation

Adjusted 5 (out of 60) low frequency modes

Reason for exit: Successful completion

Mechanics CPU Time : .02

Mechanics Wall Time: .06

SPARTAN STUDENT Quantum Mechanics Program:

(x86/Darwin) build 131kv4

Job type: Geometry optimization.

Method: UHF

Basis set: 6-31G(D)

Number of shells: 80

Number of basis functions: 229

Multiplicity: 2

SCF model: An unrestricted hybrid HF-DFT SCF calculation will be performed using Pulay DIIS + Geometric Direct Minimization

Optimization:

Step	Energy	Max Grad.	Max Dist.
1	-1417.893875	0.064403	0.119805
2	-1417.909329	0.039212	0.137941
3	-1417.918496	0.028037	0.114408
4	-1417.924359	0.022181	0.079734
5	-1417.926784	0.017939	0.045135
6	-1417.927756	0.009615	0.052139
7	-1417.927963	0.007053	0.057315
8	-1417.927763	0.011559	0.033993
9	-1417.928138	0.007006	0.026168
10	-1417.928194	0.005182	0.015042
11	-1417.928225	0.003448	0.014151
12	-1417.928242	0.002640	0.031577
13	-1417.928250	0.002098	0.018285
14	-1417.928255	0.001144	0.006480
15	-1417.928257	0.001042	0.003391
16	-1417.928258	0.000682	0.001433
17	-1417.928259	0.000619	0.001294
18	-1417.928260	0.000356	0.006187
19	-1417.928260	0.000206	0.004391

Reason for exit: Successful completion

Quantum Calculation CPU Time : 41:12.24

Quantum Calculation Wall Time: 47:52.84

SPARTAN STUDENT Semi-Empirical Program:

(x86/Darwin) build 131k

Semi-empirical Property Calculation

M0001

Solvation implemented only for closed shell systems

Energy Due to Solvation

Memory Used: 1.384 Mb

Reason for exit: Successful completion

Semi-Empirical Program CPU Time : .00

Semi-Empirical Program Wall Time: .04

SPARTAN PROPERTIES PACKAGE: MAC/P4

build 131

Reason for exit: Successful completion

Properties CPU Time : .86

Properties Wall Time: 1.01

molecule M0001 terminated normally

End- molecule "M0001" Mon Nov 16 20:02:18 2009